ANALYSIS AND RECONSTRUCTION OF DYNAMIC-STALL DATA FROM NOMINALLY TWO-DIMENSIONAL AEROFOIL TESTS IN TWO DIFFERENT WIND TUNNELS

by

Giangiacomo Gobbi

Dissertation submitted to the Department of Aerospace Engineering, Faculty of Engineering, University of Glasgow, for the Degree of Doctor of Philosophy.

March, 2009

"Certainly we are what we make of ourselves, but I wonder what we would be without wonderful examples to follow"

To my parents

PREFACE

The work described in this dissertation was carried out by the author in the department of Aerospace Engineering, during the period May 2004 to November 2007. The work is that of the author and is original in content except where otherwise stated.

Giangiacomo Gobbi

March 2009

Contents

List of figures

List of Tables

Acknowledgements

The last four years have being extremely stimulating in many ways for me and I find myself to have quite a list of people who contributed in some way or other to this thesis. I would like to express my deep gratitude to them and to take this opportunity to thank them all.

My supervisor Roderick, for continuous enthusiasm, inspiration, friendship, endless patience and advice, and without whose help this work would not have been finished. I am grateful to countless people, past and present, in the Department of Aerospace Engineering for their good, honest friendship and assistance. Among them: Wanan, Frank, Adriano and Jeremy. A special immense thank goes to Giamma. He made it possible from the beginning to the end and I will never forget his moral, and not only, support. All the friends of the research room; although engineers, I spent very good time with them during the days and, especially, at nights. I surely want to thank big Joe, Lucy, Kevin, Foti, Giacinto, Javier, Judith, Vincent, Massimo, Camilla and all the others. All those people, outside the University, who have made Glesga an incredibly nice place over all these years: Dougie, PMc, Sheano, Simy and Stevo (the original TdbT), my thoughtful flatmate Emanuela, Mark, Priscilla, Dany, the French couple: Audrey and Laurent, super Valentina, Norton, Ian, Gayle, Elaine and many others. My maiali friends from back home, their support has been always precious: Valerio, Bagabrera, TuttoIstinto, Leone, Leopoldo, Luca officially Lo Skalzo, Gigione and their ladies. To my ladies too. I like to remember the guys who shared with me my experience in Canada (Sam, Matt, Ele particularly) and Ladislav who made it happen. I cannot forget all the people from footie (neither can my legs). A mention to Mr Jack and his lovely spouse Coke without which this thesis would have been finished years ago. Last grazie goes to my parents, Renata and Aldo who have always supported and encouraged me throughout the years, and to my brothers: Tonio and Gianpa. Here comes my biggest: Thank you all, guys.

Abstract

This work is a specific investigation into low speed aerofoils. The term "low speed" is normally used to indicate free stream velocity less than Mach = 0.5 and, here, not more than 0.2 M when considering dynamic-stall. This field of investigation, for the QinetiQ aerofoil, has been somewhat ignored till now to the advantage of higher speeds starting from 0.3 M. In order to improve the knowledge of the behaviour of aerofoils under M<0.2 conditions, the University of Glasgow, in cooperation with QinetiQ, carried out two-dimensional aerodynamic tests on a RAE9645 aerofoil in 2002. By the end of November, of the same year, high quality unsteady pressure measurements from dynamic-stall tests were available. The tests were conducted on two different RAE9645 aerofoil models in two different wind tunnels. The first of these data came from the aerofoil that was tested in the Department of Aerospace's Handley Page Wind Tunnel. The second data set was from tests carried out by QinetiQ on an aerofoil in the Department of Aerospace's Argyll Wind Tunnel. The objectives of this investigation are divided in three main topics. First part considers the analysis of the data. This means (a) the assessment of the aerodynamic coefficients and consequent analysis of the various features of the dynamic-stall including the critical angle, the pitching moment and stall onset. (b) A comparison of the overall aerodynamic coefficients and (c) the carry out of final analysis of the most important quantities such as Cp deviation, vortex development and convection speed and re-establishment of fully attached flow. The assessment of the all same quantities for the second aerofoil tested by QinetiQ and the comparison of them

with the first model are the objectives of the second part of the project. Hence a most useful comparison of two data sets from two different wind tunnels will be achieved.

The third part was to establish the coefficients for the Beddoes third generation dynamic-stall model for the clean aerofoil without any flow control, using both aerofoil data. The Beddoes third generation dynamic-stall model is the last version of a model which has been in constant development over thirty years and is known as the most popular semi empirical method for assessing unsteady airloads such as lift, drag and pitching moment. This applies both to helicopters and wind turbines. The simplicity and undergoing philosophy of this method is its strength, especially compared with the current solution of Navier-Stokes or Euler equations. At the completion of this work, all the coefficients and information necessary for running the Beddoes simulating dynamic-stall model were obtained for the RAE9645 aerofoil. At the same time refinements, improvements and new guide lines were pursued in order to make the model easier and more powerful than before. Some of these changes are associated only to low Mach numbers.

It has been concluded that the Beddoes' model has been enhanced to better re-construct the RAE9645 aerofoils data of low Mach numbers.

Nomenclature

A	Calibration constant specific to a pressure transducer channel
A_q	Raw data count value
Alf_0	Angle of attack for zero lift (deg)
AR	Aspect Ratio
B	Calibration constant specific to a pressure transducer channel
c	Aerofoil chord (m)
Cm	Moment coefficient
Cm_0	Cm at α_0
Cn	Normal coefficient
C_{N1} .	Critical normal force for Beddoes' model
C_p	Pressure coefficient ($C_P = \left(\frac{p - p_\infty}{\frac{1}{2}\rho U_\infty^2} \right)$)
Ct	Thrust coefficient
D_1	Regressive coefficient by least square method, a constant for specified aerofoil
dCn/dα	Curve slope for the linear part of Cn line (1/deg)
f	Function developed by Beddoes for the separation point
f_b	Coefficients for Cm fitting
Fi	Calibration constant specific to a pressure transducer channel
Fo	Calibration constant specific to a pressure transducer channel
G	Channel gain in dB.
k	Calibration coefficient

K_1, K_2, K_3	Coefficients for Cm fitting
k	Reduced frequency (ωc/(2V))
M	Mach number
m	Coefficients for Cm fitting
n	Coefficients for Cm fitting
P	Static pressure on aerofoil surface (Pa)
p_q	Scaling factor of 1/16384
P_q	Calculated pressure for QinetiQ aerofoil (Pa)
p_s	Working section static pressure (Pa)
p_t	Tunnel settling chamber static pressure (Pa)
p_∞	Freestream static pressure and (upstream of the model) (Pa)
r	Reduced pitch rate (r=$\dot{\alpha}$ c/(2V))
Re	Reynolds number
s'	Mach number scaled non-dimensional time
S_1, S_2	Parameters for Beddoes' *f* function
t	Time (s)
T_α	New model time delay for dynamic-stall onset
T_b	Niven's modification to Beddoes' time delay
T_f	Boundary layer separation delay
T_p	Beddoes' time delay
T_r	New model time delay for re-attachment process
T_v	Non-dimensional period of the initial vortex formation
T_{vl}	Non-dimensional period for the shedding frequency
U_∞, U	Freestream velocity (upstream of the model (m/s))

V	Speed of the incoming flow (m/s)
Va	Voltage obtained from 1 from the pressure reading (V)
Vb	Voltage obtained from 1 for the temperature reading (V)
V_q	Calculated voltage (V)

Greek Symbols

α	Angle of attack (deg)
$\dot{\alpha}$	Pitch rate (rad/s)
α_a	Amplitude of aerofoil oscillation (deg)
$\alpha_{Cn\min 0}$	Incidence at the end of the convective phase (deg)
α_{ds}	Incidence of dynamic-stall onset (deg)
α_{ds0}	Critical incidence of dynamic-stall onset (deg)
α_m	Mean angle of attack (deg)
$\alpha_{\min}$	Incidence of the minimum Cn values (deg)
$\alpha_{\min 0}$	Incidence of the linear fit when it cuts the Y axis (deg)
α_1	Angle of attack for $f=0.6$ (deg)
τ	non-dimensional time after $C'_N = C_{N1}$
ω	Rotational frequency (rad/s)

Abbreviations

DS	Dynamic stall
DSV	Dynamic-stall vortex
g	Glasgow data
q	QinetiQ data

1 Introduction

Dynamic-stall is an aerodynamic phenomenon of crucial importance for many engineering applications: among these, are helicopter rotors, fighters undergoing rapid manoeuvres and wind turbine blades due to gusts and yawed flow. In the presence of this phenomenon, a dramatic increase in the aerodynamic forces is applied on the structure (2-3 times greater than the static conditions). These have consequent risks of exceeding the limits that may result severe fatigue loading, and strong unsteadiness of the flow.

1.1 Environment

The helicopter is the most practical solution thought of so far to an extremely difficult problem in aeronautics: that of combining the ability to hover economically in mid air with the ability to move through air at reasonable speed. The helicopter fascinated the human mind since very long ago [1], but its complexity delayed the first flight of rotary wings machine up to the twentieth century, and well after the first flight of a fixed wing aircraft. Unfortunately, the helicopter, as it exists, it is not without its compromises and inherent problems. They are, for the conventional type, very difficult to fly and are generally regarded as being too noisy, too slow and excessively prone to vibration. Much effort has been devoted to understanding the aerodynamic and dynamic behaviour of the helicopter with a view to reducing its noise and vibration, and improving its handling qualities and safety. The inherent complexity of the helicopter poses a distinct

impediment to its successful modeling and thus understanding, yet some significant advances have been made in recent times because the advent of very powerful computers and advanced numerical techniques.

The unsteady aerodynamics, however, which every blade of the rotor undergoes and the interaction between them, still presents a difficult challenge to the fluid dynamics researcher. The consequences of the unsteadiness in rotor aerodynamics are evident in every aspect of the rotorcraft technology. A major portion of the helicopter flight boundary is determined by excessive control loads. These arise from a form of stall flutter on the retreating blade which involves the interaction of unsteady separation phenomena with the blade torsion degree of freedom. The dynamic effects on aerofoil stall are of sufficient magnitude to influence the choice of both section geometry and structural dynamic characteristics of the rotor blade.

Moreover the diversity in the necessities, depending on the particular environment the blade will operate, lead the designer to seek a compromise between often conflicting requirements.

The complexity of unsteady aerodynamics on a rotor blade is such that it took long time to have an overall general understanding of the process it undergoes. In fact, it is true that in the early stages of rotor blade development programmes, such as Davenport and Front [2], as Dadone [3] indicated, the steady-state lift, drag and moment characteristics were used as aerofoil optimization criteria. This was due to the fact that, in the Nineteen-sixties, very little was known about the impact of the unsteady rotor environment on these forces. Again in the Sixties [4] it was eventually observed that, in forward flight, the flight envelope shaped by the rotor stall was more favorable than that predicted on the basis of static two-dimensional data.

1.2 Dynamic stall

It emerged that differences in aerofoil behaviours, resulting from unsteady aerodynamic environments, may have been the reason for those discrepancies. Early experimental studies emphasized that in high speed forward flight, the retreating blade stall of the rotor was a significant factor. The importance of these phenomena, to the understanding and analysis of blade aeroelastic problems, gave an additional reason for experimental and analytical studies on unsteady flows. As a consequence of this and the cyclic pitch of the rotor, measurements were normally carried out on aerofoils during sinusoidal pitching oscillations and of a severity characteristic of the retreating blade. One of the first investigations was by Krama [5] who observed that the boundary layer remained attached at much higher incidences, than the static stall angle, when an aerofoil was pitched at a sufficiently high rate. The net effect of this, he noted, was increased lift. Years later another effort, directed exclusively toward unsteady aerodynamic problems of blade aerofoil sections, was carried on by Liiva et al. [6]. The outcome of this investigation and of many following oscillatory tests (i.e. Ham[7], McCroskey and Fisher [8]), was the general observation of a peculiar aerodynamic behaviour which became known as “dynamic stall”.

Dynamic stall is the name given to the stalling of an aerofoil whilst subjected to significant temporal incidence variation and which exceeds through the static stall angle. Most fixed wing aerodynamics used in aeroplane design need not to consider dynamic stall, since, the range of incidence encountered is below the static stall angle and, secondly, the rate of any incidence change is slow (less than ~23 deg/s, exception made

for a gust loading). However, the branch of aerodynamics that deals with helicopter environment is intrinsically linked to understanding and modelling the dynamic-stall phenomena. This is because helicopters use cyclic pitch to overcome the difference in velocity (dynamic pressure) between the retreating and the advancing blade during forward flight. Moreover, the faster the forward flight is, the more cyclic pitch is required to trim the rotor. This eventually may lead to the dynamic stall on the retreating blade.

Today the phenomena of the dynamic stall on aerofoils in unsteady flow environments has been studied for many years. Over the last thirty years it has been established that the predominant feature of the dynamic stall is the shedding of a strong vortex from the leading-edge region. This vortex passes over the upper surface of the aerofoil, distorting the chordwise pressure distribution and producing transient forces and moments that are fundamentally different from their static stall counterparts. This behaviour is a direct consequence of the aerofoil being pitched through the static stall incidence. If the reduced frequency ($k=\omega c/(2V)$), amplitude and maximum incidence are sufficiently high, the vortex shedding is well defined and this limiting case is designated as “deep dynamic stall”. The physical process of events characterizing the dynamic stall are well noted [9], explained and illustrated in Figure 1.

These complex series of events may result in the dynamic delay of stall, to angles significantly larger than the static stall angle and dependent on the ambient environments, such as the reduced pitch rate for ramp-up or ramp-down experiments, or the reduced frequency for oscillatory aerofoils. As a result, a large overshoot of lift and a large amplitude nose-down pitching moment may be induced. Wilby reasoned that it would be beneficial to helicopter rotor performance if no break in pitching moment was

involved (i.e., prior to onset of dynamic vortex). As for the large nose-down pitching moment, it may exceed the structural fatigue limits of the pitch link mechanism and result in the failure of the structure, or cause the difficulties of control system due to the large amplitude and the possible negative pitch-damping.

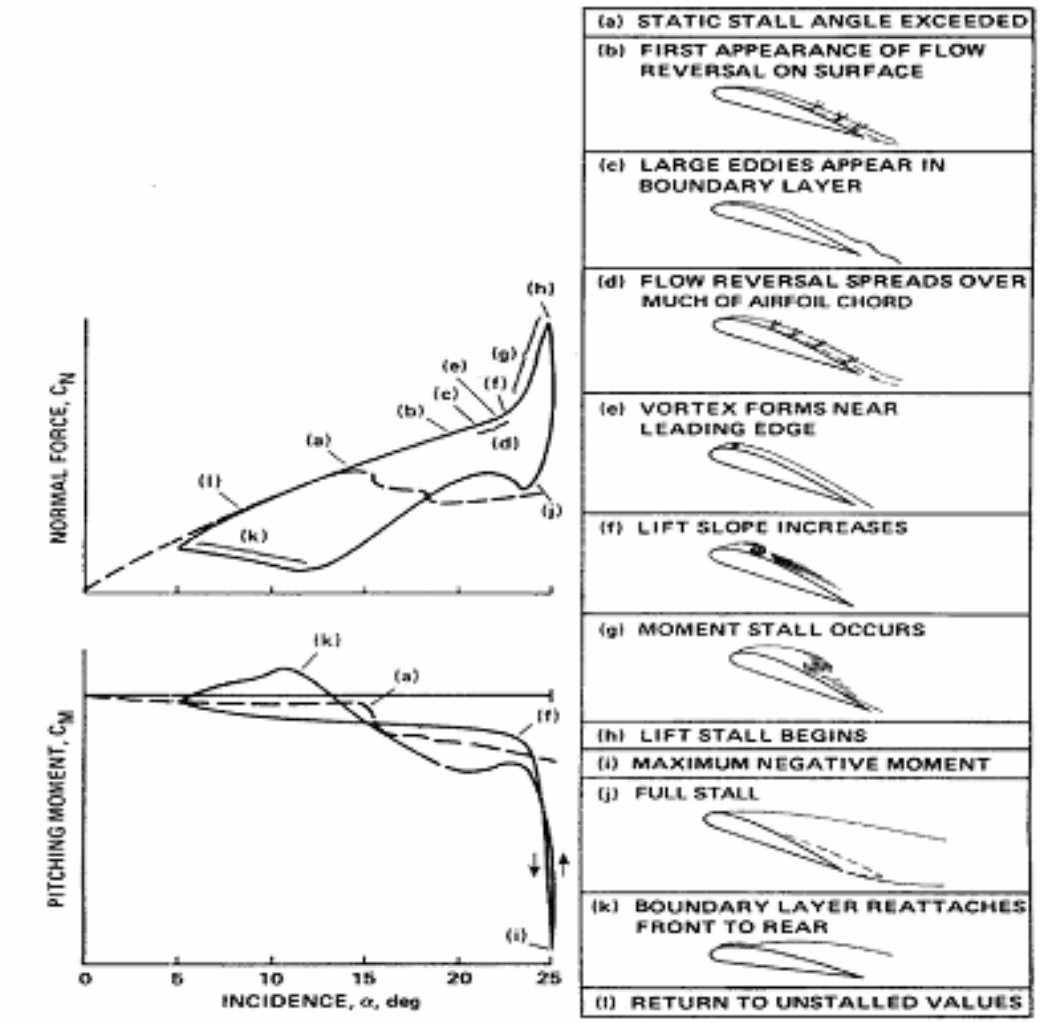

Figure 1 Events of dynamic-stall process as presented by Carr et al. [9]

Carr et al. [9, 10] gives an illustration for the events of a dynamic-stall process, shown in Figure 1. Chronologically, the dynamic-stall events actually start at point (a), where the pitching aerofoil passes the static-stall angle of attack, but without any discernible

change in the flow around the airfoil, and the flow remains fully attached. Then the flow reverses near the surface at the trailing edge region starting at point (b), but still no massive separation occurs due to the dynamic effects. This reversal moves up until the reversed flow covers much of the aerofoil chord. During the stages (c) and (d), the viscous flow no longer remains thin and attached, and a strong vortical flow develops at the leading edge region at point (e). The vortex enlarges, and traverses downstream, and finally detaches from the trailing edge, inducing a possible strong increase in lift and a strong nose-down pitching moment at points (f) and (i). After that, the flow over aerofoil upper surface is fully separated; the lift break (lift stall) occurs (j). When the angle of attack decreases continuously, the re-attachment process takes place. According to Niven et al. [11, 12], and subsequently Green et al. [13, 14], at some angle of attack (close to the static case), the leading edge re-attachment occurs, and then the process of re-establishing fully attached flow begins. Over about a three-chord distance, the very disturbed flow is convected over the entire aerofoil upper surface, away into the free stream and the lift reaches the lowest value. Depending on the reduced pitch rate the boundary layer development follows this process and so the flow proceeds to the fully attached state at the end of stage (k). The whole process of lift forms a substantial hysteresis loop [10].

It is understood that, consideration of dynamic-stall in the rotor design will more accurately define the operational and performance boundaries.

The early experimental works led to the 1970's classification of dynamic stall (Ham[15], Fisher and McCroskey[8]). They pioneered the time history pressure measurement around an aerofoil undergoing cyclic pitch change in a two dimensional

velocity field. McCroskey et al. [16] generate four different stall types depending on their characteristics:

1) **Leading-edge stall**: bursting of the laminar separation bubble that precludes a turbulent re-attachment

2) **Abrupt trailing-edge stall**: a turbulent re-separation propagating upstream from behind the laminar separation bubble

3) **Trailing-edge stall**: layer of reverse flow moving upstream from the trailing edge

4) **Mixed stall**: a combination of (1) and (3) or a modified version of (2)

1.3 The Re-attachment Process

The re-attachment phase of the dynamic stall has been, and continues to be, one of the least understood phenomena in dynamic stall. It has received only limited consideration, although dynamic-stall models have included mathematical descriptions of it [17, 18, 19, 20] reaching vary degrees of success [21, 22, 23]. To ease the problem of non-linear motions, various studies [24, 25, 26, 27, 28] have been carried out. It is also perhaps the area in which the University of Glasgow has made the largest contribution to the understanding of the physical mechanism of low speed dynamic stall. Leishman and Beddoes [29] modelled the airloads in the separated region using eq. A2.30 (Appendix 2) and the heavily lagged separation point, f (eq. A2.33, Appendix 2). As such they did not describe the physical mechanism behind the re-attachment from the fully stalled

condition. From the University of Glasgow data, it was observed that, at high reduced negative pitch rates, the normal force could be negative at a positive incidence. The Beddoes model is unable to model this phenomenon and as such Niven et al. [11] developed an improved correlation for evaluating the initial phase of re-attachment. Niven et al. chose the 2.5% chord line as a re-attachment point close to the leading edge which appeared to be insensitive to the pitch rate. They also determined that the re-attachment incidence was very close to the fully stalled steady counterpart. A pitch rate independent time delay was determined after which full chord re-attachment occurred. Niven et al. determined that rise in Cp at the 2.5% chord line was quite independent of pitch rate, and indicated the start of the re-attachment process, and the Cn followed a prescribed gradient until the local minimum was achieved. Using these two timing points a non-dimensional time delay was determined. As can be seen in Figure 2, there is a significant amount of scatter associated with the use of this methodology. This is caused by the uncertainties in the Cp-rise location and in the location of Cn_{min}. As can be seen in Figure 3, however, the inclusion of this in the Beddoes' model produced a significant improvement to the reconstruction [11].

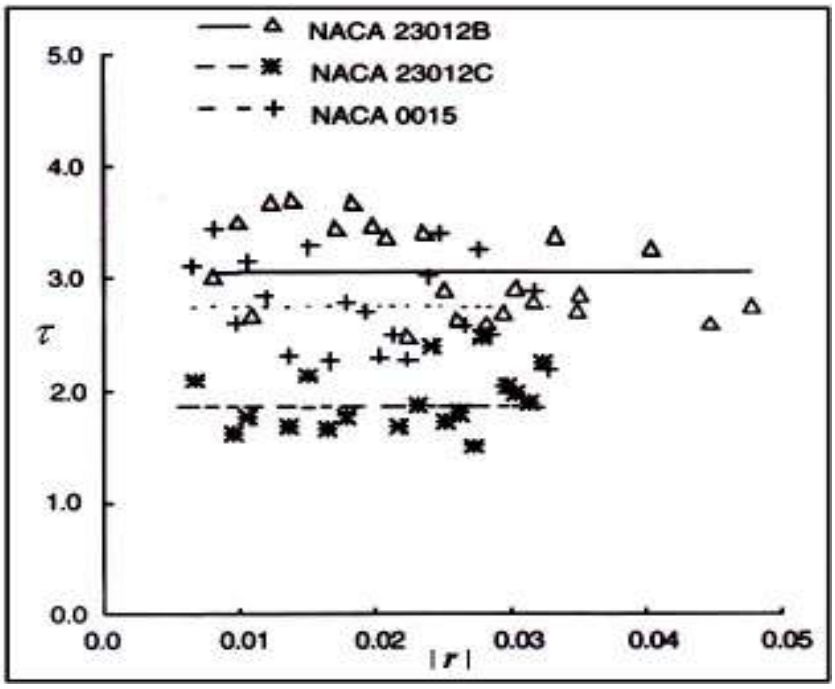

Figure 2 Non-dimensional time delay constant for re-attachment (Green and Galbraith [14])

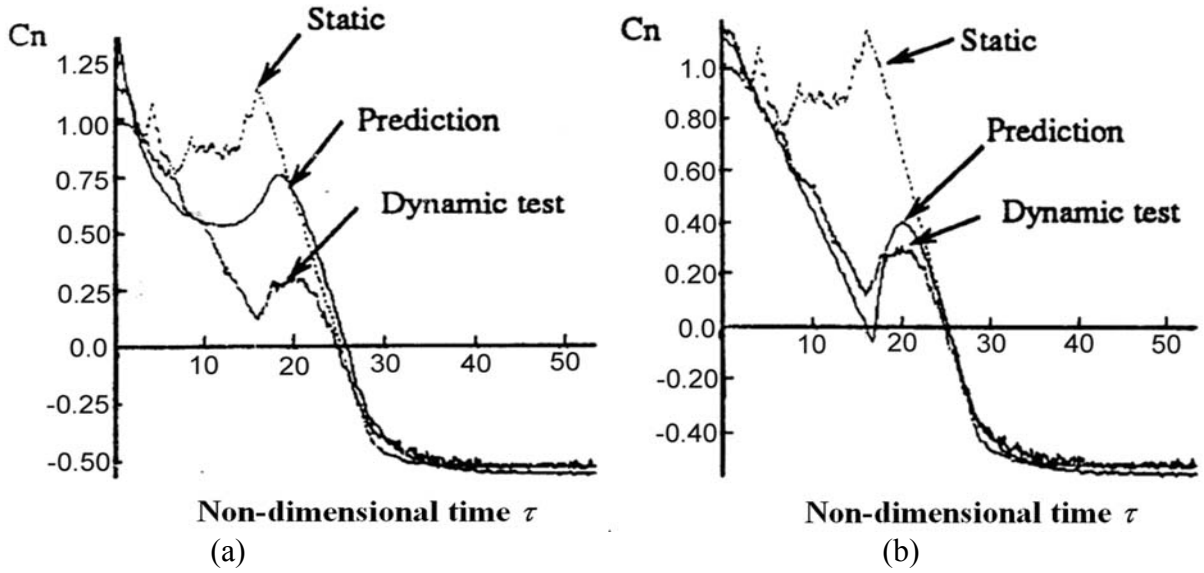

Figure 3 Beddoes' model (a) compared to Niven et al.'s re-attachment prediction (b) (from Niven et al. [11])

It was Green et al. [13] who finally managed to provide a physical reason behind the apparently anomalous data. They postulated that the re-attachment was not a single event, as observed by Kline et al. [30] for turbulent flow detachment. Instead, for the

data in the Glasgow data base, it occurred in two stages: one pitch rate independent; and the other strongly dependant on the pitch rate. The first stage in the re-attachment process was that the wake of stalled air which lies above the aerofoil is convected downstream at a rate independent of the pitch rate. Next, the full boundary layer re-establishment occurs which depends on the pitch rate. The manifestation of these phenomena are shown in Figure 4 and Figure 5.

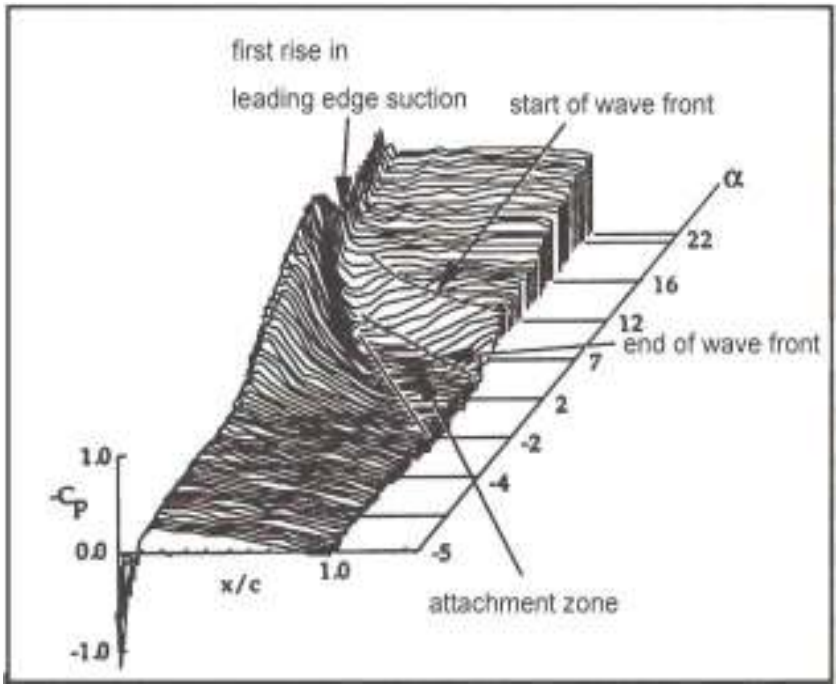

Figure 4 Chordwise pressure distribution ramp-down of NACA 23012B as function of incidence. r=-0.03 (from Green et al. [13])

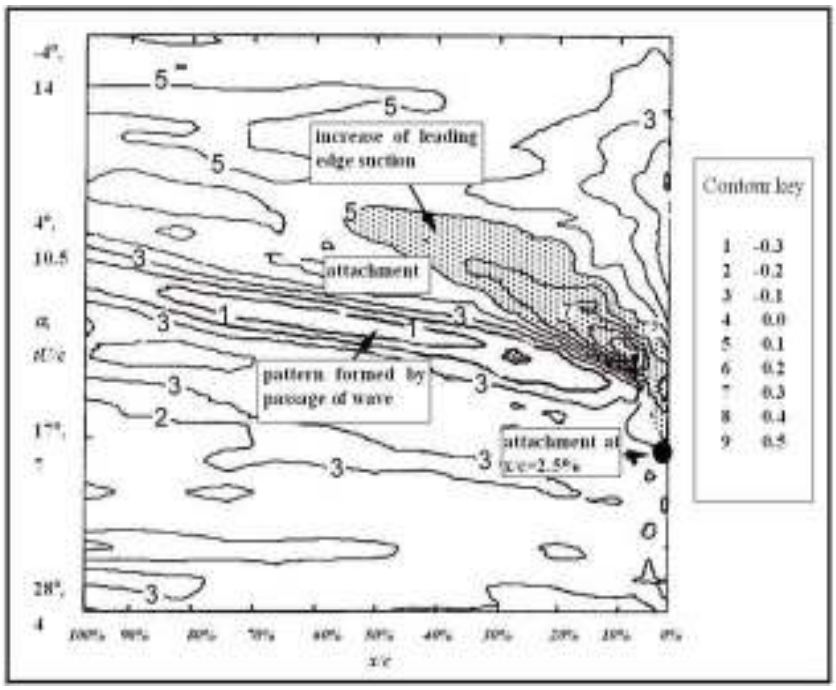

Figure 5 Time/Chordwise position contour plot of rate of change of pressure gradient. Same test parameters as Figure 4. (from Green et al.[13])

Figure 4, is a pseudo three-dimensional representation of the chordwise pressure distribution. Time increases from back to front (hence incidence decreases in the same direction). It can be clearly seen that the suction pressure (-Cp) begins its sharp rise at an incidence close to 16 deg. and a convective wave begins shortly after. The end of the convective phase is as indicated (end of wave front) and the attachment phase begins as indicated in the diagram. As Green et al. [13] stated, "the ramp down wave appears as a change in the rate of decrease suction and so is more clearly revealed if pressure data is differentiated with respect to time". Thus Figure 5 shows the contour plot of these rates. The time increases from bottom to top, hence the incidence decreases accordingly. The convective and attachment zones are easily seen and are identified in Figure 5. Further to this data analysis, a series of smoke-flow visualisations to qualitatively validate the two stage re-attachment theory were performed. These sets were carried out at a

different Reynolds number than in the wind tunnel tests and so a quantitative comparison could not be made. One ramp-down test is shown in Figure 6.

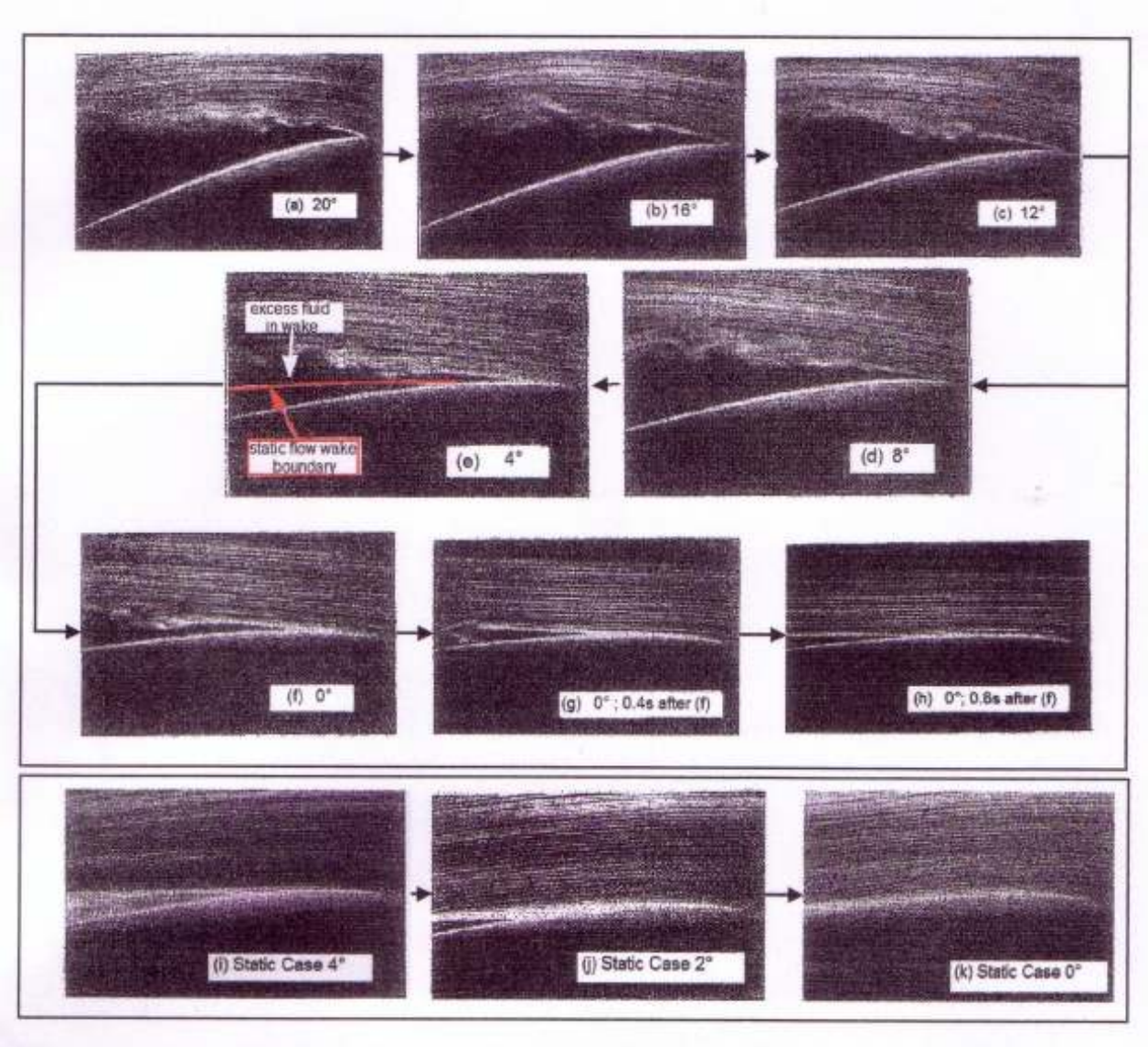

Figure 6 Smoke-flow visualisation test for NACA 0015 at r=-0.04 from 40 to 0 deg. (adapted from Green et al. [13])

Note that in Figure 6 only the first two thirds of the chord are shown and the series starts at α=20 deg because, above this angle, the flow pattern over the aerofoil is unchanged. It can be clearly seen that, as the incidence is reduced, the wake thickness is reduced. The

deflection upwards of the streamlines is visible in frame (c) and is due to the excess fluid in the wake. As Green et al. noted, if the amount of fluid together with the smoke line inclination are measured, then the wake convection may be described. The flow retains a significant amount of trailing edge separation right down to zero deg incidence, although re-attachment has occurred along the leading edge [31, 32, 33]. The static case, in comparison (frame (k)), at zero deg shows almost no separation. It is observed that, as the incidence fell, the excess wake and streamline inclination increased to a maximum at α=10 deg, and then reduced. Green et al. [14] then evaluated the time delay constant for the re-attachment process in the manner described by Niven et al. [11]. Sheng et al. [34] followed on from their new stall-onset criterion by improving the methodology to determine the non-dimensional time delay associated with re-attachment. As Niven et al. [11] had noted, the pitch rate did not affected significantly the incidence at which the maximum $|C_p|$-rise occurred at the 2.5% of the chord. As shown in Figure 7, the minimum normal force coefficient is linearly dependant on the reduced pitch rate.

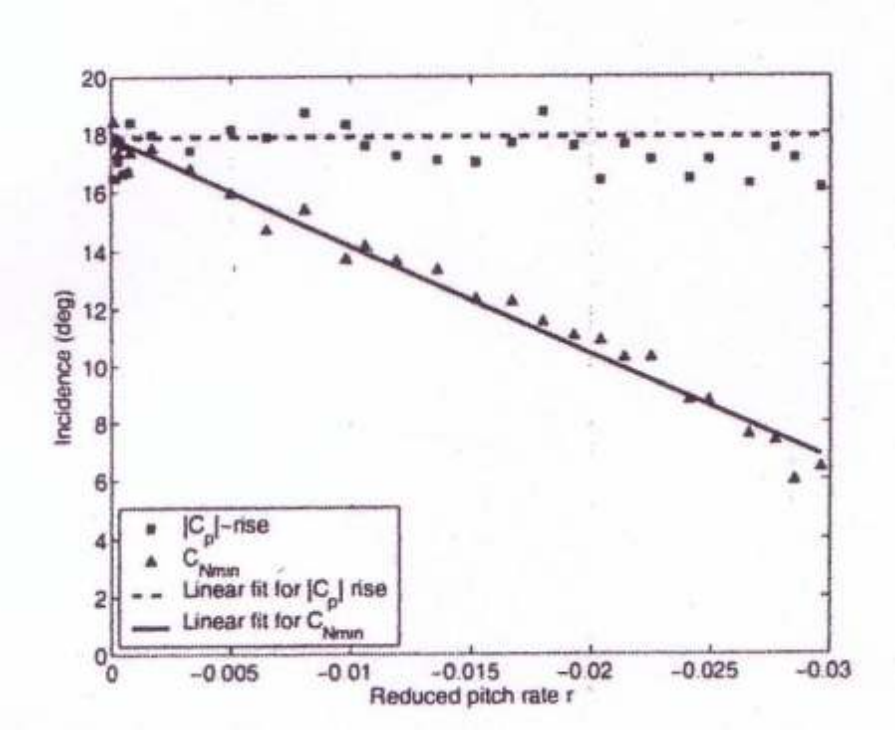

Figure 7 $|C_p|$-rise and Cn_{min} for NACA 0015 (taken from Sheng et al. [34])

Since the $|C_p|$-rise is, in effect, a horizontal line, only one linear fit is needed. The non-dimensional time constant may be found using only the linear fit applied to the Cn_{min} location (as shown in Paragraph 5.5). This methodology negates the requirement for assessing the location along the chord at which the $|C_p|$-rise occurs. The duration of the convective phase (T_r), the implied onset angle (α_{min0}) and the normal force gradient ($dCn/d\alpha$) can be easily obtained; these then provide the empirical contributions to Niven et al.'s [11] improvement to the Beddoes' Model.

1.4 Dynamic-stall models

Several approaches have been taken in the past to predict and analyze dynamic stall using various modeling techniques. Excellent reviews of the current predictive schemes

are given by Beddoes [35], McCroskey [36], Johnson [37], and Ericsson and Reding [38]. However, the computational models [39, 40] or reconstruction [41, 42, 43, 44] of such unsteady aerofoil behaviour, is both difficult and problematic.

The methods have been categorized by McCroskey [45] and Galbraith [46] into the following four types:

1) **Navier Stokes equations:** the solution of Navier-Stokes equations is fundamental to all fluid dynamic problems. However the solution is vague for the very viscous field surrounding an aerofoil during dynamic stall. The complexity of the time varying turbulent boundary layer makes it difficult to achieve a stable solution. Additionally, the computational power required to solve this, with a mesh of sufficiently granularity around an aerofoil to capture the dynamic-stall effects, would be large. Nevertheless, over the past four decades there have been substantial strides in the development of computational fluid dynamics (CFD) and there are many examples that show the success of CFD applications (Agarwal [47]). With the rapid advances of computers, in both speed and memory, new and more sophisticated computational methods have been developed, but the direct solution of the Navier-Stokes equations, with nothing to be modelled, is still far to come.

2) **Discrete Potential Vortex Method**: a potential flow is assumed over a region of flow which incorporates the boundary layer and wake. Discrete vortices are fed into this field to drive the correct computational agreement with the experimental data [48, 49, 50].

3) **Zonal Approach**: the basic premise of these models is to separate the flow field into viscous and inviscid regions which are artificially coupled by an iterative scheme [51].

4) **Empirical Models**: from the collected experimental data, a set of correlations are formed with a number of chosen parameters that are considered to influence the aerofoil behaviour (dynamic stall). These parameters are typically the aerofoil static characteristics along with parameters that describe the model motions. There have been many approaches to this kind of solution since it is the easiest to drive when a database of experimental data is available. Perhaps, the most reliable and popular method of this approach, is the one developed by Tom Beddoes [52] at Westland Helicopters and improved in subsequent versions with the help of Leishman [53]. This code has been published in various papers (among the others: [19, 29, 40]). The method has been coded by the author at the University of Glasgow and it is the one used in the present work to predict the aerofoil behaviour under different test conditions.

1.5 Present work

Experimental research into dynamic stall has been ongoing at the Department of Aerospace Engineering, at Glasgow University since 1980 under the leadership of R. A. McD. Galbraith. A dynamic-stall test facility has been developed in the departments Handley Page Wind Tunnel. The facility allows the recording of pressure time histories over an aerofoil chord whilst undergoing arbitrary motions. In fact, early investigations have shown the ability of constant pitch rate motion, such as ramp-up and ramp-down

[54, 55], to be beneficial to the understanding of the dynamic stall. In particular they have been used to investigate both vortex initiation mechanism (Niven [56]) and initial separation (Gracey [57]).

During 2002 the Department of Aerospace Engineering acquired a high quality unsteady pressure measurements from dynamic-stall tests on two RAE9645 aerofoil models tested in two different wind tunnels. The tests were conducted in low-speed unsteady-aerodynamic conditions in order to give an exhaustive view on the aerofoil behaviour in such conditions and to explore whether or not the Beddoes' model, mostly developed and used for higher Mach numbers, is still a powerful means for the re-construction such test data at low Mach numbers.

Accordingly, to investigate these aspects on the RAE9645, the present work aims and structure are the follows:

1) The two sets of data from the two different wind tunnels were processed to a uniform data format and then analyzed. All the behaviours for the three main aerodynamic coefficients, Cn, Cm and Ct, were presented for all the typologies of the tests performed (ramp-up, ramp-down and oscillating). The main aerodynamic characteristics of the profile, for each wind tunnel and each test typology, were discussed. Leading factors and major relationships were carried out from the tests in order to obtain common rules and laws which may governor the aerofoil behaviour in unsteady conditions for every different test set-up.

2) It is well known that different wind tunnels lead to different aerodynamic behaviours [58] even for the same aerofoil section. Due to the nature of the tests, a direct comparison was available between the facility in the Handley Page Wind tunnel and that

of the larger Argyll Wind Tunnel at the University of Glasgow. The two wind tunnels have different sections and set-ups. Considerations of the aerodynamic coefficients were made in order to asses the differences between the aerofoil characteristics. These may be influenced by the test facilities and set-ups.

3) The latest version of the Beddoes model (third generation [40]) was applied to the data in order to define all the coefficients and information necessary for tuning the re-constructive stall model. In particular, attention was focused on the parameters which define the dynamic-stall onset and on the re-attachment process from fully stalled condition. With all the parameters required by the model assessed, several simulations were run and are presented for several different test conditions: ramp-up, ramp-down and oscillating. The strengths and weaknesses of the 3rd generation Beddoes' model for low speed aerodynamics are highlighted.

4) With the additional understanding of the deep dynamic-stall onset and the subsequent re-attachment process, suitable modifications to the Beddoes' model have been made, for the RAE9645 aerofoil, via an updated stall-onset criterion and re-attachment modelling. These updated methods gave a better re-construction of these salient aspects of the aerofoil behaviour.

An in depth consideration is given to all the ramp-down tests, which are very important for the flow re-attachment reconstruction and often not considered in the literature. It is shown that the convective phase, not included in the Beddoes' model, plays a key role in the overall process and it must be taken in account for the appropriate reconstruction of

the process. The re-attachment criterion is very accurate and fulfills the task where the Beddoes' model shows its weakest area in low Mach number flows. It is concluded that the accuracy of the re-construction of the convective phase of the re-attachment process validates the existence of it.

Perhaps a very significant contribution to the field of study was the rescuing of the QinetiQ data from obscurity. As a consequence of the closure of their (QinetiQ) site, their experiments were their last and redundancy loomed for the researchers involved at Glasgow. Accordingly, when Glasgow received their data, all those involved were no longer available and, uncharacteristically, the data were not recorded in an easy decipherable way. It took one year to map their data onto a format compatible with the Glasgow data. The main difficulty was that there was no information about the QinetiQ data format and it turned out that the sequence of collection and storage was obscure. Such was this that several attempts, prior the present author, had been made, unsuccessfully, to rescue the data.

2 The data sets and their reduction

In order to improve the knowledge of the behaviour of aerofoils under low-speed unsteady-aerodynamic conditions, and in particular dynamic-stall (DS), the University of Glasgow, in cooperation with QinetiQ, carried out two-dimensional aerodynamic tests on a RAE9645 aerofoil during 2002. These tests were meant as an investigation into the DS of a specific low-speed aerofoil. The term "low speed" is used to indicate free stream velocity at low Mach numbers and, for the current work, not more than M=0.2. The wind tunnel tests produced high quality unsteady-pressure measurements from RAE9645 aerofoil models in two different wind tunnels. The first of these data came from a model tested in the Department of Aerospace's Handley Page Wind Tunnel. The second data set was from tests, carried out by QinetiQ and Glasgow University, on an aerofoil model mounted in the Department of Aerospace's Argyll Wind Tunnel. The two different wind tunnels had different test set-ups, employed different data acquisition systems, different teams and, consequently, stored the measured data in two different formats. In order to have a clear and accessible common database for all data, the data from the QinetiQ tests, were re-formatted onto the Glasgow standard. Hence all the Glasgow software was available for the analysis. To achieve this, the first action was to reduce and transform the QinetiQ data to the Glasgow University's format. It should be noted, however, that the QinetiQ data, as received, were not in a readily decipherable form. The recovery took one year and thanks must go to all who helped and, in particular, Professor Coton and Galbraith. Once completed, both sets were analysed with the same computer codes to gain an

insight into the dynamic-stall characteristics of both the data sets and to compare and assess any obvious differences.

2.1 University of Glasgow data

The University of Glasgow test data were acquired from the Department of Aerospace's Handley Page Wind Tunnel. The tests were carried out for four different types of motion: static, oscillatory, constant pitch-rate ("ramp" in both positive and negative directions) and triangular wave motions. These tests were normally performed for the same Reynolds and Mach numbers. For the ramp tests, both the start and end angle of attack were fixed for all reduced pitch rates. The collected data were all reduced and presented in archived departmental reports [59, 60]. In these reports, the main characteristics of the aerofoil, such as normal force, thrust and pitching moment (Cn, Ct and Cm) were plotted against the angle of attack and in non-dimensional time. The upper surface pressure coefficients (Cp's) were plotted in isometric projection and all other relevant data provided.

2.1.1 Wind tunnel and test set up

The first series of tests were conducted on a RAE 9645 airfoil in University of Glasgow's Handley Page low-speed closed-return type wind tunnel, with a maximum airflow speed of 60m/s (Figure 8). The model was mounted vertically in its working section of width 2.13m and height 1.61m and large corner fillets. It was pivoted about

the quarter chord position on two tubular steel shafts connected to the main support via two self aligning bearings, with the weight being taken by a single thrust bearing on the top support beam. The dynamic and aerodynamic loadings from the aerofoil were reacted to the wind tunnel framework by two transversely mounted beams as shown in Figure 9.

The angular movement of the model was obtained using a linear hydraulic actuator and crank mechanism. The model was instrumented with 30 dynamic pressure transducers, positioned along the mid-span chordline, plus 10 positioned along the span. The transducers were of a vented gauge type with one side of the pressure-sensitive diaphragm open to the ambient pressure outside the wind tunnel. The aerofoil shape and the locations of the pressure transducers along the mid-span are shown in Figure 10 and listed in Table 1.

Output signals from the transducers were taken to a signal-conditioning unit with its own control board. On instruction from the computer, the control board automatically removed all offsets to below the A-D converter resolution and adjusted all gains as necessary. The gain adjustment was done, during a typical test, by the computer sampling the maximum and minimum of each transducer output and adjusting the gains to maximize the data acquisition resolution. The measurement system has a capability of measuring up to 200 channels with each A-D channel having a maximum sampling rate of 50kHz. Such a high sampling rate was required to capture the fine detail of the dynamic-stall process, especially at relatively high oscillatory frequencies and reduced pitch rates.

An angular displacement transducer, geared to the model's main spar, assessed the instantaneous angle of attack of the aerofoil. The signal voltage from the transducer was

fed into an amplifier/splitter to produce three signals for recording the aerofoil's angle of attack, for initiation of data sampling when a preset angle (voltage) was reached and for a feedback signal to the hydraulic actuator controller.

The following expression was used to calculate the surface pressure coefficients, C_P,

$$C_P = \left(\frac{p - p_\infty}{\frac{1}{2}\rho U_\infty^2} \right) = \frac{p - p_s}{K(p_t - p_s)} \qquad 2.1$$

A micro manometer measured the difference between the static pressure in the working section, 1.2m upstream of the leading edge, and the static pressure in the settling chamber. Calibrating the wind tunnel produced the following expression:

$$C_P = \frac{p - p_s}{1.1392(p_t - p_s)} \qquad 2.2$$

The single element RAE 9645 aerofoil section model had a chord, c, of 0.5m, a span, b, of 1.61m and a thickness of 0.06m (12% thick and 5% camber). The model had a solid aluminium spar with an outer epoxy glass fibre skin. Though not forming part of the current work, the model had an aluminium plenum chamber with a width of 40mm, height of 20mm, thickness of 2mm and the length approximating the span of the aerofoil model. The plenum was able to supply Air-jet vortex-generator (AJVG's) embedded flush with the model's surface. The plenum was unpressurized during all the work reported here; for completeness, Figure 11 contains a photograph of the model including the AJVG's.

All the procedures and equipment used has been detailed and reported in references [59, 60].

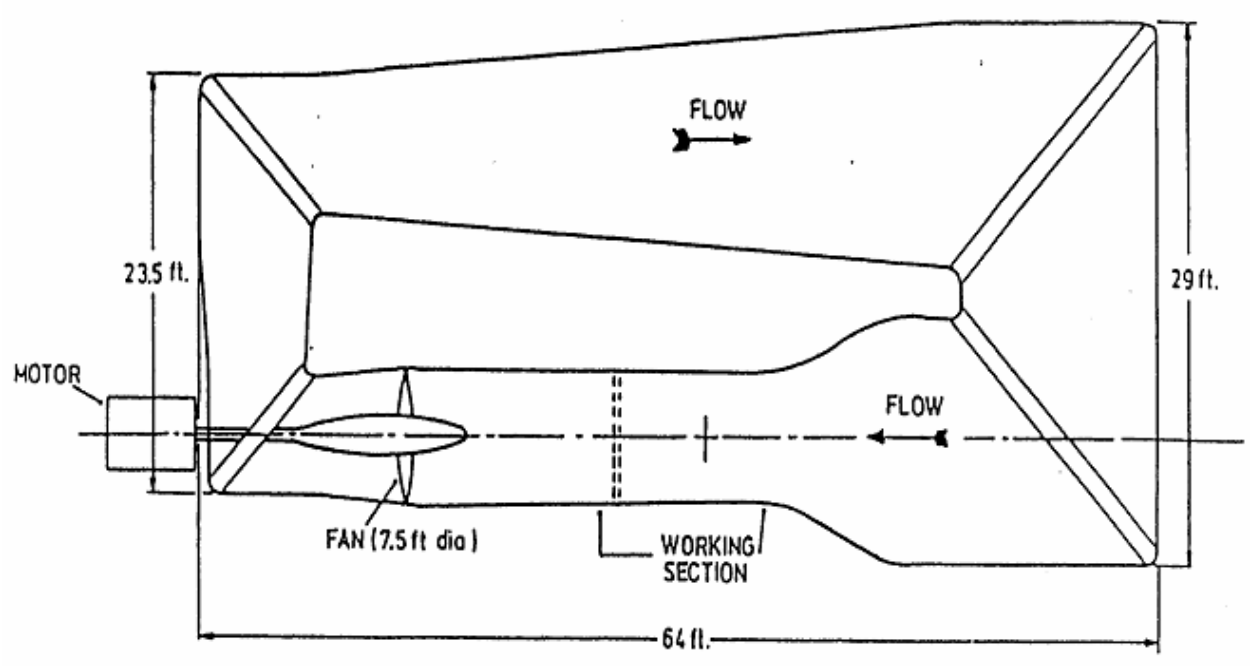

Figure 8 Plan view of the Glasgow University's "Handley Page" 7ft X 5ft 3in Wind Tunnel.

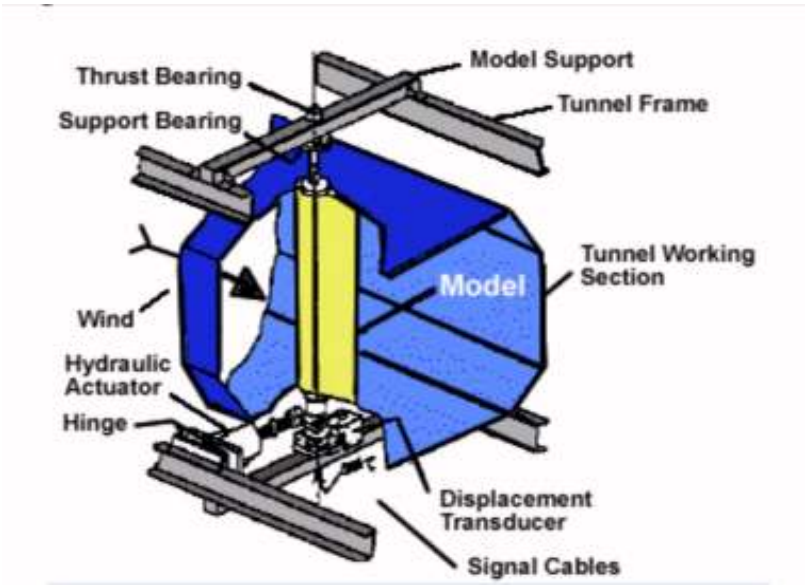

Figure 9 Glasgow University's dynamic-stall rig

Orifice	X (mm)	Y (mm)
1	485	2
2	450	9
3	410	17
4	370	24
5	330	28
6	290	33
7	250	37
8	210	40
9	170	41
10	135	42
11	100	41
12	70	37
13	50	34
14	38	30
15	25	25
16	13	18
17	5	11
18	2	6
19	1	5
20	0	0
21	1	-2
22	4	-5
23	10	-7
24	25	-10
25	50	-13
26	100	-16
27	200	-18
28	325	-14
29	400	-8
30	475	-2

Table 1 Transducer locations

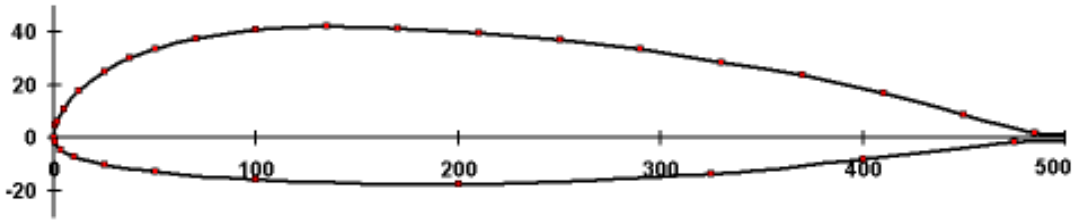

Figure 10 Chordwise profile of the RAE 9645 aerofoil section indicating pressure transducer locations

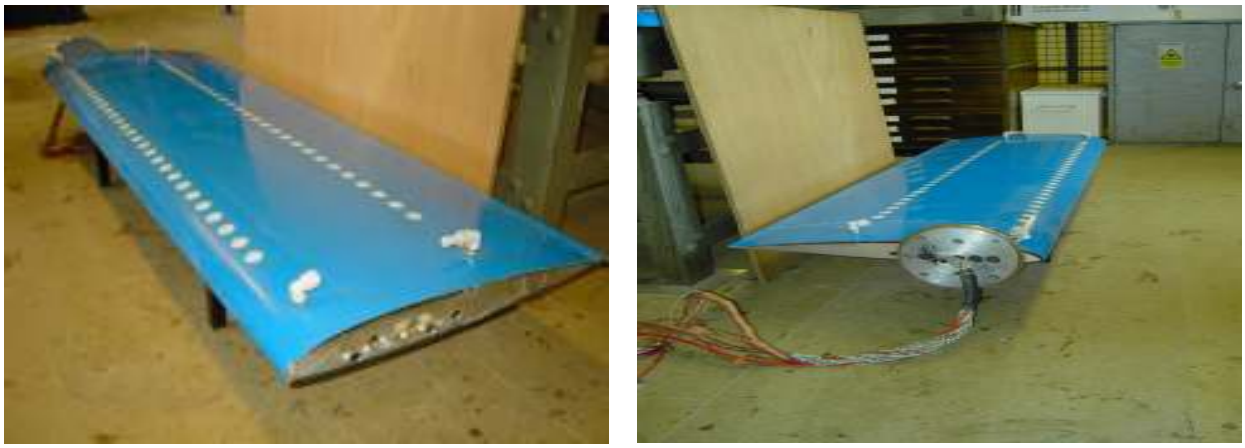

Figure 11 Photograph of the RAE 9645 with AJVG's

2.1.2 Tests

The test programme considered four types of motion: static, oscillatory, constant pitch-rate ("ramp" in both positive and negative directions) and triangular wave motions.

The test Reynolds number was ~$1.5 \cdot 10^6$ and the Mach number was ~0.13 based on the chord and freestream condition. The airflow speed was ~44m/s and the angles swept by the profile for the ramp tests were normally from 0 to 40 deg.

Static tests were conducted for an angle of attack range -5^0 to 26^0, in 1^0 increments, utilising 32 sampling blocks each collecting 1000 samples per angle of attack.

For a sinusoidal test the model was oscillated about its quarter chord with a sinusoidal pitching motion defined by:

$$\alpha = \alpha_m + \alpha_a \sin(\omega t) \qquad 2.3$$

The oscillatory tests were conducted over 4 continuous cycles with each cycle utilising one sampling block giving a total of 4 sampling blocks collecting 8000 samples per sampling block (or cycle).

The constant pitch rate tests (ramp up and down) and the triangular wave tests (ramp up-down) were conducted over 4 continuous cycles with each of the sampling blocks containing 8192 samples. The results over the 4 cycles were then averaged. The pitch rates performed in deg/s were: 2, 7, 20, 35, 79, 120, 160, 200, 240 and 280.

The pressure measurement test procedure involved running the wind tunnel up to the desired speed with the aerofoil angle of attack set at $\alpha = 0^0$. For the static tests, once a settled test flow field was established, the desired angle of attack was set and the measurements taken. Similarly for the constant pitch rate tests, the aerofoil was set at the desired starting angle of attack and pitched, either in the positive or negative direction.

The execution of the oscillatory, as well as the triangular wave, tests also necessitated a stable test flow to be established at the desired wind tunnel speed with the angle of attack set at $\alpha = 0^0$. After this, the mean angle of attack was set, i.e. $\alpha_m = 15^0$, and effective oscillation motion attained prior to the acquisition of pressure measurements.

In the present work all the wave tests were not investigated being of not of primary interest for a helicopter environment. The test data, here analyzed, is grouped for each motion type, with compact details of the specific tests given in Appendix 1 in Tables 1A to 3A. Surface pressure distributions and integrated force and moment coefficients are presented for a few cases. Data presentation of all the "Handley Page" tests are contained in references [59, 60].

2.1.3 Data and data reduction

The Glasgow's data presented here is the average of four cycles. Individual runs have been presented in other sources [59, 60], where it may be seen that, whilst minor random

differences do exist from cycle to cycle, the salient features were highlighted by the averaging process. The given data may be considered as typical of aerodynamic behaviour in a given individual cycle. This is particularly relevant when considering the detailed flow phenomena of separation and re-attachment.

For the University of Glasgow data, the pressure measurements were taken in sets of ~8000 steps during the whole test irrespective of the type of motion or the pitch rate. In each of these steps there were fifty-one measurements where the first forty were the pressure transducers placed on the upper and lower surfaces of the aerofoil and the last eleven channels carried different information including the angle of attack. As the analysis of the data was meant to be two-dimensional only the first thirty transducers along the mid-span section were used for the calculation of Ct, Cn and Cm. The last ten were positioned along the span of the blade and hence not suitable for this particular case. Moreover, one of the transducers (13th) was found to be faulty during the entire test set and it had to be replaced by a linear interpolation of the two values before and aft of it. All the files with the pressure measurements were archived with a "csXXXc.out" name (where XXX always was the number of the test) and start with a block of twenty-four numbers that are specific for each test. This set of values accounts for the main characteristics of the test such as temperature, static pressure, pitch rate, samples, date, type of test, flow speed, Reynolds number, Mach number and so on.

Only the twenty-nine measures, plus the angle of attack, were read by a specific program for calculating the coefficients for the Cn, Ct and Cm of the profile. In order to simplify and lighten further work with the files, the code only read one set of measures in every twenty. In this way, the files generated by the program reported only ~400 values for Cn, Cm and Ct, compared to the ~8000 of the particular data set. The data

were written in three columns along with the angle of attack at each step and archived with a name “9645clXXX”.

2.1.4 Formats and Results

2.1.4.1 Formats

All the files have been processed utilizing two different programmes to plot the main coefficients. The first graphs were created by a Matlab code. These graphs display only one coefficient at the time plotted against the angle of attack. The data then went through averaging process before being plotted. In fact, a number of ~400 values on an arc of 40 deg still gave a little scatter in representation. Averaging these data in groups of five to eight values brings to better readable graphs as show in Figure 12, Figure 13 and Figure 14. Also, the University of Glasgow developed a standard format used for the reports on the collected data on aerofoils. The data plotted in this standard University of Glasgow format present the aerofoil behaviours for the Cn, Ct, Cm against the angle of attack and the non-dimensional time, Ut/c. Moreover, a pseudo 3D graph highlights the Cp behaviour throughout the angles of attack and a time dependent angle of attack history was plotted. This way a complete overview on the whole aerofoil characteristics is given [59, 60]. The static characteristics were also plotted and reported. Figure 15 gives an example of this layout.

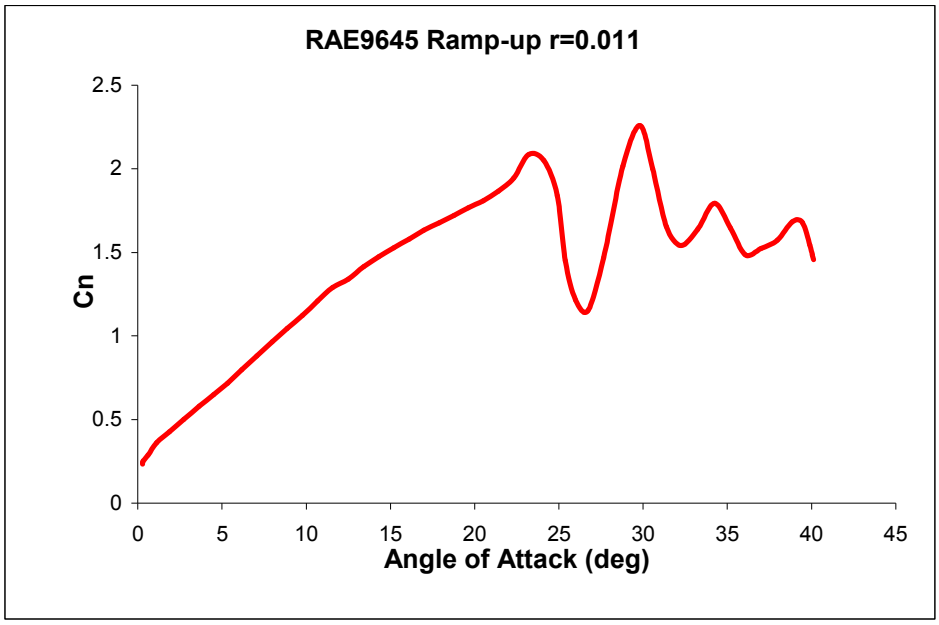

Figure 12 Standard Matlab format for Cn

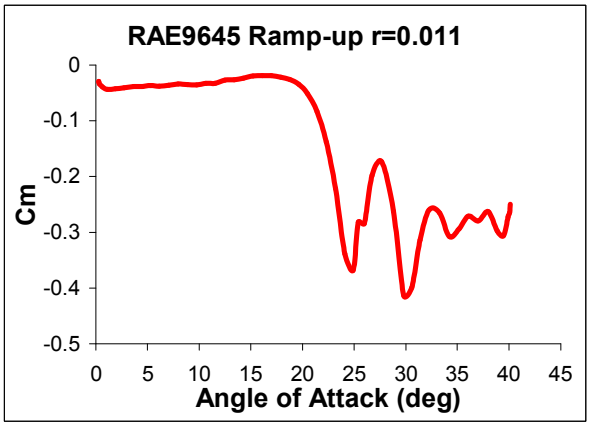

Figure 13 Standard Matlab format for Cm

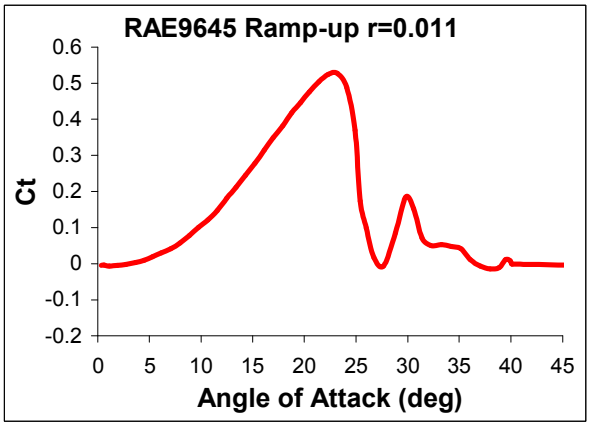

Figure 14 Standard Matlab format for Ct

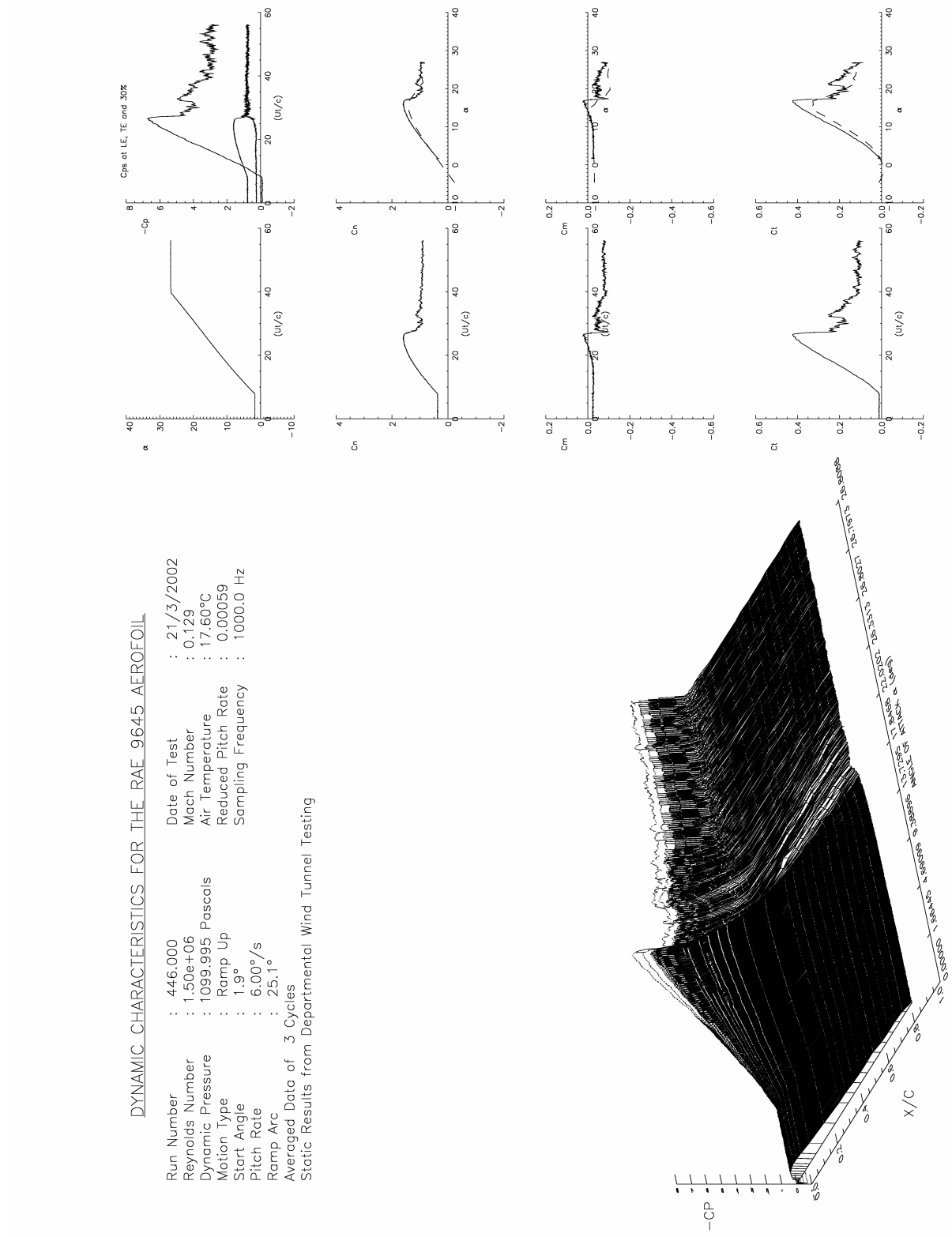

Figure 15 University of Glasgow format

2.1.4.2 Results

1) Static

The "static" data were important for defining the classical behaviour of the aerofoil; all other "unsteady data" were compared to them. Figure 16, Figure 17 and Figure 18 represent the behaviour of the RAE9645 profile under static conditions. The three main coefficients do not present any particular behaviour, even though, from Figure 16, the development of a trailing edge separation may be observed. When the angle of attack exceeds ~8 deg the Cn slope (about 0.096 per degree during the linear phase) begins to decrease until the profile stalls reaching a maximum Cn value of ~ 1.42 at ~15.6 deg. The Cm plot also indicates that, depending on the definition of stall, it occurs somewhere between an incidence of 15 to 16 deg. It can be also noticed in Figure 17 that the Cm is never equal to 0. This does not happen even during the linear behaviour of Cn. With the pitching moment axis at the quarter of the chord from the leading edge, this means that the zero-moment axis is located more towards the trailing edge. When the angle increased from 0 to 26 deg, the centre of pressure moves up stream until the stall takes place and the detached flow pulls it back again with a minimum value of ~-0.105. The last Figure illustrates the Ct curve. The line presents the commonly observed trend of other airfoils and any particular characteristics can be notice.

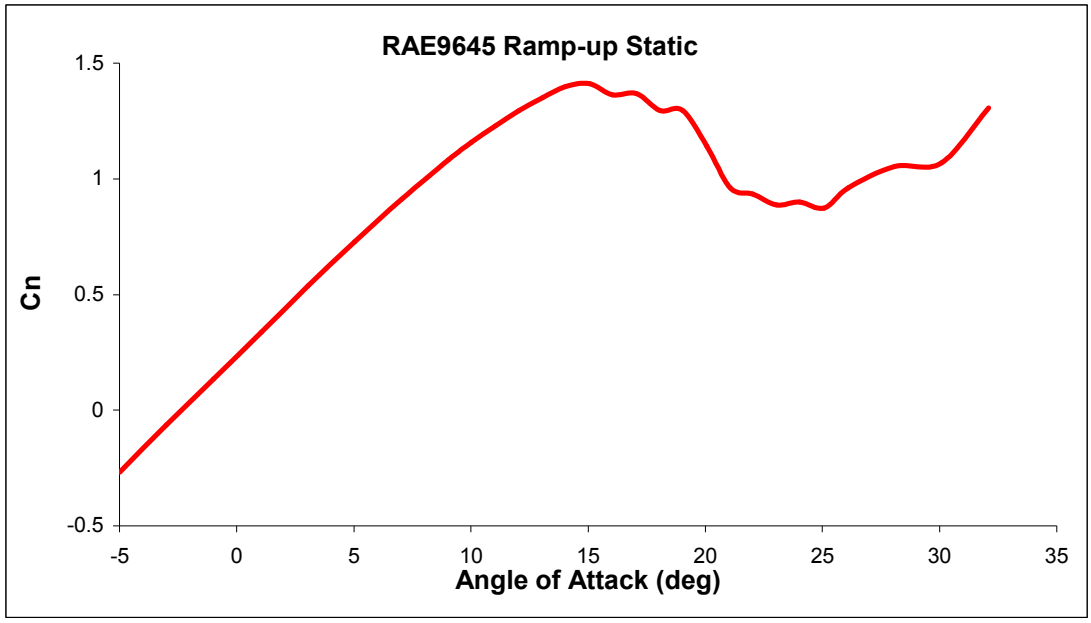

Figure 16 Cn static test

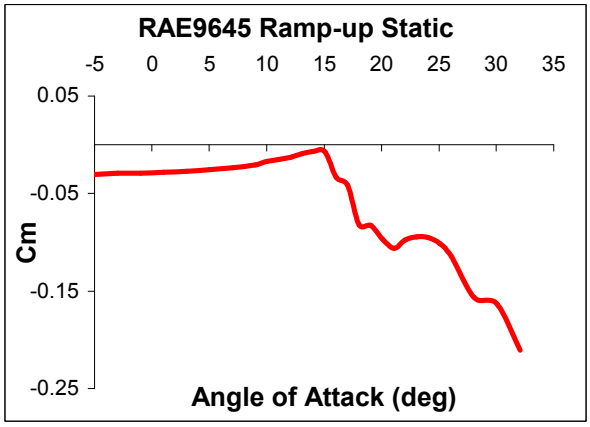

Figure 17 Cm static test

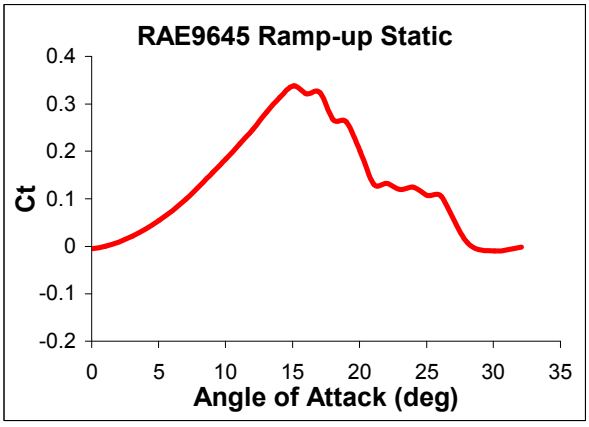

Figure 18 Ct static test

2) Ramp up

The ramp-up tests performed at the Handley Page wind tunnel follow the trend showed by the static case. In fact, what looks like a trailing edge separation, is more noticeable the slower the pitch rate, (can be clearly seen in Figure 19 and Figure 20). In dynamic cases the dynamic-stall vortex shedding usually hides this kind of separation, due to

reversed flow moving upstream. This is usually addressed to the time scale of the phenomenon. Trailing edge separation takes time to develop and to affect the global circulation of the profile. In this way, a significant non-steady condition, due to a high pitch rate, can compensate this loss by suppressing or, at least, delaying the process.

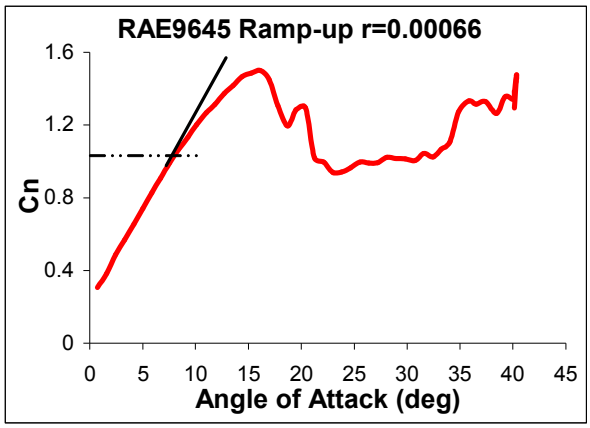

Figure 19 Trailing edge separation for a pitch rate of 7 deg/s (r=0.0006)

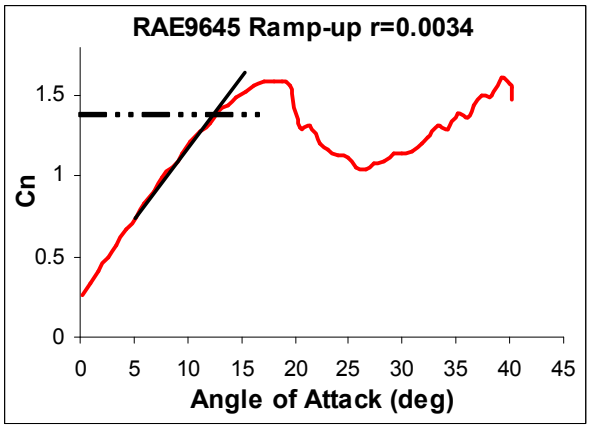

Figure 20 Trailing edge separation for a pitch rate of 35 deg/s (r=0.0034)

In Figure 21 is given an example of pressure distribution at low reduced pitch rates (r=0.0034, Figure 20). In fact what it was taken to be trailing edge separation in the Cn graph may be better observed considering the pressure data. In Figure 21 (a) the incidence is 10 deg and the pressure distribution does not present any evidence of trailing edge separation. The increased angle of attack of 12 deg (b) begins to show a light trailing edge separation towards the last two pressure taps. When the incidence reaches 15 deg(c), and the Cn slope begins to decrease significantly, the separation has moved upwards towards the last 25% of the chord. The separation point continues to move towards the leading edge and when the angle of attack is equal to 18 deg (d), and the lift coefficient is about to collapse (Figure 20), the stalled surface covers almost the 70% of the entire profile.

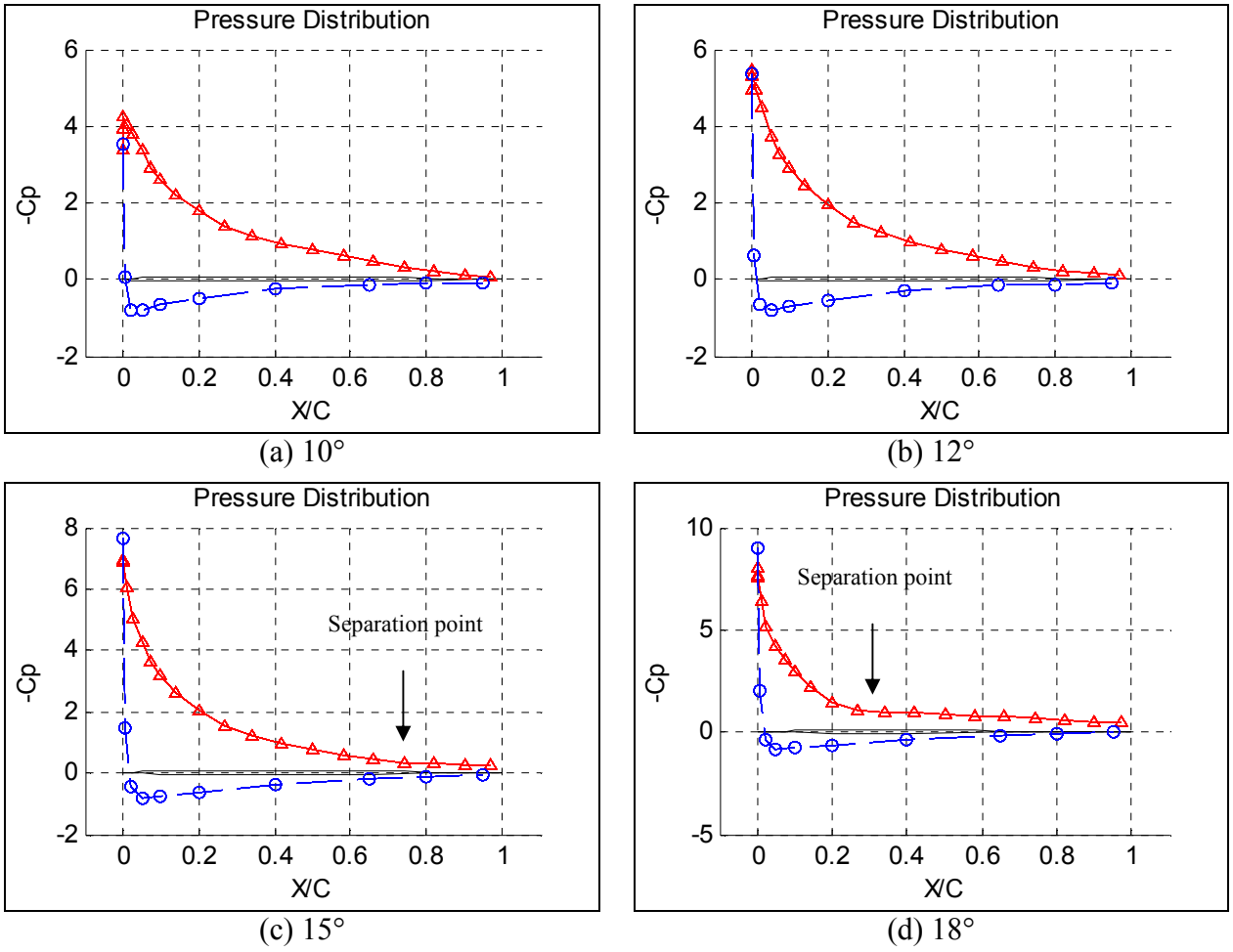

Figure 21 Chordwise pressure distribution for r=0.0034 and for angles of attack equal to 10(a), 12(b), 15(c) and 18(d) deg. ("Δ" upper surface, "o" lower surface)

However, for thicker and more cambered profile sections, which are more commonly used, trailing edge separation influences the behaviour of the aerofoil.

In these tests it is evident that, even for the highest pitch rates carried out in this wind tunnel, as shown in Figure 22, after an angle of attack of ~19 deg, the lift curve slope declines due to the trailing edge separation.

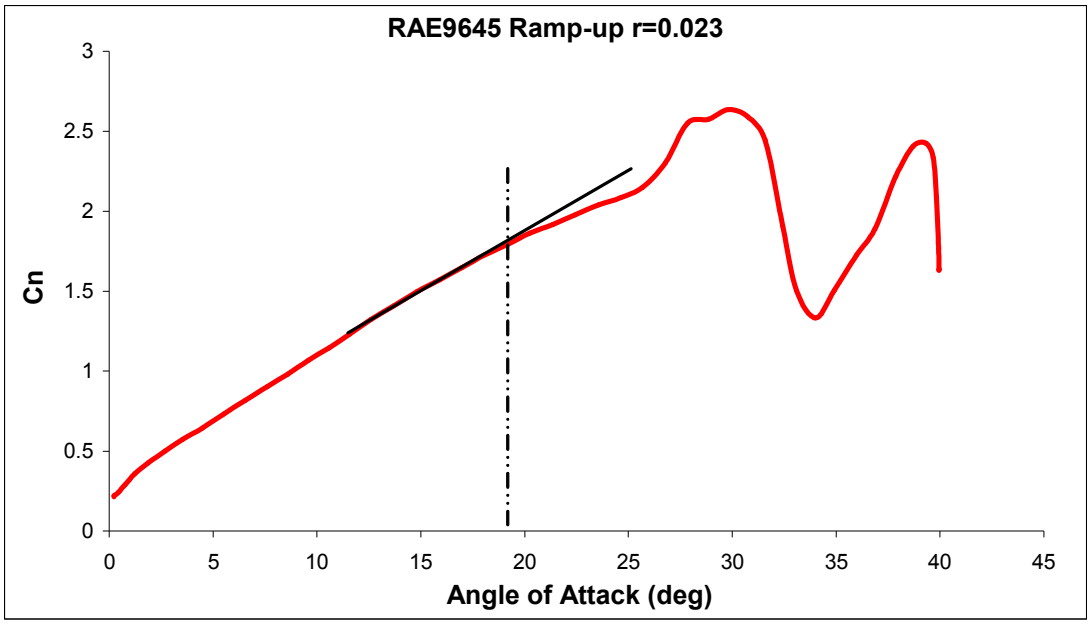

Figure 22 Trailing edge separation for higher pitch rates after 19 deg of incidence

The pressure data for r=0.023 throughout the incidences where the trailing edge separation, from Figure 22, looks to take place are reported in Figure 23. In this case the pressure distribution is quite regular for the first picture (16 deg, (a)), but starts to show a trailing edge separation from picture (b-c) which becomes more evident as the incidence increases. For the angles of attack equal to 23 deg (c) and 25 deg (d) the separation point seems to move upstream from a position of ~25% to ~35% of the chord. The last two pictures show the coexistence of the trailing edge separation with the onset of the dynamic stall vortex. It is clear from Figure 22 that around 26 deg the curve slope start to increase, in the same way picture (e) of Figure 23 (together with Figure 22) shows that the loss in lift due to the separated flow is compensated and overcome by an enhancement of the –Cp coefficient about the 20% of the chord. The last picture of the sequence (28 deg of incidence) shows a trailing edge separation almost unchanged, but with a more powerful vortex moving downstream over the aerofoil.

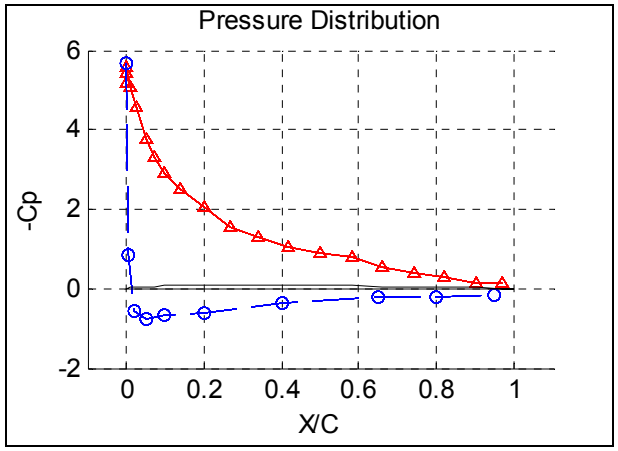

(a) 16°

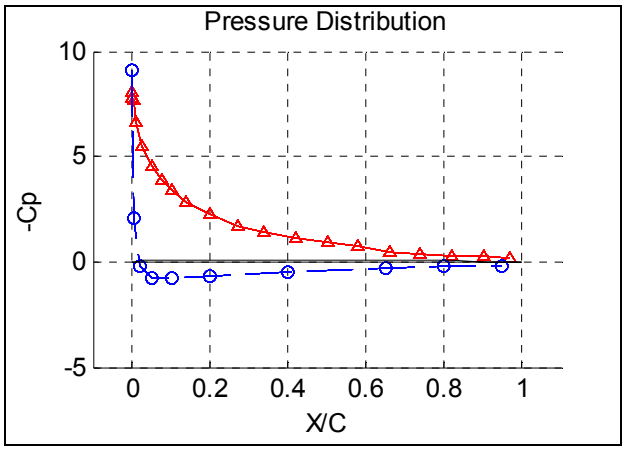

(b) 18°

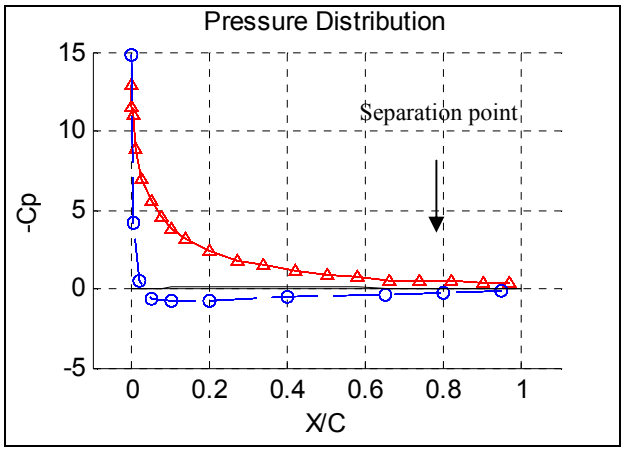

(c) 23°

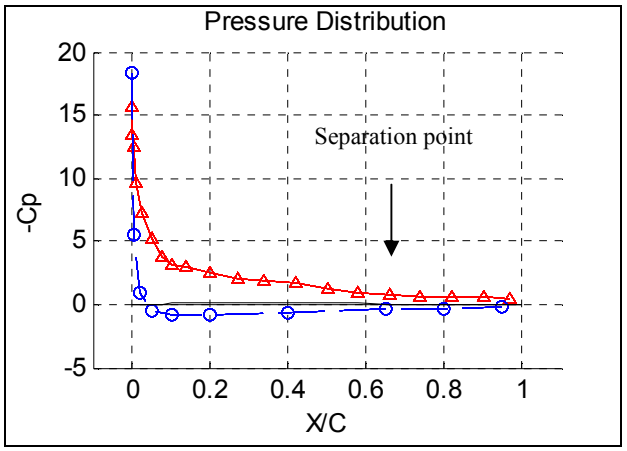

(d) 25°

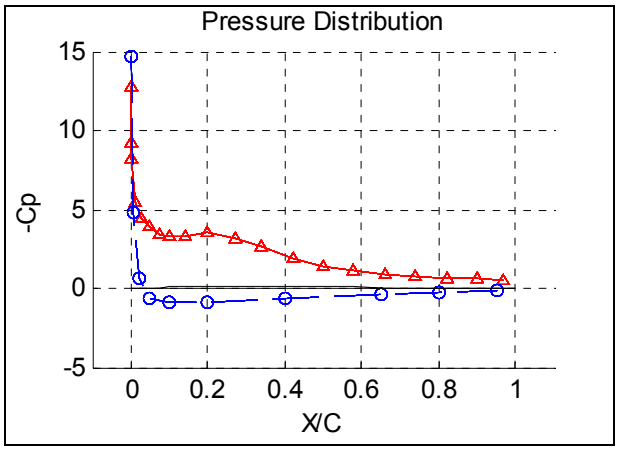

(e) 27°

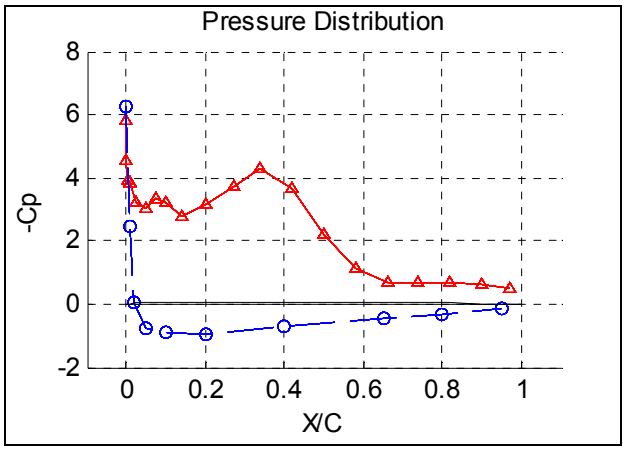

(f) 28°

Figure 23 Chordwise pressure distribution for r=0.023 and for angles of attack equal to 16(a), 18(b), 23(c), 25(d), 27(e) and 28(f) deg. ("Δ" upper surface, "o" lower surface)

It has to be kept in mind, however, that the faster the pitching motion the higher is the induced camber effect and, at the stall, the stronger is the dynamic-stall vortex, generated at the leading edge. The final result is always an interaction of all these aspects and it cannot easily be assessed which one of these effects will dominate, as shown by the comparison between Figure 22 and Figure 23. This behaviour has been already observed for other profiles and reported by others, e.g. J. G. Leishman and T. S. Beddoes [19].

Additionally, it is also well known [61] that the wind tunnel features can influence the aerofoil characteristics and that a given profile, tested in different facilities, can yield significantly different values of the coefficients [58]. The influence of this last aspect will be explored in detail in Chapter 3.

The comparison between the Cn ramp-up tests shows the typical behaviour of aerofoils under such conditions. As already mentioned, and well documented by other tests [29, 62], during dynamic motions at the same Mach number, the Cn curve displays significant lags in the aerodynamics and these become more severe with the increased pitch rates. This means that, for a given angle of attack the value of Cn will depend on the pitch rate. The unsteadiness of the flow causes delay in the lift force to build up. Hence, the lift curve slope decreases in value with the increasing angular speed. Figure 24 highlights this aspect by plotting only the first part of the Cn data. However, the appropriate parameter, in such comparisons, is the non-dimensional reduced pitch rate given by:

$$r = \dot{\alpha}\, c/(2V) \qquad 2.4$$

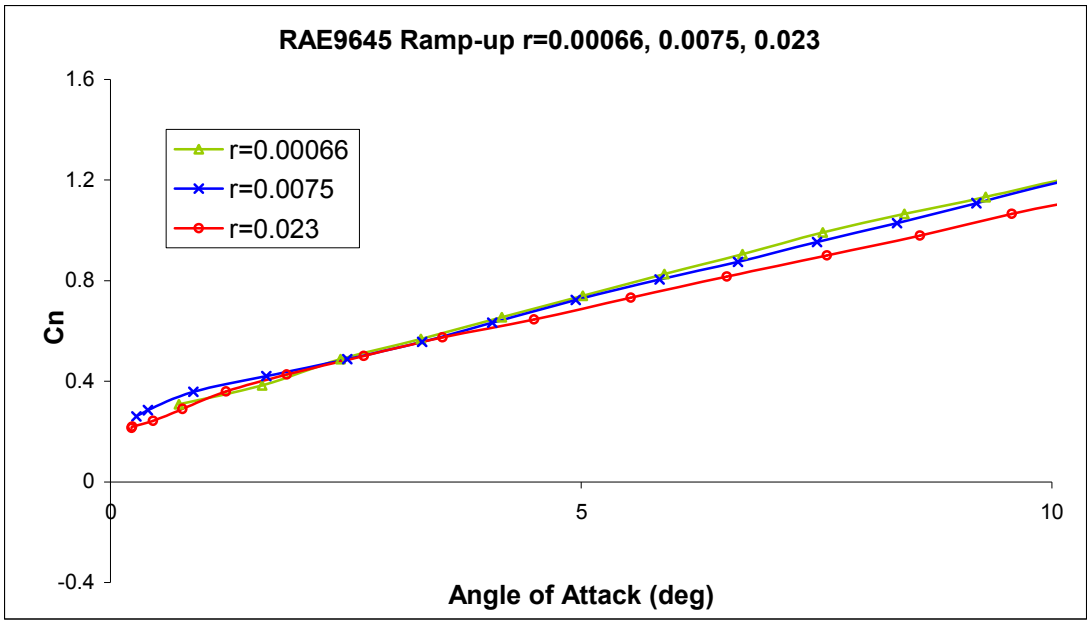

Figure 24 Cn decreasing tangent values with the pitch rate

Hence the greater the reduced pitch rate, the more the slope decreases. Also the reduced pitch rate will be fundamental to determine the division of the aerofoil dynamic behaviour between the "quasi-static" and the deep dynamic stall. Another peculiar aspect about the curve slope may be noted in Figure 25 where ramp-up tests are presented together with the static test (black line). As stated before, it has always been reported, [53, 63, 64] for the approximation of lift response and [65, 66, 67] for test data, that the dynamic motion decreases the lift curve slope and is dependent on the reduced pitch rate. For the RAE9645, tested in the Handley Page wind tunnel, this is true, but, at this Mach number, the lift curve slope may appear to be greater than the static value ($dCn/d\alpha \sim = 0.096$ deg^{-1}). For example in Figure 25 the Cn curve for 7 deg/s (r=0.00066), in fact, begins from the same values of the static one, but reaches higher values of normal coefficient for the same angles with a curve slope equal to ~0.097 deg^{-1}. Even at these low pitch rates it would appear that significant trailing edge separation suppression is occurring together with minimal circulation delay. The same behaviour applies to the

other pitch rates until they are above 79-120 deg/s (r=0.075-0.011). Above that pitch rate, all the tests stay underneath the steady state curve.

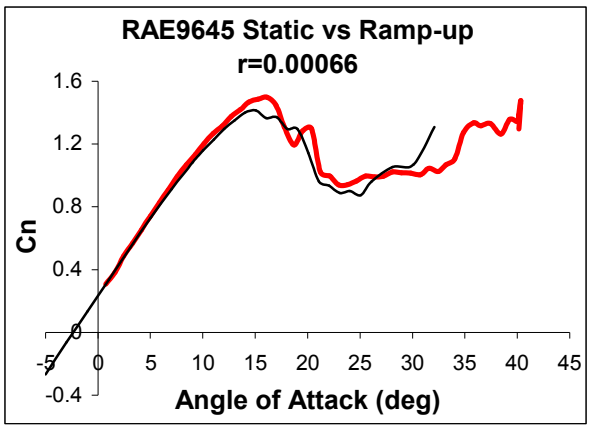

a) Cn for r=0.00066

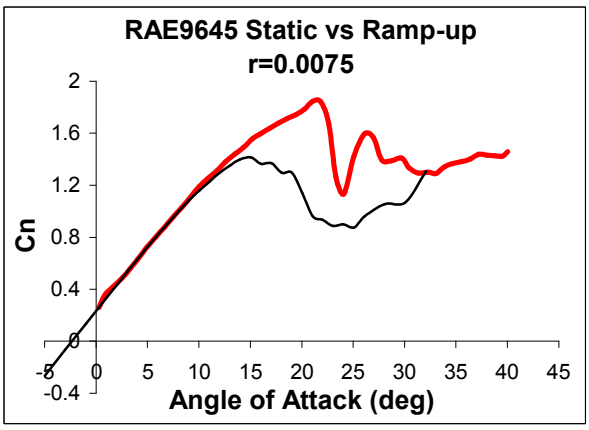

b) Cn for r=0.0075

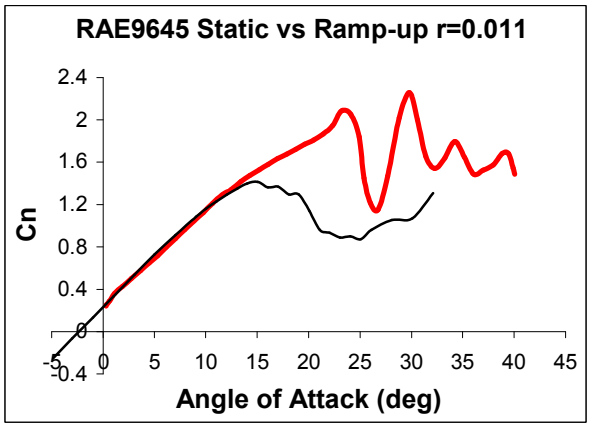

c) Cn for r=0.011

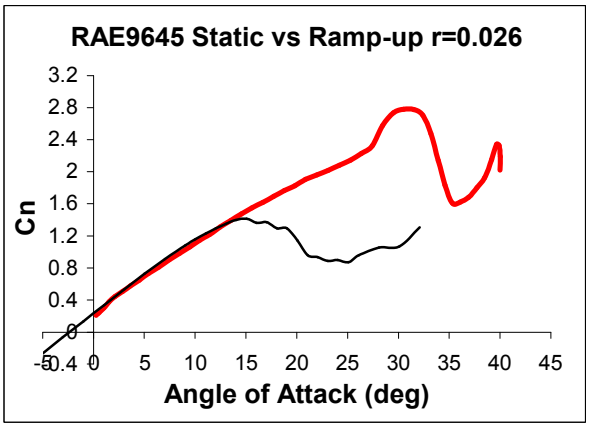

d) Cn for r=0.026

Figure 25 Different Cn slopes for different pitch rates (red line) compared to the static case (black line)

The second notable point is that the reduced pitch rate of 0.0075 and 0.011 are also the boundary of two different Cn curve shapes. The profile behaviour is the same as the static one until the pitch rate gets to 79 deg/s (r=0.0075). There is an increasing of the maximum Cn for every higher pitch rate, but there is no discernable change in the *Cn* - α curve slope before this reduced pitch rate. For reduced pitch rates below 0.0075, though modified, the lift curves have a similar form in as much as there is a well

rounded stalling indicative of the trailing edge or turbulent stall. At, and above this value of r, and more pronounced at higher values, e.g. 0.011 and 0.024 (Figure 25), the stall takes on the form of a deep dynamic stall by exhibiting the characteristic Cn curve associated with the development and convection of a dynamic-stall vortex over the upper surface (Figure 26). This has been noticed on all other aerofoils tested [68] and in general the deep dynamic-stall is visible for reduced pitch rates greater than r=0.01. At a lower reduced pitch rate, the pressure profile characteristics are qualitatively similar to those in steady conditions, but with some lift and moment "overshoot" (quasi-static/steady stall) [68]. However, other profiles had already shown an earlier transition between quasi-static and dynamic-stall. Accordingly, for instance the S809 aerofoil at a Reynolds and Mach numbers of $1.5 \cdot 10^6$ and 0.12 respectively, the division between quasi-static and dynamic stall is for r=0.005 [68].

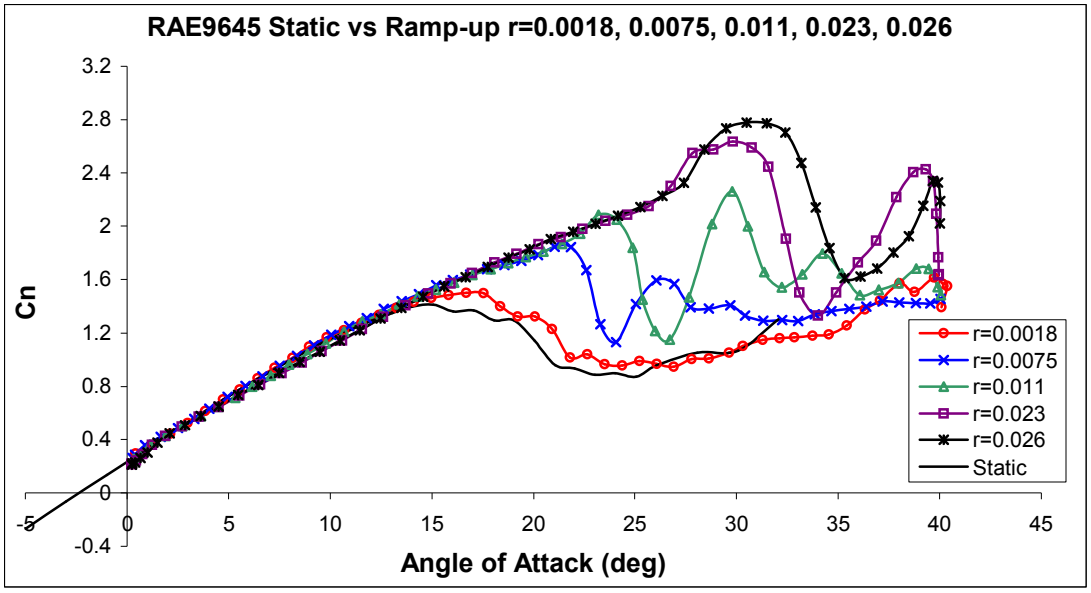

Figure 26 Differences between quasi-static and dynamic behaviour for the RAE9645

In the same way, Beddoes [69], noted that a different and deeper dynamic stall occurs only when the pitch rate exceeds some small positive value. According to Seto and

Galbraith [28] this value has to be searched for in the reduced frequencies domain and it was found to be 0.01.

Also for the RAE9645 the pitch rate of 79 deg/s is slightly below the r=0.01 and it is, in fact, the first where the deep dynamic-stall may be seen. In Figure 26, considering the Cn curves for the two highest values of r, all these noted features of dynamic stall may be observed very clearly. For higher values of r the phenomenon is evident. Hence this value of the reduced pitch rate (i.e. r=0.01) divides the aerofoil behaviour into two states. The first state, and more visible, is the characteristic deep dynamic-stall curve shape, that is absent at lower values of r and it establishes the point at which the tangent of the Cn curve falls below static value. For smaller values than 0.01 the flow does not develop the characteristic of a large dynamic-stall vortex and the induced camber effect is of second order magnitude.

The reduced pitch rate is important to compare characteristics of different profiles tested in different conditions or to carry out general considerations. Since all the tests judged in this section were from the same wind tunnel and for a given wind speed, the considerations on the pitch rate would lead to the same results.

Throughout the range of the pitch rates tested, the aerodynamic Cn coefficient attained values that, at the higher rates, could double its static value (See Chapter 2.1.4.2 part 1, where the highest Cn achieved was 1.42 at an angle of attack of to 15 deg). The most severe test performed had a pitch rate of 280 deg/s (r=0.026) and the value of maximum Cn was 2.8 at 30 deg of incidence. Considering the linear part of the curve (i.e. up to the stall onset), Cn still achieves a 50% overshoot. In this linear range, the lift attains higher values without involving any “break” in the Cm curve (Figure 27, Figure 28 and Figure 29).

As noticed for both the static and for the dynamic cases, the Cm curve has a non-zero value of C_{m0} (i.e. C_{m0}=0.03) indicating an offset between the pitching axis and the aerodynamic centre of the aerofoil. Moreover it can be seen that this offset does not stay constant throughout the pitch rates tested. The C_{m0} decreases in values as the pitch rates increase. This is due to the fact that, with a pitching up rotational speed, the profile compresses the air (pressure increases) over the fore-upper and lower-aft part of the section whilst the effect of the motion is opposite on the fore-lower and aft-upper part of the aerofoil where the pressure diminishes. This event is stronger at high pitch rates and causes the movement of the linear part of the Cm lines towards more negative values as the pitch rate increases. In Figure 27, Figure 28 and Figure 29 the Cm curves are presented against the static counterpart. In Figure 27 the three pitch rates presented (2, 7 and 20 deg/s) illustrate the near comparability with the static test in the linear range of the curve. Albeit there are minor differences in the Cn break at the stall, these are dependant on the definition adopted. The Cm break is usually accepted, by the Wilby [61] definition, as angle of the pitching moment when the value of Cm has dropped by 0.05 below the maximum value achieved. Using this definition, the Cm break for these cases is, more or less, at the same angle of attack. In fact the curves reach their maximum values (from -0.01 to 0) at different angles of attack, but, after a drop of 0.05 in Cm value, they experience the same Cm at the same angle of attack. Only for the Cm line at r=0.0002 appears to be a slightly difference. In this case the ramp-up test is close to the static one at Cm=~-0.7, after a drop of ~0.06 from its maximum value, however very close to the value indicated by Wilby. Hence, according to Wilby, no Cm break delay can be discerned between these tests (Figure 27).

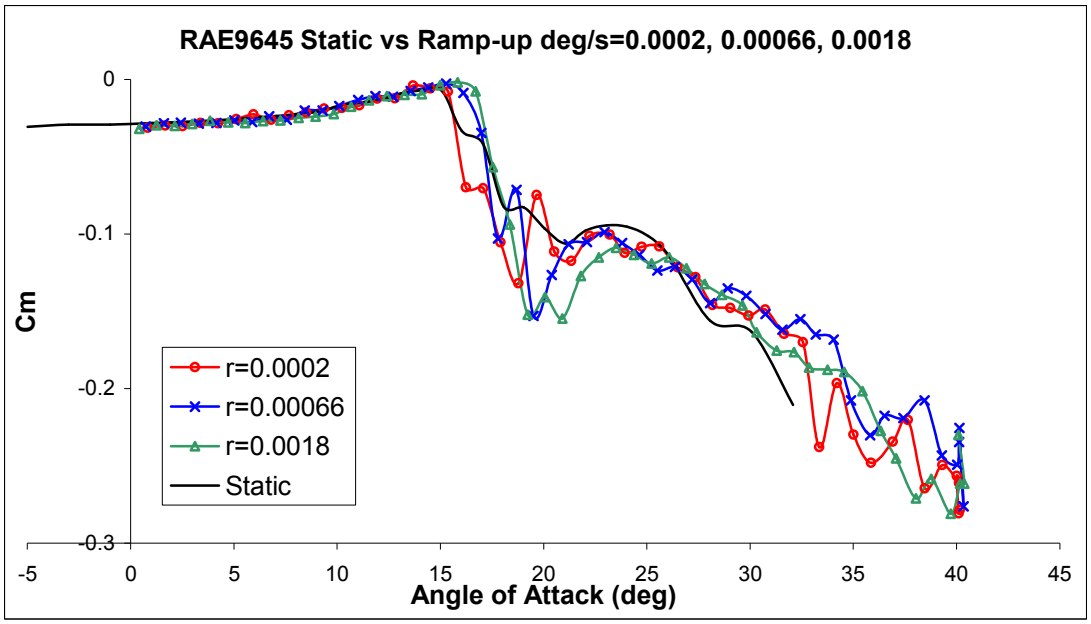

Figure 27 Cm coefficients for the first three pitch rates tested compared to the static test (black line)

After the stall, the three curves plunge down on similar paths following the static behaviour until the pitch rate is greater than 20 deg/s where upon the dynamic behaviour of the aerofoil differs from the static case. Figure 28 depicts the pitch rates from 35 to 120 deg/s. To each of these angular speeds is associated a different value of C_{m0} and it diminishes as the pitch rate increases. Further confirmation is given in Figure 29 which depicts the high pitch rate tests. For these cases, a significant delay in the Cm break may be observed. Once again, this Cm break delay increases with the pitch rate from a value of $\Delta\alpha$ ~1.5 deg to approximately 9 deg for 280 deg/s. For this case (280 deg/s), the dynamic behaviour maintains the Cm value close the C_{m0} until the stall at an angle about a 50%, above the static case. It may be noticed that, at this angular speed, the value of C_{m0} is close to -0.06. This value is double that for the static case. However, such a constant behaviour, up to a higher angle of attack, allows the blade to reach incidences with greater values of Cn coefficient without involving any unacceptable moment coefficient excursion or hysteresis loops. Additionally the way the Cm break occurs is

much influenced by the reduced pitch rate. As the reduced pitch rate increases, the Cm break appears to be smoother; the 35 deg/s is very different from the 280 deg/s. In the first case, the Cm stalls very suddenly and, once it starts to decrease, it achieves the minimum values after a few additional degrees of angle of attack. For the fastest ramp-up (280 deg/s) the stall manner is more benign since the Cm coefficient profile rolls over instead of exhibiting a sharp drop. The pitch rates in between follow this trend and the way the Cm break is reached becomes smoother the faster the ramp rate.

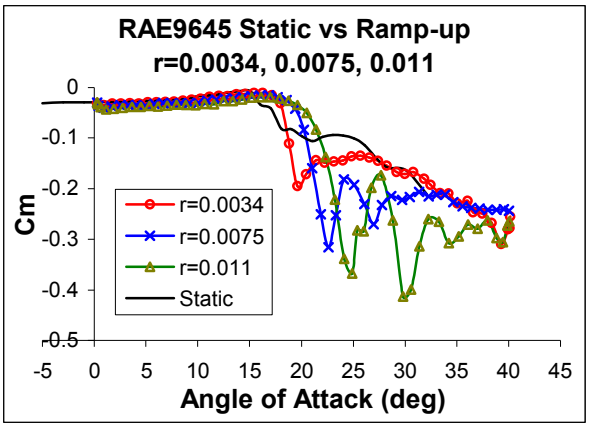

Figure 28 Cm coefficients for r=0.0034, 0.0075, 0.011

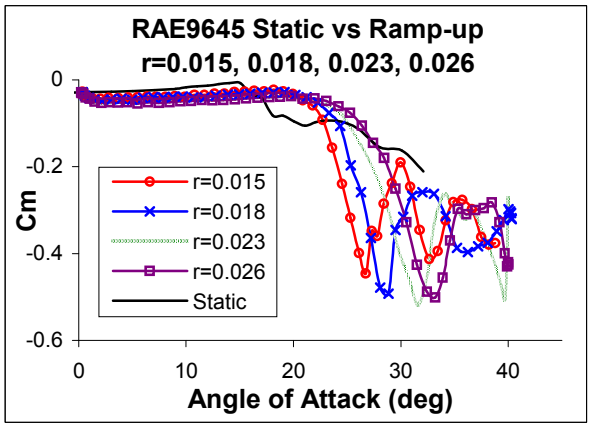

Figure 29 Cm coefficients for r=0.015, 0.018, 0.023, 0.26

As the stall incidence is exceeded, the value of Cm deviation becomes progressively larger until it gets to the lowest point. The absolute value of Cm (min) increases until a reduced pitch rate of r=0.018 (200 deg/s), after which it remains relatively constant at ~-0.5; Table 2 presents the minimum values of the moment coefficient along with the pitch rates. In Figure 30 these data are plotted and a linear correlation, up to r=0.018, may be observed.

The last coefficient considered was the thrust or chordal coefficient (Ct).

Pitch Rate (deg/s)	r	Min |Cm|
35	0.0035	0.22
79	0.0078	0.31
120	0.012	0.37
160	0.015	0.45
200	0.02	0.49
240	0.024	0.51
280	0.022	0.5

Table 2 Minimum Cm values for reduced pitch rates

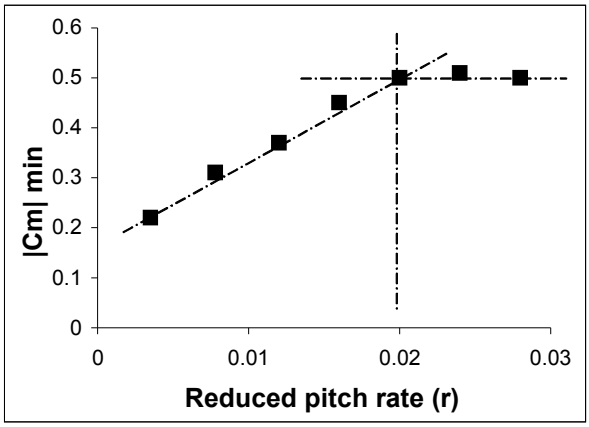

Figure 30 Linear correlations between reduced pitch rate and minimum Cm

The lift and moment are in fact the main forces that can generate the critical loads for both the structure and the aerodynamic limits. Accordingly only a brief analysis of the Ct is presented here. It will be discussed, in Chapter 5, where the Beddoes' model stall-onset criterion was modified using the Ct as indicator of the dynamic-stall onset [68, 70]. In Figure 31 the Ct profiles for a selection of reduced pitch rates are plotted together with the static case. Two aspects of the data are most prominent. First, albeit the initial forms of the curves are similar, there is an obvious and increasing lag as the reduced pitch rate is increased. Second, with increasing the pitch rate there is an obvious increasing in Ct max. That maximum value is well defined. This latter feature is illustrated in both Table 3 and Figure 32. As may be observed, there is a good linear correlation over the majority of the data. At the lower reduced pitch rates, however, this linearity is less clear. More interesting, though, is the similar relationship between the reduced pitch rate and the angle of attack at which the maximum value is reached. This is shown in Figure 33 and detailed in Table 4. These are important data and will be a key factor for the modelling of the dynamic-stall onset (Section 4.1).

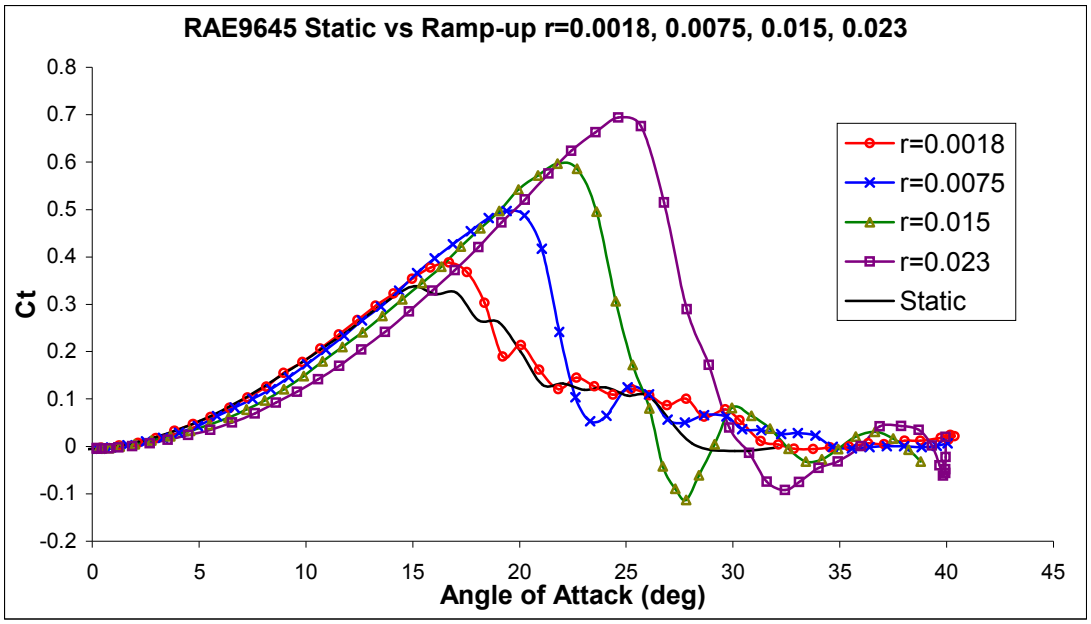

Figure 31 Ct decreasing tangent with the pitch rate

Pitch Rate (deg/s)	r	Max Ct
0	0	0.350
20	0.0019	0.399
35	0.0034	0.436
79	0.0076	0.498
120	0.011	0.536
160	0.015	0.599
200	0.018	0.636
240	0.023	0.696
280	0.026	0.734

Table 3 Maximum value of Ct per each pitch rate

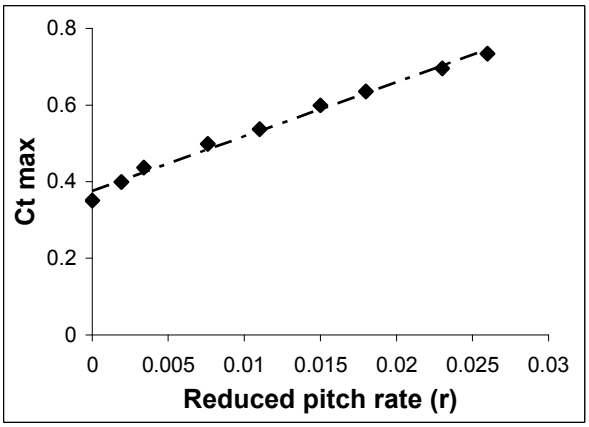

Figure 32 Linear relationship between the reduced pitch rate and the maximum values of Ct

Pitch Rate (deg/s)	r	α_{Ctmax}
0	0	15
20	0.0019	16.5
35	0.0034	17.8
79	0.0076	19.8
120	0.011	21.2
160	0.015	22.5
200	0.018	23.5
240	0.023	25
280	0.026	26.5

Table 4 Angle of attack at each maximum Ct per each pitch rate

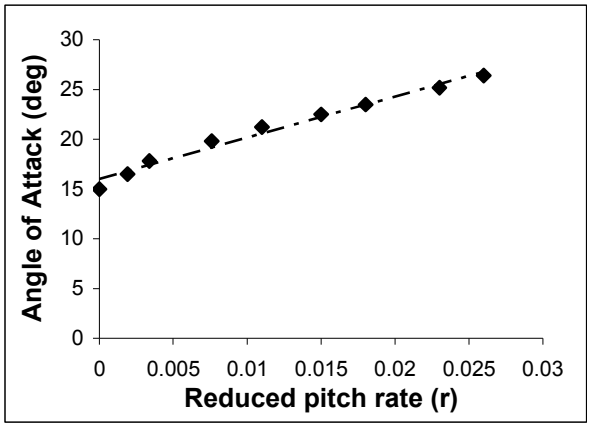

Figure 33 Linear relationship between the reduced pitch rate and the angle of maximum values of Ct

3) Ramp down

Ramp down tests are important to assess and appreciate the process of re-establishing fully attached flow over the aerofoil from the fully stalled state. From these, the associated phenomena and their modelling may be described and archived. Re-establishment of fully attached flow has always received only partial attention over the years. This, in part may have been due to its complex nature and to the limited data available from ramp-down tests. The normal coefficient behaviour for various pitch rates is illustrated in Figure 34 and Figure 36. As with the ramp-up data, the two figures demonstrate two different behaviours of the section. As with the ramp-up tests, here the reduced pitch rate of r~0.01 divides the Cn lines from above to below the static test. Figure 34 presents all the pitch rates up to 79 deg/s. This is the last pitch rate that reaches its values of Cn at 0 degrees from above the "static" line. The r value of 0.01 delimits the boundary between two different behaviours of the same aerofoil: the quasi-

static and the dynamic one. During ramp-down tests, the data are always scattered, especially towards the beginning of the test, due to the natural unsteadiness of the flow undergoing the re-attachment process.

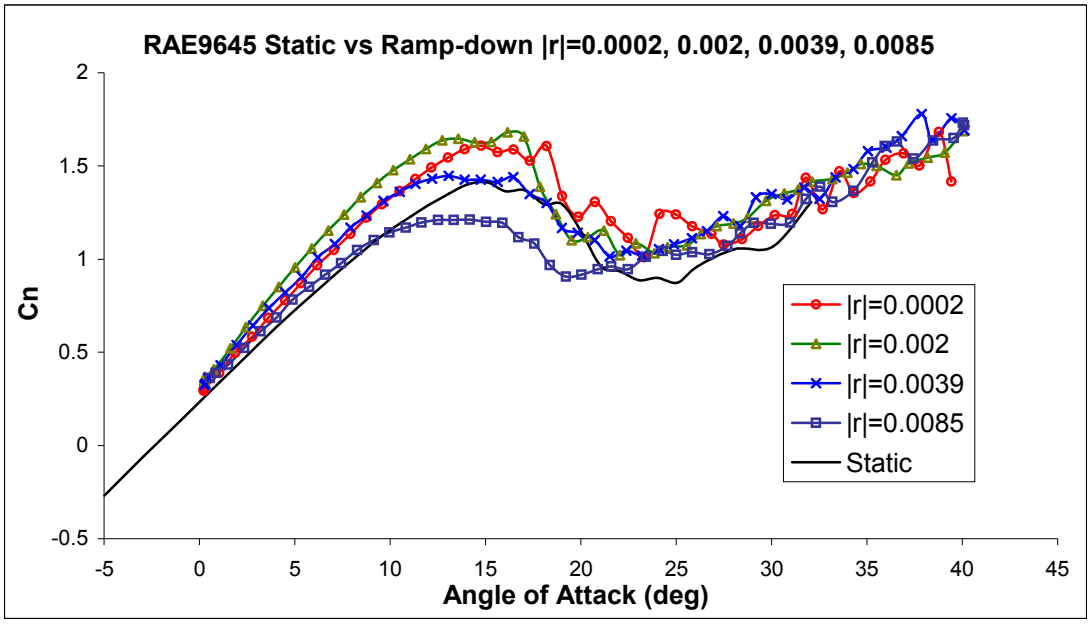

Figure 34 Ramp-down tests for |r|= 0.0002, 0.002, 0.0039, 0.0085 versus the static test

Hence it is always difficult to describe the details of the process. This refers particularly to the re-attachment procedure itself and to the conclusion of the convective phase, Sheng et al. [34]. In fact, although it is very clear from the graph that all the Cn lines, for the quasi-static rates, are well above the static one, and get to higher values of maximum Cn, it is difficult to define a specific angle for the conclusion of the convective phase. When the process takes place, the unsteadiness of the phenomenon produces fluctuations in the Cn values. It may, however, be presumed that the convective phase is concluded when the tangent of the Cn line changes its sign. By applying linear fits and interpolation of the two branches of the line an estimate of the change may be made [71]. Figure 35 gives an example of this and it may be seen that all the quasi-static

ramp-down data yields an incidence close to the static case. The r=0.0085 (79 deg/s), has already been assessed as the transition from quasi steady to deep dynamic-stall, for ramp-up tests. Like the ramp-up, this is also the first angular speed [magnitude of] where the behaviour changes for the ramp-downs. In the fully dynamic case, the flow yields a lower angle of attack for Cn_{min} as ramp-down rates increase.

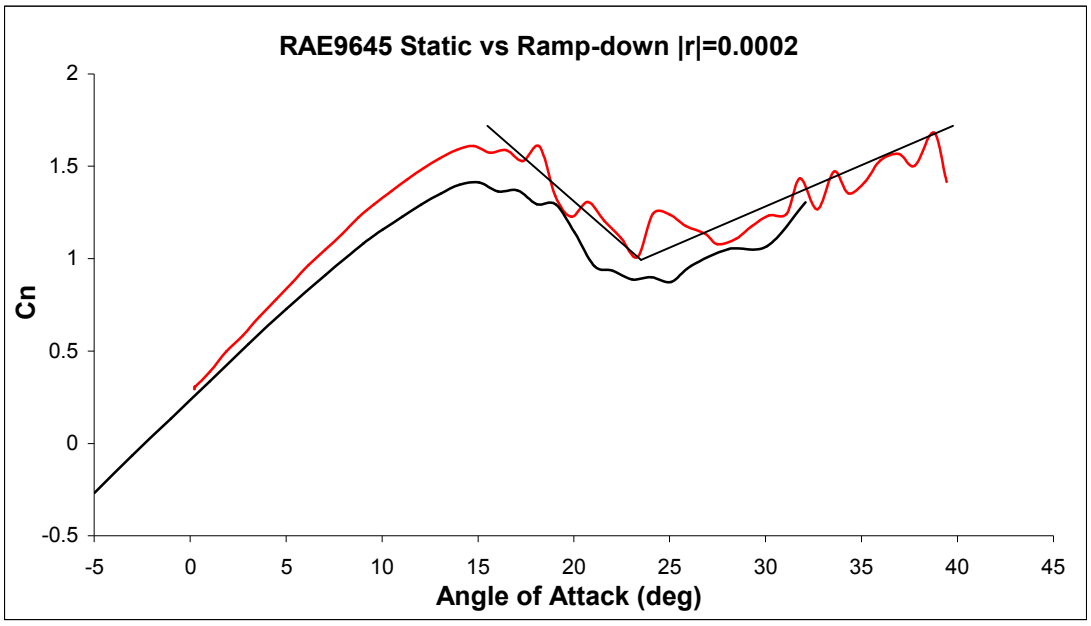

Figure 35 Example of angle of attack for the beginning of the re-attachment process compared to the static test (black line)

In Figure 36 all the negative reduced pitch rates above |0.01| are plotted against the static case. Although the difficulties above mentioned, and the fact that for high pitch rates curves does not always show clearly the characteristic Cn_{min} observed elsewhere, it is possible to define the Cn_{min} angles. These are given in Table 5 and depicted graphically in Figure 37. Here may be observed that there is a strong indication of the expected linearity of the data.

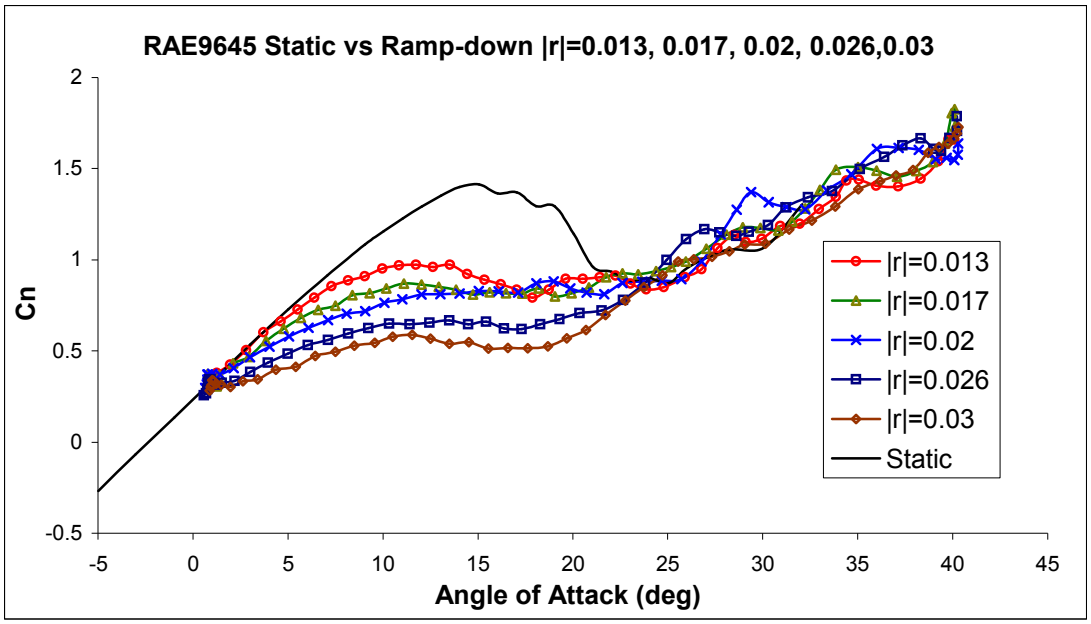

Figure 36 Re-attachment process for |r|>0.01 up to 0.03

In Table 5 the value for r=-0.0165 (-160 deg/s) is set equal to 17.6 deg as, for the test, the Cn stays constant for ~5 deg, from 20 deg to 15 deg, and a simple average is made. The same value will be found by the linear trend-line interpolation shown for |r|<0.01. Unfortunately one test (200 deg/s, blue line in Figure 36) out of the five could not be used for the values in Table 5 because it difficult to obtain an unambiguous Cn_{min} incidence assessment.

$\alpha_{Cn\min 0}$ (deg)	-r	Pitch Rate Deg/s
16	0.03	-280
16.5	0.026	-240
17.6	0.017	-160
18.5	0.0125	-120
19.5	0.0085	-79

Table 5 Angle of attack to begin the re-attachment process

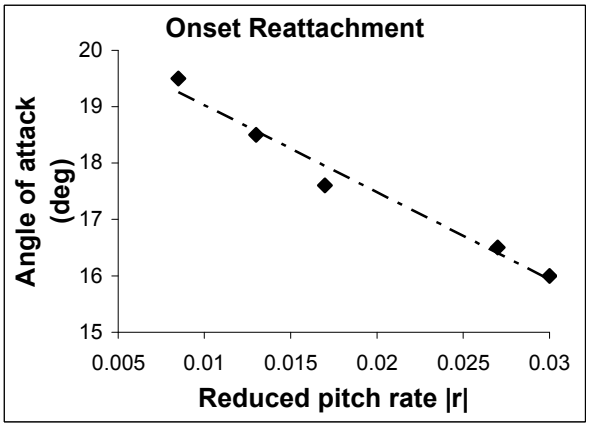

Figure 37 Linear relation between r and the angle of attack when the re-attachment begins

A linear relation between the reduced pitch rate and the angle of attack at, which the convective phase is assumed concluded, has already been observed by Glasgow University for another set of profiles [34], and a value of r~-0.01 was assessed to be the point of the change from quasi-steady to fully dynamic re-attachment process. The RAE9645 exhibits this behaviour a little earlier, but close to the value of the previous works. Hence, it can be inferred that when the pitch rate reduces to the extent that the convective phase is over before the aerofoil incidence is within the fully attached flow region, then the influence is small and the aerofoil behaves in a quasi-static manner.

Additionally the Cm coefficient exhibits an analogous response to its ramp-up counter part. Figure 38 presents these data for a selection of reduced pitch rates that illustrate the main aspects. As with the ramp-up tests, the ramp-downs start, at the low pitch rates, to follow closely the static trend. No significant differences can be identified until -35deg/s after which significant deviations occur. It may be observed that there is a similarity between the pitch up and down tests in as much as, for the fastest ramp-downs, the values of Cm lag the steady state. This is normally associated with the time required by the re-attachment process to develop.

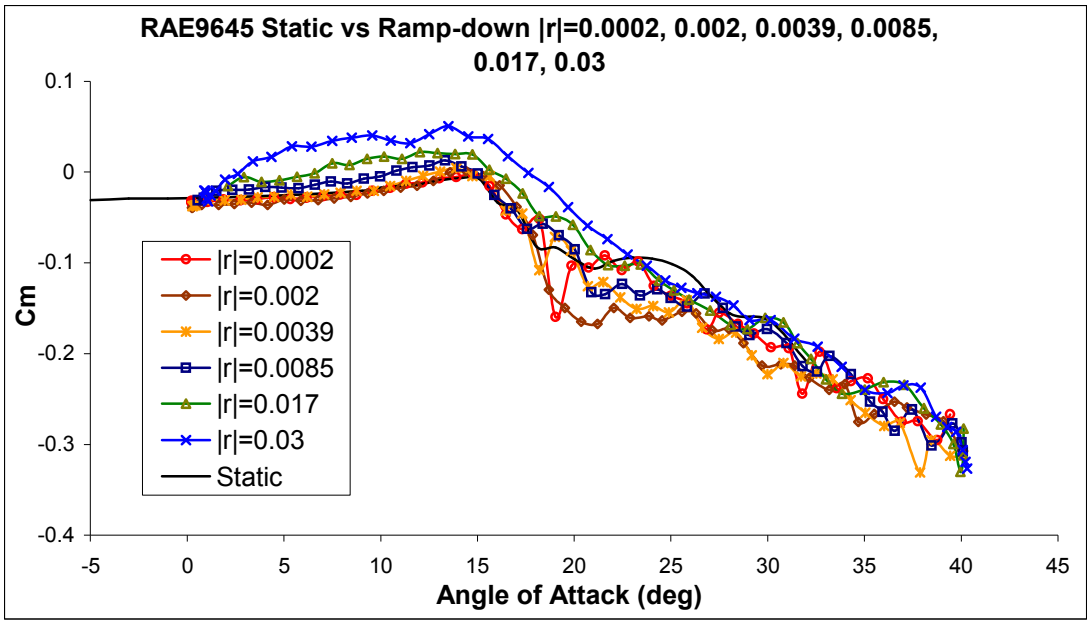

Figure 38 Ramp-down Cm coefficients for |r|=0.00021, 0.002, 0.0039, 0.0085, 0.017, 0.03 plotted with the static test

4) Oscillatory

The oscillating tests performed at University of Glasgow, and here analysed, are all for amplitude of 8 degrees and a mean angle that goes form 2 degrees up to 20 degrees in step of 2 degrees per test. The oscillation frequencies, defined as rad/s, are four: 0.72, 1.45, 2.89 and 4.34.

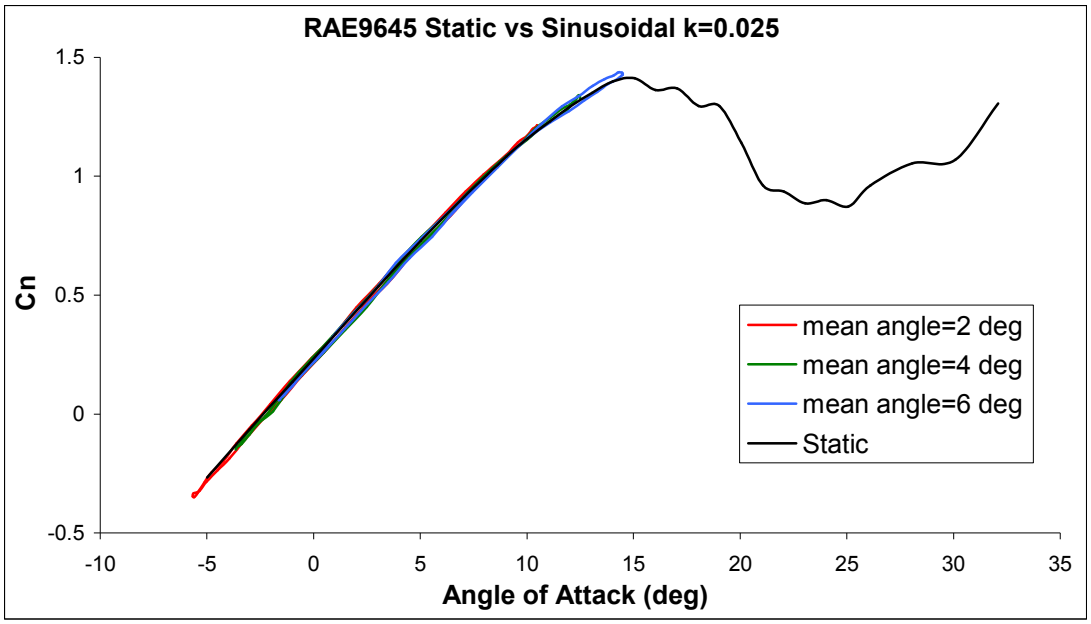

Figure 39 Sinusoidal tests for k=0.025 (0.72Hz), amplitude =8 deg and mean angle =2, 4, 6 deg

During sinusoidal movement a profile may show three different kinds of behaviour depending on the angle of attack, the oscillating frequency and a combination of them. The RAE9645 behaviour in these three cases are plotted in Figure 39, Figure 40 and Figure 41. In the first graph is given the example for k=0.025 (0.72Hz) and the maximum angle of attack lower than the static stall angle (Figure 39). The Cn moves on the same line, according with the frequency, both if it is pitching up and down.

Also for the other three frequencies tested, the Cn lines stay all on the same path, only with minor differences, and well fit the static Cn values for those angles of attack. This behaviour does not appear affected by the angular speed, but by the maximum incidence reached. In fact as long as the maximum angle of attack is smaller than the static stall angle, the tests present the same behaviour for any frequency. Instead, in Figure 40 are plotted the two tests that reach 16, 20 degrees for the four pitch rates. For these maximum angles of attack the profile follows two different paths during the ramp up

and the ramp down parts, generating a hysteresis loop [72]. For all the frequencies the curves have the same kind of shape and the biggest differences may be noted during the ramp down branch when the re-attachment process takes place. Depending on the frequencies and the maximum angle of attack, during the pitching up part, the section can begin to stall (smaller Hz) or not (higher Hz), but none of them stall deeply and completely. However in all these cases, when the section starts its pitch-down part of the loop, it always begins from an angle of attack higher than the static stall angle. As already noticed, in the former paragraph, when the stream reattaches during a ramp down motion it behaves in different ways depending on the pitch rate.

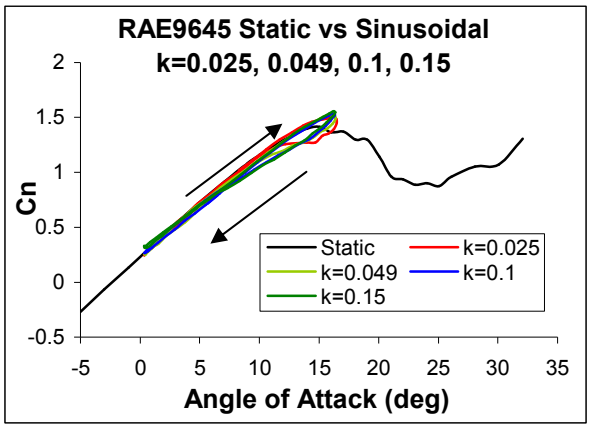

a) Sinusoidal tests for α max=16 deg

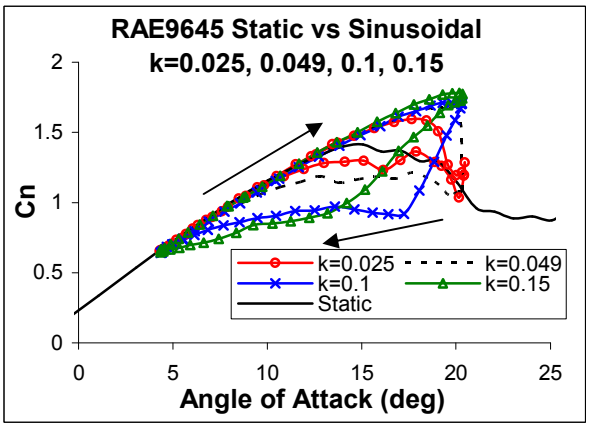

b) Sinusoidal tests for α max=20 deg

Figure 40 Sinusoidal tests for the four frequencies tested. (amplitude=8 deg, mean angle =8 and 12 deg)

The higher the reduced frequency, the longer (in terms of angle of attack) the stall surface will stay on the profile and the later the re-attachment process (intended as the change of the Cn slope during the ramp-down part of the cycle) will start. The stall is then deeper along with the frequency and the flow begins to reattach at lower angles of attack. This gives also an indication on the long time scale necessary for the flow to re-

order after the profile overtakes the static stall angle and to permit conditions for the re-attachment process to occur.

Up to these incidences no dynamic stall can still be seen and the oscillating speed influences only the re-attachment process. In the last picture of the series for the Cn (Figure 41), the maximum angle of attack goes from 22 up to 28 degrees. Through this range is the frequency that mostly shapes the Cn curves more than the angle of attack. Only for the two highest angular speeds the profile shows the typical "raising up" of the Cn slope due to the ongoing dynamic stall. It may be seen for the lowest range of angles of the set, but it becomes clearer as the maximum incidence increases. On the other hand, the two lowest sinusoidal rates do not demonstrate any evidence of the phenomenon for any amplitude. According to Leishman [73] the flow, in oscillating cases, can be considered steady for a reduced frequency k between 0 and 0.05. For frequencies above 0.05 the flow is considered unsteady and the dynamic effects become significant with the generation of a "deep" dynamic stall [16, 74]. The RAE9645 confirm this kind of separation. The four tests plotted in all Figures are for the reduced frequencies k=0.025 (0.72Hz), 0.049 (1.45Hz), 0.1 (2.89Hz) and 0.15 (4.34Hz), from the lowest to the highest Cn reached respectively. It is clear that the dynamic stall starts to appear when the incidence is big enough, but only for those reduced frequencies above 0.05 (Figure 41d. in the picture k=0.025 (0.72Hz) is not reported because of the failure of the test). When the angle of attack is big enough it may be seen a slight enhancement also for k=0.049, which is very close to 0.05 (Figure 41d). Nothing like this can anyway be noticed, for the same value of k, in all the other tests.

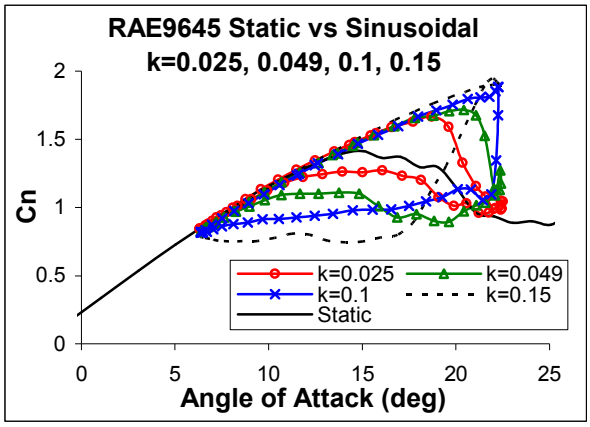

a) Sinusoidal tests for α max=22 deg

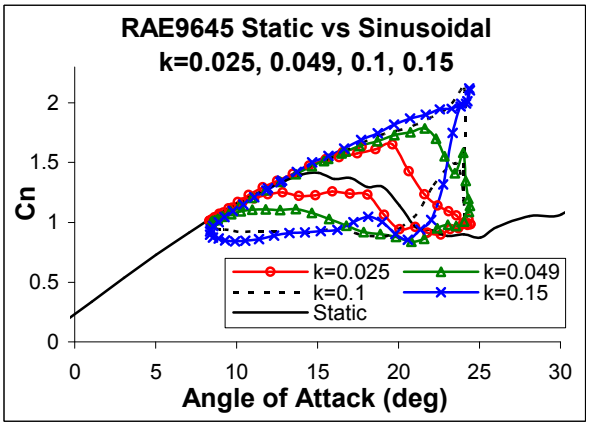

b) Sinusoidal tests for α max=24 deg

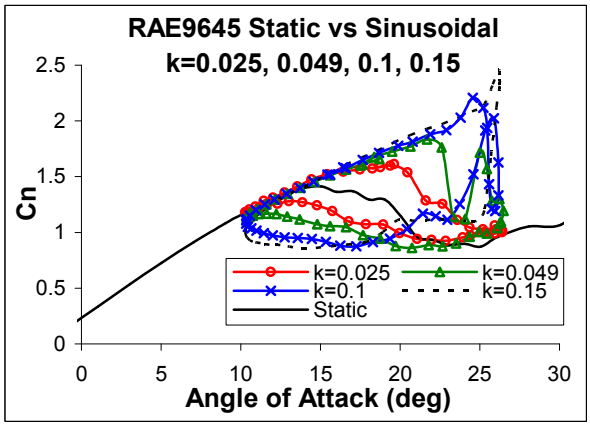

c) Sinusoidal tests for α max=26 deg

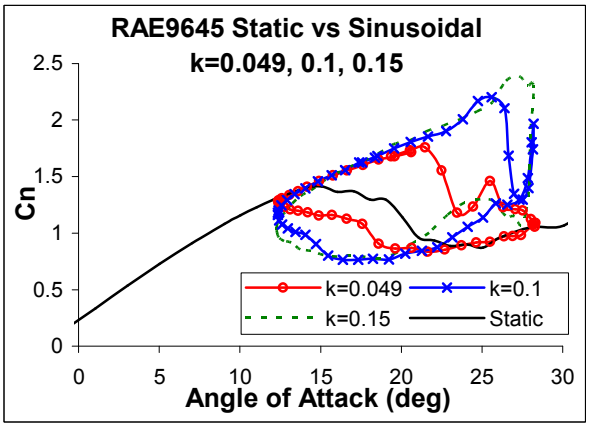

d) Sinusoidal tests for α max=28 deg

Figure 41 Sinusoidal tests for the four frequencies tested. (amplitude =8 deg, mean angle =14, 16, 18, 20 deg).

Comparing all the unsteady tests with the static counterpart it becomes evident that they agree better with Cn static tangent for small angles of attack. It is clear that, for the smaller mean angles, the oscillating tests stay exactly on the linear part of the static line, but for the bigger ones, the slope of the curve decreases in value. This means that an oscillation at higher mean angles will have lower tangent values of the up-stroke cycle, than the same test performed at smaller mean angles. This behaviour has to be kept in mind when, in the next sections, the Beddoes' model was adapted to the profile data.

The Cm graphs plotted in Figure 42, Figure 43 and Figure 44 show three different behaviours of the RAE9645 section, depending on the maximum angle reached and the

oscillating frequencies. For those tests spanning angles of attack below the static breaking moment point, Figure 42, the behaviour is a classical anti-clockwise circular line where the lower part represents the pitching up and the upper one the pitching down.

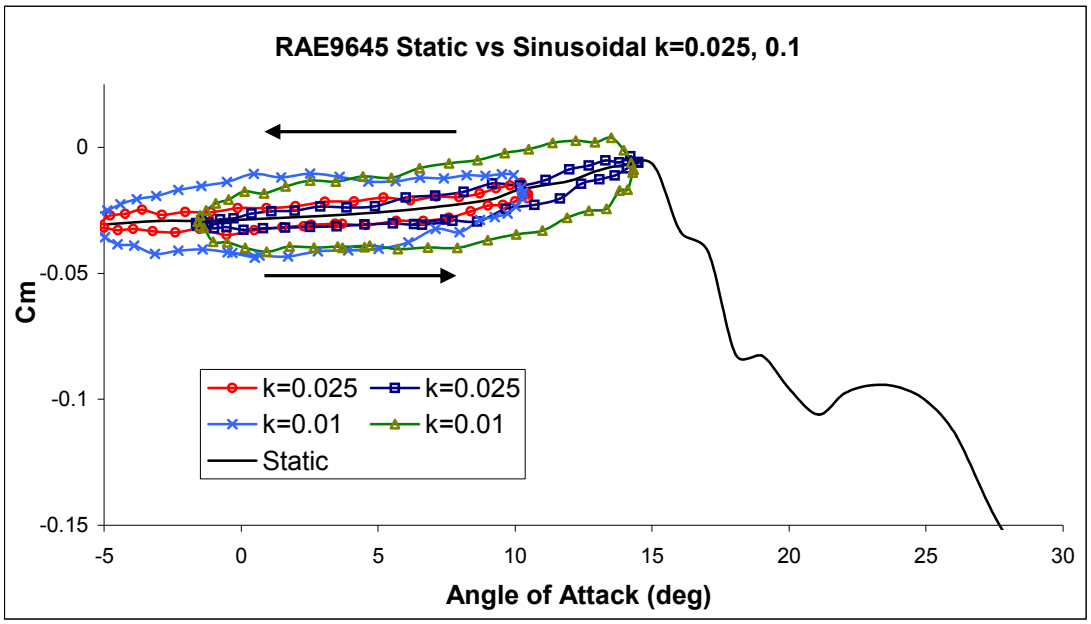

Figure 42 Sinusoidal cycles for Hz=0.72, 2.89 and maximum angles=10, 14 deg

Within this range the general behaviour does not appear to be influenced by the maximum angle of attack. The effect of the oscillation frequency is mainly to enlarge or reduce the size of the hysteresis loop.

Once the amplitude exceeds the static stall angle, the behaviour of the profile changes and a deep break in the Cm curve may be seen. Among these cases, however may be seen two different stalling characteristics.

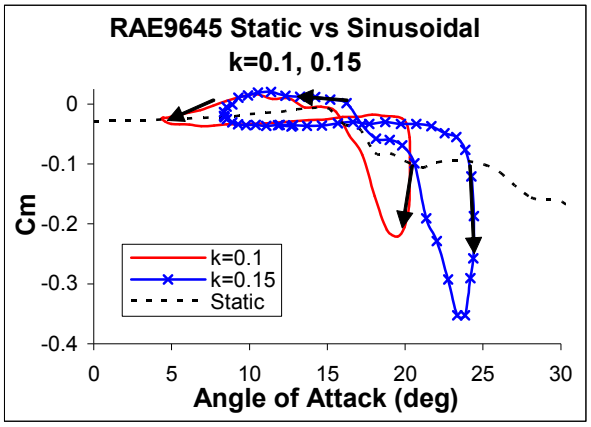

Figure 43 Cm light dynamic-stall

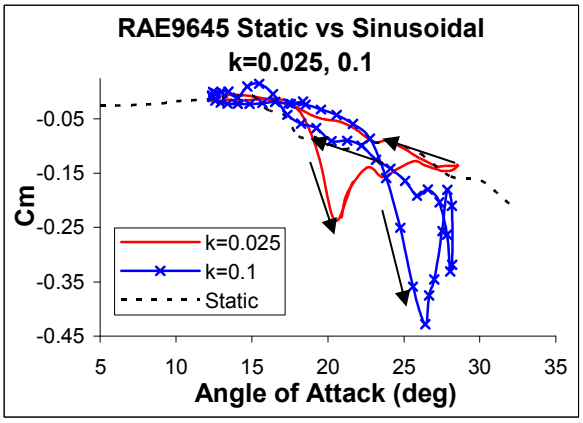

Figure 44 Cm deep dynamic-stall

Figure 43 and Figure 44 underline these differences in what was defined as deep or light dynamic-stall by Carr et al. ([10], [65]) and McCroskey et al. ([23], [74], [75]). In Figure 43 the mean angle is high enough to cause a large nose-down pitching moment due to the leading edge vortex shedding. Nevertheless the flow does not detach completely and the dynamic-stall vortex has not left the trailing edge yet (lift stall) when the maximum incidence is reached (Figure 41 (b) for k=0.15 and Figure 40 (b) for k=0.1). Hence the downstroke of the cycle begins exactly at the lowest Cm. This introduces a clockwise circle into the curve that leads to a reduction of the torsional aerodynamic damping with possibly aeroelastic problems. Furthermore, in Figure 43 for k=0.15 the area of the clockwise is clearly bigger than the counter clockwise circle. In this case the value of the integral of the whole rotation is positive (~0.5) which means that energy is put into the system at each cycle giving aeroelastic problems. The third case shown is Cm curves presenting a deep dynamic-stall. This can be achieved with or without the typical strong enhancement of the Cn coefficient (the dynamic behaviour instead of quasi-static) depending on the oscillation frequency, Figure 41. The profile undergoes this kind of stall only when the flow is fully separated, as it can be seen via a comparison of these figures with those for the Cn (Figure 41 (d)). In these cases, the Cm

curve follows a different path during the pitching down motion than those in Figure 43. All these figures present a second counter clockwise circle big enough to produce a torsional damping.

2.2 QinetiQ data

Experimental tests conducted at University of Glasgow Argyll Wind Tunnel by QinetiQ were aimed at studying the behaviour of the aerofoil RAE9645 rotating about the quarter chord axis under three types of motion: oscillatory and constant pitch-rate ("ramp" in both positive and negative directions) motion. As for Glasgow's tests, the data have been plotted in the standard University of Glasgow format which present the lift, drag and pitching moment against the angle of attack and the non-dimensional time Ut/c. Moreover, a pseudo 3D graph highlights the Cp behaviour throughout the angles of attack [76, 77].

It has to be said, on a cautionary note, that the details of the tests are rather skimpy as a consequence of a lack of information about the model construction, transducer type, actuation system and data logging. These were all the property of the main funding body QinetiQ. Due to changes in company strategy, the information became unavailable. Two reports [76, 77] were then produced with all the tests analysed for the present work and archived at the Aerospace Engineering Department of the University of Glasgow.

2.2.1 Wind tunnel and test set up

The experiments were conducted in University of Glasgow's Argyll low-speed closed-return type wind tunnel (Figure 45). The tunnel has a working section essentially rectangular of width = 2.65 m, height = 2.04 m and a contraction ratio of 5:1. The model was mounted horizontally and it was pivoted about the quarter chord position on two steel shafts. The dynamic and aerodynamic loadings from the aerofoil were reacted to the wind tunnel framework by four vertically mounted beams as shown in Figure 46.

The angular movement of the model was obtained using a hydraulic motor at one end (see Figure 47) and controlled via a custom designed controller.

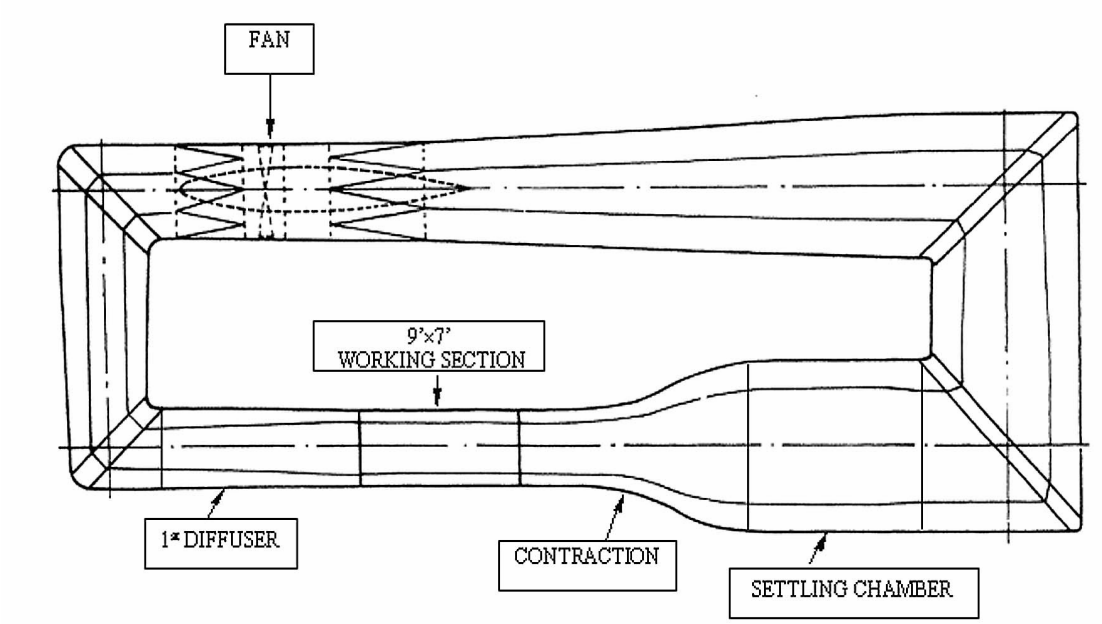

Figure 45 Picture of the Glasgow University's "Argyll" 2.65m x 2.04m wind tunnel

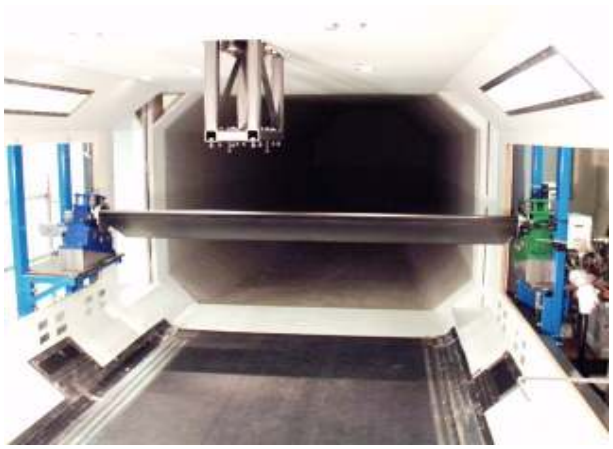

Figure 46 Argyll's dynamic-stall rig

Figure 47 Argyll's dynamic-stall rig

The single element aerofoil section, RAE 9645, had the same geometrical characteristics as the Glasgow one, but the span, b, of 2.4m. The model was constructed of carbon fiber. To provide the chordwise pressure distribution at the mid-span, fifty-two transducers, were installed just below the surface of the centre section of the model. The transducers were of an absolute type. The locations of the pressure transducers in the model are shown in Figure 48 and Table 6. Other transducers were placed along the span of the blade, but they are not here considered. Output signals from the transducers were taken to a specially designed signal-conditioning unit with its own control board.

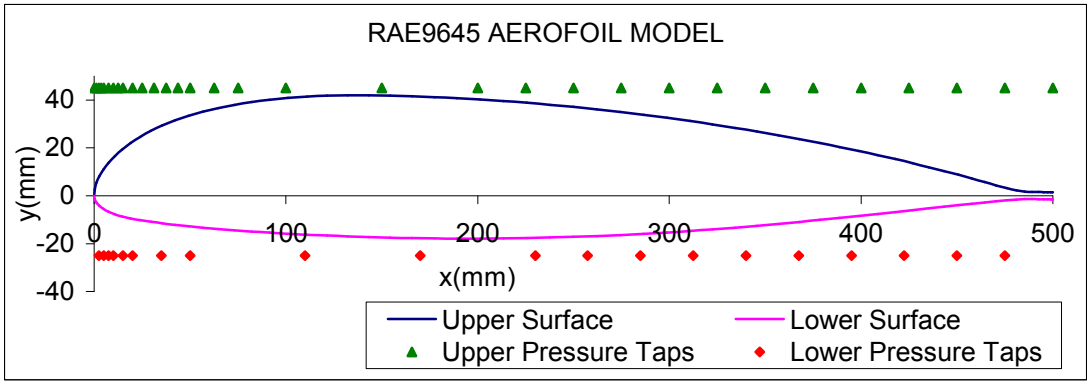

Figure 48 Chordwise profile of the RAE 9645 aerofoil section indicating pressure transducer locations

Orifice	X (mm)	Y (mm)
1	500	1.5
2	475	3.3
3	450	8.7
4	425	13.6
5	400	18.3
6	375	21.6
7	350	26
8	325	29.6
9	300	32.4
10	275	35
11	250	37
12	225	38.8
13	200	40.2
14	150	41.5
15	100	40.5
16	75	38.3
17	62.5	36.2
18	50	33.5
19	43.75	32.2
20	37.5	30
21	31.25	27.7
22	25	25
23	20	23
24	15	19.3
25	12.5	17.4
26	10	16.3
27	7.5	13.6
28	5	11
29	3.75	9.45
30	2.5	8
31	1.25	5.4
32	0	0
33	2.5	-4
34	5	-5.6
35	7.5	-6.6
36	10	-7.6
37	15	-8.7
38	20	-9.7
39	35	-11.4
40	50	-12.8
41	110	-16.2
42	170	-17.7
43	230	-17.5
44	257.5	-16.9
45	285	-15.9
46	312.5	-14.5
47	340	-12.9
48	367.5	-10.9
49	395	-8.4
50	422.5	-6.2
51	450	-3.8
52	475	-1.8

Table 6 Pressure transducers location along the profile

2.2.2 Tests

The experimental regime was divided into three types of motion: oscillatory and constant pitch-rate ("ramp" in both positive and negative directions) motion. The typical test Reynolds number was ~1.5 million and the Mach number was ~0.13 based on the chord and freestream condition. The airfoil model had a chord of 0.5m and an aspect ratio of 4.8. The typical airflow speed was ~44m/s. Some tests were carried out for two different flow speeds and, consequently, different Re and Mach number. These have not been considered herein. Nonetheless the stream velocities were 29 and 59 m/s with Mach numbers of 0.085, 0.172 and the $Re=1\cdot10^6$, $2\cdot10^6$ respectively.

Static tests were not conducted and the present work will use, if necessary, either the comparable data from Glasgow's Handley Page tunnel for an angle of attack range -5^0 to 26^0, in 1^0 increments, utilising 32 sampling blocks each collecting 1000 samples per angle of attack or the QinetiQ slow ramp data. For a sinusoidal test, the model was oscillated about its quarter chord with the sinusoidal pitching motion defined for Glasgow University's tests. The oscillatory tests were conducted with 1 continuous cycle utilising one sampling block collecting from 2000 to 36000 samples depending on the frequency. The constant pitch rate tests (ramp up and down) were conducted over from 3 to 6 cycles with each of the sampling blocks containing from 6000 to 38000 samples depending on the pitch rate.

The oscillating tests were mainly done keeping the amplitude fixed at 5, 8 or 10 degrees and varying the mean angle from 8 to 20 deg with a two-degrees step between each mean angle. For any amplitude a range of frequencies was tested starting from 0.0028 rad/s going up to 7 rad/s. All the ramp up and ramp down tests were over an angle of

25.1 deg, beginning from 1.9 and ending at 27 deg, for the ramp up and the reverse for the ramp down. The pitch rates tested, in deg/s, were: 3, 6, 15, 30, 60, 90, 120, 150, 180, 200, 250 and 300.

The test data were grouped for each motion type, with compact details of the specific test given in Appendix 1 (Tables 4A and 5A). Surface pressure distributions and integrated forces (aerodynamic coefficients) are presented for each case in references [76, 77].

2.2.3 Data and data reduction

The data for each test were saved in three different files. The files with extensions ".buf" give details as the tunnel conditions, the sample rate, the block size etc. It also contains the list of the channels and transducers used with the mean, RMSD, max and min values. The files with the ".raw" extensions, two for each test, contain the temperature (004) and pressure (005) measurements of the test. They have been stored in binary format and as "ADC counts". A FORTRAN code was used to convert the files in a readable ASCII format. Then they were changed to volts as follow:

$$V_q = A_q p10^{(-G/20)} \qquad 2.5$$

$$P = A + B\frac{(V_a + F_i)}{(V_b + F_o)} \qquad 2.6$$

Another FORTRAN code has been then developed to calculate the aerodynamic coefficients Cn, Cm and Ct from the pressure measurement and to store them in the typical University of Glasgow format. Where possible the results over the cycles were then averaged.

The main data for the ramp up and ramp down tests presented in this report are the average of a number of cycles. This was not possible for the sinusoidal tests as they were performed only for one complete cycle. By the averaging of the process the salient features are highlighted and the minor random differences, that do exist from cycle to cycle, are cancelled. The given data may be considered as typical of aerofoil behaviour in a given individual cycle. At the end of this process all the files, as the tests had all a different number measures depending on the frequencies, were then reduced to 1024 measures per each ramp-up and down test and to 256 steps for the oscillating ones. Moreover some transducers were not suitable for the calculations. Four out of the fifty-two transducers were found not to work properly and their values had been interpolated with the values of the ones right before and after them. At the trailing edge the last two pressure gauges on the upper surface and the last one on the lower surface were not found at all among the pressure measures.

As final result the pressure measures were collected in files named "9645cpsqXXXtot.dat". The file presents fifty-one columns (forty-nine for the transducers, one for the angle of attack and one for the time), and either 1024 or 256 rows. On the same way another file is generated, "9645cplXXXtot.dat", with the three coefficients at each angle of attack, the incidence and the time.

2.2.4 Formats and Results

2.2.4.1 Formats

The formats for the QinetiQ data are the same as the University of Glasgow's (Figure 12 to Figure 15 show the typical plots). No further reduction of the data was required.

2.2.4.2 Results

The results have been already discussed for the Handley Page data set. The present Chapter will describe common characteristics and any new aerodynamic behaviour, not observed before, will be highlighted. In further sections, a comparison between the two behaviours will give a better understanding of the influence of the test conditions (different set-ups and wind tunnels) on the aerofoil aerodynamic coefficients. The following analysis cover the range of tests performed at Mach=0.13, $Re=1.6 \cdot 10^6$ and wind tunnel airflow speed=44m/s. These are the same parameters tested at the Handley Page tunnel and were chosen to have a common base for comparison.

1) Static

QinetiQ conducted no static tests. It was therefore not possible to compare the dynamic behaviour with the static one. The static test carried out by the University of Glasgow can be use only as an indication, but, being performed in a different wind tunnel and under different condition, does not make it suitable for any conclusion about the section

behaviours in the two conditions. A possible solution to the lack of the static test, adopted in some cases, will be to compare the dynamic tests with the slowest ramp-up performed by QinetiQ (r= 0.0003).

2) Ramp up

The ramp-up tests are divided in two main categories. The first one, shown in Figure 49, represents the Cn behaviour without the deep dynamic-stall. For these tests the trailing edge separation starts to be apparent around 12 degrees of incidence and the normal force curve tends to bend clearly towards lower values of the tangent. The way the profile then stalls completely is sudden and rapid, dropping from almost the maximum value of Cn reached to the minimum within very few degrees. The range of pitch rates represented in Figure 49 goes from 3 to 30 deg/s (r=0.0003 to 0.003).

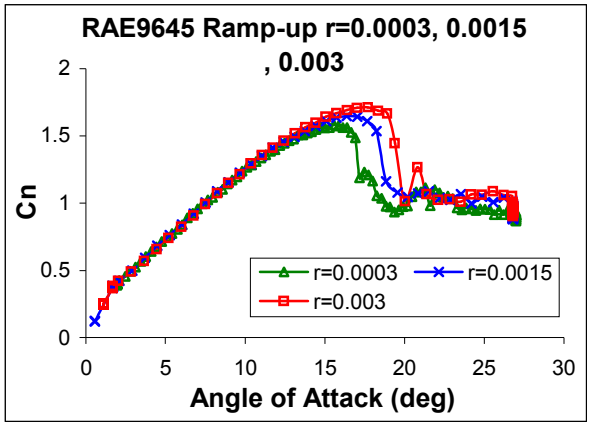

Figure 49 Cn for QinetiQ low pitch rates

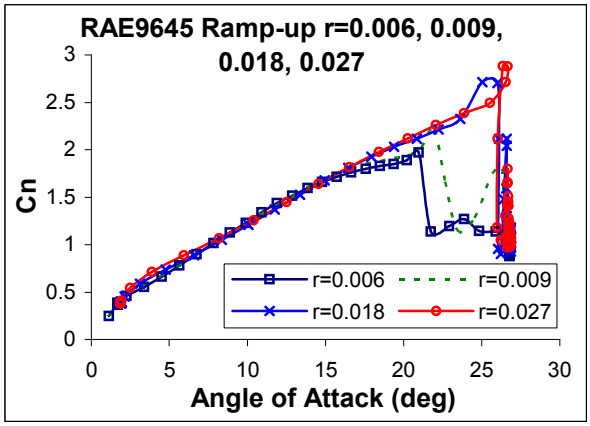

Figure 50 Cn for QinetiQ high pitch rates

Figure 50 illustrates some tests for which the dynamic-stall process is visible. Unfortunately the angles spanned are not large enough to appreciate the full

development of the vortex at the highest pitch rates. Nevertheless, looking at the lowest angular speed of this range, an interesting observation may be made. The first two curves have a value of r=0.0059 (60 deg/s) and 0.0089 (90 deg/s). The second value of r is close to the "border value" of 0.01, separating the dynamic behaviour from the quasi-static one. So too, however, does the first value of ~0.006, displaying, albeit a weak, a dynamic-stall vortex. The RAE9645 section, therefore, shows evidence of dynamic stall well before the limit value of reduced pitch rate chosen for other profiles [28, 69]. This does not appear to be a peculiar aspect of the tests in this particular wind tunnel. In fact the same behaviour has been noted for the University of Glasgow's tests, although for a higher pitch rate, but still below the "edge" value. From Figure 50 it is also clear how, what looks like trailing edge separation (Cn curve slope begins to decrease after a certain angle of attack), become less important with the increasing pitch rate. As for the Glasgow data, it is even more noticeable for the lowest angular speeds and it almost completely disappears for the highest values. A confirmation that is effectively a trailing edge separation that takes place at lower reduced pitch rates, and it is less important, instead, for the fastest ramp-ups, is given in Figure 51 and Figure 52. These two figures show the pressure distribution along the chord at different angles of attack for two different reduced pitch rates: 0.006 and 0.027 respectively. In frame (a) of Figure 51 the angle of attack is equal to 15 deg and no trailing edge separation can be discerned over the profile. Comparing this pressure distribution with the Cn line (Figure 50) at the same angle of attack it can be noticed that up to this incidence the Cn curve slope has not changed yet, but it starts to bend towards a lower value of the tangent around this point. At 17 deg of angle of attack the Cn curve slope has changed and decreased in value. It can be noticed that in frame (b), corresponding at the same angle of attack, the last 20%

of the chord is now showing the presence of detached flow. Frames (c) and (d) give the pressure distribution for the angles of attack equal to 19 deg and 21 deg. It is clear from the pictures that the trailing edge separation is progressing upwards covering almost 80% of the profile in frame (d) that shows the pressure field around the aerofoil at an incidence right before the beginning of the dynamic stall (as illustrated in Figure 50).

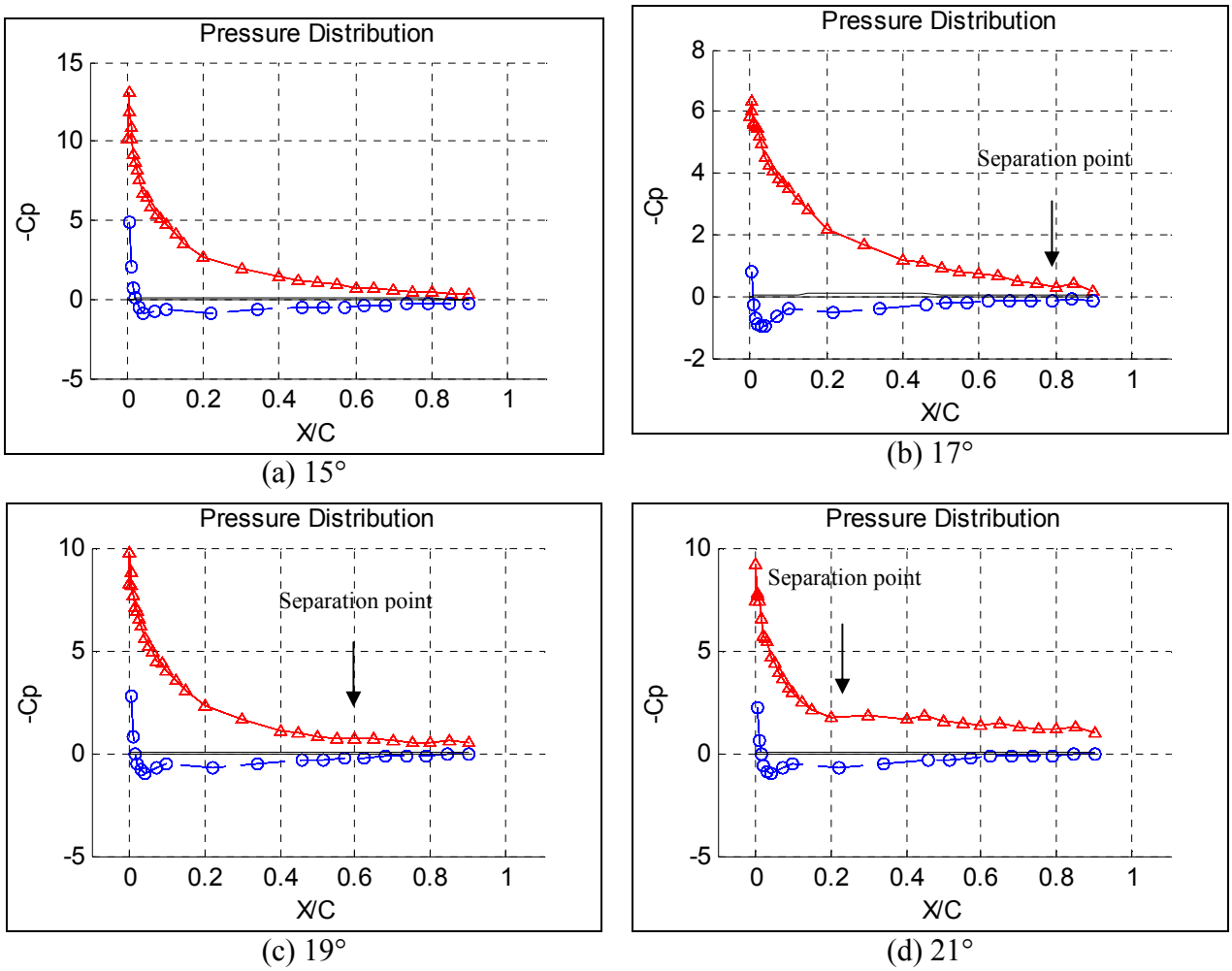

Figure 51 Chordwise pressure distribution for r=0.006 and for angles of attack equal to 15(a), 17(b), 19(c) and 21(d) deg. ("Δ" upper surface, "o" lower surface)

On the other hand for a fast pitch rate the trailing edge separation appears almost not to occur at all on the upper surface of the aerofoil. In Figure 52 it is clear how, for a pitch

rate of 270 deg/s, there is no discernable detached flow at an incidence of 23 deg (c) and even at the highest angle of attack here presented (frame (d) =26 deg), which is again the incidence right before the beginning of the dynamic stall (as shown in Figure 50), only the last 20% of the profile chord shows the presence of trailing edge separation.

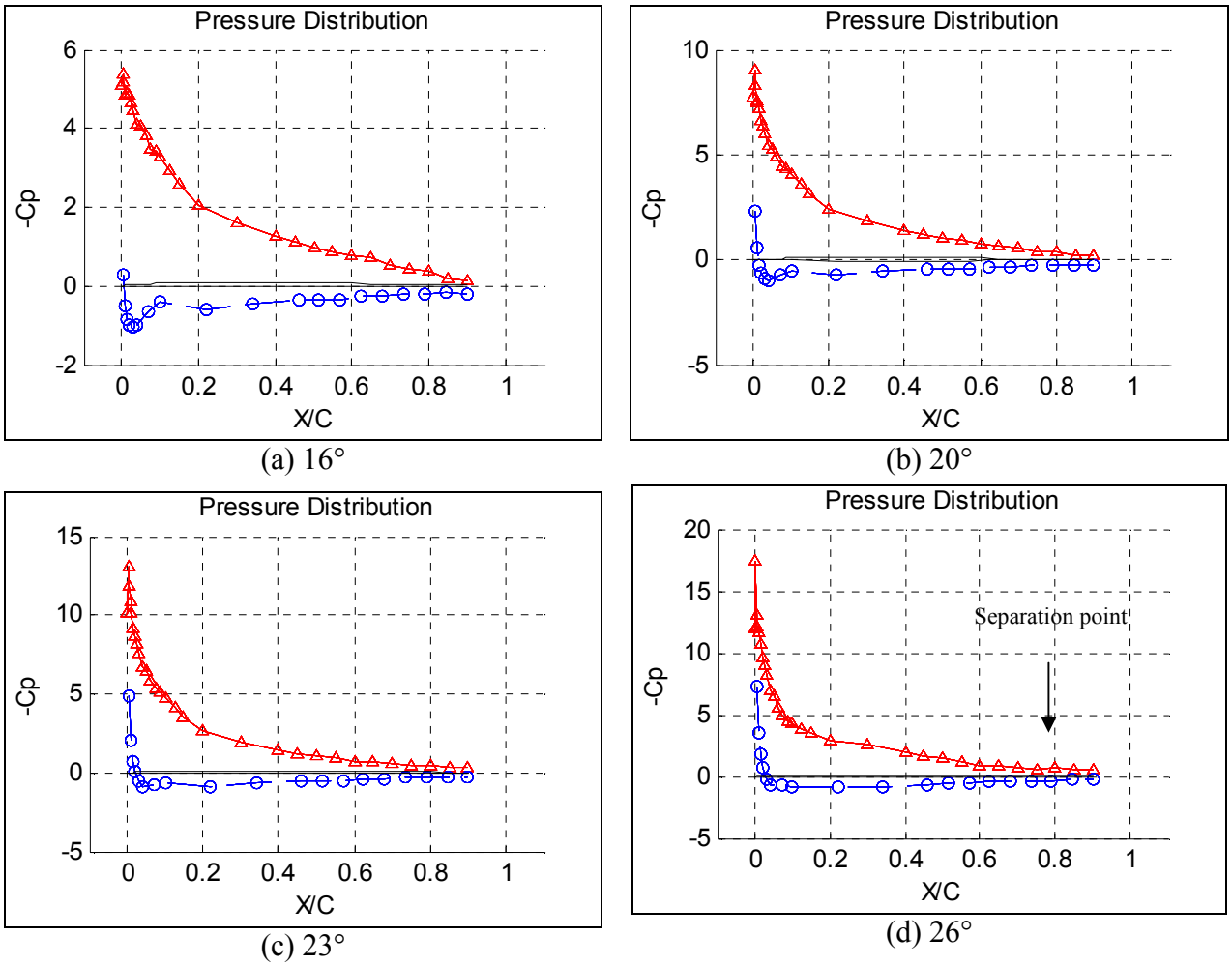

Figure 52 Chordwise pressure distribution for r=0.027 and for angles of attack equal to 16(a), 20(b), 23(c) and 26(d) deg. ("Δ" upper surface, "o" lower surface)

The Cm curves begin from a value of ~-0.03 decreasing to -0.06 for the highest reduced pitch rate. This means that the pitching axis is positioned in front of the centre of pressure and it moves backwards with the increasing pitch rate. In Figure 53 (a & b) could also be inferred that, during the pitching-up motion, before the stall of the profile,

especially at the lower rates, the pressure distribution varies a lot, with the centre of pressure moving upstream beyond the pitching axis and the Cm coefficient changes its sign, becoming positive.

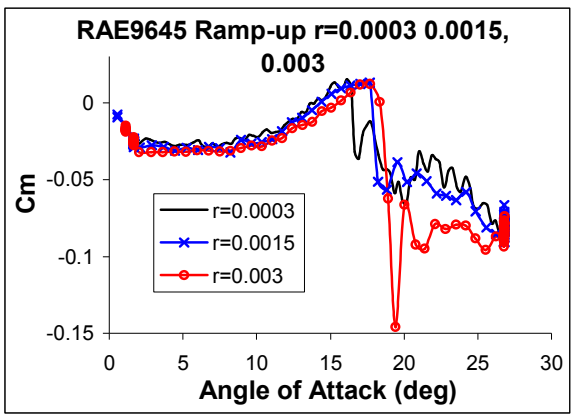

a) Low reduced pitch rates

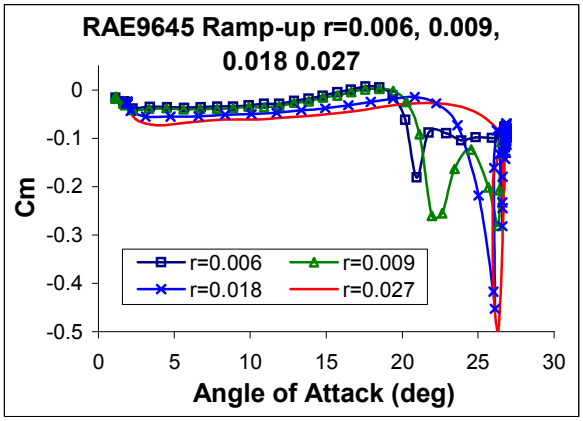

b) High reduced pitch rates

Figure 53 Cm coefficients throughout the range of reduced pitch rates tested by QinetiQ

As seen for the Glasgow tests (Figure 28 and Figure 29) the Cm break becomes smoother with increased pitch rate resulting in a more gradual dip towards negative values. Unfortunately, due to the set-up of the tests, the minimum Cm values for the highest pitch rates cannot be seen.

Figure 54 presents the Ct coefficient behaviour for the reduced pitch rates starting from a value at which the first dynamic-stall may be observed (r~=0.006).

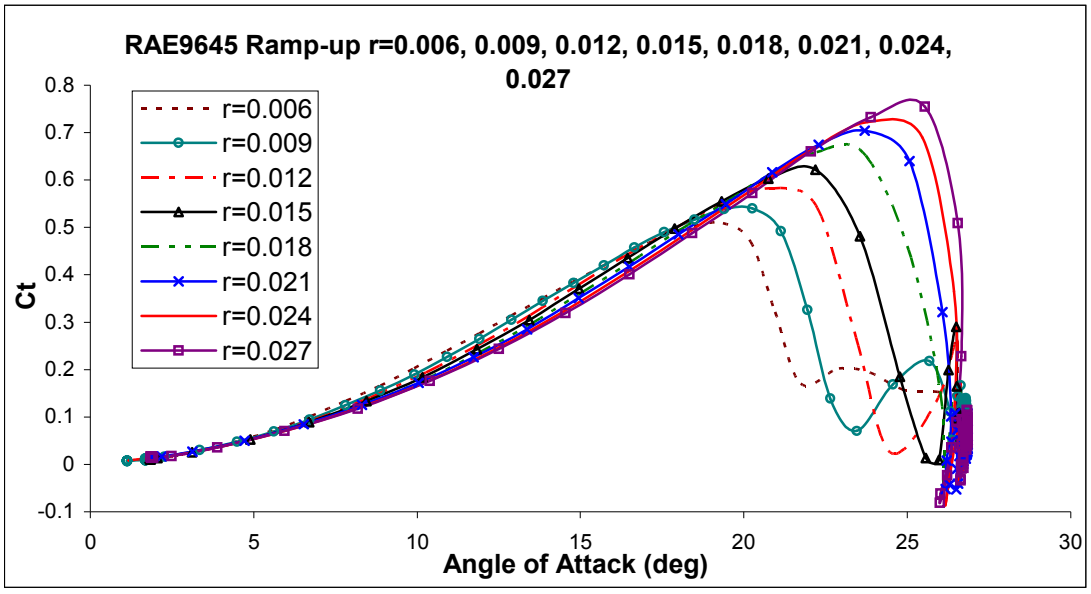

Figure 54 Ct curves for reduced pitch rate above r=0.006

The trend in Ct, depicted in Figure 54, is clear and the maximum value achieved at various pitch rates is shown in Figure 55 and listed Table 7. It is clear that up to a value of r=0.025 the maximum Ct varies linearly with r. Albeit the linearity does not appear to be maintained above r=0.025, it is likely that the non-linearity is simply a consequence of the system motion limitations. Sheng et al. [70] had previously observed this and were able to demonstrate that the non-linearity in Ct_{max} at large r was simply a consequence of non-linearity in the ramp motion as the model was near to the maximum α of the test and so in the slow-down sector of the ramp function. Accordingly the last few data points for Ct_{max} are low because of this.

Pitch rate	r	α max Ct
60	0.0059	19.1
90	0.0089	20
120	0.0119	21
150	0.0149	22
180	0.0178	23
210	0.0208	23.8
240	0.0238	24.7
270	0.0268	25.3
300	0.0297	25.8
330	0.0327	26

Table 7 Maximum value of Ct per each pitch rate

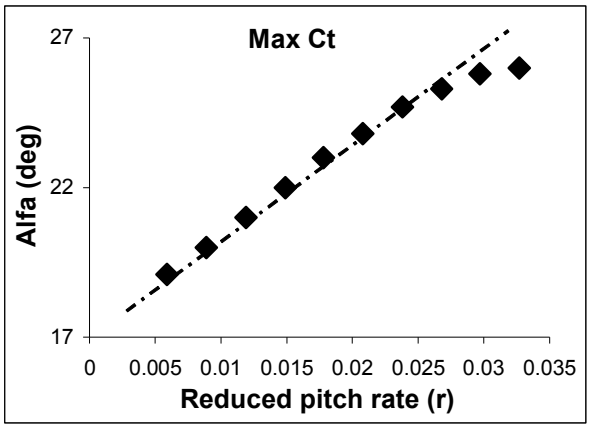

Figure 55 Linear relationship between the reduced pitch rate and the angle of maximum values of Ct

3) Ramp down

The starting angle of 27, QinetiQ data, degrees results in a re-attachment process that is unclear for low pitch rates. Figure 56 illustrates the data for pitch rates up to r=0.012 (120 deg/s). A slight delay may be observed in the re-attachment process, and that this delay becomes clearer with increasing pitch rate, but up to this value it is difficult to define a precise angle for the re-attachment process to begin. Adopting the same procedure used for the Glasgow data (Figure 35), it appears; however, to be close to the starting angle (around 23.5/25 degrees). This is the same as that from the Glasgow data and is close to the static values.

Considering Figure 56, in which is also plotted the data for the lowest ramp-up rate, it is interesting to note that the max Cn, for the ramp-down test, is greater than that for the smallest ramp-up rate. This simply indicates that, although the slowest ramp-up rate may be considered to be close to the "static" data, the mechanism of stall and re-attachment,

even at low pitch rates, yield different results in the region of the stall. The re-attachment process becomes clearer at larger ramp-down rates, as depicted in Figure 57 and the behaviour is radically different. Although not all the data are included in the figure, the trend is apparent, comparable to previous tests and, even with the low ramp-down start angle, the non classical convective phase of the process is clear. In fact, in keeping with the methodology of Sheng et al. [34], the angle of minimum Cn, assumed to be the conclusion of the convective phase, is unmistakably identifiable in Figure 57 and depicted in Figure 58 and Table 8. The close linearity of the data is unmistakable and indicates a beginning of the convective phase of just over 22 deg. Here after the boundary layer continues its re-establishment process together with the pressure distribution and hence Cn reacting to the reducing incidence.

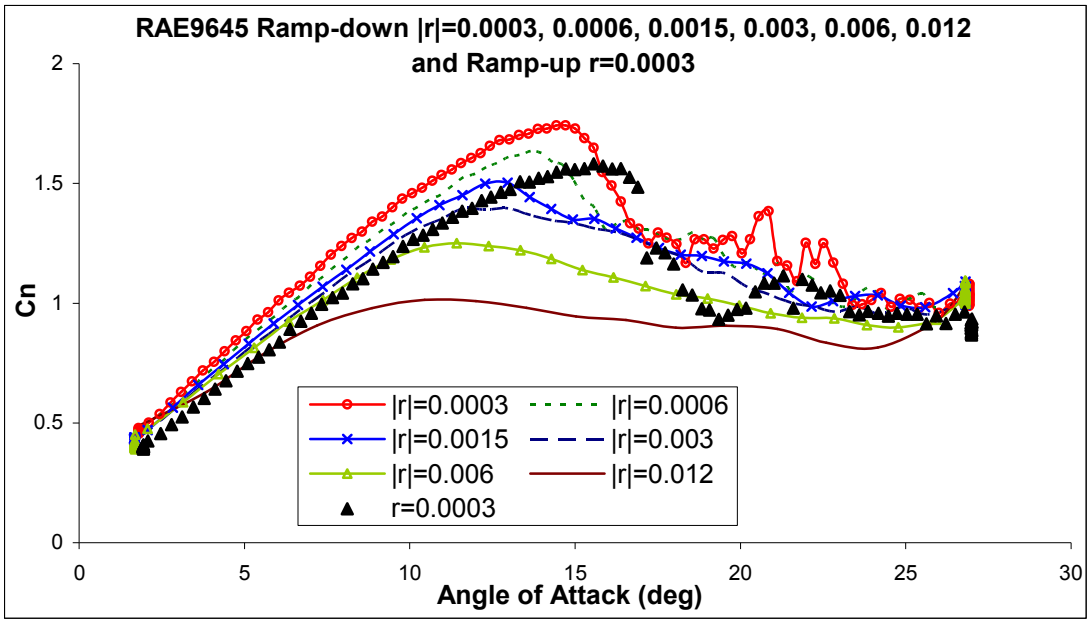

Figure 56 Cn for QinetiQ ramp-down tests for |r|=0.0003, 0.0006, 0.0015, 0.003, 0.006, 0.012 compared to the slowest QinetiQ ramp-up test (r=0.0003)

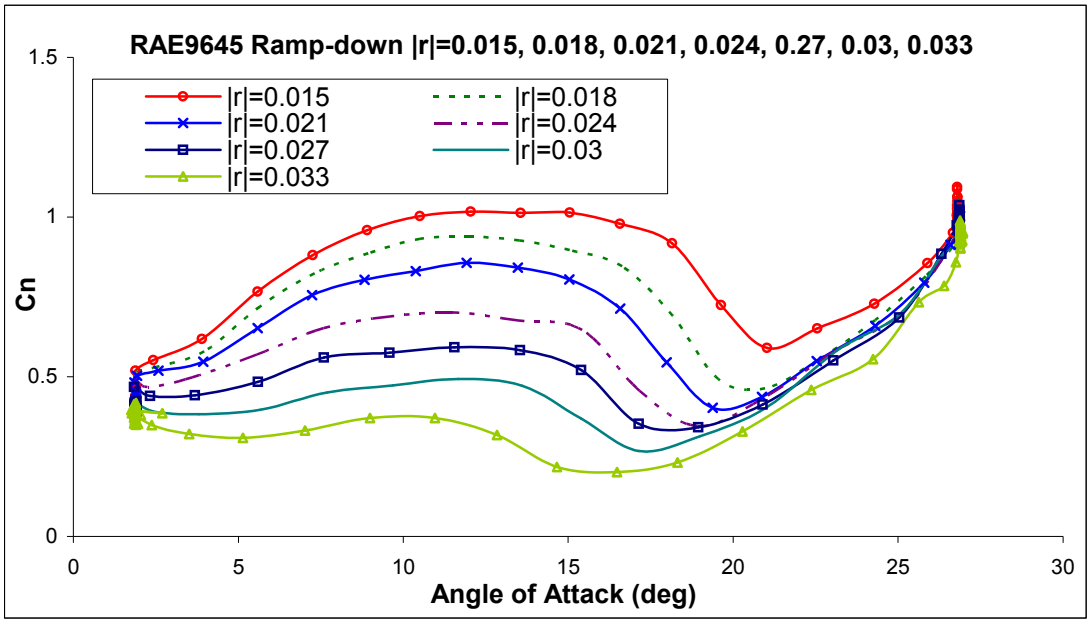

Figure 57 Cn coefficient for ramp-down motion performed at |r|=0.015, 0.018, 0.021, 0.024, 0.027, 0.03, 0.033

Pitch rate	|r|	$\alpha_{Cn\min 0}$ (deg)
150	0.0149	21.3
180	0.0178	20.5
210	0.0208	19.8
240	0.0238	19
270	0.0268	18.1
300	0.0297	17.2
330	0.0327	16.2

Table 8 Angle of attack to begin the re-attachment process

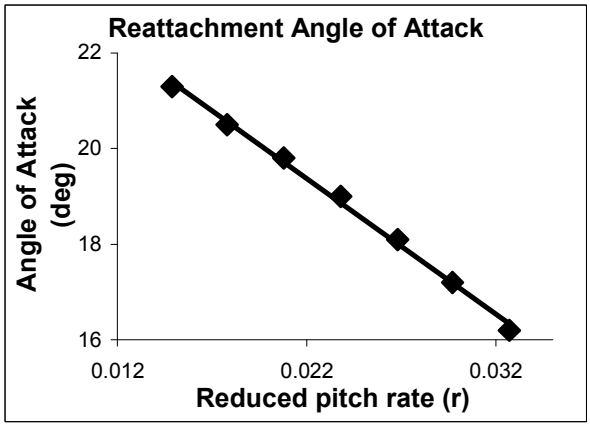

Figure 58 Linear relation between r and the angle of attack when the re-attachment begins

The Cm coefficient for the QinetiQ data presents a similar, to Cn, and unusual behaviour. As for the Cn, the pitch rate of 120 deg/s seems to define a distinct change in coefficient profile. The angular speeds up to 120 deg/s are shown in Figure 59.The Cm behaves like most other profiles [78] and the curves present the typical rounded form which suggests how the centre of pressure moves along the chord. At these low pitch

rates the Cm progresses from its minimum negative value (i.e. start of the ramp-down), towards its maximum, in an obvious quasi-static nature. Clearly, however, the -120 deg/s pitch rate, as expected, is in the transition from quasi-steady to fully dynamic. When Cm achieves its maximum value this appears to be the start of boundary layer re-establishment. As the boundary layer develops over the aerofoil chord, from the leading edge, the Cm reduces until it achieves the "static" value (Glasgow tests). At pitch rates -30 deg/s and less, the Cm profile appears close to the static value over the entire incidence range. Above this value clear dynamic effects may be seen, but still in the transition from quasi-steady to dynamic.

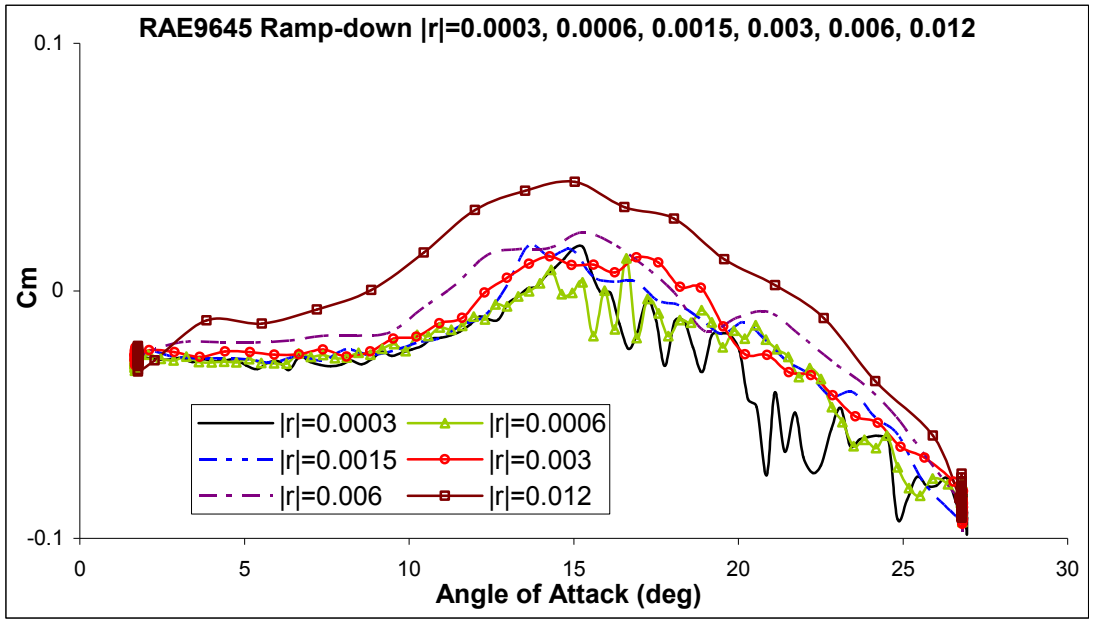

Figure 59 Ramp-down Cm coefficients for |r|=0.0003, 0.0006, 0.0015, 0.003, 0.006 and 0.012

For pitch rates higher than 120 deg/s the aerofoil response may be considered to be fully dynamic. It can be seen in Figure 60 that at the highest angular speeds the Cm lines, from the maximum angle of attack, start to move toward positive values of the coefficient, but when they reach the maximum the curves drop suddenly to move up

again and carry on with the typical Cm shape already observed for the lower pitch rates. Beside this characteristic peak, all the curves present behaviours similar to the lower angular speeds and to the Cm line obtained by Glasgow University experiments (Figure 38). The explanation to this behaviour may be found by observing and comparing the Cm and Cn curves together with the unsteady pressure profiles. The tip of the Cm curves is always slightly delayed, in term of angle of attack, with respect to what was defined as the end of the convection phase during the re-establishment of fully attached flow. Figure 57 illustrates this well defined location on the Cn curves. The subsequent rise in Cn indicates that boundary layer re-establishment is fast. Such a re-attachment, from the leading edge to the trailing edge of the aerofoil, is also manifest in a big difference in the pressure field and a movement of the centre of pressure. This displacement gives an abrupt drop of the line right after the onset of the re-attachment process.

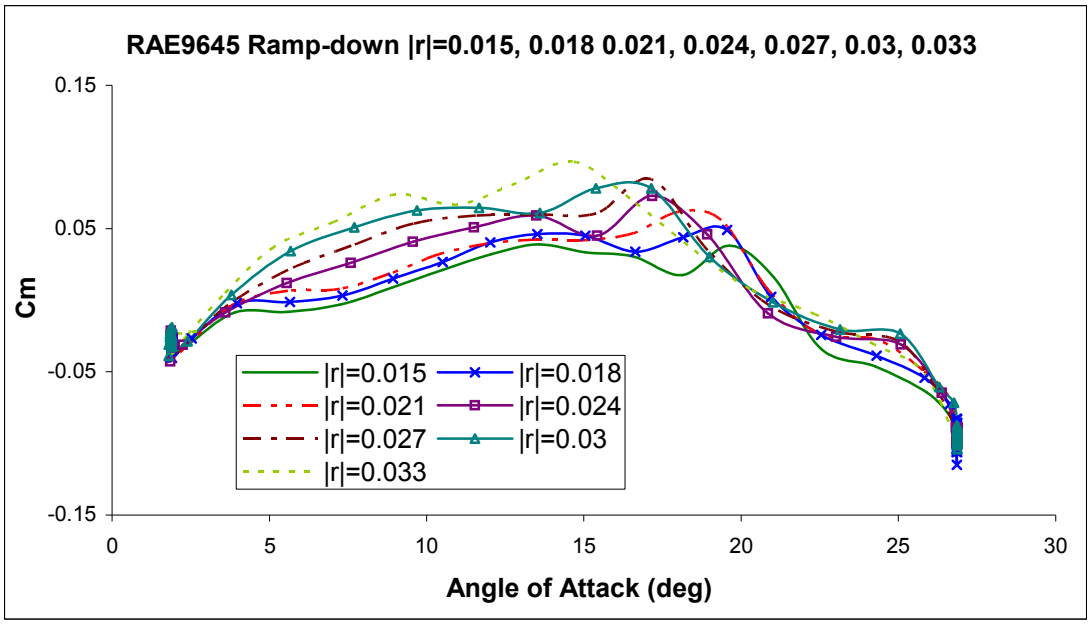

Figure 60 Ramp-down Cm coefficients for |r|=0.015, 0.018, 0.021, 0.024, 0.027, 0.03, 0.033

In fact, looking at the pressure field [76, 77] brings to the same conclusions and highlights how the pressure on the upper surface changes along with the angle of attack. Figure 61 presents the "pseudo-3D" graphs for three different tests: two at high pitch rates (b and c) and one at a low angular speed (a).

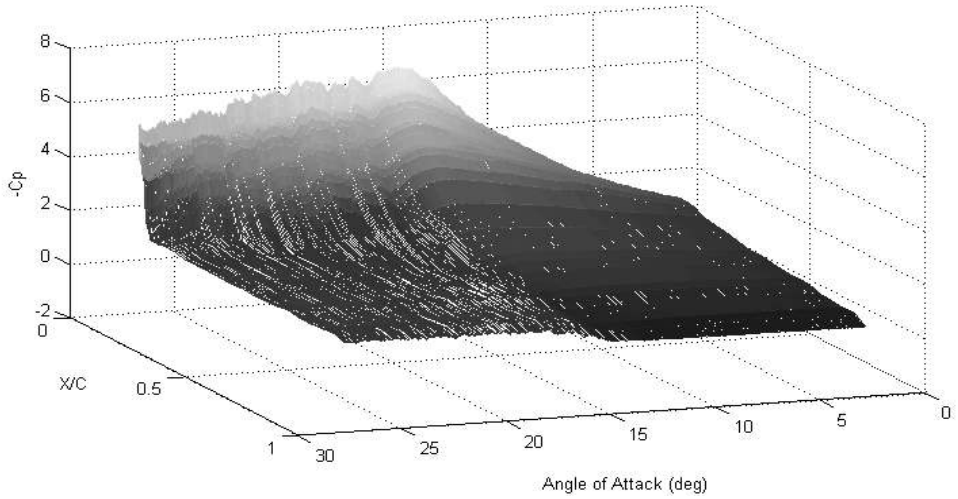

Figure 61 (a)

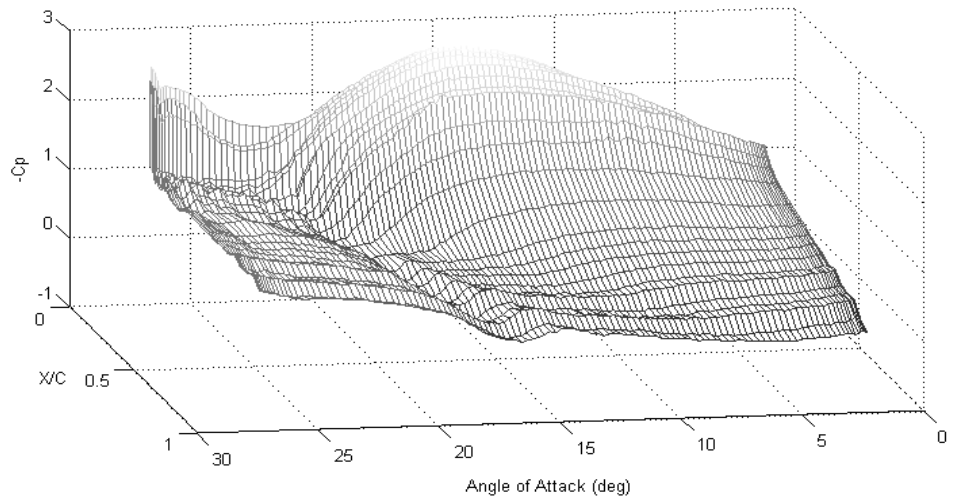

Figure 61 (b)

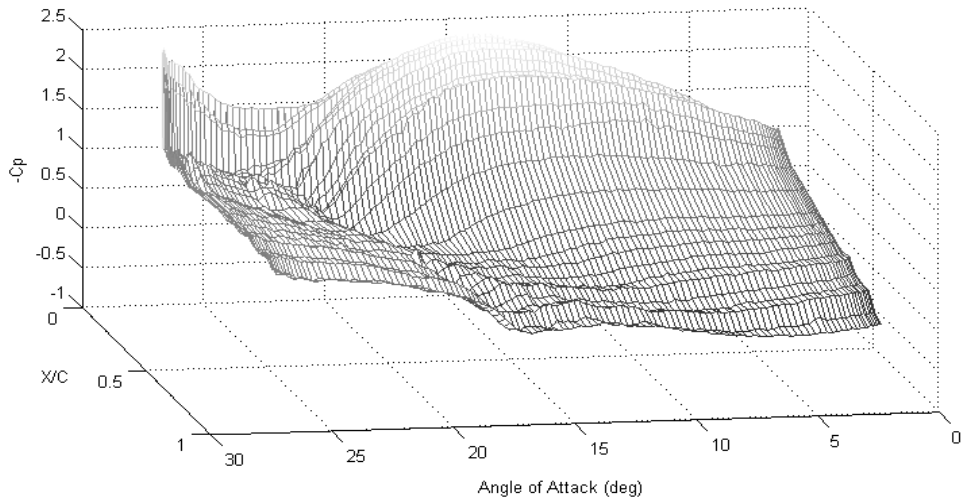

Figure 61 (c)

Figure 61 Comparison between Cp coefficients for different pitch rates (a-> r=0.0006 [6 deg/s], b->r=0.024 [240 deg/s], c->r=0.027 [270 deg/s])

It may be observed, once the re-attachment process is initiated, that the Cp changes very suddenly for the highest speeds compared to the lowest one. Moreover, for (b) and (c) the values of Cp at the leading edge, and close to it, are very similar and start to rise at about the same incidence, indicating that the process begins not only in one point of the profile leading edge, but almost at the same time over a certain length of the fore part of the chord. The re-attachment process is, instead, more progressive in (a).

The Ct coefficient closes the analysis of the ramp-down test. Some examples of Ct curves are given in Figure 62. However, the Ct, during ramp-downs, is not of primary importance in the present work. The results reported show the typical trend for the Ct coefficients and no anomalous behaviour can be notice throughout the entire range of pitch rates tested by QinetiQ.

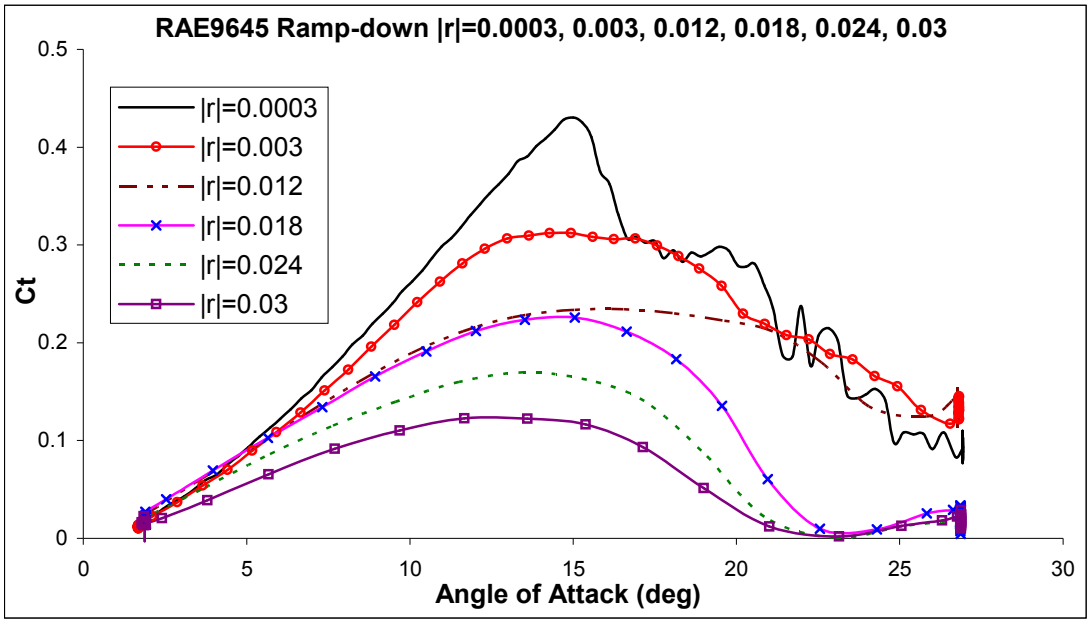

Figure 62 Ct coefficients for some pitch rates tested by QinetiQ

4) Oscillatory

Oscillatory data from QinetiQ data set cover a wider range of reduced frequencies and combination of mean angles and amplitudes than Glasgow series. What was said for the previous sinusoidal data (Chapter 2.1) applies to the QinetiQ data. The QinetiQ data may be used, however, to underline a few more features that could not be so clearly seen in the Glasgow data. The first evident aspect is the influence of the reduced pitch rate on the Cn curve for low angle of attacks. In Figure 63 (a, b and c) the classic behaviour of aerofoil, whilst undergoing sinusoidal pitching motions below its stall, is illustrated.

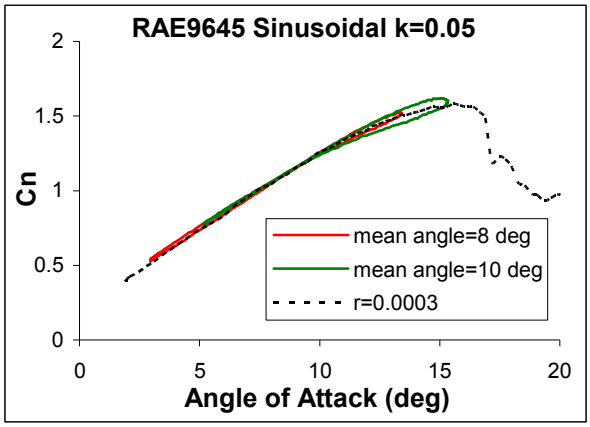

a) Sinusoidal test (k=0.05) for mean angle of 8 and10 deg and amplitude of 5 deg

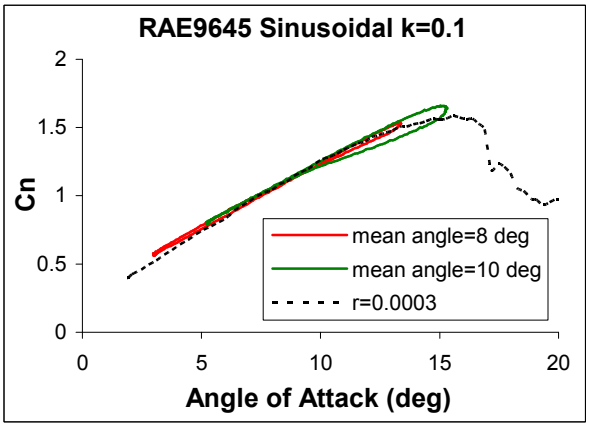

b) Sinusoidal test (k=0.1)for mean angle of 8 and10 deg and amplitude of 5 deg

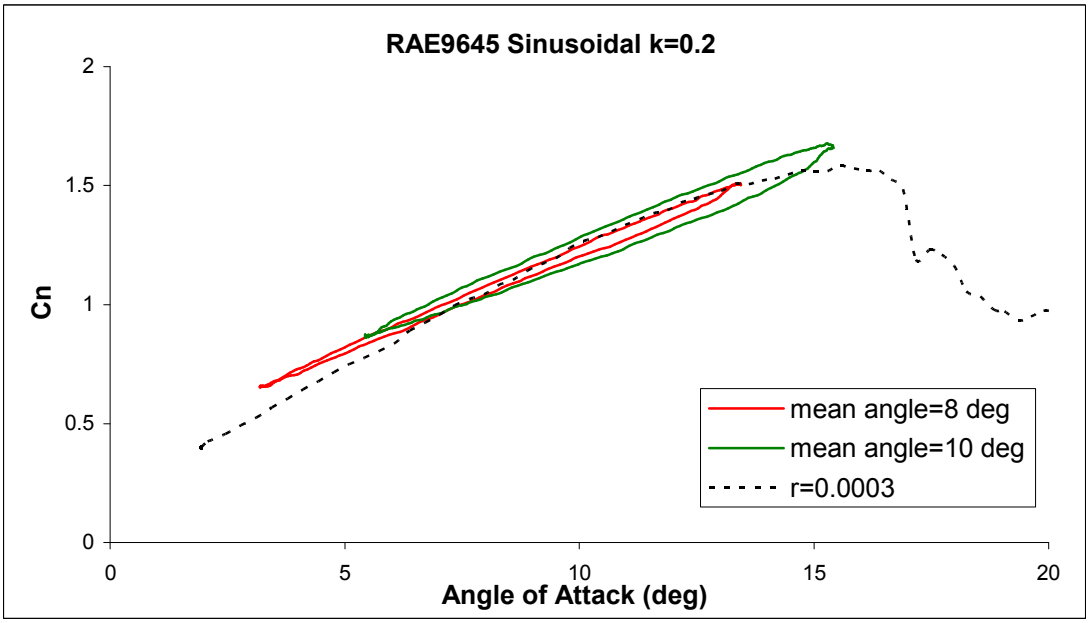

c) Sinusoidal test (k=0.2) for mean angle of 8 and 10 deg and amplitude of 5 deg

Figure 63 Sinusoidal tests performed at three different pitch rates for angles of attack below the static stall incidence and slow rump-up r=0.0003

However, if the pitch-up parts of the loop appear similar, during the pitch-down process, the reduced frequency affects the values of Cn. As the frequencies increase so does the hysteresis. This outcome is very marked and it is due to the so-called induced camber effect that, for the same angle of attack, produces lesser values of Cn as the absolute angular speed increases. Figure 64 and Figure 65 present three Cn and Cm graphs for reduced frequencies of 0.2 (5.6 Hz), 0.15 (4.2 Hz) and 0.05 (1.4 Hz) at higher maximum

incidence. For the lowest pitch rate the profile displays a light dynamic-stall as may be noticed by the moment break around 17 deg. At this incidence the aerofoil is about to change direction.

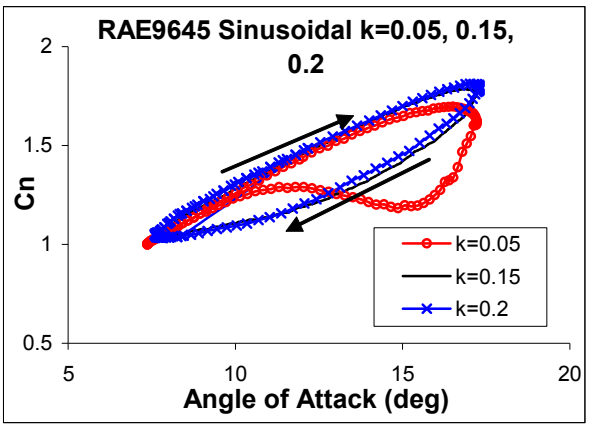

Figure 64 Cn for oscillating tests up to17 deg of incidence (k=0.05, 0.15 and 0.2)

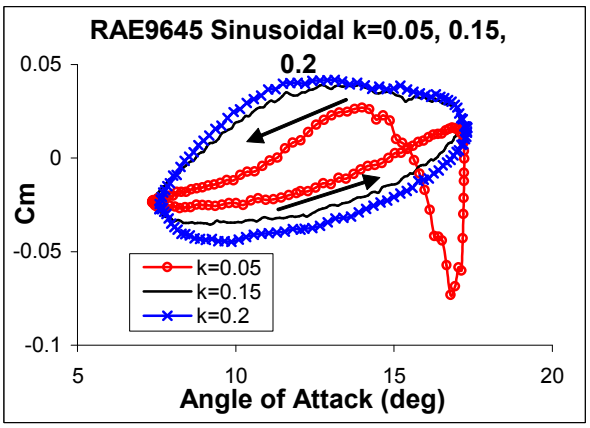

Figure 65 Cm for oscillating tests up to 17 deg of incidence (k=0.05, 0.15 and 0.2)

The aerofoil does not appear to develop a substantial stall vortex on the upper surface (no Cn overshoot), but simply appears to display a quasi-steady stall. When the profile changes its motion, the Cn curve shows the classic return from the stalled state, with the re-establishment of a fully boundary layer that begins around 14 deg.

The other two cases have the same nominal angle of attack forcing, but higher reduced frequencies. The Cm graphs do not present any break and any angle and the Cn curves follow the behaviour shown in Figure 63 for attached flow. The dynamic effect delays the stall. This is also due to the induced camber, because this effect lightens the leading edge pressure gradients for a given value of lift and hence the separation and stall are delayed to higher angle of attack [73]. If the reduced frequency is high enough this effect can prevent flow separation to be initiated at any point of the cycle (k=0.2, 0.15).

These data illustrate how the stall can be delayed (dynamic overshoot) by the motion of the aerofoil and that the higher the frequency the longer the delay. The delay does, however, have a limit called the onset of the dynamic-stall. This aspect is not normally observed in the Glasgow data because of the test points chosen. Figure 66 and Figure 67 present two reduced frequencies (k=0.15, 0.2), for an amplitude of 5 deg and mean angles from 14 deg up to 20 deg. The effect throughout the different mean angles is clear.

For the lower frequency (Figure 66) stall occurs for all mean angles of attack. For the 14 deg mean angle of attack there is no evidence of deep dynamic stall and hence no significant stall vortex. For all other mean angles the effect on Cn of stall vortex can be seen clearly and a secondary vortex is evident for the two highest mean angles. As may be expected (Figure 67) at the higher frequency the stall is delayed beyond that for the lower frequency. Also, at the lowest mean angle, the stall is suppressed. At the largest mean angle a large secondary vortex is evident.

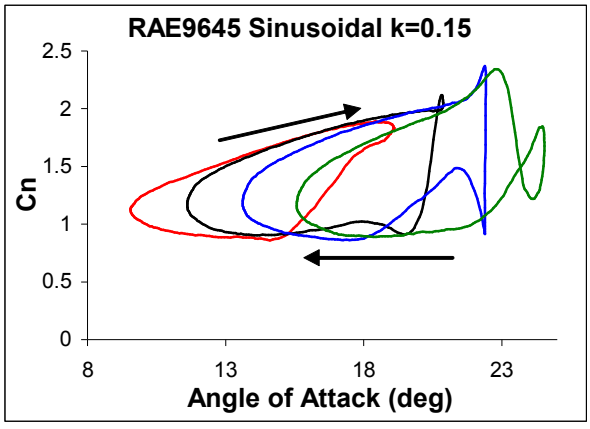

Figure 66 Re-attachment process for 4.2Hz (k=0.15), same amplitude (5 deg) and different mean angles (14, 16, 18 and 20 deg)

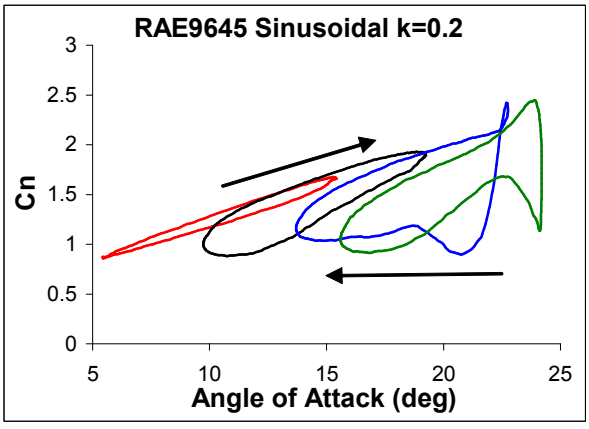

Figure 67 Re-attachment process for 5.6Hz (k=0.2), same amplitude (5 deg) and different mean angles (14, 16, 18 and 20 deg)

3 Comparison between the data

It has been previously recognized, that different wind tunnels, and different test set ups, can, for the same aerofoil, yield different results (Wilby [61]). This Chapter will compare the QinetiQ and Glasgow sets for the RAE 9645 aerofoil.

Unfortunately, no static tests were performed by QinetiQ. For the present work the comparison, for the static behaviour, was made using the QinetiQ slowest ramp-up test of 3 deg/s. As stated in the previous Chapter, these two sets of tests were carried out for different pitch rates, and with different test models, in both of the Glasgow University low-speed wind tunnels. The two wind tunnels have different working sections. First, in the primarily octagonal Handley Page tunnel and, second, in the essentially rectangular Argyll tunnel. Since the experiments were carried out in different wind tunnels it is to be expected that the different flow characteristics of each tunnel will affect the aerofoils behaviour. The precise nature of each tunnels flow states are unavailable at present because the Argyll wind tunnel was never fully re-calibrated after the transfer from Hatfield and its re-construction at Glasgow. The precise differences that one would look for are flow angularity, constancy of working section velocity over the entire area, the static pressure along the working section centre line together with turbulence intensity. Unlike the Argyll wind tunnel, the Handley Page tunnel was fully calibrated (over many months during 1982 by Richard Gordon) and flow angularity in the cross stream direction (yaw) was -1 deg at the centre line and the vertical value was 0.5 deg. Except close to the walls, the percentage difference in tunnel speed was 2%. Turbulence measurements were made, but are no longer available.

The second series of tests used a QinetiQ model designed to fit in the formally RAE eight foot transonic wind tunnel at Bedford (UK). The model profiles were identical since they had both been constructed using the same mould plug.

The two profiles were, however, instrumented with different makes of transducers and the data were taken and processed with a different data acquisition system from the Glasgow system. Hence it is not possible to discern completely the influence of the different facilities from the different set ups. This is primarily due to the fact, that the author was not present or involved in the experiments. Geometrically, however, the Argyll wind tunnel data were obtained from a model that did not completely span the working section and was mounted horizontally. At one end a "blister" was put around the support, that was in the tunnel, in an attempt to smooth out the flow (see Figure 46 which illustrates the support in the working section). Additionally, the working section had a floor raised by about 63mm due to the presence of a moving ground. The effect this had on the tunnel flow has never been investigated. The question to be answered is: did the tunnel modifications affect, and in which way, the flow angularity at the measuring station?

Hence, the observed differences may be taken as an indication how the test environment may affect the aerofoil behaviour. On the other hand, the similarities, analogies, common trends and relations will point out what can be considered independent from the test environment. This gives a more confident attitude in assessing tests from different facilities for a given aerofoil.

3.1 Static

The comparison presented in this section is not between two static tests performed in the two different wind tunnels and is due to the lack of the QinetiQ performing steady performance tests. Conversely, it seems to be possible, and reasonable, to use the slowest ramp-up tested in the Argyle wind tunnel as representative of the static behaviour for the QinetiQ profile. Although it was observed (Chapter 2), for the Glasgow aerofoil, that slow pitch rates may affect the aerodynamic coefficients (e.g. maximum Cn and Cn curve slope), for very low values of r, such as 0.0002/0.0003, the discrepancies with the static test may be assumed to be small. In this regard, the slowest QinetiQ ramp-up test was carried out at a reduced pitch rate equal to 0.0003 which may be considered to be reasonably representative of the static behaviour. Accordingly, these data were used for the steady performance comparison and referred to as quasi-static.

Figure 68 presents the two tests (static and quasi-static) along with the slowest Glasgow ramp-up (2 deg/s, r=0.0002) as an illustration of the effect of even slow ramp rates. Considering the two Glasgow tests, it may be observed that the Cn slope and Cn_{max} have increased in value while the angle of attack at which the maximum Cn occurs appears little affected. For this work, the most important aspect, with regard to the application of the Beddoes' model, is the percentage increase in the curve slope. Particularly, in this case, the specific increment is of about 1%. Accordingly, it may be expected that the QinetiQ quasi-static test would show the same kind of behaviour when compared to the corresponding static test. Hence, with the actual curve slope equal to ~0.108 deg^{-1}, it seems reasonable to assume that the static test would have had a gradient of about 0.107 deg^{-1}.

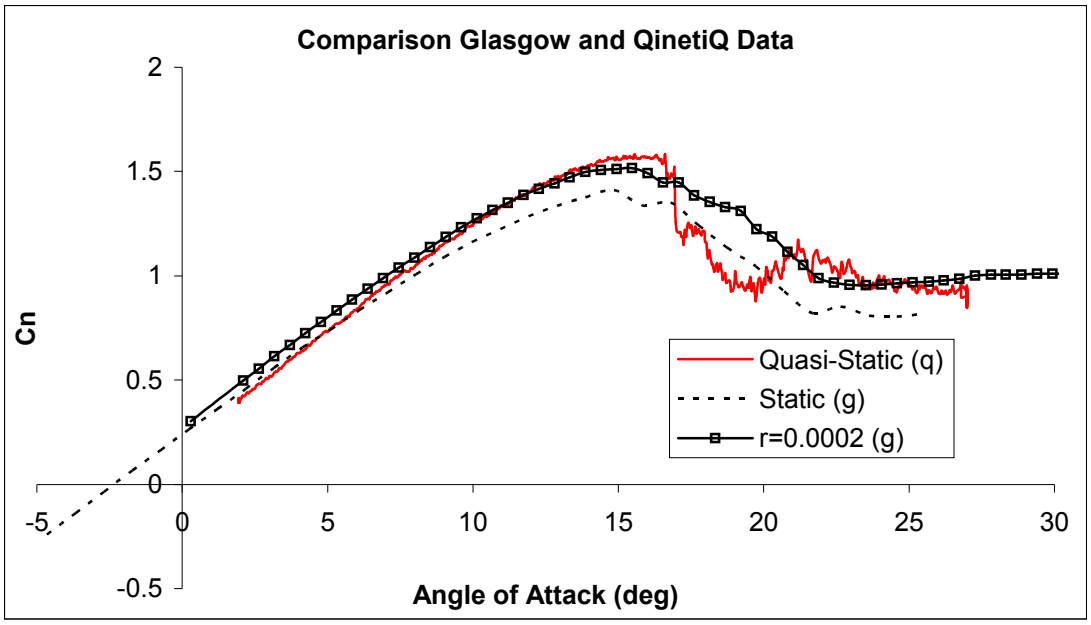

Figure 68 Glasgow static and r=0.0002 tests compared to QinetiQ test for r=0.0003

However, it has to be considered that all these assumptions are made comparing two behaviours from two different wind tunnels and different set-ups. Hence the relationships found between the data carried out from one tunnel may not be satisfied from another. Alternatively, finite wing theory could be adopted here to calculate the static test curve slope of the QinetiQ tests and, knowing that from the Glasgow data, the value found could be used as an indication of the goodness of the assumptions. The Cn slopes are given by equation 3.1 using the two different aspect ratios.

$$dCn/d\alpha = \frac{2\pi}{1+\frac{2\pi}{\pi AR}} \qquad 3.1$$

The two aspect ratios, for the Glasgow and QinetiQ profiles, are 3.22 and 4.8 respectively. Using eq.3.1 it can be found a ratio between the two curve slopes (QinetiQ dCn/dα over Glasgow dCn/dα) of 1.144. The value attained for the QinetiQ dCn/dα,

multiplying this number by the Glasgow curve slope, is 0.11. This value is close to the one found for r=0.0003 and to the one assumed for the static test. However, it must be remembered that eq. 3.1 relies on the assumption of an elliptical loaded wing. Because of the different set-ups, the pressure and lift distributions along the span were for sure different over the two models and, particularly, the Glasgow profile spanned the tunnel from wall to wall. It is not known the overall effect of the walls, but it is reasonable to accept that this condition did obtain a better $dCn/d\alpha$ than that predicted by an elliptical distribution of the lift. Nevertheless, it is concluded, that the assumption of a static $dCn/d\alpha$ equal to ~0.107 for the QinetiQ aerofoil is reasonable for the data here presented.

Although the QinetiQ test begins at an incidence of 1.9 deg, Figure 68 already suggests that each test has a zero lift angle that is different to that of the Glasgow curves. In fact, extrapolating the QinetiQ data to the value of zero-lift angle gives a zero lift angle of about -2 deg whilst that from the Handley Page wind tunnel was ~-2.3 deg. This difference may be due to the flow angularity in the Argyle wind tunnel, an offset in the incidence measurements or three dimensional effects of the flow around the profile. A specific reason can not be evaluated in the present work as the experiments were conducted autonomously by QinetiQ and there is no evidence of any of the reasons mentioned in the data recorded. Nevertheless, the difference is small and it does not appear to influence significantly the general conclusions. Figure 69 and Figure 70 present the pressure distributions for the two cases. As expected they are very similar and no major differences can be noted. However, the QinetiQ profile seems to have a sharper drop in the leading edge pressure after stall. This is also clear when looking at Figure 68.

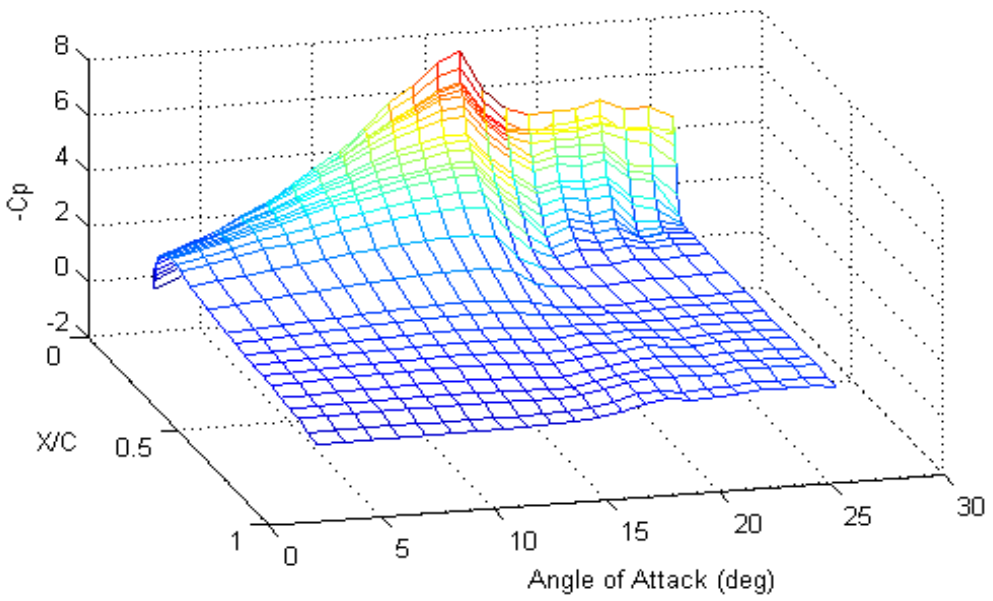

Figure 69 Pressure distribution for QinetiQ test at r=0.0003 (3 deg/s)

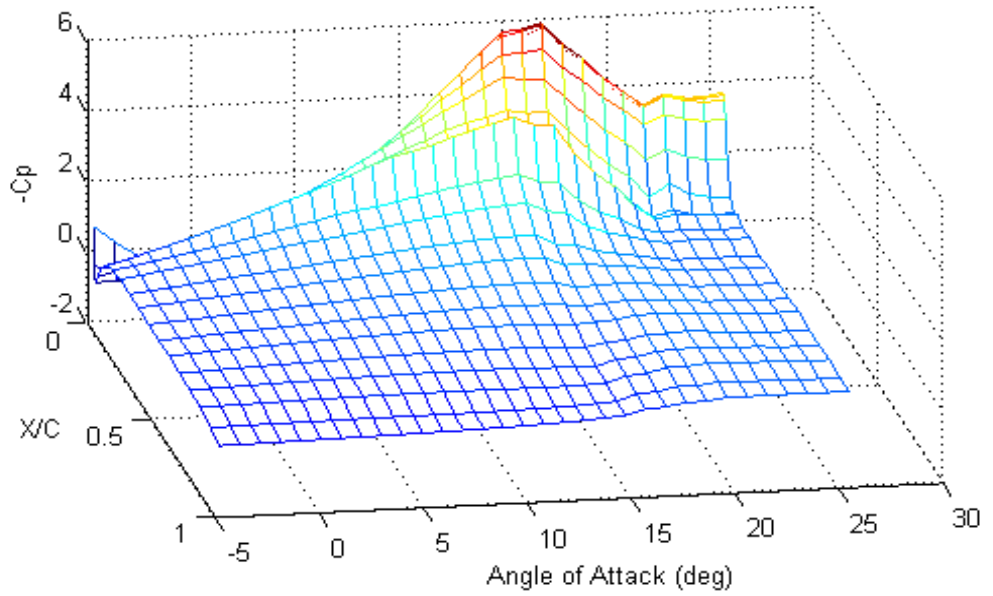

Figure 70 Pressure distribution for Glasgow's static test

3.2 Ramp-up

The leading comparative factor for the aerodynamic coefficients is the reduced pitch rate r. Hence, albeit the tests, in the two different wind tunnels, were performed for different pitch rates, the comparison can still be made for those which have equal or very similar r values. The reduced pitch rate (r) is here the only feature kept in account for a consistent assessment since the Mach and the Reynolds numbers were comparable for both set-ups. All the tests were performed within the "low-speed" aerodynamic range. The Mach number was about 0.12 and small variations between the tests points had no significant influence on the results. It has been also said [68] that, for the most of the profiles, and for reduced pitch rates lower than about 0.01, the stall process is usually categorized as quasi-static. The large enhancements in the force and moment profiles, for more severe ramps, do not exist. In the present work the comparisons for the two different wind tunnels are, then, only made for those tests that have r value greater than 0.01.

Although the RAE9645 develops a deep dynamic-stall at lower reduced pitch rates than 0.01, as shown in Table 9, there are no suitable comparable angular speeds below this value of r (the five that are available are highlighted). Figure 71 (g=Glasgow data, q=QinetiQ data) presents some of these five reduced pitch rates in Table 9. Qualitatively the profile tested by QinetiQ has a larger lift curve slope than that for the Glasgow data. Additionally it will be seen that the incidence range for the QinetiQ data is much lower than the Glasgow tests.

Pitch rate (deg/s)	r	Pitch rate (deg/s)	r
		2	0.000196
3	0.000297		
6	0.000595		
		7	0.000661
15	0.001487		
		20	0.001828
30	0.002975		
		35	0.003369
60	0.00595		
		79	0.007518
90	0.008925		
120	0.0119	120	0.011205
150	0.014875	160	0.014658
180	0.01785	200	0.017815
210	0.020825		
240	0.0238	240	0.023066
270	0.026775	280	0.02638
300	0.02975		
330	0.032725		

Table 9 QinetiQ (left) and Glasgow's (right) reduced pitch rates for ramp-up tests

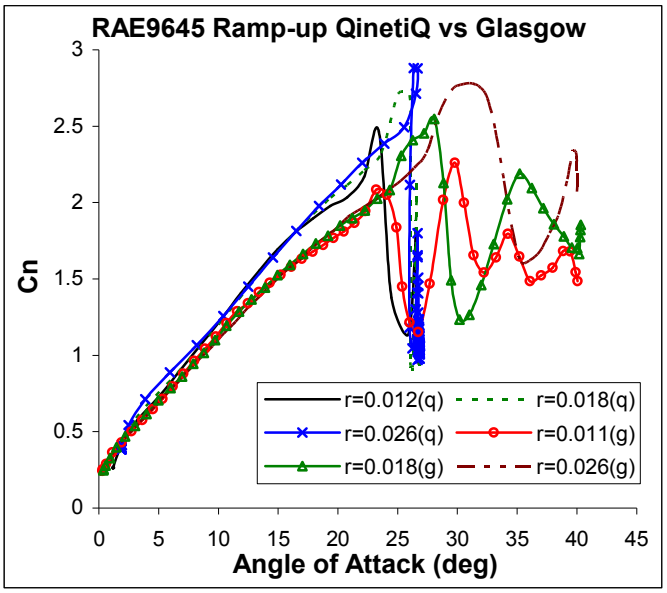

Figure 71 Examples of ramp-ups tests performed for r~=0.11, 0.18, 0.26 by QinetiQ (q) and University of Glasgow (g)

These Figures also highlight the evident differences between the two sets of data prior to the occurrence of the dynamic stall. Once initiated, the dynamic tests diverge and the QinetiQ data achieve larger Cn values. Hence this may have resulted in different amounts of trailing edge separation, vortex strenght and so stall development. The differences are probably due both to the geometric set ups and the better incoming flow's quality of the Argyll Wind Tunnel. As α increases, both models undergo deep dynamic-stall. Two tests were chosen for further consideration and these correspond to a reduced pitch rate of 0.015 and 0.018 respectively (Figure 72 and Figure 73).

When the dynamic stall takes place its onset and effect are clearly visible in the Cn graphs. Figure 72 and Figure 73 present the two Cn curves for each test together with

the “static” or “steady” data (both steady data are Glasgow’s). Intriguingly, albeit the different Cn starting values, the inception of the dynamic stall appears to be at the same angle for both aerofoils, as indicated by the rapid Cn build up due to the dynamic-stall vortex (DSV) formation. The vortex continues to develop over the surface until it is swept away by the oncoming stream and the lift collapses.

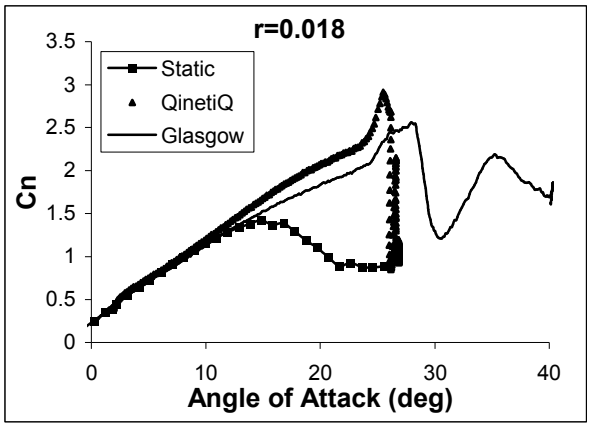

Figure 72 Cn vs. Angle of attack for r=0.018

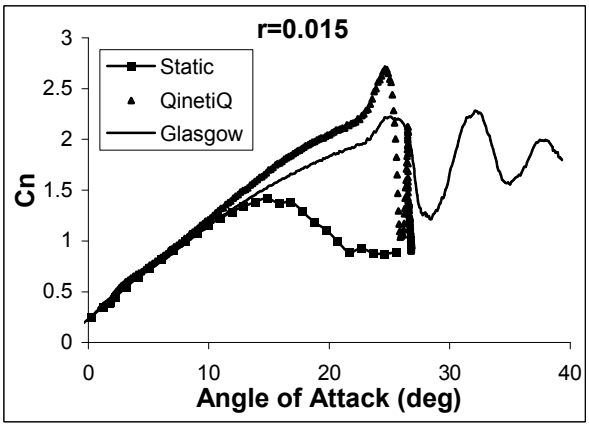

Figure 73 Cn vs. Angle of attack r=0.015

Again the limited range of the QinetiQ data is obvious and it masks the subsequent nature of the stall when viewed in terms of incidence. Nevertheless the data are adequate to asses the inception of the dynamic stall through all the aerodynamic coefficients depicted Figure 74 and Figure 75 for the Ct and Figure 76 and Figure 77 for Cm. the criterion adopted for the dynamic stall is the angle at which the Ct reaches its maximum; as per Sheng et al. [70]. Compared to the alternatives, this criterion is well defined. However the phenomenon, along with comparisons between different ways to determine its onset, will be examined further in Chapter 4 where the reasons of this choice are explained. The trend lines of the Ct are shown in Figure 74 and Figure 75. The two Ct, per each graph, have the same behaviour and, although the maximum values are different, the important aspect is that they occur at the same angle of attack for the

corresponding reduced pitch rate. This indicates, in each case, one single angle for the onset of the dynamic stall.

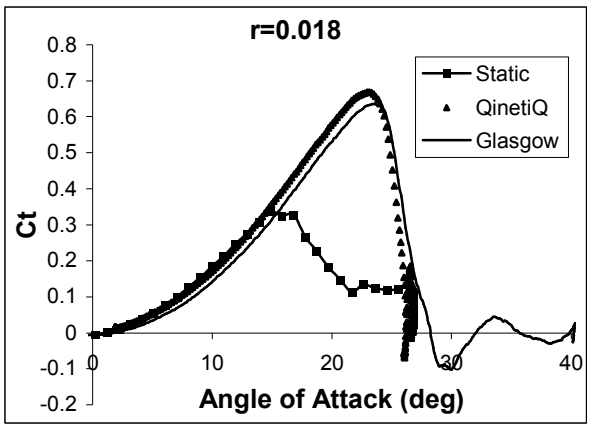

Figure 74 Ct vs. Angle of attack for r=0.018

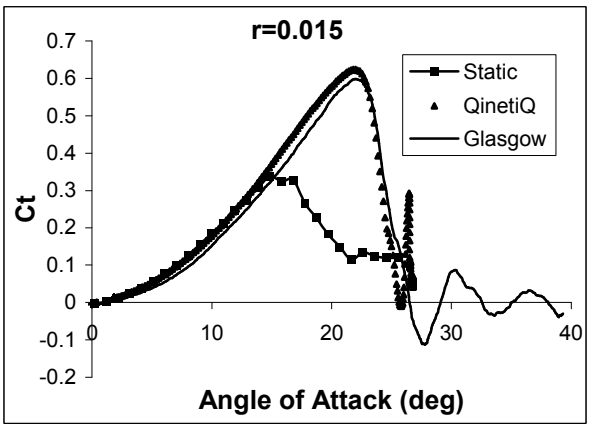

Figure 75 Ct vs. Angle of attack r=0.015

With regard to the Cm, except for some expected differences in the values, the Cm lines follow the same patterns (Figure 76 and Figure 77) and it may be observed that the Cm breaks, like the Ct, occur at the same angles. The two profiles reached close minimum values. The QinetiQ data, however, present a more abrupt change in the slope. This could be foreseen also by the higher climb rate of the Cn curves in Figure 72 and Figure 73.

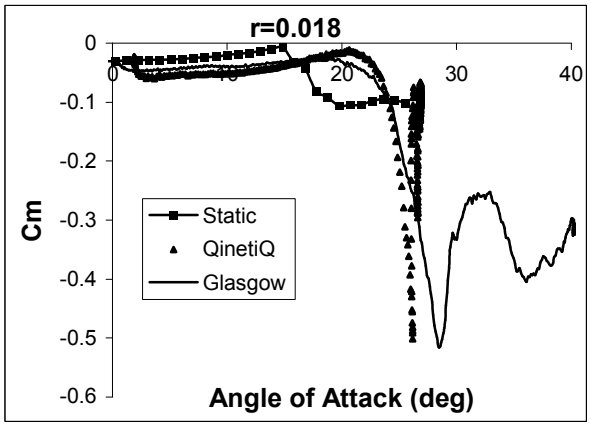

Figure 76 Cm vs. angle of attack for r=0.018

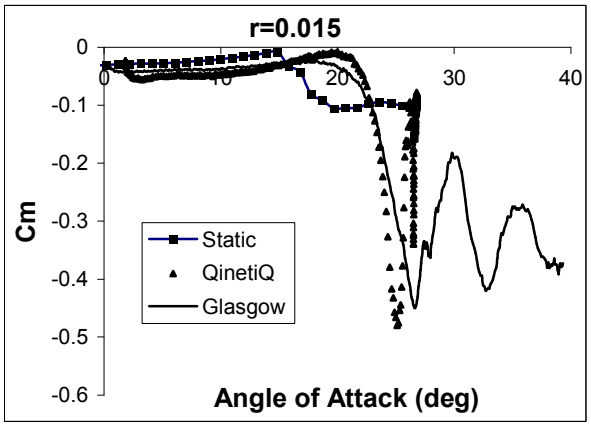

Figure 77 Cm vs. angle of attack r=0.015

Figure 78 to Figure 81 illustrate the temporal response of the associated pressure distributions, since they are for ramp data they are presented in terms of incidence. As a consequence of the different ways in which the tests were recorded, the University of Glasgow data appear to have a better resolution.

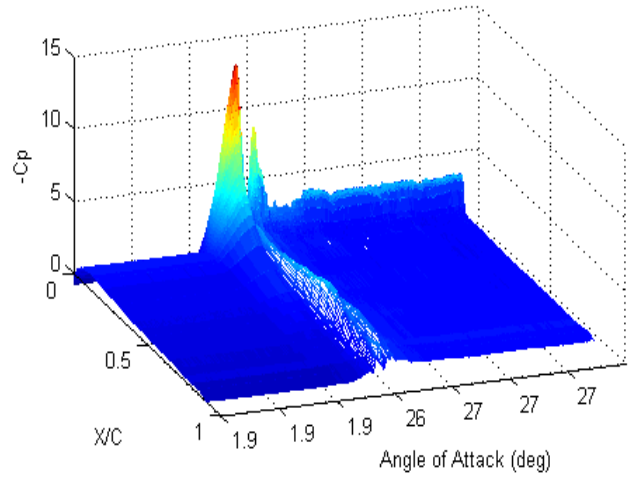

Figure 78 QinetiQ test for r=0.015

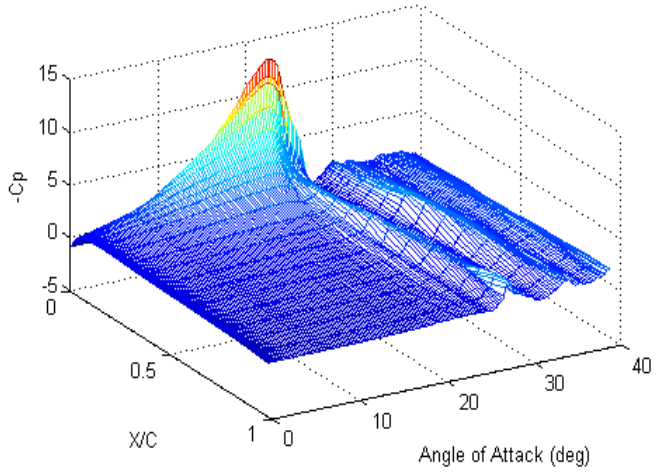

Figure 79 Glasgow test for r=0.015

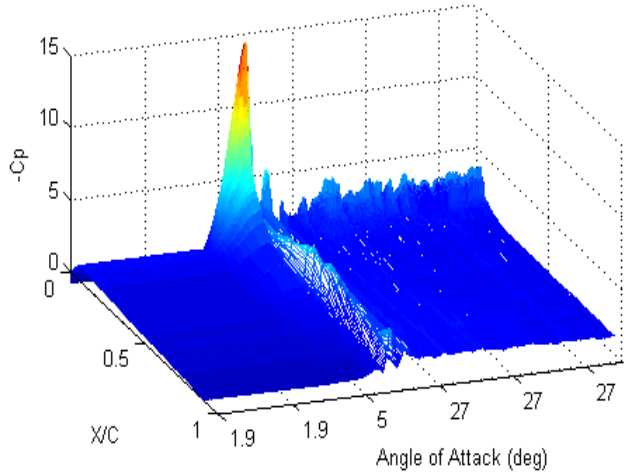

Figure 80 QinetiQ test for r=0.018

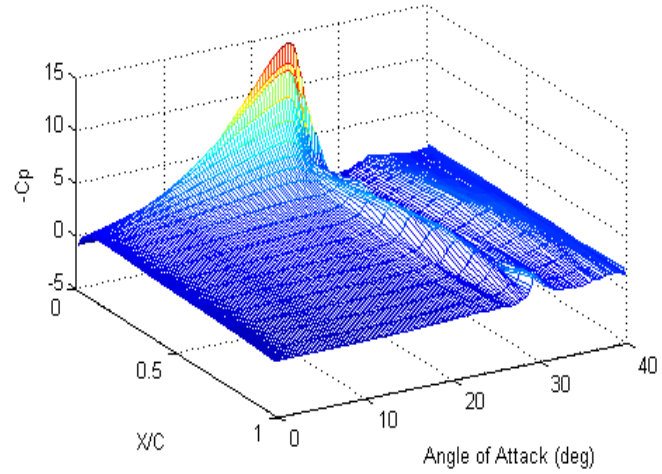

Figure 81 Glasgow test for r=0.018

It is clear that for both data sets there is an initial suction rise close to the leading edge. The QinetiQ data appear to have a more rapid build up, but that appearance is simply due to the plots initial profiles. These are for the aerofoils at fixed incidence just before

the ramp start. Both data sets illustrate the suction wave of the dynamic-stall vortex as it travels the chord. The peak suctions during this phase show slight unexpected differences in as much as there is a double peak in the QinetiQ data. The second wave in the Glasgow data, due to vortex shedding, is also present in the QinetiQ data, but less clear due to the data compaction. It is evident, however, in the region of the trailing edge (it disappears at the fastest frequencies and this is simply due to the stop angle of the ramp: Glasgow 40 deg and QinetiQ 27 deg). The difference can be further illustrated with Figure 82 and Figure 83, where the angle of attack against the time is plotted. Clearly the Glasgow data are recorded over the complete aerofoil motion, whereas the QinetiQ data included much when the aerofoil was stationary. However, the general behaviour and shape for the two data sets are similar as are the maximum Cp values achieved.

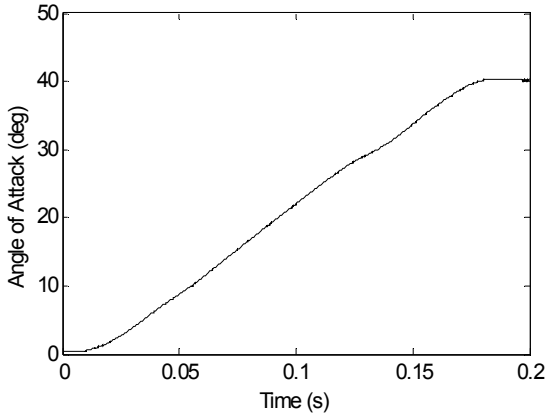

Figure 82 Angle of attack against time for Glasgow test (r=0.018)

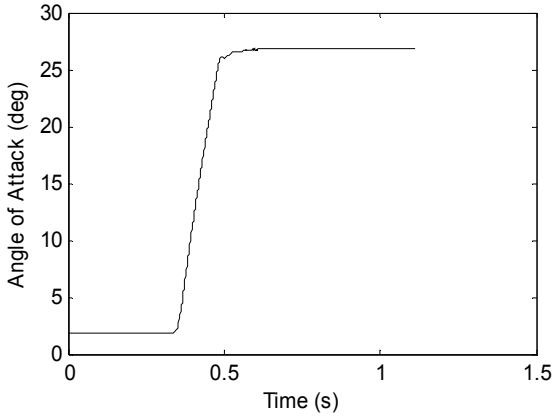

Figure 83 Angle of attack against time for QinetiQ tests (r=0.018)

Plotting the aerodynamic coefficients against non-dimensional time, instead of incidence, provides a better illustration of the behaviour of the QinetiQ aerofoil during the phases after the inception of the dynamic stall. Similarly the corresponding pressure

distribution plotted against non-dimensional time gives a clearer presentation for the QinetiQ data. In Figure 84 the Cn coefficients and the angles of attack are plotted for three different pitch rates. The QinetiQ data were shifted to have the start of the ramp motions to coincide with that of the Glasgow data. This "phase locking" is most noticeable in Figure 84 (f).

Immediately noticeable is the similarity of the frequency of the vortex moving along the chord and shedding in the wake. The period of these two events is very similar, if not equal, for each r. More interesting, is that the second vortex, for the QinetiQ tests, is always shed during the steady part of the motion, whilst the Glasgow one model is still in motion. This leads to the conclusion that the second vortex, beside differences of the strength, may not be affected by the motion of the aerofoil, but its inception and timescale may be influenced by other factors such as the Stroutial number of bluff bodies. The second observation that can be made is about the forcing. Figure 84 (b, d and f) shows that the two aerofoils were follow very similar paths during the constant part of the ramp-up tests. Obviously the two lines begin to diverge when the QinetiQ profile starts to decelerate towards the end of the test.

Plotting the QinetiQ pressure data for the ramp-up part of test, against non-dimensional time, gives a better illustration of the pressure profile development. It may be observed (Figure 85 and Figure 86) that the second peak mentioned early in this Section (see Figure 78 and Figure 80) is the second wave as observed in the Glasgow data. Qualitatively, therefore, the flow phenomena of both data sets are similar.

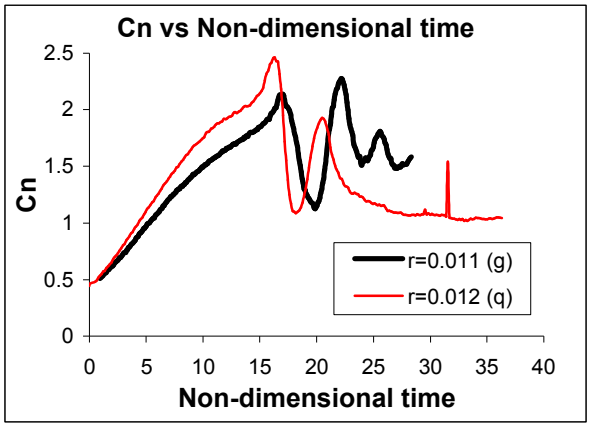

(a)

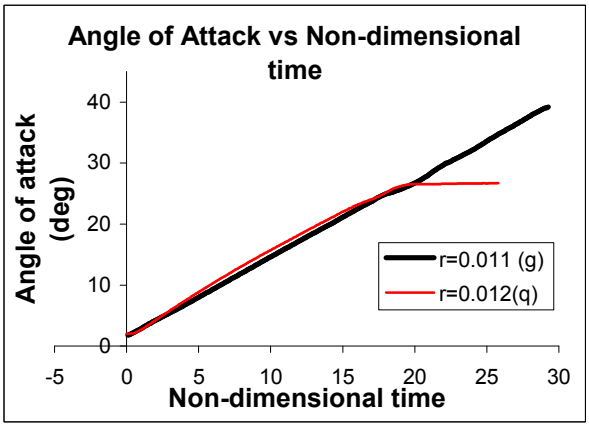

(b)

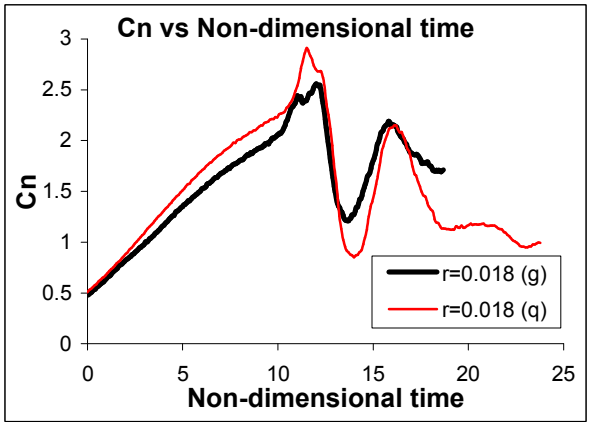

(c)

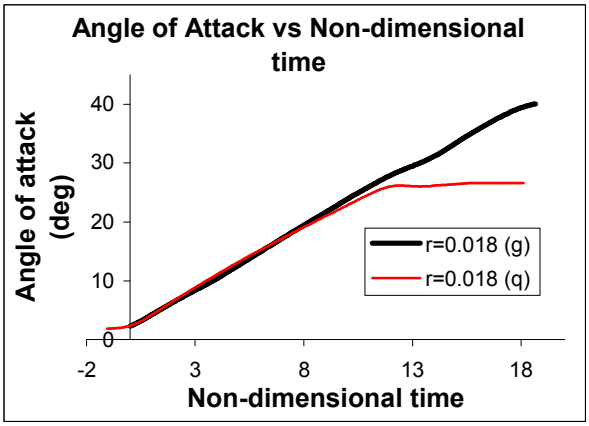

(d)

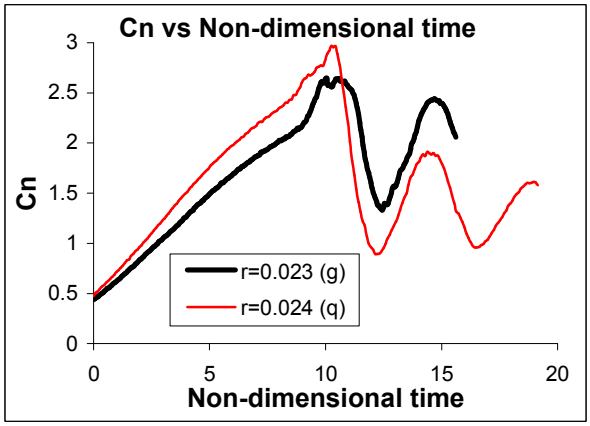

(e)

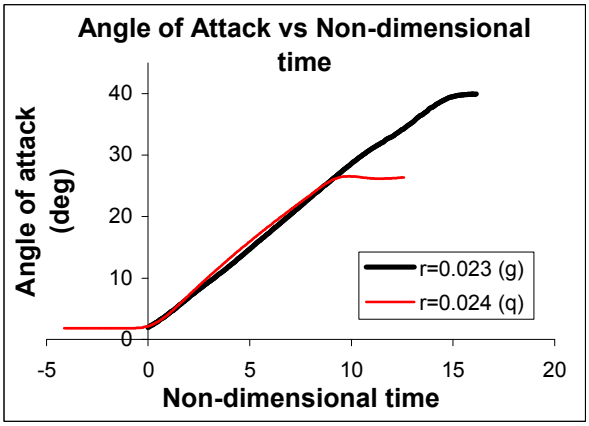

(f)

Figure 84 Glasgow and QinetiQ Cn coefficients and angles of attack plotted against non-dimensional time for three different reduced pitch rates.

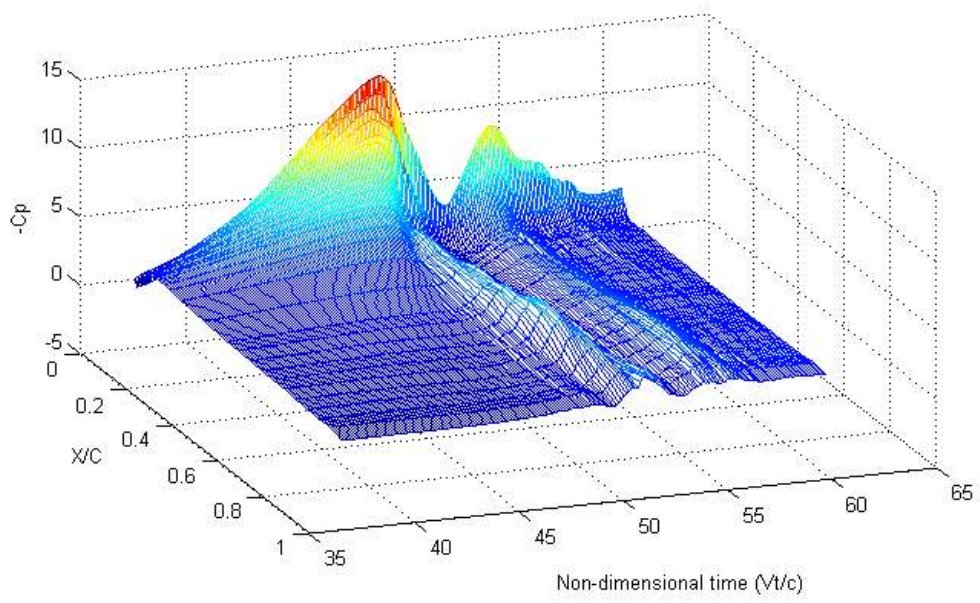

Figure 85 Pressure distribution against time on the QinetiQ aerofoil for r=0.015

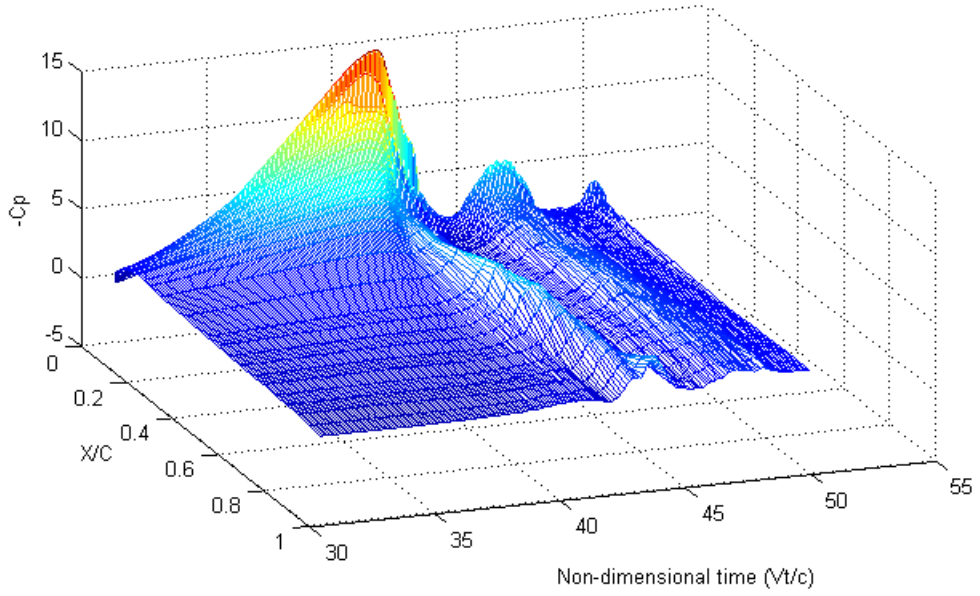

Figure 86 Pressure distribution against time on the QinetiQ aerofoil for r=0.018

3.1.1 Discussion

Other factors that may influence the pressures and hence the coefficients include:

- The test procedure and the data recording
- The different test environments

The data acquisition systems were different, with different sensitivities and different transducer distributions. The two wind tunnels were very different both by sections and (suspected) by the quality of the free stream. These two factors could lead to different results in terms of pressure or maximum and minimum absolute values. The more noticeable differences were for the lift coefficient, rather than for thrust and moment coefficients. This implies that, despite the different absolute values of Cn for a given angle of attack, the two pressure distributions over the surfaces at the same incidence are mostly similar. Thus, only their integrated coefficients (resultant forces) are most obviously affected by the test environment; a result worthy of further investigations.

Conversely these issues do not seem to affect the dynamic-stall onset of the airfoils and the overall results, for the stall onset, were the same for both experiments. As was previously mentioned, it is important, for the helicopter flight envelope, to know the dynamic-stall inception in order to avoid dangerous loads for the blades and the initiation of non-linear hysteresis. Accordingly the observation of stall onset similarity is an important result. The observed independence of the phenomenon for the two test set-ups may be observed in Figure 87. This Figure presents all the incidences corresponding to the associated Ct breaks (the angle of attack at the maximum value of Ct) against the reduced pitch rate r. These are for all the tests carried out by the University of Glasgow and QinetiQ. It can be noticed that for the tests in Table 10 the values found for the

onset are very close. Especially for the two analysed in detail, where the reduced pitch rates were the same, the stall onset angles co-incide.

Pitch rate (deg/s)	r	α Ct$_{max}$	Pitch rate (deg/s)	r	α Ct$_{max}$
			2	0.000196	15.5
3	0.000297	16.5			
6	0.000595	16.9			
			7	0.000661	16
15	0.001487	17.2			
			20	0.001828	16.5
30	0.002975	18.1			
			35	0.003369	17.8
60	0.00595	19.1			
			79	0.007518	19.8
90	0.008925	20			
120	0.0119	21	120	0.011205	21.2
150	0.014875	22	160	0.014658	22.3
180	0.01785	23	200	0.017815	23.5
210	0.020825	23.8			
240	0.0238	24.7	240	0.023066	25.2
270	0.026775	25.3	280	0.02638	26.4
300	0.02975	25.8			
330	0.032725	26.3			

Table 10 Comparison between QinetiQ (left) and Glasgow's (right) incidences for maximum Ct

Figure 87 also illustrates another central aspect of the two aerofoils' behaviour. Over all the range of pitch rates tested the angle of the dynamic-stall onset, for both data sets, increases linearly with the reduced pitch rates for r ~> 0.01.

It should be noted, however, that when the reduced pitch rate is equal or greater than ~0.024, the onset values start to deviate from the trend line. This refers to the last three tests, performed by QinetiQ. This is primarily due to a limitation of the test set-up, since the maximum angle of attack reached was always 27 deg. Towards the end of the

pitching up motion the angular speed becomes, necessarily, non linear, as the rotation has to slow down, and the angle of attack of the maximum Ct is affected by this. This aspect was also observed by Sheng et al. [70].

Furthermore, as noted previously (Chapter 2), the RAE9645 shows the presence of the dynamic-vortex for frequencies below r=0.01. As illustrated in Figure 87 this linearity can be truly extended backwards to include almost all the reduced pitch rates. For the RAE9645, this behaviour follows what it was shown by Wilby [79] that, beyond a certain reduced pitch rate, a linear relationship exists between the onset of dynamic stall and the reduced pitch rate. The value of 0.01 can be then taken as the upper minimum value for the existence of a DSV, but for the profile here examined, the linear relation can extend to lesser r.

Although the linear relationship between the DSV onset and the reduced pitch rate was already noticed for other profiles [80], and here confirmed for the RAE9645, the data were only from Glasgow and obtained using the Handly Page wind tunnel. This result leads to the important conclusion, that the dynamic-stall onset is not influenced by the two different test environments.

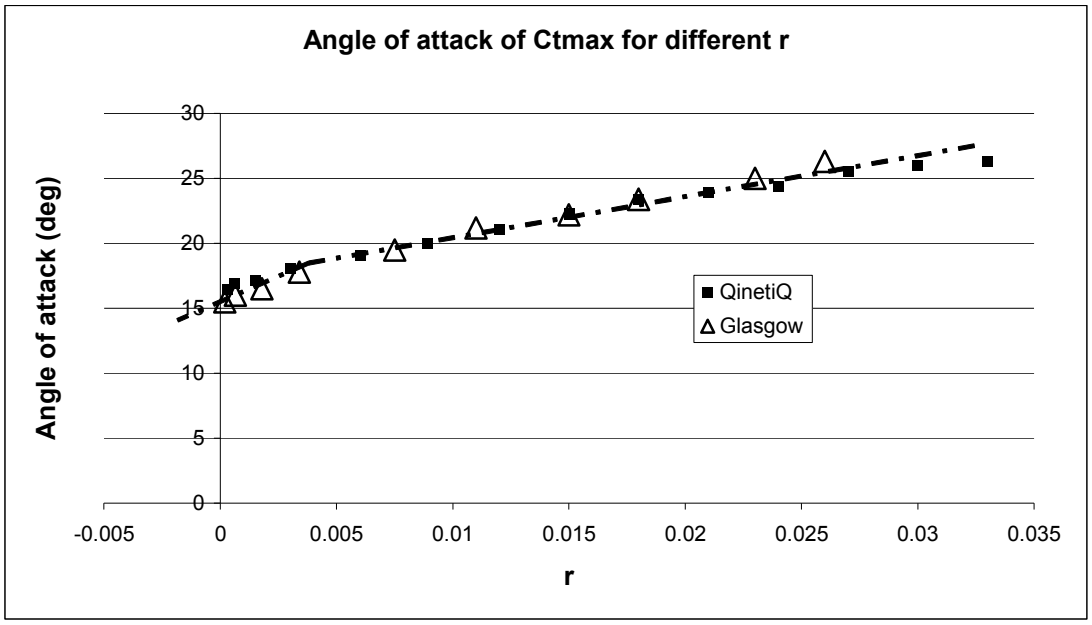

Figure 87 Angles of attack for Ct breaks against the reduced pitch rate

Figure 87 shows that, for the RAE9645, this linearity cannot be extended back as far as the {ordinate-abscissa} for it ceases at a reduced pitch rate of 0.006. It can be seen, however, that, for the other tests with smaller r, another linear relationship exists but with a different gradient. Albeit the tests are few, it is clear that the dash line closely fits the data and a linear approximation can be adopted. The two lines meet at about 0.004 that can be assumed to be the first reduced pitch rate where the dynamic stall starts to appear for the RAE9645. In other words, it is the transition point at which the flow changes from quasi-static to fully dynamic stalling.

3.2 Ramp-down

For the process of re-establishing attached flow from the fully stalled state it has been observed [11, 12, 34, 68] that it comprises of two different processes. First, a convective

phase in which all the large eddy/vortical flow on the upper surface is removed by the action of the free stream. Second, a motion dependent phase in which the fully developed boundary layer forms. These two phases may co-exist, but it is likely that that co-existence will diminish as pitch rate (|r|) increases. Typical Cn profiles for ramp-downs are presented in Figure 88 where it may be observed that, albeit there are significant differences in coefficient values, there is an undoubted qualitative similarity in form. That is, an initial relatively linear reduction in Cn until an approximate minimum is reached. The aerofoil displays no tendency to progress towards the steady data during the convective phase. Once the Cn minimum has been achieved the coefficients then tend to the normal values; this is the fully attached boundary layer being established.

That stated above has recently been expanded by Sheng et al. [34, 68] who had little difficulty in obtaining the values of Cn_{min}, and hence the assumed termination of the convective phase, from the Glasgow data base. This particular aerofoil was not included in that study and, by inspection of Figure 88, it may be seen that the Glasgow data is more indistinct than those from the QinetiQ tests. None the less values of Cn_{min} have been assessed and presented in Table 11. It may be noticed the Cn_{min} is achieved at higher angles of attack for the QinetiQ data, albeit the differences are relatively small. As the reduced pitch rate (|r|) decreases the α_{Cnmin} values tend to the same value for both aerofoils (Figure 89). Typical profiles for Cm and Ct coefficients are given in Figure 90 and Figure 91. Once again, as with the Cn, there are significant differences in coefficient magnitude but also distinct similarities in the trends. This is in spite of the significant differences in pitch rate. Close inspection, however, will again show that the completion of the convection phase is similar. When considering Figure 92 a strong argument could

be posed against this statement, but a consideration of the temporal pressure distributions (Figure 93 (a) and (b)) will elucidate the differences in the trends.

Deg/s	|r|	α (deg)	Deg/s	|r|	α (deg)
150	0.0149	21.3	120	0.013	18
180	0.0178	20.5	160	0.017	17.6
210	0.0208	19.8			
240	0.0238	19			
270	0.0268	18.1	240	0.027	16.6
300	0.0297	17.2	280	0.03	16.2
330	0.0327	16.2			

Table 11 Comparison between QinetiQ (left) and Glasgow's (right) reduced pitch rates for re-attachment

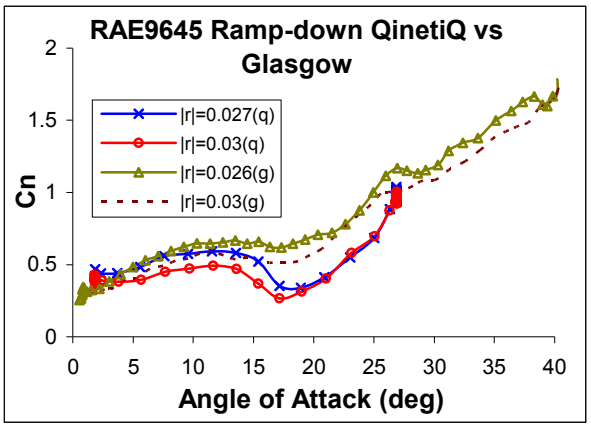

Figure 88 Ramp-down tests performed by QinetiQ and University of Glasgow for reduced pitch rate r=0.027 and 0.03

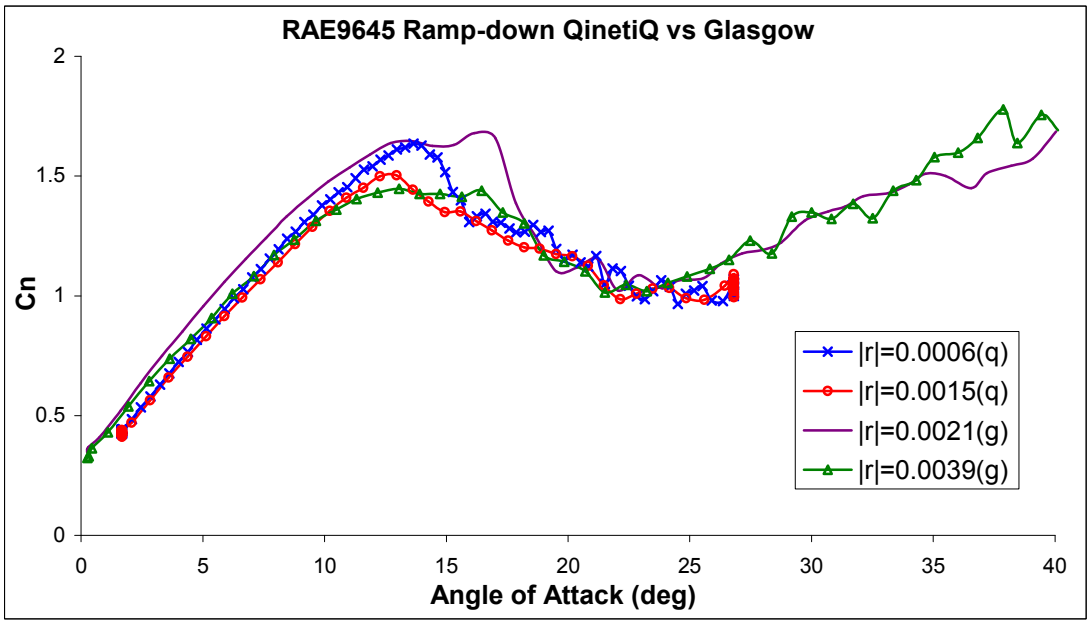

Figure 89 Ramp-down tests for reduced pitch rates below r=0.015

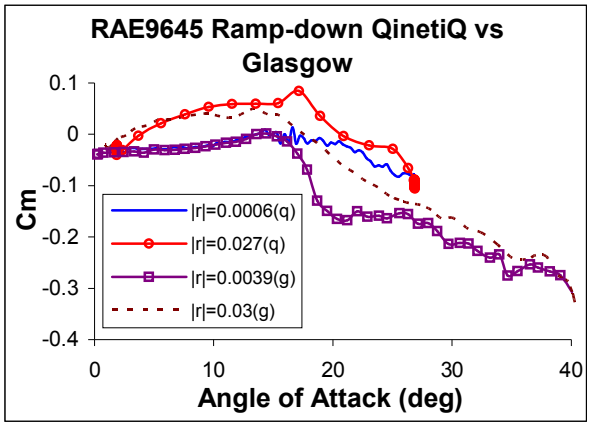

Figure 90 Comparison between two Cm for high and low reduced pitch rates

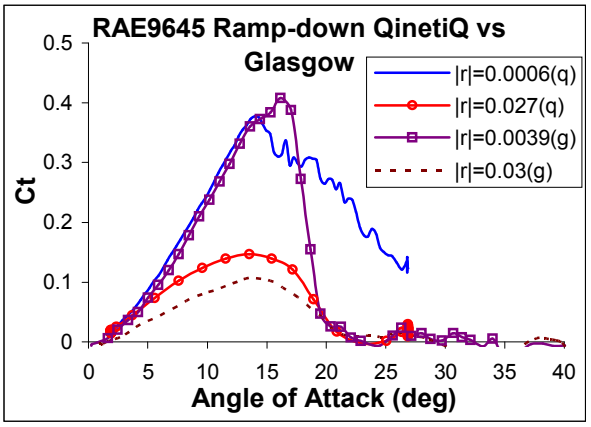

Figure 91 Comparison between two Ct for high and low reduced pitch rates

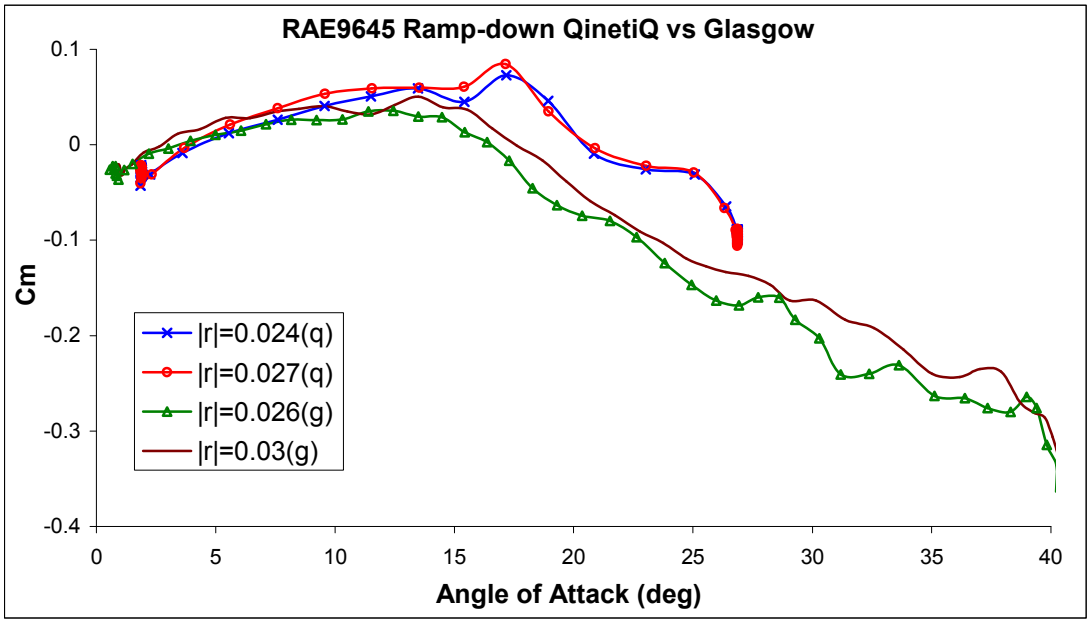

Figure 92 Comparison between QinetiQ and Glasgow's Cm's at high pitch rates

Considering the Glasgow data (Figure 93 (a)) in conjunction with Figure 92, with time effectively going from left to right, it may be observed that there is a limited pressure increase in suction close to the leading edge (uncharacteristic of all other Glasgow data) but the aerofoil is essentially fully stalled. After a short while this tends to reduce prior the full re-attachment process beginning. This leads to some uncertainty in the start of the process by introducing undulations in the Cn profile. The QinetiQ data, however,

have a different detailed development though predominantly the same. First, the pressure at the leading edge displays a rather large suction ridge together with a small suction region behind and in front of the fully stalled region. This would inevitably lead to higher values of Cn than the Glasgow data. However, it should be remembered that the QinetiQ ramp-downs were initiated from around 27 deg incidence. If one now looks closely at the Glasgow data it may be observed that this incidence corresponds to the small region of suction at the leading edge. In other words, the apparent gross differences in the initial phase of the data sets are exaggerated by the test procedures and do not exist in general. There are two very significant differences, however, and these are at the start of the re-attachment process:

1) The Glasgow data exhibits a smooth transition from the stalled condition to the fully attached phase. In the QinetiQ data, however, there appear to be a collapse of the pressure followed by what appears to be a sharper peak suction.
2) In the QinetiQ data the re-attachment process begins almost simultaneously over the foremost part of the profile.

Remembering that, at the start angle of QinetiQ data, a higher value of Cn could be expected, the collapse in the suction would lead to a reduction in Cn, and the larger surface involved at the beginning of the re-attachment process would give a steeper Cn slope during the onset of this phase, as can be observed in Figure 88. It is interesting that after this part all the data for Cn are similar and the differences are minimal.

This particular aspect of the work is an area well worthy of further and more detailed investigation. Although the re-attachment process of the aerofoils appears very different they are fundamentally similar. The investigation would require to look in detail at the

pressure profiles and individual temporal traces with some additional experiments at Glasgow to mimic the QinetiQ motions.

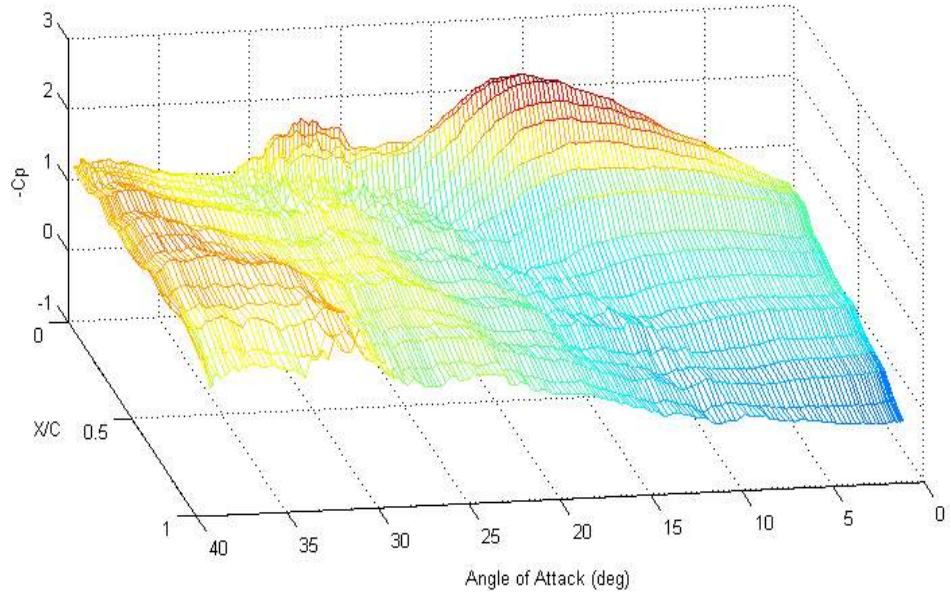

(a) University of Glasgow

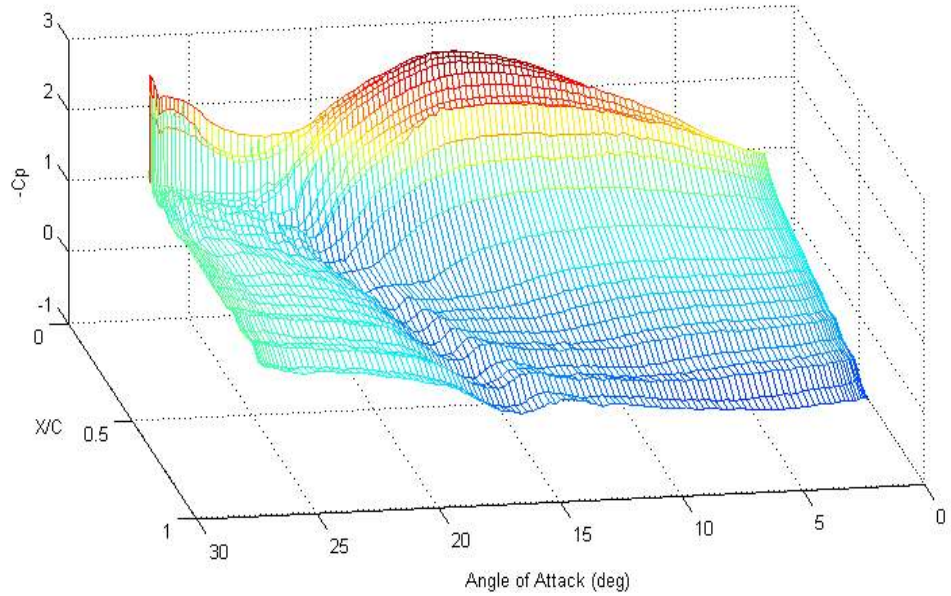

(b) QinetiQ

Figure 93 Comparison between the Cp upper surface coefficients for the two data sets at |r|=0.027

However a comparison between the angular forces against non-dimensional time shows that the two profiles followed very similar paths during the pitching down as it was observed for the ramp-up tests. Figure 94 presents the incidence against the non-dimensional time for three tests with same reduced pitch rates: 0.017 (a), 0.027 (b) and 0.03 (c). Once again the QinetiQ tests have been shifted in time in order to have the tests passing by the initial angle of attack at the same time as Glasgow. It is clear from the Figures that, since the pitching down motions are so similar, the different behaviours at the re-establishment of the attached flow are not dictated by this particular aspect of the test.

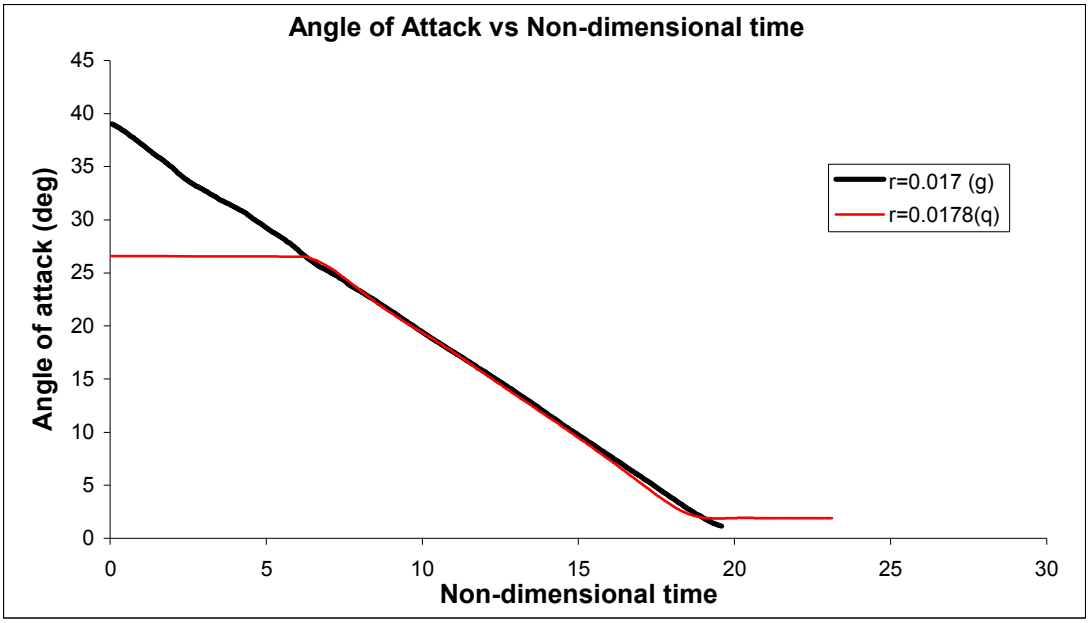

Figure 94 (a)

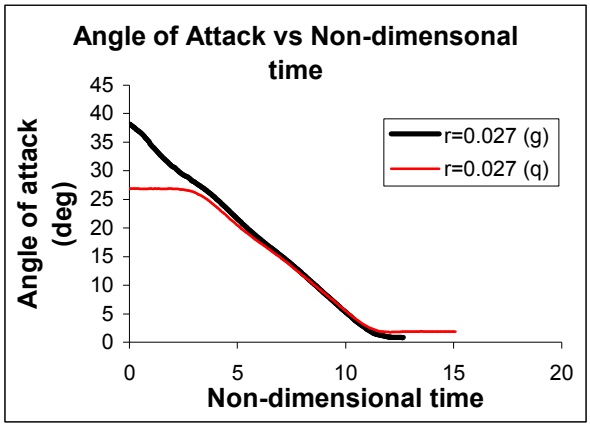

Figure 94 (b)

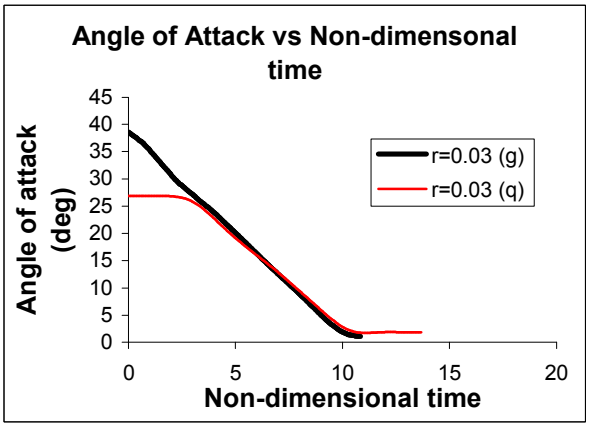

Figure 94 (c)

Figure 94 Glasgow and QinetiQ angles of attack plotted against non-dimensional time for three different reduced pitch rates: |r|= 0.018, 0.027 and 0.03.

3.3 Oscillating

Despite the wide range of reduced frequencies tested in each facility, it is still very difficult to compare sinusoidal test. Among the range of the tests only three sets have the characteristics suitable for a comparison. First, all the tests must have either equal or very similar values of reduced frequencies and second, the cycle must span the same angles of attack. This means equal mean angles and equal amplitudes. The tests reported in Appendix 1 in Table 2A and 4A satisfy these conditions only for k=0.05, 0.1 and 0.15 with an amplitude 8 deg and mean angle from 8 to 18 deg. Even under these conditions, general conclusions are difficult to make. In fact, during an oscillating test, it is more difficult to have the same motion for the two test facilities than for the ramp experiments. It is understandable, that what can introduce differences between the behaviours is the nature of the oscillations. The dynamic-stall inception and its strength are, in fact, well influenced by the angular speed at which it takes place. For an oscillating profile there are two moments during the cycle, during the approximate

ramp-up and ramp-down motion, per each cycle, where the angular speed is relatively constant, or can be considered as, and, provided stall and return from stall occur in these regions, the tests can be better compared. On the other hand, when the inversion of the motion takes place, the profile has to slow down and speed up again to that relatively constant value. These accelerations and decelerations influence the aerofoil behaviours especially whilst the DSV is developing. To have comparable tests, the two set-ups should consider equal oscillating accelerations. The tests performed by QinetiQ and Glasgow's University, as shown in Figure 95 (a and b) for the same reduced frequency (plotting the incidence against non-dimensional time), do not have the same shape. The difference that was noticed between the two oscillating motions is mainly in the region of the oscillation when the profile is about to change direction of the motion. In this area the Glasgow data present a faster changing in direction with a higher deceleration and acceleration. Although, with this difference, they still appear, by inspection, to be acceptable for qualitatively comparison purposes.

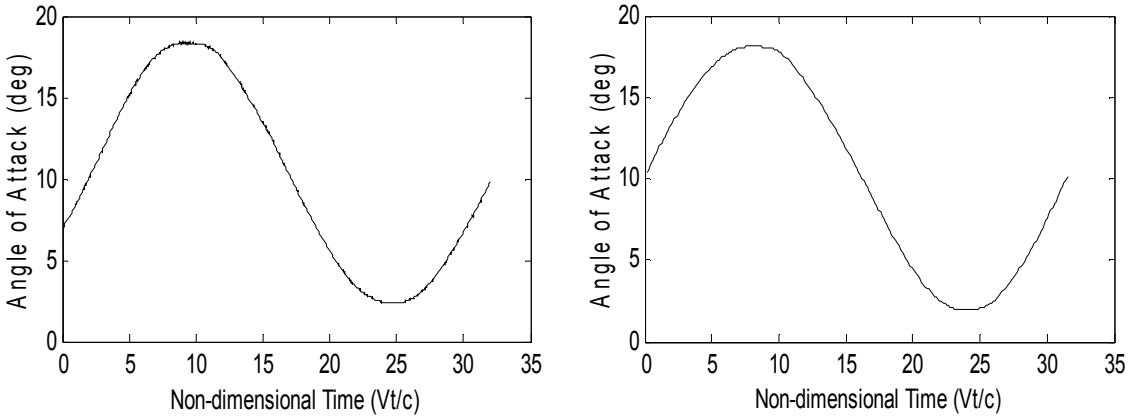

a) Glasgow oscillating law b) QinetiQ oscillating law

Figure 95 Comparisons between the two oscillating laws performed by University of Glasgow and QinetiQ for the same reduced frequency (mean angle=10 deg, amplitude=8 deg)

The comparisons are depicted in Figure 96 and Figure 97 (for Cn). There are several striking features. First, the QinetiQ data, on the upstroke, parallels at higher value, the Glasgow data. This is different from the ramp-up data where the two data sets diverge from a common start value (Figure 72 and Figure 73). Additionally the starting values of Cn are different. This, once again, implies differences in the two test set-ups. It is almost as though there were either errors in recording the incidence or an offset in the pressure measurements. The Glasgow incidence is simply the geometric incidence of the chord line to the centre line of the tunnel working section and was measured via a calibrated high specification angular displacement transducer via an anti-backlash gearing set-up. Flow angularity at the pitch axis and tunnel axis for the "clear" condition is 0.5 deg (Richard Gordon, 1982, no report exists, but the data are archived at the Department of Aerospace Engineering, University of Glasgow). The QinetiQ data were collected via a dedicated QinetiQ system assembled and installed independently of Glasgow University. The incidence set and measurement system details were not available for the present work and indeed may be lost.

A similar result has been reported (Sheng et al. [80]) when comparing the S809 aerofoil data from Glasgow with those from Iowa State University.

It may be concluded that mismatches in the Cn magnitudes should not seriously affect the general conclusion regarding the nature of the data.

Considering the stall of the aerofoils, it may be observed that the QinetiQ data do so prior to the Glasgow data.

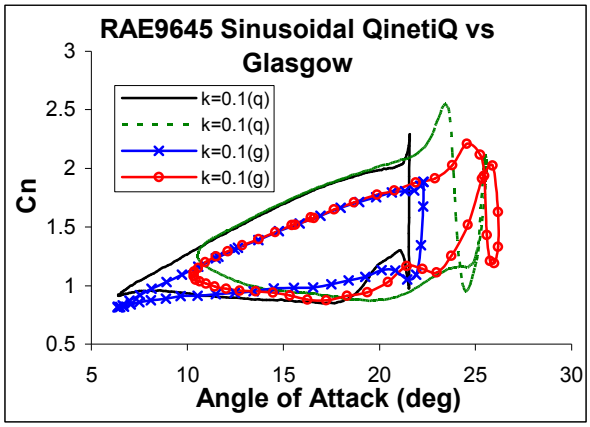

Figure 96 Oscillating tests for k=0.1, Amplitude of 8 deg and mean angles of 14 and 18 deg

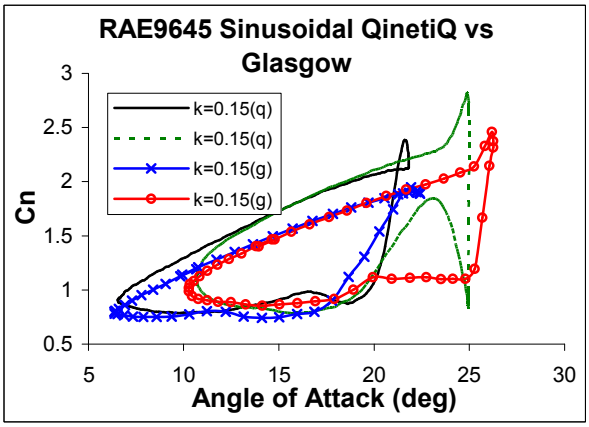

Figure 97 Oscillating tests for k= 0.15, Amplitude of 8 deg and mean angles of 14 and 18 deg

Recalling that, for the ramp-up data, both aerofoils stalled at the same incidence, and then this early stall may seem perplexing. Fortunately the explanation is somewhat straight forward. Once the critical incidence is reached (Sheng et al. [70]) there is then a fixed non-dimensional time delay before stall onset. The QinetiQ test did not achieve the incidence of the Glasgow equivalent and so had slowed down as it approached the peak of the incidence curve. Since the time delay from the same critical angle is constant, the QinetiQ data stalls at an earlier incidence. This is more obvious in Figure 97 where, for the mean angle of 14 deg, the incidence is on the point of reversal at the stall and an anti-clockwise loop appears. Large secondary vortices are evident, but interestingly all the data converge during the downstroke, indicating that the aerofoils are essentially fully stalled. Figure 98, which depicts the corresponding Ct data, from which, on the ramp-up data, the stall onset was assumed to be at the maximum value, clearly illustrates the differences in stall onset angle simply due to the data being presented against incidence rather than non-dimensional time. Again there is the almost constant offset on the upstroke, the evident secondary vortices and the near equivalence on the down stroke. In Figure 99 the Ct curves are presented against non-dimensional time to better

observe the stall onset for the two aerofoils. The two cases presented are for k=0.1 and 0.15 and for the maximum mean angles illustrated in Figure 98 (a and b). In the non-dimensional time domain, it is evident that the differences observed, in Figure 98, are no longer so visible and the onset of the dynamic stall appears to happen approximately at the same time. The Glasgow data were adjusted in order to begin at the same angle of attack as QinetiQ.

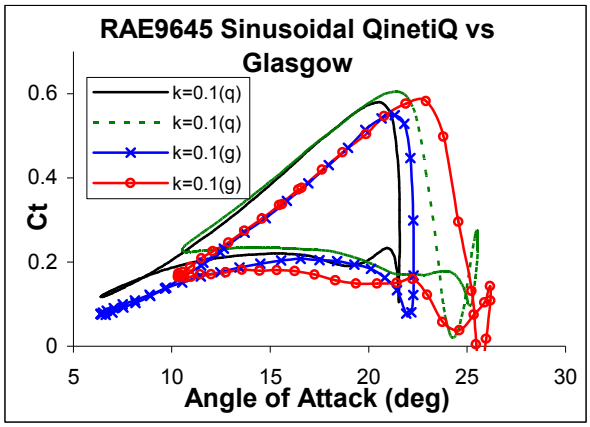

a) k=0.1 and mean angles of 14 and 18 deg

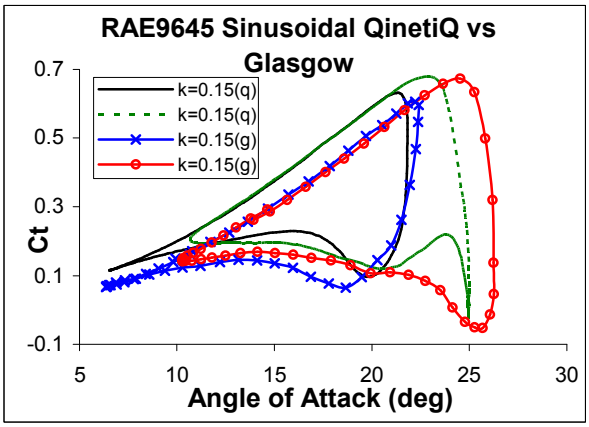

b) k=0.15 and mean angles of 14 and 18 deg

Figure 98 Comparisons between University of Glasgow and QinetiQ data for the chord-force coefficient for two different reduced frequencies and mean angles.

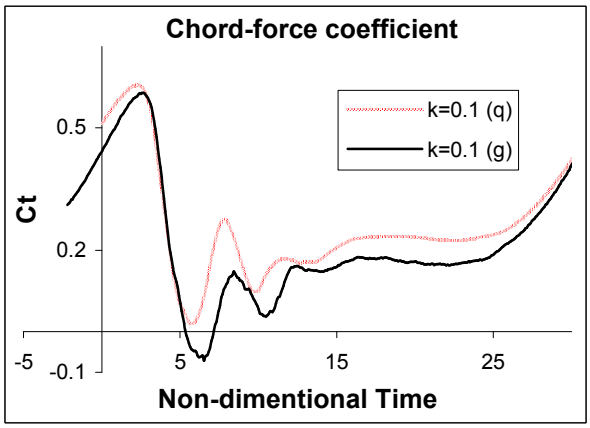

a) k=0.1 and mean angle 18 deg

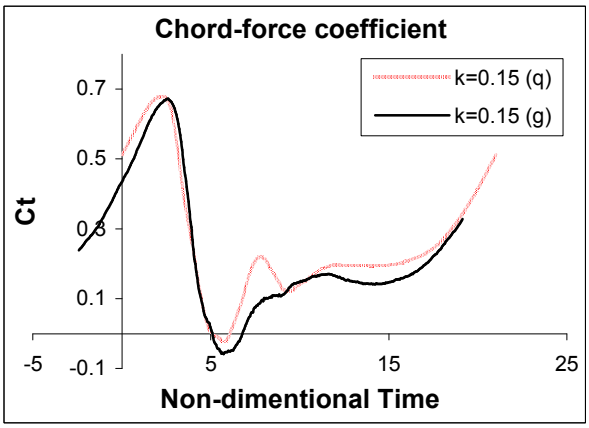

b) k=0.15 and mean angle 18 deg

Figure 99 Comparisons between University of Glasgow and QinetiQ data for the chord-force coefficient for two different reduced frequencies and mean angles in non-dimensional time domain.

With regard to the pitching moments, Figure 100, the different incidences of stall angle and the minimum Cm are all too obvious as is the overall general agreement of the form of the profiles.

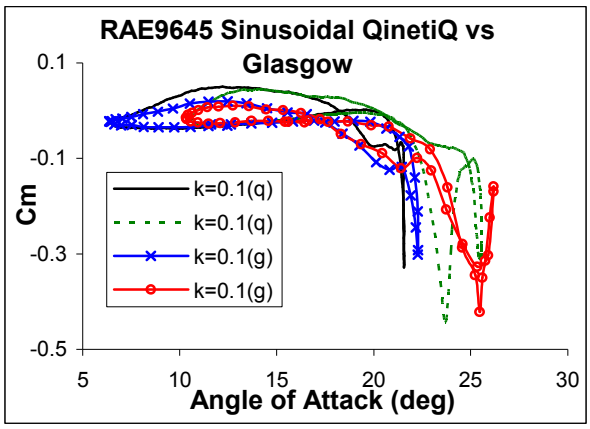

a) k=0.1 and mean angles of 14 and 18 deg

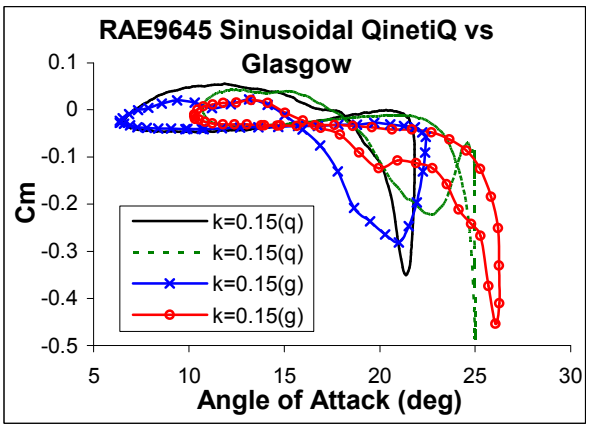

b) k=0.15 and mean angles of 14 and 18 deg

Figure 100 Comparisons between University of Glasgow and QinetiQ data for the moment coefficient for two different reduced frequencies and mean angles.

4 The Beddoes' Model

Experimental analysis, if properly conducted, will always advance a better understanding or description of the phenomena associated with dynamic stall. To apply this knowledge to engineering problems, however, requires the development of a quantitative analytical method in order to assess and construct the flow and aerodynamic coefficients. Potentially, very theoretical methods (i.e. CFD) still require very considerable computational effort. Many such methods have been proposed [39, 81, 82, 83]. Alternatively several very fast semi-empirical methods have been developed for routine uses in aerofoil applications [20, 84, 85, 86, 87]. An extensive and comprehensive review was given by McCrosky [88] and Beddoes [35] gives a good synthesis of all the most important methods for DS prediction. Unlike many others, the Beddoes dynamic-stall model is deeply founded in the physical mechanisms active in dynamic stall. Accordingly, the model will apply to a broad variety of aerofoils and reduced frequencies [89]. Therefore, Beddoes' (or Leishman-Beddoes) dynamic-stall model is very popular both in helicopter and wind turbine aerodynamics.

Beddoes' dynamic-stall model was developed in 1970s, when Beddoes observed and used two time delays to form his first dynamic-stall model. After much refinements and improvements (Beddoes [90, 91, 92, 93] and Leishman & Beddoes [29, 94, 95], the latest version of the Beddoes' dynamic-stall model was finalised in 1993 and titled the 3rd generation dynamic-stall model [40].

1st Generation Model (Beddoes model, 1976&1978):

Features:

- Attached flow by the Mach-number scaled indicial functions;
- Leading edge pressure and lift lagged with time constant T_p;
- Criterion for separation: Evans-Mort (low Mach number)/ Shock reversal (high Mach number);
- Two time delay constants: one for delay to the divergence of pitching moment, and another for the vortex shedding subsequently;

Validation:

- General success because of the deep knowledge and appreciation of the basic physical processes involved;
- The model only describes leading edge separation, but ignores trailing edge effects.

Chordwise effects are not included;

2nd Generation Model (Leishman 1987a & b, Leishman & Beddoes 1989, Beddoes 1983&1984):

Features:

- Revision on forcing representations by including unsteady oncoming flow, pitch rate, and plunging effects;
- Attached flow by the revised Mach-number scaled indicial functions;
- Leading edge pressure and lift lagged with time constant T_p;

- Separated flow by Kirchhoff theory, and a time delay constant T_f lagging the flow separation under dynamic conditions;
- Criterion for separation: Evans-Mort / shock reversal criterion;
- Vortex induced loadings by a revised dynamic-stall model, including vortex formation and travelling over chord of aerofoil;

Validation:

- The improvement in forcing representations, to wider unsteady cases, including dynamic inflow, plunging motion, etc;
- Involvement of Kirchhoff separation theory for nonlinear effect of trailing edge separation;
- Vortex shedding is modelled in a more physical way;
- Chordwise effects are not included;

3rd Generation Model (Beddoes, 1989&1993).

Features:

- A revision of forcing representations in a more general way by considering the chordwise effects;
- Simplifications of indicial function responses for attached flows;
- Nonlinear effect of trailing edge separation by Kirchhoff method, and a time delay constant T_f delaying the flow separation due to the unsteady conditions;
- Criterion for separation: Evans-Mort / shock reversal criterion;
- A revision in pitch moment calculation;
- Involvement of modelling vortex formation and development;

Validation:

- More general representations in forcing may be easier to implement in BVI or other complicated cases;
- Vortex shedding modelling is in more realistic way than 2nd generation dynamic-stall model;
- The revised pitching moment may give better fitting to the test data, but too many parameters in pitch moment may cause difficulties in fitting test data;

In this work, however, only 3rd generation dynamic stall is used, except where the author thinks the modifications and refinements are required for low speed aerofoils. In Appendix 2 a quick overview on the model theory, as it was applied and coded by the author, is given.

4.1 Modelling Onset of Dynamic Vortex

Dynamic stall is a term often used to describe a phenomenon that, under unsteady conditions [96], the aerofoil undergoes a process where the flow remains attached when the angle of attack significantly exceeds that of static stall during rapid pitching. Generally, the process will result in a significant increase in lift/normal force (overshoot). When the aerofoils pitches up further, a strong concentrated vortex (dynamic vortex) may be formed. The vortex, on the aerofoil upper surface, induces a further increase in the lift/normal force (additional overshoot) and a large nose-down pitching moment.

4.1.1 Definitions of dynamic vortex onset

According to Leishman [97], consideration of dynamic stall in the rotor design will more accurately define the operational and performance boundaries. However, the accurate prediction of dynamic-stall onset, as well as the prediction of the subsequent effects of dynamic-stall on blade loads and behaviour, is certainly not an easy task [98]. Beddoes [69] emphasized that it is critical to model the point at which the separation process is started.

Due to the complexity of dynamic-stall process [99], several researchers have explored the incipient dynamic-stall from experiments. Some have involved the examination of air loads [19, 100, 101, 102], while some others have involved the examination of flow field data [28, 103] and smoke flow visualizations [104].

Beddoes [69, 90] concluded that, to a first order, each dynamic-stall event is governed by a distinct universal non-dimensional time constant which exists between the aerofoil pitching through the static stall incidence and experiencing both moment stall and maximum lift. He pointed out that, if the leading edge is critical in determining separation, then the angle of attack for pitching moment break forms a reasonable criterion. The static stall incidence is defined as being the angle of attack at which there was an abrupt drop in the pitching moment curve. This definition as well as the following one can be titled as the C_m break.

Wilby [61] reasoned that aerofoil sections which exhibit, in oscillatory conditions, the ability to attain high incidence values without involving a break in pitching moment would be beneficial to helicopter rotor performance, and defined dynamic stall occurring

at the incidence at which the coefficient of pitching moment had fallen by 0.05 below its maximum pre-stall value for ramp experiments.

Scruggs et al. [101] defined dynamic-stall onset occurring at the incidence at which there is a sudden deviation in the gradient of the aerofoil of the lift curve, termed as *Cn* deviation.

Daley et al. [104] defined the stall occurring at the incidence at which the boundary layer separated at the quarter-chord. Smoke-flow visualization and pressure data were used to determine this location.

Seto & Galbraith [28] suggested that early indications of incipient stall may be disguised or hidden due to the air loads being calculated by integrating the recorded pressure coefficient values around the surface of the aerofoil, and during vortex initiation the formation of any localised disturbance within the boundary layer might be indicated immediately by the response of the local pressure coefficient. By examining the individual pressure traces, they established a criterion for indicating that the stall process has been initiated, termed C_p deviation. The stall onset was assumed to have had occurred when the pressure coefficient diverged at somewhere near the ¼-chord location.

Figure 101 shows results of onset of dynamic stall for different definitions, and Figure 102 gives the comparison of the onset of dynamic stall for different definitions. Generally, these definitions give a very similar result. All definitions give acceptable results. Therefore, the onset of dynamic vortex can be decided by any of them. As stated in Chapter 2, the onset of dynamic vortex is here considered as the angle at which the chord force reaches its maximum. The choice is based on the following considerations:

- It is easy and feasible to asses;

- Chord force is a result of integration; therefore, the local disturbance may not affect the general result;

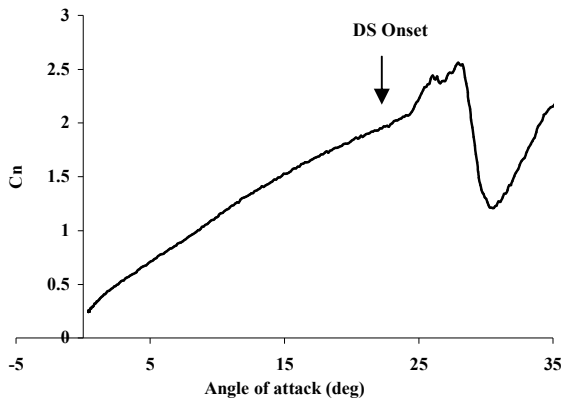

(a) Cn deviation

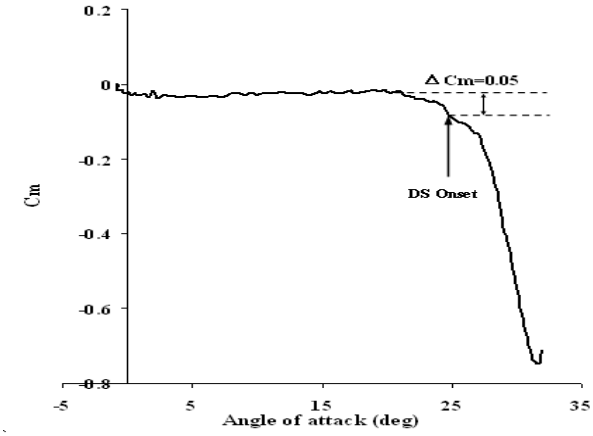

(b) C_m break ($\Delta C_m = 0.05$)

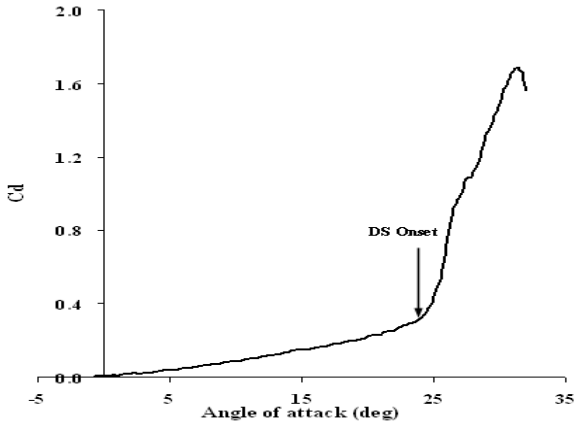

(c) C_d deviation

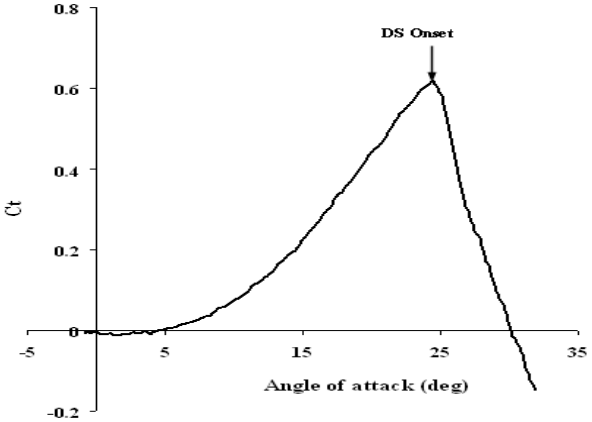

(d) C_t maximum

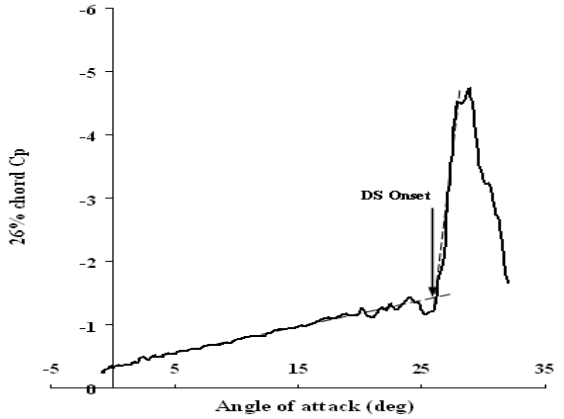

(e) C_p deviation

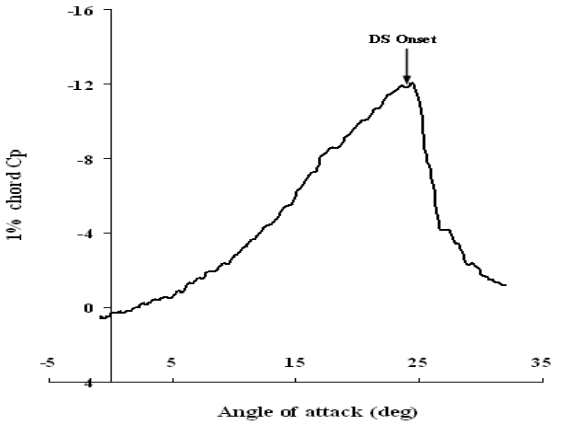

(f) C_p collapse at LE

Figure 101 Definitions of onset of dynamic-stall (DS Onset, Sheng et al.[70])

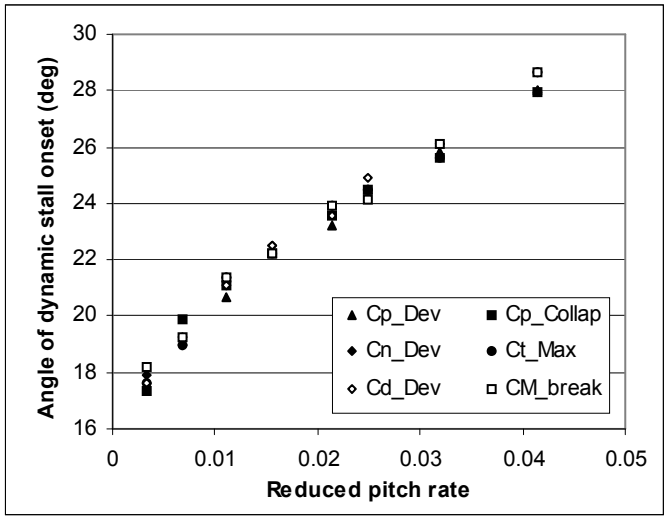

Figure 102 Onset of dynamic-stall by different definitions (NACA 0012)

4.1.2 Modelling of dynamic vortex onset in Beddoes' models for the RAE 9645

In the Beddoes models, the Evans-Mort correlation is employed to give the critical normal force C_{N1} for low speed airfoils, and the criterion for high Mach number (M>0.3) was extended by Beddoes, forming the Evans-Mort/shock reversal criterion, shown in Figure 152 and Figure 153 (in Appendix 2).

As was shown in Chapter 3 both QinetiQ and Glasgow data sets gave the same result for the stall onset. According to Seto and Galbraith [28] the reduced pitch rate of 0.01 delimits the boundary of quasi-static and dynamic effects. (The RAE9645 profile, actually shows the presence of the dynamic effects earlier than r=0.01, around a value that seems to be ~0.004 (Figure 87), but that can not be confirmed because of the lack of tests at that reduced pitch rate). At lower reduced pitch rate, the characteristics are qualitatively similar to those in steady conditions with significant lift and moment

overshoot, while at higher reduced pitch rates, the dynamic-stall vortex plays a significant part in the stall process and response is associated with dynamic stall. Beddoes also mentioned that the leading edge is critical for the initiation of the separation process only when the pitch rate exceeds some moderately small positive value, but he did not give the value of this [105]. In Chapter 3 it was shown that the incidences of dynamic-stall onset increase linearly with reduced pitch rate, when the reduced pitch rate is larger than ~0.01. Moreover, the relationship has been extended backwards to the first reduced pitch rate (r=0.0059) where the dynamic-stall is noticeable, showing that for the RAE9645 the boundary value of 0.01 does not apply to the data. The Beddoes' criterion, for the onset of the dynamic stall, should then be appropriate until this angular speed. However in the RAE9645 aerofoil case, it has been difficult to apply this criterion properly due to a lack of data and the difficulties caused by the low Mach number. The author was not able to find the C_{N1} vs Mach number graph for this aerofoil and not a single common value for T_p (Table 12) has been found for the complete range of reduced frequencies.

deg/sec	r	T_p		
		1% chord	2.5% chord	14% chord
2	0.00020	/	/	/
7	0.00066	/	/	/
20	0.0018	/	/	/
35	0.0034	/	/	/
79	0.0075	1.9	1.9	1.9
120	0.011	2.4	2.4	2.4
160	0.015	3.4	3.4	3.4
200	0.018	3.8	3.8	3.8
240	0.023	4.3	4.3	4.3
280	0.026	5.3	5.3	5.3

Table 12 T_p laggings for different r and different chord percentages (Glasgow data)

It is clear from Table 12 that the values obtained from the data for the T_p are very different for every pitch rate they refer to and changing the measuring point forwards or backwards does not yield any improvement.

A second noticeable thing is that the values of T_p remain constant (for each reduced pitch rate) at least until the first 14% of the chord. Other points of measurement, not reported here, have been taken between the leading edge and the 14% leading always to the same results. As stated before, what appears also clear from Table 12 is that there are no pressure lags due to the ramp up process if the reduced pitch rate is lower than r=0.0075. For the RAE9645 (QinetiQ) aerofoil the value of 0.0059 for r is the first one where a slight increase in the Cn - α curves slope can be noticed. Lower values have no effect while with higher values the phenomenon can be observed more clearly.

In Figure 103 some of the Cn - C_p curves are shown for different reduced pitch rates and different percentages of chord.

It was not possible to find a common value for T_p over the tests carried out. According to the experiences of the author, with T_p values already known in literature for higher Mach numbers for this profile and with the simulations obtained with the Beddoes' 3rd generation dynamic-stall model, the best value to fit the purpose has been chosen equal to 3.5 averaging the values for each pitch rate.

In predicting unsteady air loads, the prediction of dynamic-stall onset is very important. In Beddoes model, the onset of dynamic-stall is said to be triggered when

$$C'_N > C_{N1}$$

as mentioned above the Evans-Mort/shock reversal criterion (as showed in Appendix 2, Figure 153) is not here applicable because of the lack of the curve for the RAE9645

airfoil. Thus the C_{N1} value has been found using the method suggested in Leishman and Beddoes paper [29].

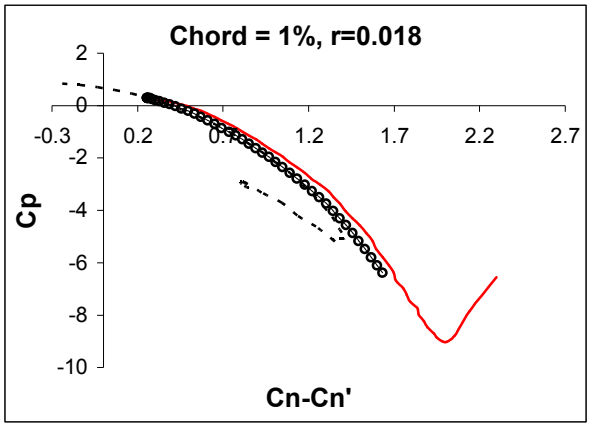

a) Normal force lagged at r=0.018

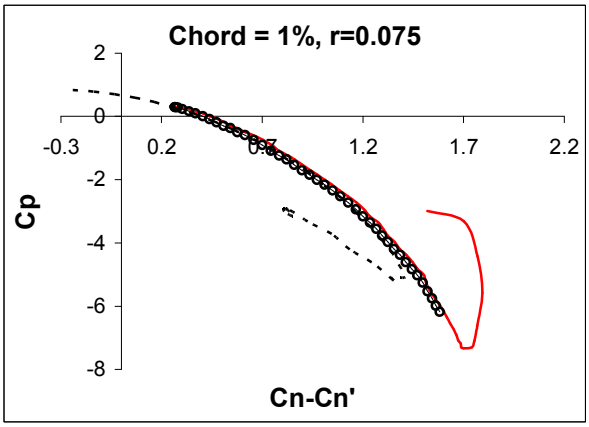

b) Normal force lagged at r=0.0075

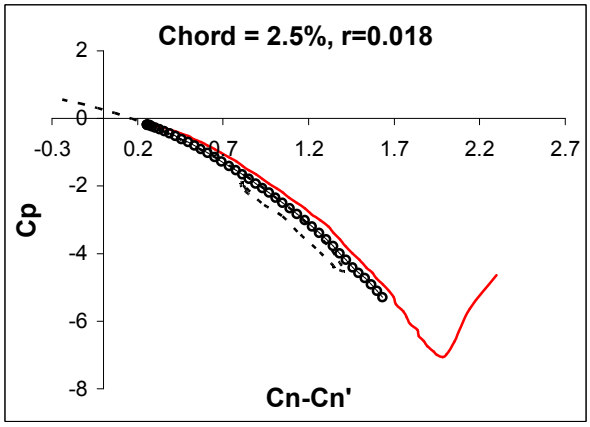

c) Normal force lagged at r=0.018

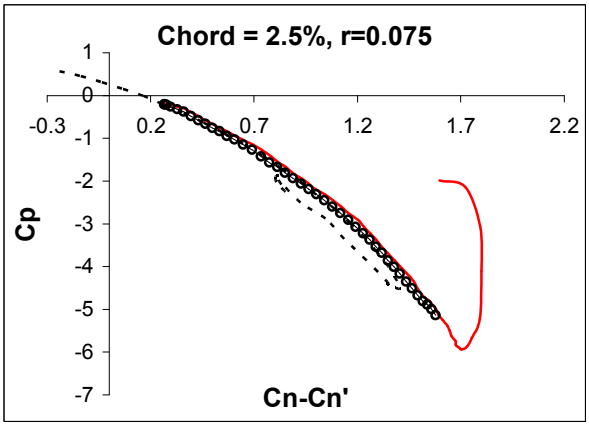

d) Normal force lagged at r=0.0075

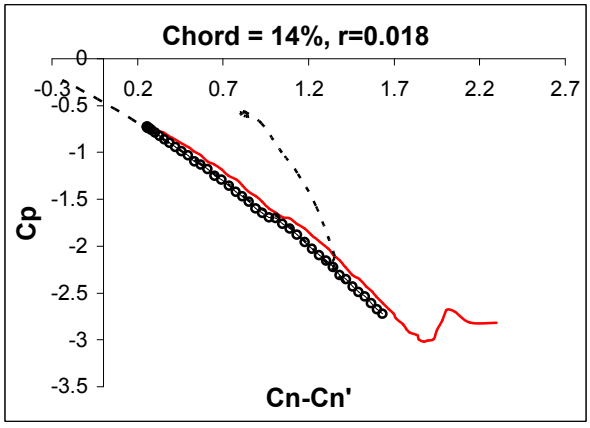

e) Normal force lagged at r=0.018

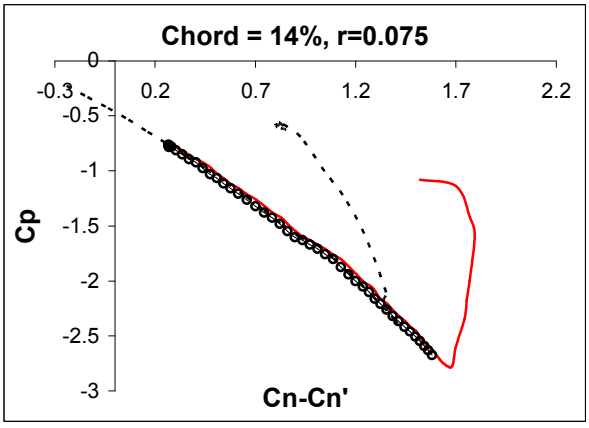

f) Normal force lagged at r=0.0075

Figure 103 Normal force lagging ------- Static case, T_p lagging ◦◦◦◦◦◦◦, _____ Dynamic case. Values of T_p as in Table 12: 3.8 and 1.9 respectively.

In this way the C_{N1} is found at the intersection between the vertical line passing by the static stall α and the extension of the fully attached flow lift-curve slope. The stall α value for the static case has been chosen with the C_t maximum criterion that gives an angle of 14.8 deg. Figure 104 shows the method.

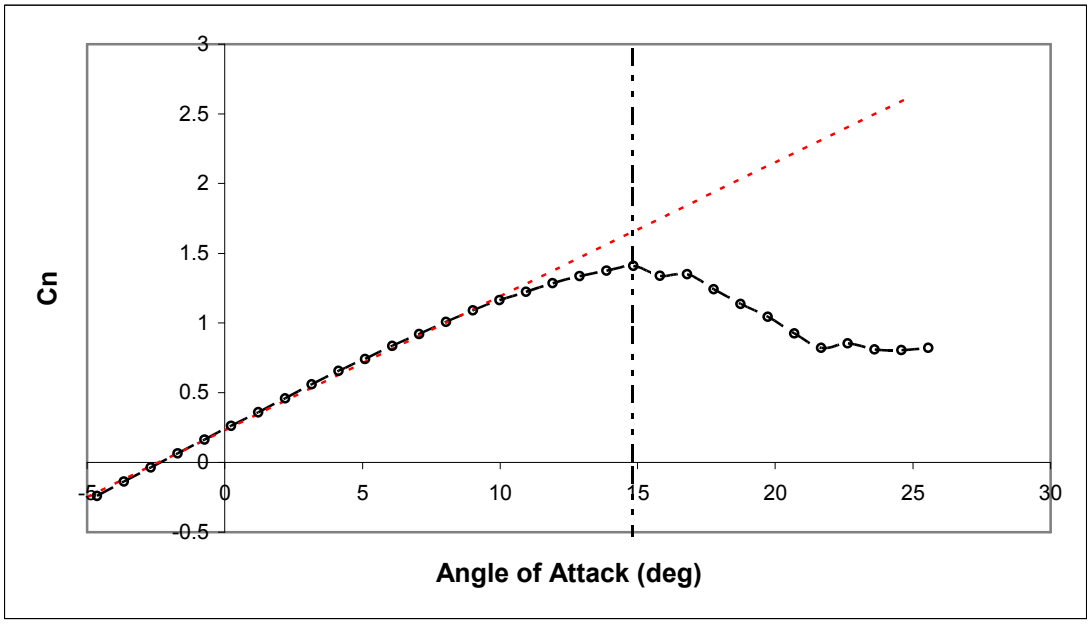

Figure 104 Leishman and Beddoes C_{N1} method for Glasgow's data

The C_{N1} obtained in this way for the Glasgow's data is around ~1.64 that is close to the best value found to fit the dynamic test curves. The QinetiQ data do not have any static test data; hence it was not possible to find a value for C_{N1}, not even with this method. For the following discussion the value adopted for these tests will be of 1.75, which is the one extrapolated, using the Leishman and Beddoes method, from the assumptions made in Chapter 3. All the coefficients used for the Beddoes' model will then be given in later sections when all the cases have been modelled.

However, as shown in Appendix 2 Figure 153, and Niven's research [62], for low speed cases of Mach number < 0.2, the T_p lagging tends to under predict the incidence of dynamic-stall onset. In Figure 105 are shown the angles of attack predicted by the T_p for the RAE9645 and the actual incidences when the dynamic-stall starts to appear. The dynamic-stall onset, using T_p, is clearly trigged too early. As said before, the value of T_p, used, is not, the one found by comparing the pressure measurements at the leading edge, as it was not possible to obtain a unique value, it is an average of those.

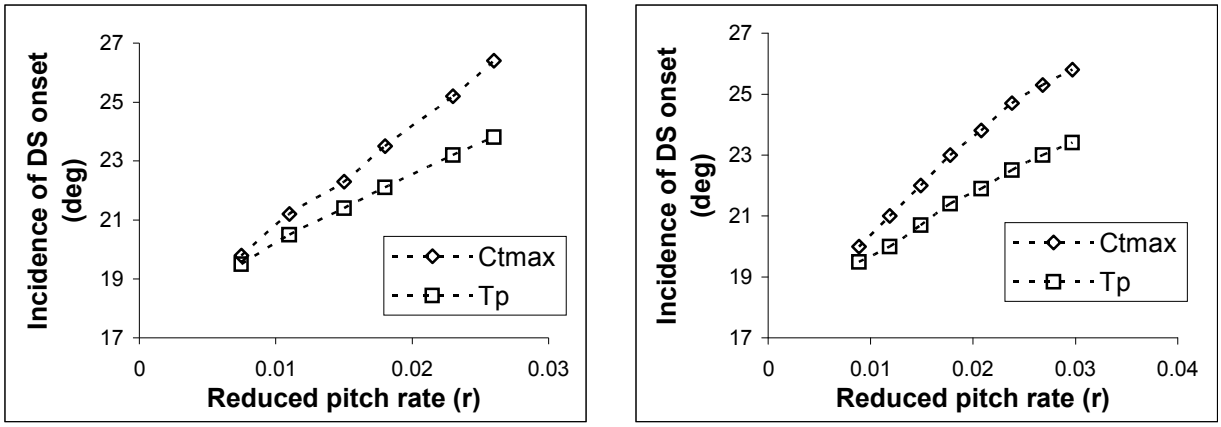

a) Glasgow's Dynamic-stall onsets b) QinetiQ Dynamic-stall onsets

Figure 105 Dynamic-stall onsets predictions using T_p for the RAE9645 profile

Although it is larger than the ones found for the lowest pitch rates of the set, it can be seen, from Figure 105, that it still triggers the onset of the stall too early.

The T_b modification proposed by Niven [62] significantly improved the calculation of dynamic-stall onset, as may be seen in Figure 106 (T_b =1.8). It can be seen that T_b modification gives much closer results to experimental data.

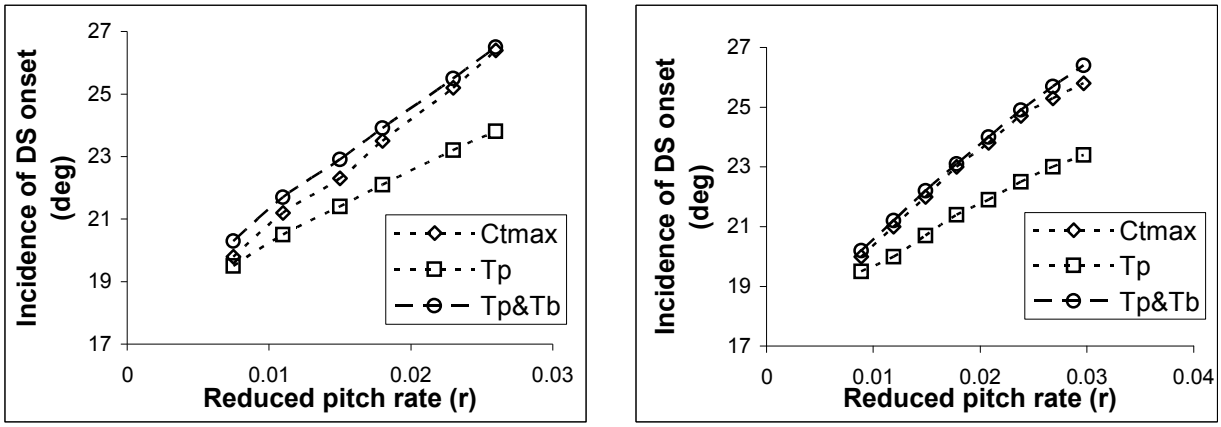

a) Glasgow's Dynamic-stall onset b) QinetiQ Dynamic-stall onset

Figure 106 T_b modification for prediction improvement of onset of dynamic-stall for the RAE9645 profile

It is clear from Figure 106a that T_b modification tends to over predict the onset of the dynamic-stall for lower reduced pitch rates but the difference reduces with the increased reduced pitch rate. The QinetiQ data however, display the opposite trend. This is not due to a gap in the method, but it is only a consequence of the set-up. In fact, in the former Chapter 2, it was noticed that for the QinetiQ tests it is difficult to get a good prediction of the dynamic-stall onset for the high reduced pitch rates. This was due to the tests stopping too soon to show a clear evidence of the stall onset. It is also initiated during the non-linear fraction of the pitching up process. As a consequence, the dynamic-stall onset angles leave the linear path and tend to show DSV earlier. Considering Figure 106, it seems evident that to achieve an agreement a lower value could have been chosen for T_b. However a better and closer agreement at lower reduced pitch rates would have produced a lesser precision for the faster ramps. It is not possible, for this aerofoil, to avoid the over or under prediction throughout the range of frequencies.

For the range here tested, the predictions are close to the measured data and so it can be said that the Niven's modification improves the T_p method for low Mach numbers. The

value of 1.8 was chosen as the best available for future analysis when using the Beddoes' model. On the other hand T_b and T_p are values carried out for tests with two different set-ups and in two different wind tunnels. The idea of having only one value for each result is a compromise between the values for each set. The predictions, however, appear to be very satisfactory.

4.1.3 A new model for reconstructing dynamic-stall onset

As discussed in Section 4.1.2 the T_p lagging together with the C_{N1} are not always sufficient for a good prediction at low Mach numbers and it was necessary to apply the additional T_b modification to obtain more accurate or satisfactory results. The development of a criterion that does not require these three parameters would be desirable. Furthermore, for the RAE9645 profile, other problems can arise from the test data. Indeed, in some cases, it looks impossible to obtain only one value for the T_p irrespective of the procedure applied. In this regard the matter apparently lies with the starting angle of the tests. The QinetiQ are severely limited by the high starting angles of attack. Hence it is clear that the T_p lagging requires not only an analysis of pressure and lift data, but the analysis of the test cases that can vary from profile to profile and that cannot be known a priori. As shown in Chapter 3, that although the DSV in both experiments was initiated at very similar incidences at the same reduced pitch rate, the two set-ups influenced the way the tests reached that angle. The omission of static data for the QinetiQ tests renders the assessment of C_{N1} problematic. In order to avoid all these problems, the University of Glasgow conducted and investigated unsteady tests of

many airfoils looking for different parameters that could result in reduced uncertainties for the stall onset [70]. A new method was developed that depends only on one coefficient that can be found by an easy and quick examination of the dynamic tests. The investigation, to which the author contributed, was aimed at more consistent stall onset model for the Beddoes' dynamic-stall model.

The method uses the dynamic-stall angles for every reduced frequency and fits them with a linear equation given by:

$$\alpha_{ds} = D_1 r + \alpha_{ds0} \qquad 4.40$$

Figure 107 below shows the fitting for airfoil RAE9645

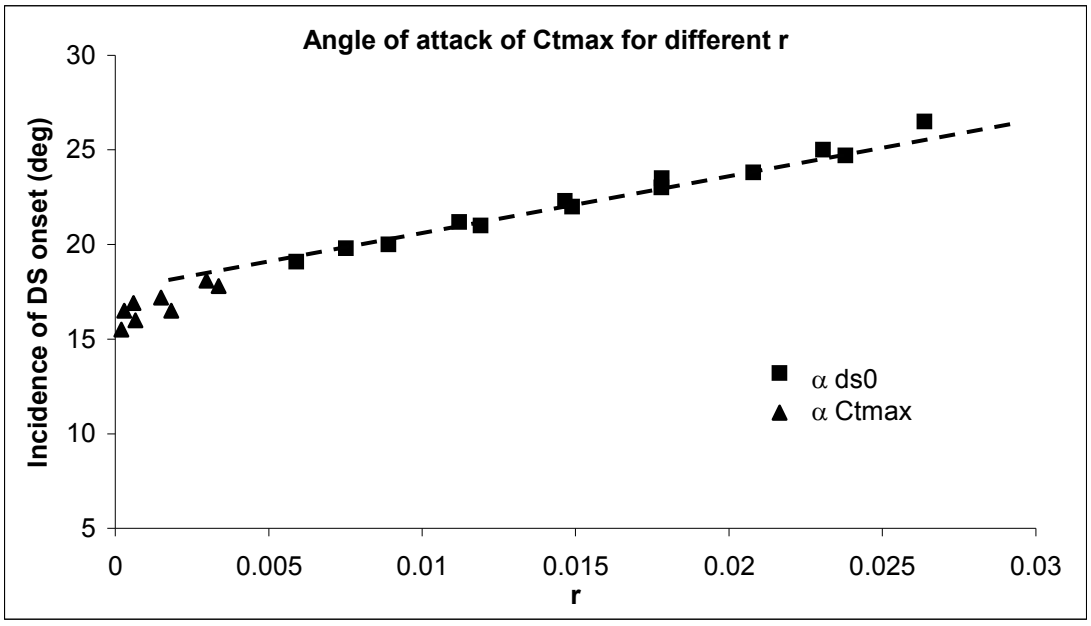

Figure 107 Incidence of dynamic-stall onset and its linear fitting

The fit works well for the higher frequencies but, once again, does not satisfy the lower values. This is no more than a confirmation that for slow pitch rates the aerofoil behaviour is quasi-steady. The trend line, evaluated with the least square method, intercepts the y-axis at the value of 17.15 deg.

Based on these coefficients a new time delay can be introduced by the equation:

$$T_\alpha = \frac{\alpha_{ds} - \alpha_{ds0}}{\dot{\alpha}} \cdot \frac{2V_\infty}{c} = \frac{\alpha_{ds} - \alpha_{ds0}}{r} \cdot \frac{\pi}{180} = \frac{\pi}{180} D_1 \qquad 4.41$$

That leads to the new non-dimensional time constant T_α. The value of T_α for the RAE9645 carried out with the above coefficient is: 5.9. The new time delay constant T_α is applied on the angle of incidence by

$$\Delta\alpha'(s') = \Delta\alpha(s')\left[1 - e^{-s'/T_\alpha}\right] \qquad 4.42$$

and from Figure 108 it is clear that the new lagged angles are very close to the critical angle value for reduced frequencies starting from r~=0.01 onwards.

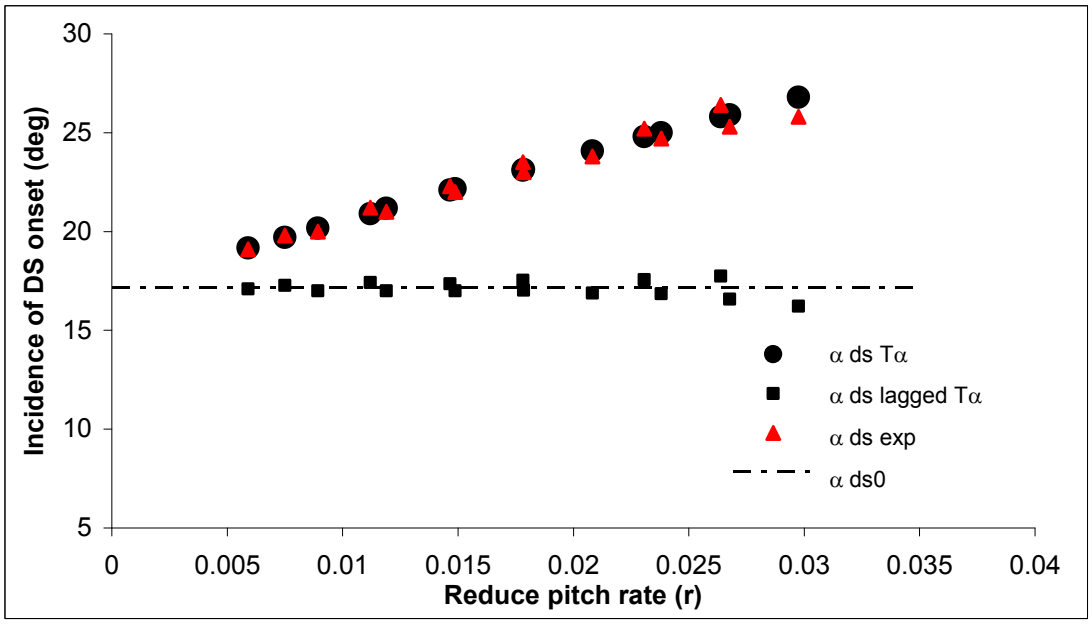

Figure 108 Dynamic-stall angles lagged by T_α

In Table 13 are reported all the values used for the graph in Figure 108. The table presents, in the first column, the values of all the reduced pitch rates tested. In the second column are the angles of attack at which the dynamic stall is taken to occur using

the above method. The third and fourth columns report the "real" angle of attack for the DSV onset (Ct max) and the values of the lagged angle of attack.

It can be seen that there is a very good agreement throughout all the range, albeit the agreement deteriorates at higher values. Additionally the values in Table 13 contain the results of the two wind tunnels.

The values of T_α attained this way are very close and so the use of a common value is acceptable. Furthermore this choice simplifies the problem to only one coefficient (i.e. T_α) for both data sets. The analysis and comparisons presented in the next Section demonstrate the reliability of the choice.

The dynamic stall is triggered when the new α lagged angle overcomes the new critical angle α_{ds0}. Hence the last column of Table 13 shows the lagged incidence at which the maximum Ct occurs.

r	α Stall T_α	α Ct max	α lag at Ct max
0.0059	19.16	19.1	17.1
0.0075	19.7	19.8	17.27
0.0089	20.17	20	16.99
0.0112	20.9	21.2	17.42
0.0119	21.17	21	16.99
0.0146	22.1	22.3	17.36
0.0149	22.16	22	17
0.0178	23.1	23.4	17.53
0.0178	23.13	23.5	17.03
0.0208	24.08	23.8	16.88
0.0231	24.8	25.2	17.57
0.0238	25	24.7	16.86
0.0264	25.8	26.4	17.75
0.0268	25.9	25.3	16.57
0.0298	26.8	25.8	16.22

Table 13 Dynamic-stall angles lagged by T_α (Glasgow's data in grey)

As illustrated in the next Chapter, the results are more accurate than the ones obtained with the "classical" method. There is a real simplicity of the procedure that does not possess the uncertainty of the classical methods three parameters and is more deterministic.

4.1.4 Result Analysis

In the previous section it has been shown 1) the difficulties associated with obtaining the three parameters for the Beddoes' model, 2) even if they are available, they may require modification to fit the data 3) deficient data sets are even more problematic. In this section will be presented the results obtained using the T_α modification to carry out the incidence of the dynamic-stall onset for low speed aerofoils.

The onset of the dynamic stall is illustrated in Figure 109 where are included the predictions using the T_α and T_p+ T_b.

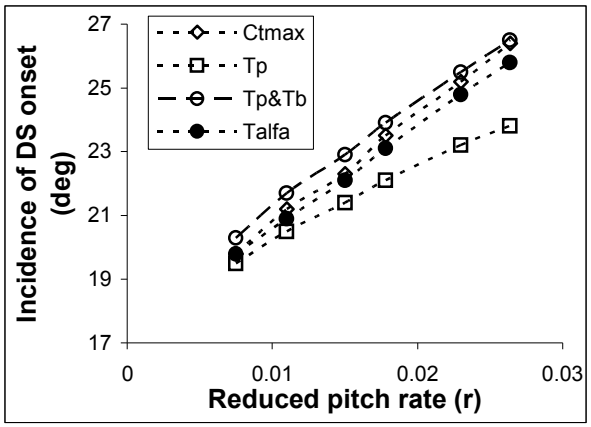

a) Prediction for the Glasgow tests

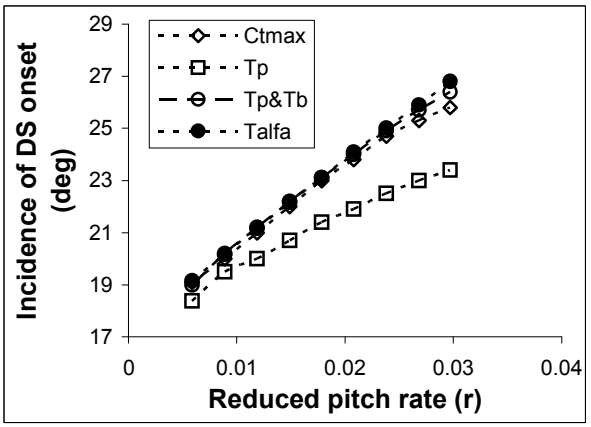

b) prediction for QinetiQ tests

Figure 109 Prediction of dynamic-stall onset with the three different laggings

For clarity, the graphs have been split in two between the two test facilities. As it is clear from the Figures 93 a) and b) the values carried out with the T_α lagging are close to the measured data and better than the classic method. This is further illustrated by Table 14 where the numerical values are compared:

Pitch rate (deg/s)	r	α max Ct	Stall with T_p	Stall with T_b	Stall with T_α
60	0.0059	19.1	18.4	19	19.16
79	0.0075	19.8	19.5	20.3	19.7
90	0.0089	20	19.5	20.2	20.17
120	0.011	21.2	20.5	21.7	20.9
120	0.0119	21	20	21.2	21.17
160	0.0146	22.3	21.4	22.9	22.1
150	0.0149	22	20.7	22.2	22.16
200	0.017815	23.4	22.1	23.9	23.1
180	0.01785	23.5	21.4	23.1	23.1
210	0.0208	23.8	21.9	24	24.08
240	0.023	25.2	23.2	25.5	24.8
240	0.0238	24.7	22.5	24.9	25
280	0.02638	26.4	23.8	26.5	25.8
270	0.0268	25.3	23	25.7	25.9
300	0.0297	25.8	23.4	26.4	26.8

Table 14 Stall angles with different laggings (Glasgow's data in grey)

In conclusion, it can be said that the Beddoes' model for the prediction of the dynamic-stall onset does not work properly for low speed airfoils even with the Niven corrections. The parameters required are three and a precise defining is problematic. Alternatively the new T_α method is more precise and easier to be applied. It needs just few ramp-up tests at different pitch rates and only one linear interpolation of these values to have the onset of each stall at any frequency. Additionally the tests do not have to come from the same facility. In fact, for the examples here examined, it always gave very good results for both data sets.

5 Beddoes' third generation model re-construction

The present section presents the results obtained using the Beddoes' third generation model for ramp-up/ramp-down and oscillatory tests (see Appendix 2). The results of the indicial-based semi-empirical stall model are compared to the experimental unsteady aerofoil data collected for the RAE 9645. The model was developed for a range of Mach number from M~=0.3 up to M~=0.9. A version of this model has been coded at Glasgow University by the author from the relevant equations mostly cited in reference [29, 40, 94, 95]. Some of the simulations, for the Cn's, have been already presented in the previous sections in order to highlight the topic aspect of the onset of the dynamic stall. This section covers most of the tests focusing on the entire dynamic-stall process, and not just on a particular aspect. Although the Beddoes' model was adopted for higher Mach numbers, no major modifications have been included for the following representations. The method is applied as it is described [40] and all the factors/coefficients are the best found for the profile undergoing these tests. It has been used this way to better understand what are the conditions and the parameters that mostly effect a good or bad re-construction for the RAE9645 aerofoil at low Mach number.

5.1 Beddoes' Model forcing terms

The forcing terms used for the re-construction are calculated as describe by Beddoes in [40] and here reported in Appendix 2, Section 1.1 for a given increment in the angle of

attack. This means that the method is not driven by the real motion of the profile during the test, but by a "perfect" movement. In this Section some of the ramp-up, down and oscillating test motions are compared to the ones re-constructed by the Beddoes' model in order to understand if there are main differences between the method and the tests and what kind of consequences these may have on the re-constructions. However, it is observed that the motions well match each other for all the types of test performed and the differences are minimal. In Figure 110 are shown six ramp-up tests from both QinetiQ and Glasgow University.

Beside the obvious difference due to the "time-shifting" depending on the difference between the data recording start and the beginning of the motion, it is clear that, at each reduced pitch rate, the two lines are parallel for the most of the motion. The same gradient of the lines indicates the same angular speed for the simulation and the test which guarantees the closest re-construction for the Beddoes' model. Nevertheless, the model motion does not consider the acceleration and deceleration part, visible at the beginning and end of each test. What is more important for these tests, is the slowing down part of the ramp. In fact, this may cause problems for the right assessment of the dynamic-stall onset and development, when the dynamic stall occurs within, or right before, this phase and it may generate discrepancies between the test and the re-construction.

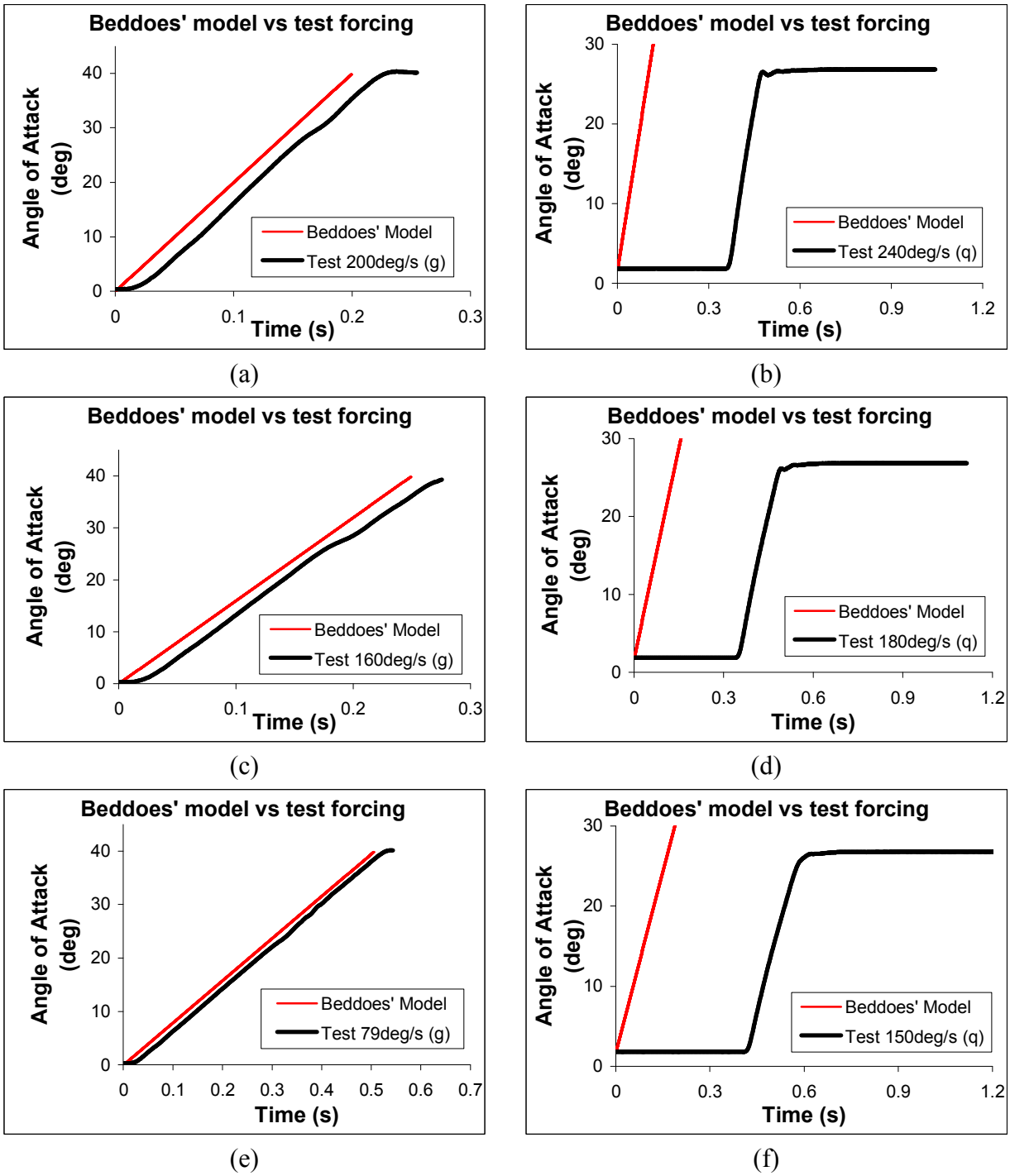

Figure 110 Pitching up motion comparison, between the Beddoes' model and Glasgow (a, c, e) and QinetiQ (b, d, f) tests, at different pitch rates.

Due to the different maximum angle of attack reached by the two aerofoils, this may be the case only for some QinetiQ test, as it was already noticed in Chapter 2 and 3. In

these cases the Beddoes' model may not be very accurate. Section 5.4 presents some re-construction for the QinetiQ data where this aspect is reported.

Some ramp-downs from both facilities are shown in Figure 111.

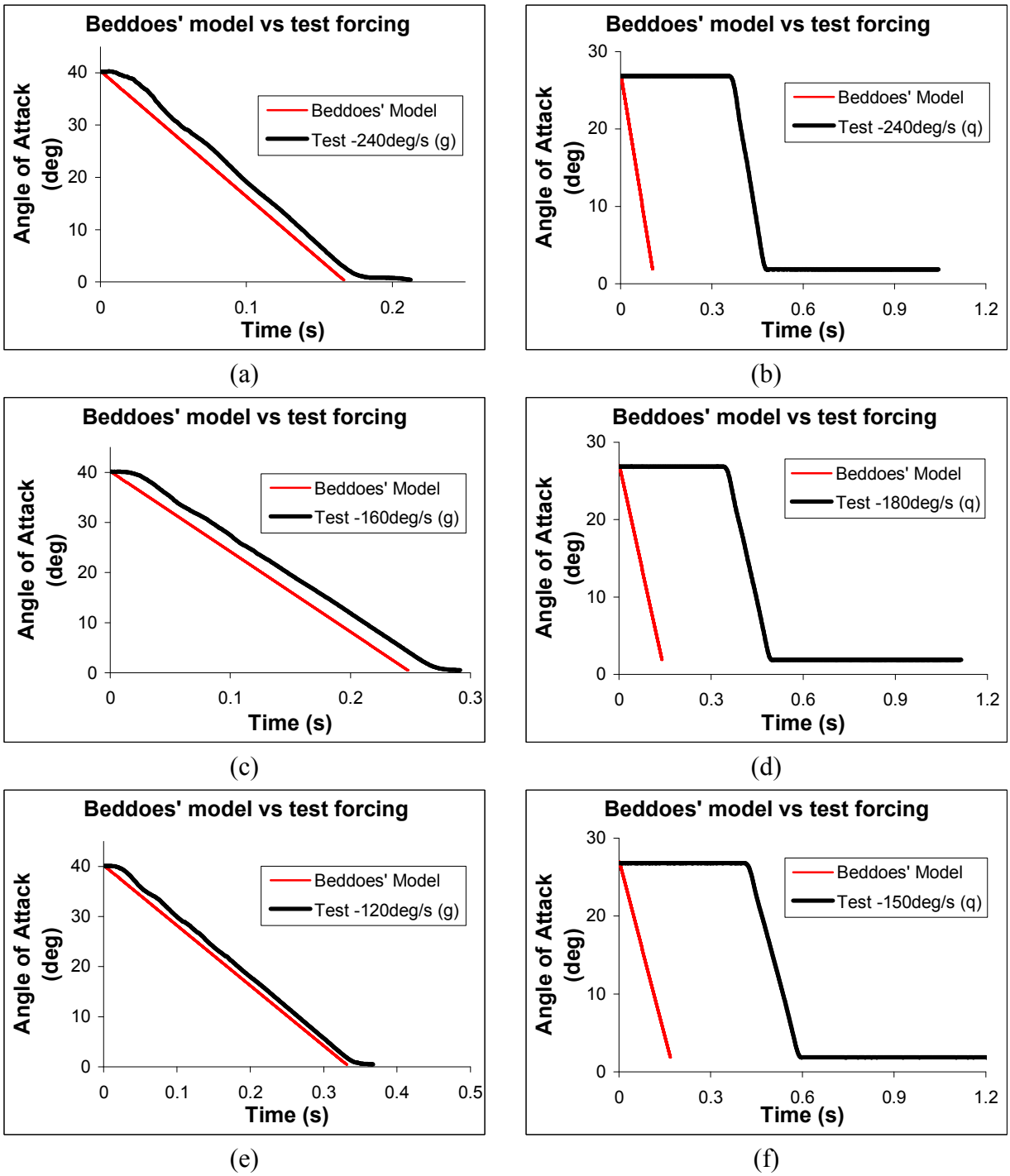

Figure 111 Pitching down motion comparison, between the Beddoes' model and Glasgow (a, c, e) and QinetiQ (b, d, f) tests, at different pitch rates.

Once again the accuracy of the re-constructed motion is clear and the two lines are mostly parallel for each pitch rate. More over, for the negative pitching motion considered in this work, the accelerating and decelerating parts of the curve are less important, even for the QinetiQ data, as they happen when the profile is fully stalled or recovered from the stall. Hence they not influence the key moments of the reattachment process.

The last comparison is between the oscillating motions. Figure 112 shows that the tests where conducted with a very good approximation of the oscillating law:

$$\alpha = \alpha_m + \alpha_a \sin(\omega t) \qquad 5.1$$

also used to reproduce the motion in the Beddoes' model. Differences are minimal and appear to be very small for the Glasgow data, while the QinetiQ ones have a slightly less steep line during the pitching down part of the cycle. However, overall it may be said that the reconstructed motions are satisfactory for all the three motion types and they should not be main causes of discrepancies in the Beddoes' model re-constructions.

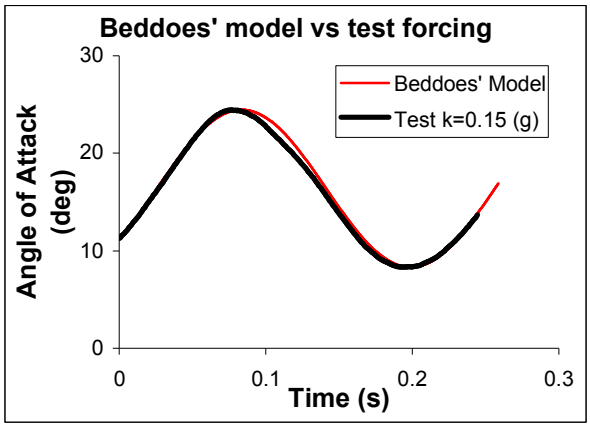

(a)

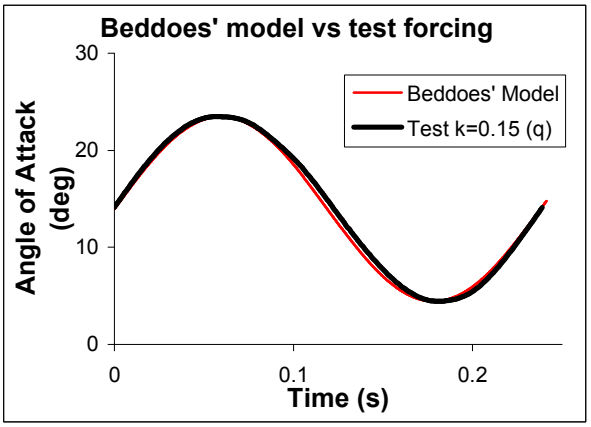

(b)

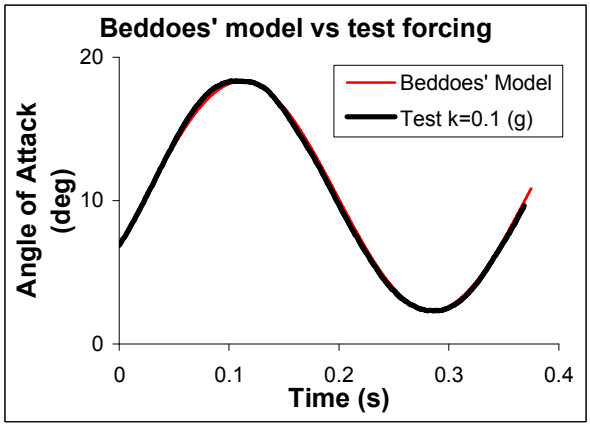

(c)

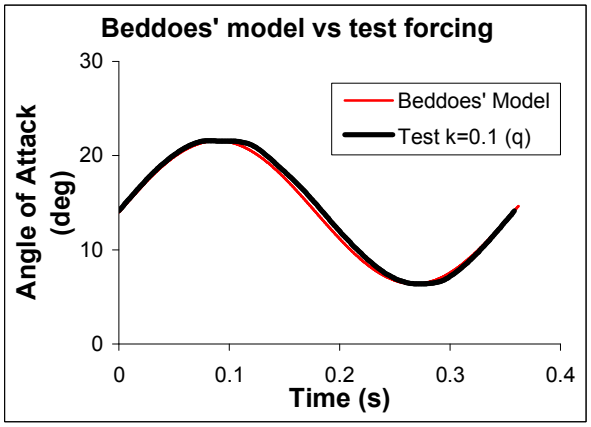

(d)

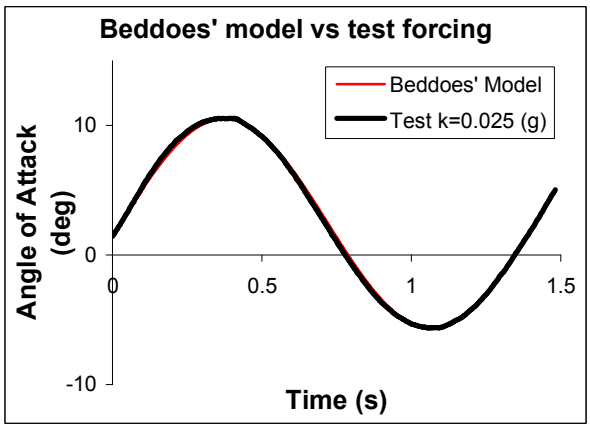

(e)

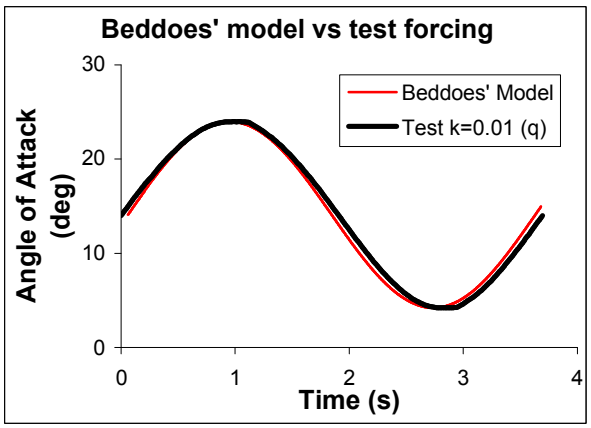

(f)

Figure 112 Oscillating motion comparison, between the Beddoes' model and Glasgow (a, c, e) and QinetiQ (b, d, f) tests, at different reduced frequencies.

5.2 Beddoes' Model Inputs

As presented at the beginning of Chapter 4, the Beddoes' model is a semi-empirical model which requires a number of empirical inputs. Some of the parameters were obtained from the static characteristics of the profile, whilst others from dynamic tests and a third group has no better explanation than the best inputs to satisfy the dynamic behaviour during re-construction.

It is of primary importance for the model that there is a good "static test" of the aerofoil. From these data are obtained the first set of parameters unique to that aerofoil. Figure 113 and Figure 114 present the static test conducted at University of Glasgow for the Cn and Cm coefficients.

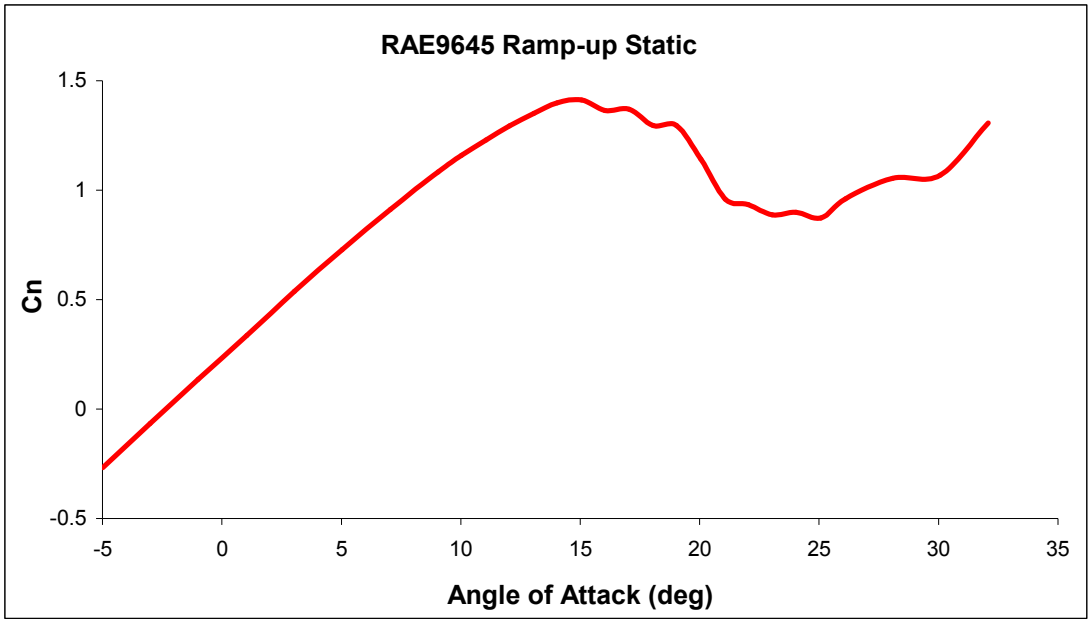

Figure 113 Cn static test at Glasgow's University

The following are obtained from the Cn data:

1) The lift curve slope for the linear part of the line (dCn/dα),

2) The angle of attack for zero lift (α_0),

3) The C_{N1}. coefficient for the onset of the dynamic-stall (as calculated in Figure 104) and

4) The α_1 parameter for the "*f*" function (eq. A2.31) as developed by Beddoes.

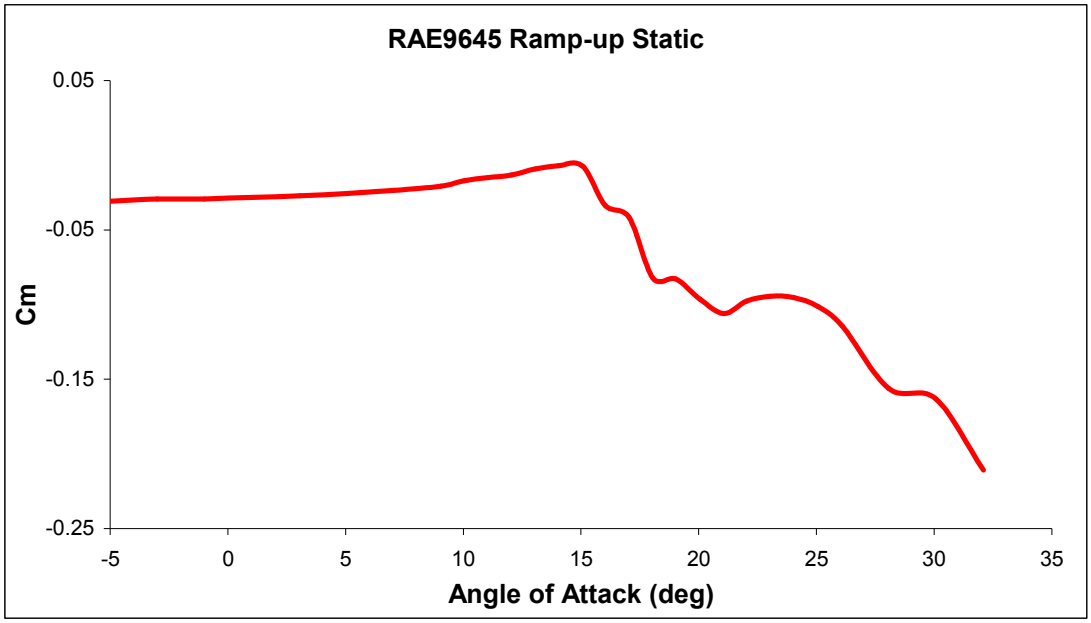

Figure 114 Cm static test at Glasgow's University

Figure 114 depicts the moment coefficient and from it the value of Cm_0 may be obtained. Figure 113 and Figure 114 then provide more information about other parameters. Following the theory presented in Appendix 2, the static test also provides all the missing parameters for the re-construction of the lift and moment "static" curves:

1) S_1 and S_2 values for Kirchhoff theory (eq. A2.31)

2) K, m, n and f_b coefficients for Cm fitting (eq A2.32)

However, in the present work, the Cm curve was reproduced by equation (5.2) as is represented in [95]:

$$\frac{C_m}{C_n} = K_0 + K_1(1 - f^n) + K_2 \sin(\pi \cdot f^m) \qquad 5.2$$

This equation gives a good representation of the Cm coefficient, always in close agreement with eq.A2.32, and does not require the arbitrary coefficient: f_b.

Figure 115 and Figure 116, illustrate re-construction of the normal and moment coefficient. In Table 15 lists all the parameters needed for these representations.

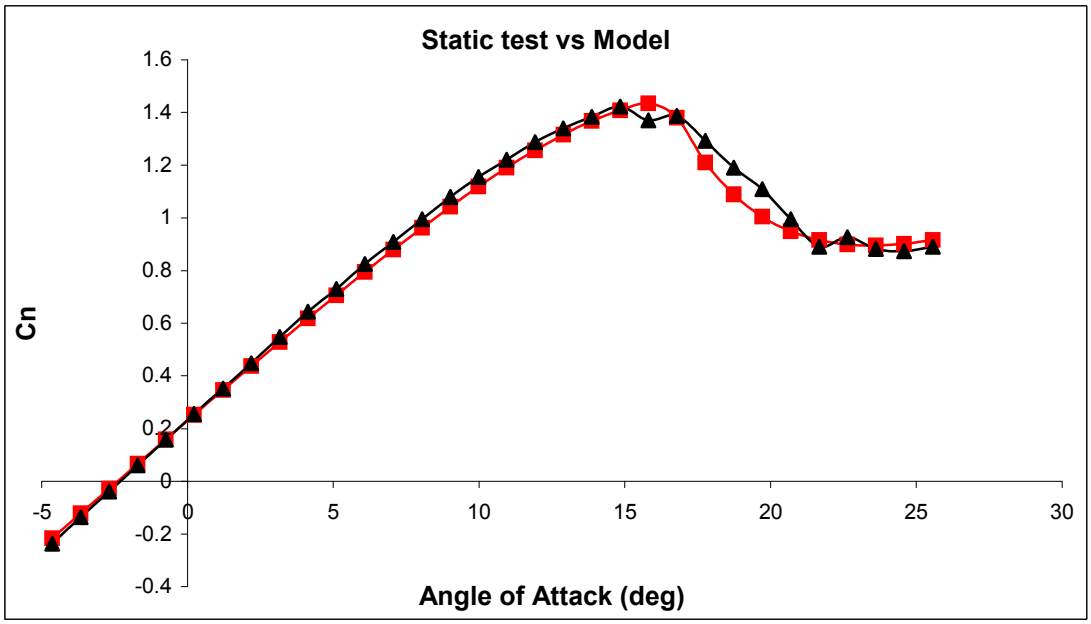

Figure 115 The Cn coefficient for Glasgow static test (red line) compared to the model (black line)

K0	K1	K2	α_1	α_0	S1	S2	Cm_0	dCn/dα	m	n
0.0005	-0.095	0.04	16.5	-2.40	6	2	-0.0315	0.096	1	1.5

Table 15 Coefficients for static reconstruction

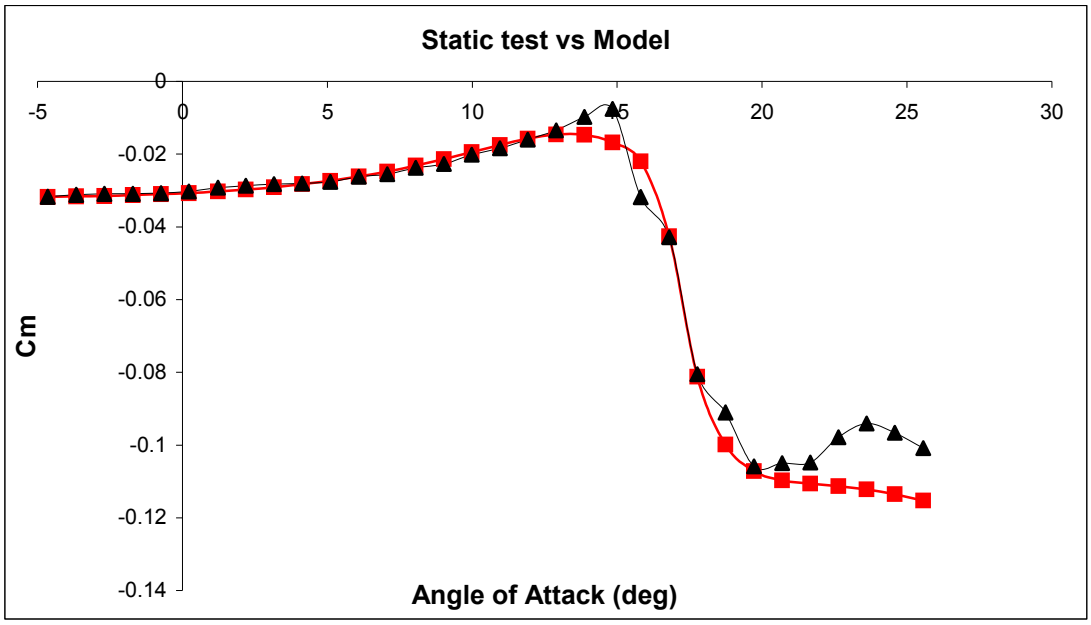

Figure 116 The Cm coefficient for Glasgow static test (red line) compared to the model (black line)

It may be noticed that Figure 113 to Figure 116 are representative of two different static tests. As reported in Appendix1, Table1A, the University of Glasgow run more than one static test. In this case the data sets plotted are listed and labelled in Table1A as 10000 and 10010, respectively. Minor differences between data sets may be noticed, but these do not change the general behaviour of the aerodynamic coefficients and do not affect the parameters in Table 15. Accordingly the choice of one static test over another does not largely influence the final results for the coefficients.

Nonetheless it must be accepted that these parameters may be slightly altered once the method is applied to the dynamic cases. Furthermore, the choice of the parameters is not unambiguous as other sets and combinations may be satisfactory for the re-construction of the static tests. Those parameters in Table 15 are, perhaps, the best fit.

Moreover, only the University of Glasgow performed static tests have been used and so the chosen parameter values are from one facility. It is logical, however, from what has been analyzed in Chapter 3, to expect that these tests may have lead to different

coefficients. Also in this case, as already done for other parameters before (i.e. time delays in Sections 4.1.2, 4.1.3 and 4.1.4), the conventional choice would have been a "weighted average" between the two sets. Therefore the coefficients would have changed for this case.

In the following section are presented the simulations for oscillating tests and it will be clear how and which of these parameters have been changed, if necessary, to fit better the dynamic data.

The parameters found with the static test are insufficient to apply the Beddoes' model. What cannot be established with the static test is the whole series of delays that the method needs to represent the dynamic behaviour of the section. Section 4.1 provided an overview on the choice of the first two delays the method requires. The T_p delay was chosen as an average value between the 6 values carried out with Beddoes' technique (T_p=3.5). Instead, for the T_b delay the uncertainty associated with the Evans-Mort upper and lower criterion cause the choice of it to be somewhat difficult and personal. Figure 117, however, gives a representation of how these two parameters perform and illustrates why the choice of T_b=1.8 is reasonable. Chapter 4 described how the dynamic-stall vortex is triggered by the Cn coefficient overtaking the value chosen for C_{N1}.~1.64 (dash line in the graph). Figure 117 shows clearly that the dynamic-stall would initiate too early with only the T_p delay and leaves only one appropriate choice for the selection of the T_b coefficient. That choice is made by the value that forces the delayed Cn curve to cross the C_{N1} line at the same angle of attack of the onset of the dynamic stall.

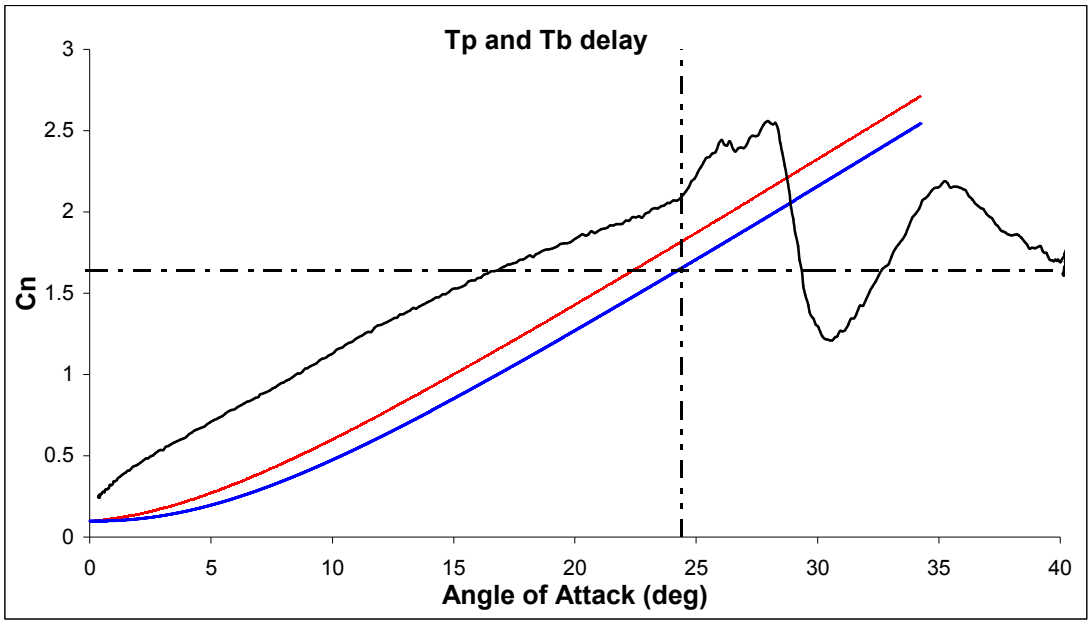

Figure 117 T_p (red line) and $T_p + T_b$ (blue line) delays compared to the C_{N1} coefficient and the onset of the dynamic-stall

To run the model for the Cn coefficient in a Ramp-up motion there are still two parameters to be defined. In fact, when the leading edge vortex starts to build up two new time constants are required to represent its effect on the aerodynamic coefficients. As they are named in Reference [95] and will be referred as T_{vl} and T_v. These parameters give the non-dimensional time for the dynamic-stall vortex to grow and move across the profile upper surface. Two parameters are also fundamental for the reconstruction of Cm. The centre of pressure will vary with the chordwise position of the vortex and a representation of its behaviour (as position in time) is necessary for the reconstruction of the Cm coefficient (equation 4.38). According to the ramp-up tests, a reasonable choice gave the same value for the two parameters (as expected from Section 3.2). This was done essentially by "trial & error":

1) $T_v = 3.2$

2) $T_{vl} = 8$

Hence the Beddoes' model was initially applied to the RAE9645 profile using these parameter values and also those for the static test. Table 16 lists all of these and Figure 118 and Figure 119 are examples of the Beddoes' model reconstruction for Cn and Cm coefficients for a reduced pitch rate of r=0.018 (200 deg/s).

dCn/dα	α_0	α_1	S_1	S_2	K_0	K_1	K_2	Cm_0	C_{N1}	T_p	T_b	T_f	T_v	T_{vl}	m	n
0.096	-2.4	16.5	6	2	0.0005	-0.095	0.04	-0.0315	1.64	3.5	1.8	5	3.2	8	1	1.5

Table 16 Beddoes' parameters as found from the static test and dynamic observations

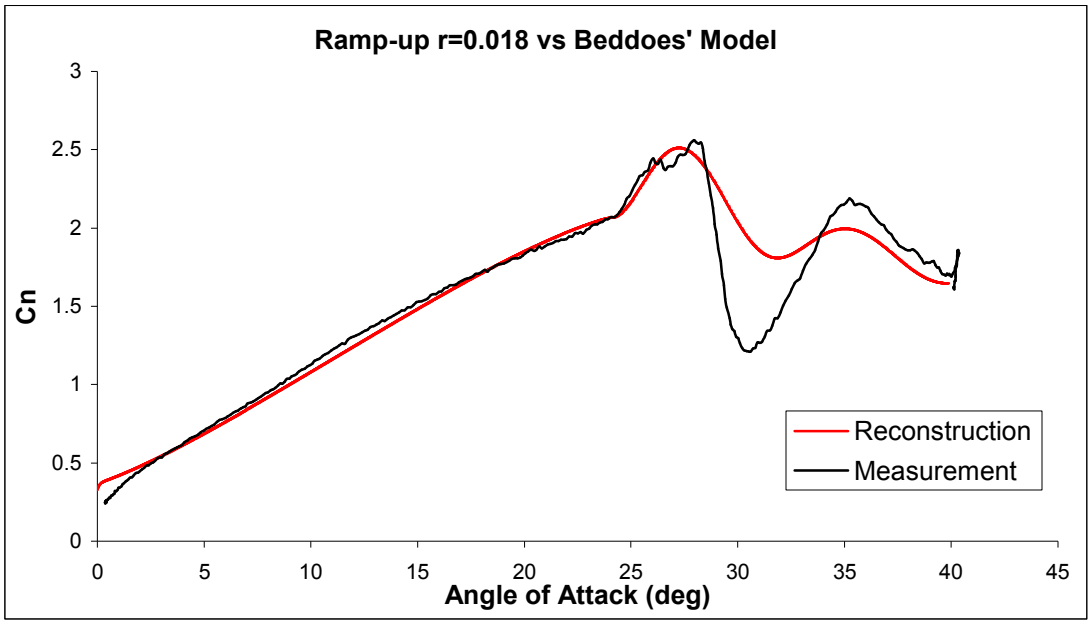

Figure 118 Cn coefficient ramp-up simulation for r=0.018 (200 deg/s)

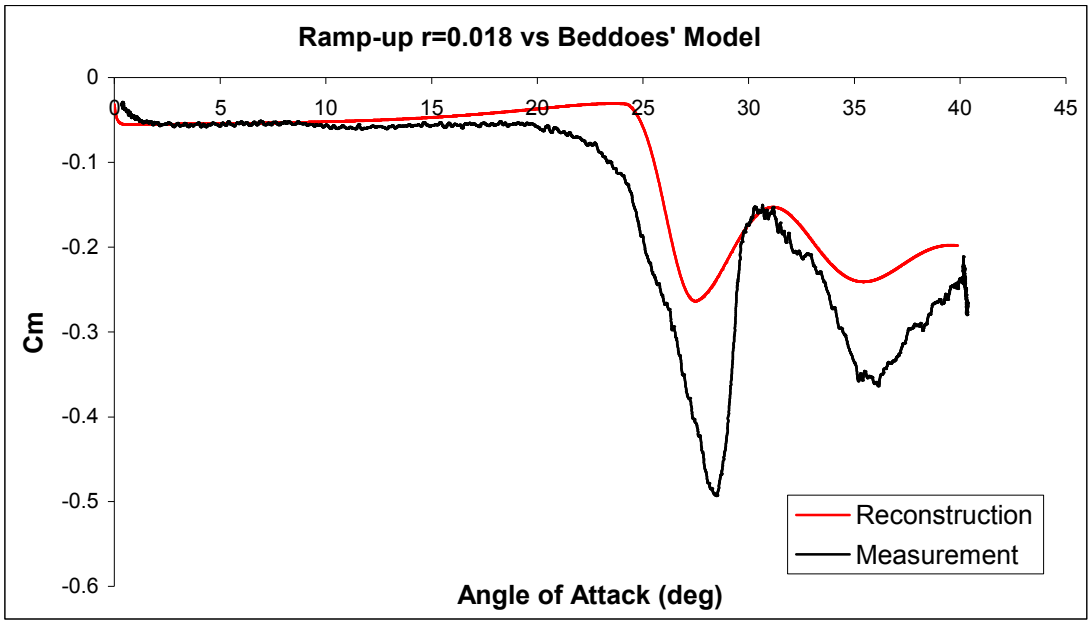

Figure 119 Cn coefficient ramp-up simulation for r=0.018 (200 deg/s)

Whilst Figure 118 and Figure 119 depict good general reconstructions, the empirical parameter values were adjusted to obtain appropriate improvements.

In particular, it may be noticed in Figure 118 that the Cn coefficient follows, in the good agreement, the first part of the curve. The accuracy becomes less when the trailing edge separation starts to take place (around 17 deg) and the onset of the dynamic-stall vortex (sudden rising up of the curve) is slightly delayed. Conversely, after these minor discrepancies, the maximum Cn achieved and the period of the sinusoidal/oscillating part are in reasonable good agreement with the data set. The reconstructive discrepancies are even more noticeable in Figure 119 (the Cm coefficient). It is clear (Figure 119) that the trailing edge separation, the onset of the dynamic vortex and the shedding of it are too delayed compared to the test performed. This deviation may also influence the post stall response in terms of maximum and minimum values achieved. However, before a detailed consideration of the Cm coefficient, it is prudent to have a closer consideration of the Cn curve and, in particular, the dynamic-stall onset. The two

aspects of the stall onset have already been noted and the parameters that influence these features are:

1) S1, S2 and Alf1 for shaping the "*f*" function;

2) C_{N1} being the trigger for the dynamic-stall onset.

Nevertheless, all the parameters used in the Beddoes' model are coupled (Appendix 2) and it is not possible, to change one without minor corrections on the others to achieve the best possible reconstruction. On the other hand, the parameters cannot be significantly altered, but should stay close to the ones obtained from the static and ramp-up tests. All Glasgow's ramp-up data have been analyzed and a better selection of the parameters are given in Table 17, where only the dCn/dα, α_0 and C_{N1} were altered slightly.

dCn/dα	α_0	α_1	S_1	S_2	K_0	K_1	K_2	Cm_0	C_{N1}	T_p	T_b	T_f	T_v	T_{vl}	m	n
0.095	-2.3	16.5	6	2	0.0005	-0.095	0.04	-0.03	1.62	3.5	1.8	5	3.2	8	1	1.5

Table 17 Beddoes' model parameters for Glasgow's data for the RAE9645 profile

Table 17 gives the final set of constants, required by the Beddoes' model, which were used for all the reconstructions carried out on the Glasgow data.

No static tests were performed by QinetiQ and so it was not possible to obtain all the parameters required for the Beddoes' model. On the other hand, following the analogies and the differences shown between the two sets of tests, it was likely to know which coefficients would have been different among the two static tests. All the QinetiQ dynamic tests confirm a higher gradient of dCn/dα that would result in a higher value of C_{N1}. It is, then, reasonable to think that, for a better reconstruction of the QinetiQ

data, these two parameters should be increased accordingly. Moreover, the analysis conducted in Chapter 3 suggests the goodness of these assumptions.

It is different for the Cm coefficient where a deductive reasoning is more complicated. However, it was decided to change the least possible number of coefficients in order to have more or less the same set of parameters between the two data sets. The result is given in Table 18.

dCn/dα	Alf_0	Alf_1	S_1	S_2	K_0	K_1	K_2	Cm_0	C_{N1}	T_p	T_b	T_f	T_v	T_{vl}	m	n
0.108	-2.3	16.5	6	2	0.0005	-0.095	0.04	-0.03	1.76	3.5	1.8	5	3.2	8	0.5	1.5

Table 18 Beddoes' model parameters for QinetiQ data for the RAE9645 profile

5.3 Oscillating

This Section presents an overview of some of the sinusoidal tests performed in the two wind tunnels. These tests cover the Beddoes model re-constructions for all the cases illustrated in Sections 2.1.4.2 and 2.2.4.2 (case 4). The first group of data is from the Handley Page tunnel. For each frequency is pictured a selection of mean angles and amplitudes to highlights the method's strengths and weaknesses in low speed aerodynamics.

For the first two reduced frequencies, Figure 120, Figure 121, Figure 122 and Figure 123, the method is in good agreement, both for the Cn and the Cm coefficients. The only major discrepancies are for the minimum value reached by the Cm's, when the light and deep dynamic stall occurs, and the path followed by the method during the pitching down phase of the cycle. Considering a range of angles of attack, for the same frequency, it may be seen that this difference increases with increasing maximum angle

of attack and, therefore, with the influence of the unsteadiness of the flow (e.g. Figure 120 and Figure 121).

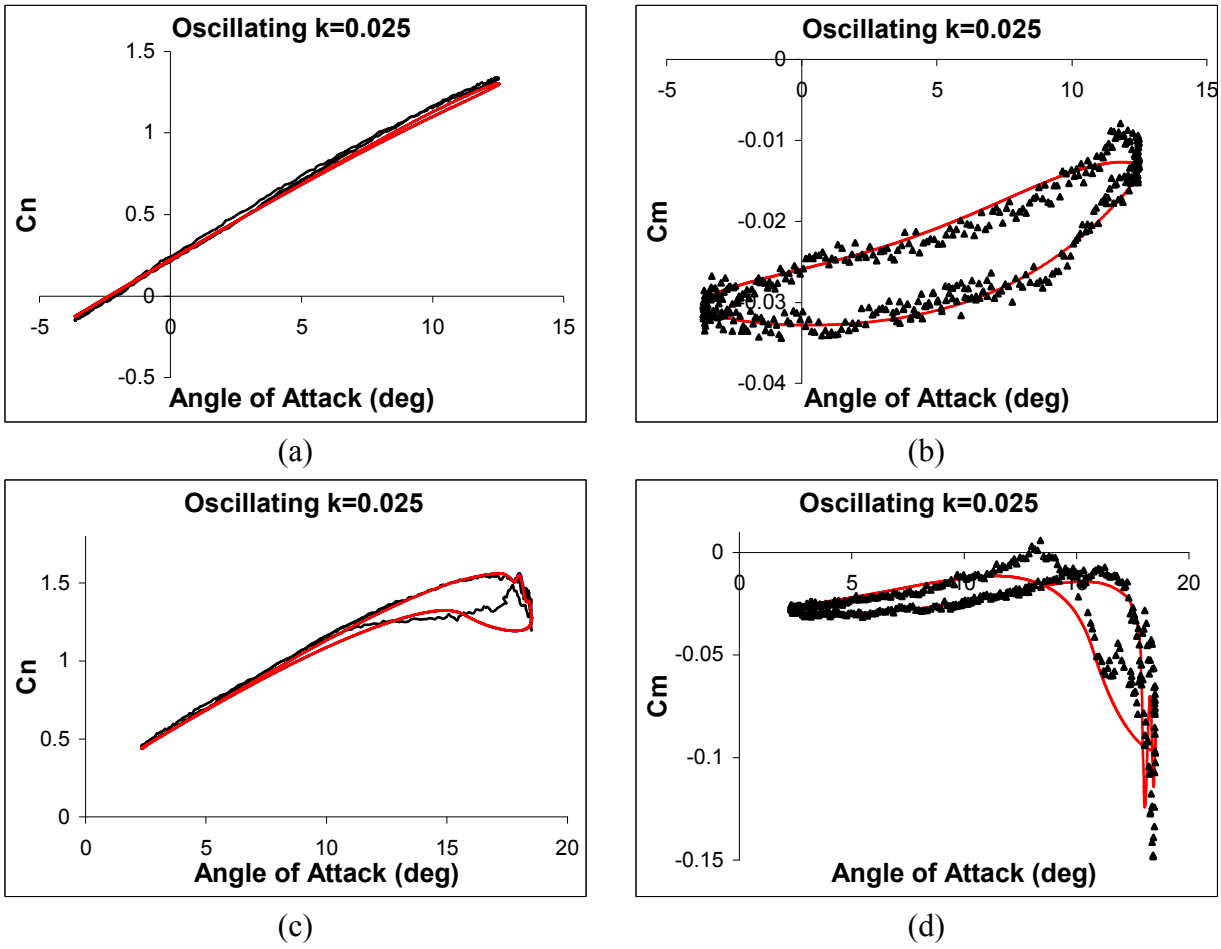

Figure 120 Beddoes' model reconstructions (red line) for the RAE9546 profile tested by University of Glasgow at k=0.025 (4.52rad/s) for different mean angles and same amplitude

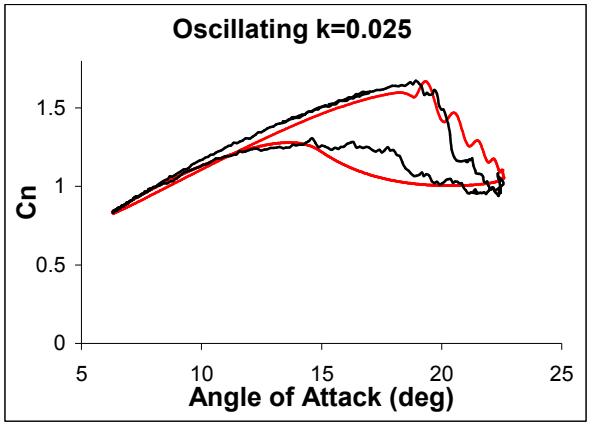

(a)

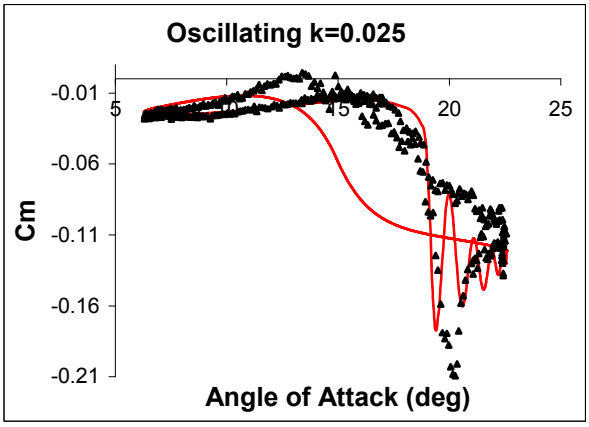

(b)

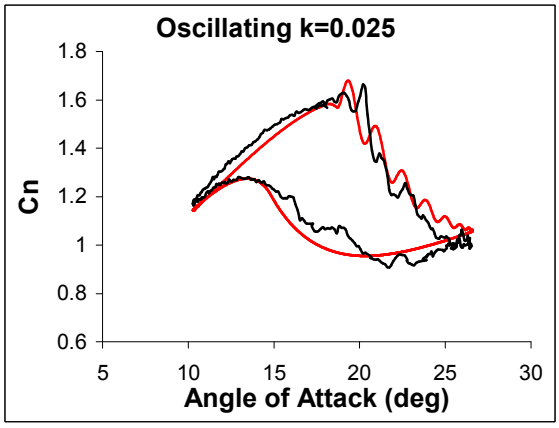

(c)

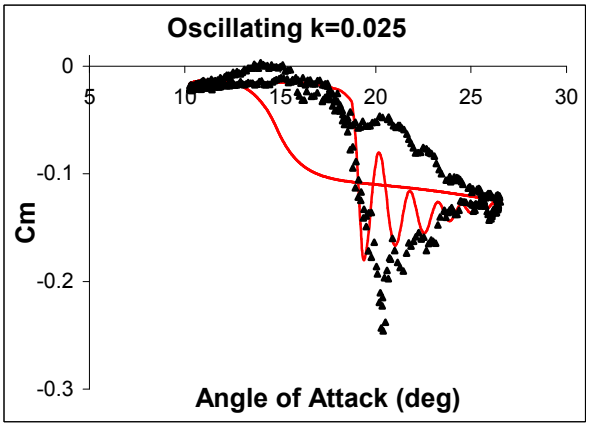

(d)

Figure 121 Beddoes' model reconstructions (red line) for the RAE9546 profile tested by University of Glasgow at k=0.025 (4.52rad/s) for different mean angles and same amplitude

Comparing the two different frequencies for the same mean angle and amplitude, however, it may be observed that the divergence between the minimum absolute values of Cm (test data and Beddoes' model) amplifies along with the increasing frequency (e.g. Figure 120, Figure 121 and Figure 123). This tendency is confirmed by the higher reduced frequencies (Figure 125 and Figure 126). Such behaviour could have been already foreseen from Figure 119 where the minimum Cm achieved by the Beddoes' model is less than the one reached by the test although the maximum Cn's appear to be in agreement (Figure 118). The problem may have its origins in a poor choice of the

pitching moment coefficients. Although it is difficult to define a good choice of these coefficients, as there are many combinations that can satisfy the static test, the chosen set of parameters was tested against all the tests performed and appeared to be a good choice for all of them. Conversely, a set of coefficients that may give a better fitting for the dynamic cases may not satisfy the static case. Hence what, may be a possible real reason, in these cases, is that in low speed aerodynamics the effect of the unsteadiness and vortex shedding on the Cm's is stronger than for higher Mach numbers. In this way the Beddoes' model may not always be a good reconstruction to the experimental data. This difference may be appreciated better by considering Figure 120 (c-d) where the profile still does not show any deep dynamic stall and the maximum Cn is similar to those of the static tests (Figure 115). Nevertheless, the aerofoil does experience the effects of the dynamic behaviour and the minimum value for the Cm is, roughly, 35% greater than the static test. As the reduced frequency increases, and the dynamic behaviour of the flow becomes more important, this difference appears to be bigger and clearer.

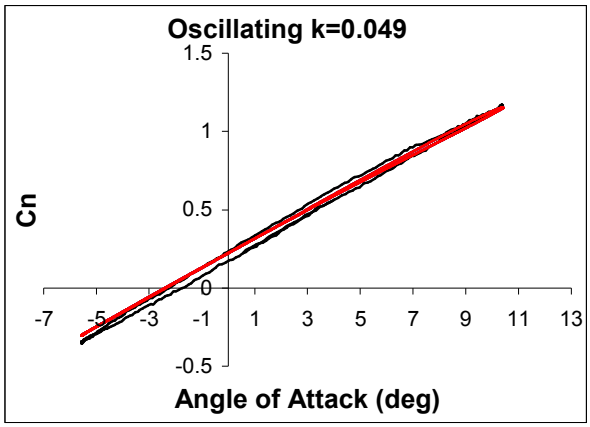

(a)

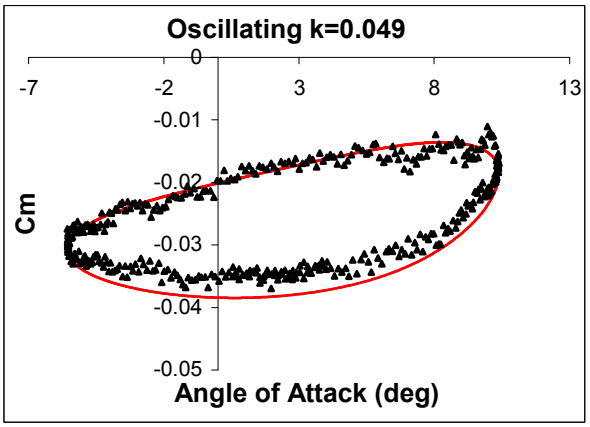

(b)

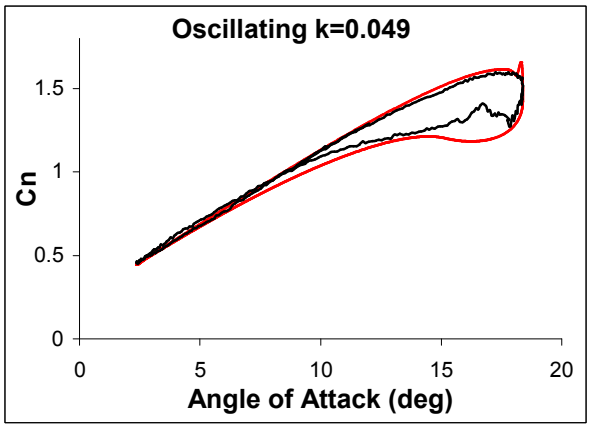

(c)

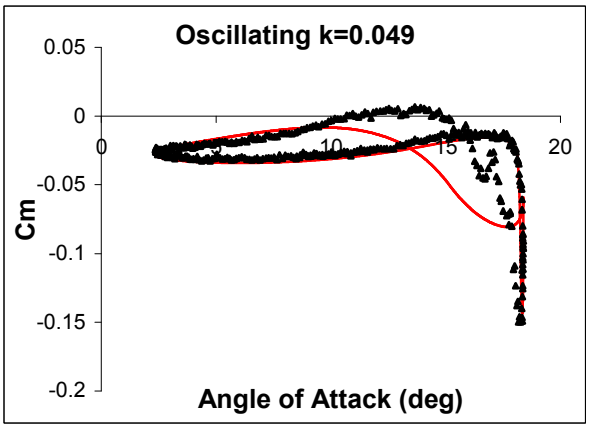

(d)

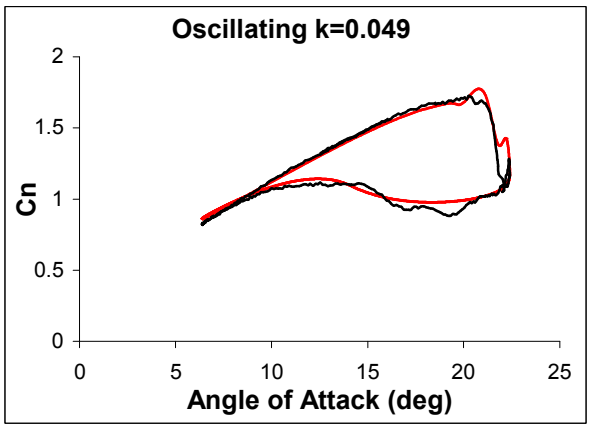

(e)

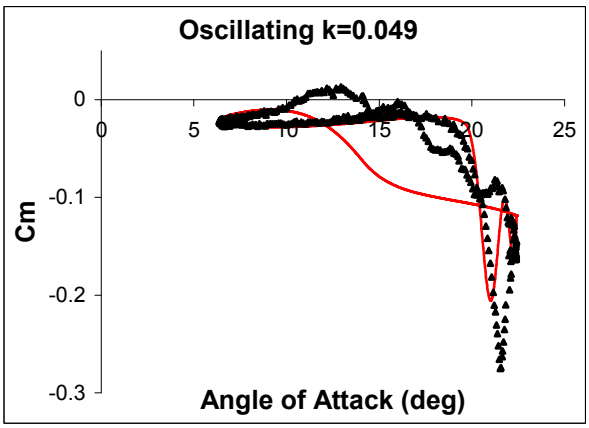

(f)

Figure 122 Beddoes' model reconstructions (red line) for the RAE9546 profile tested by University of Glasgow at 9.1rad/s for different mean angles and same amplitude

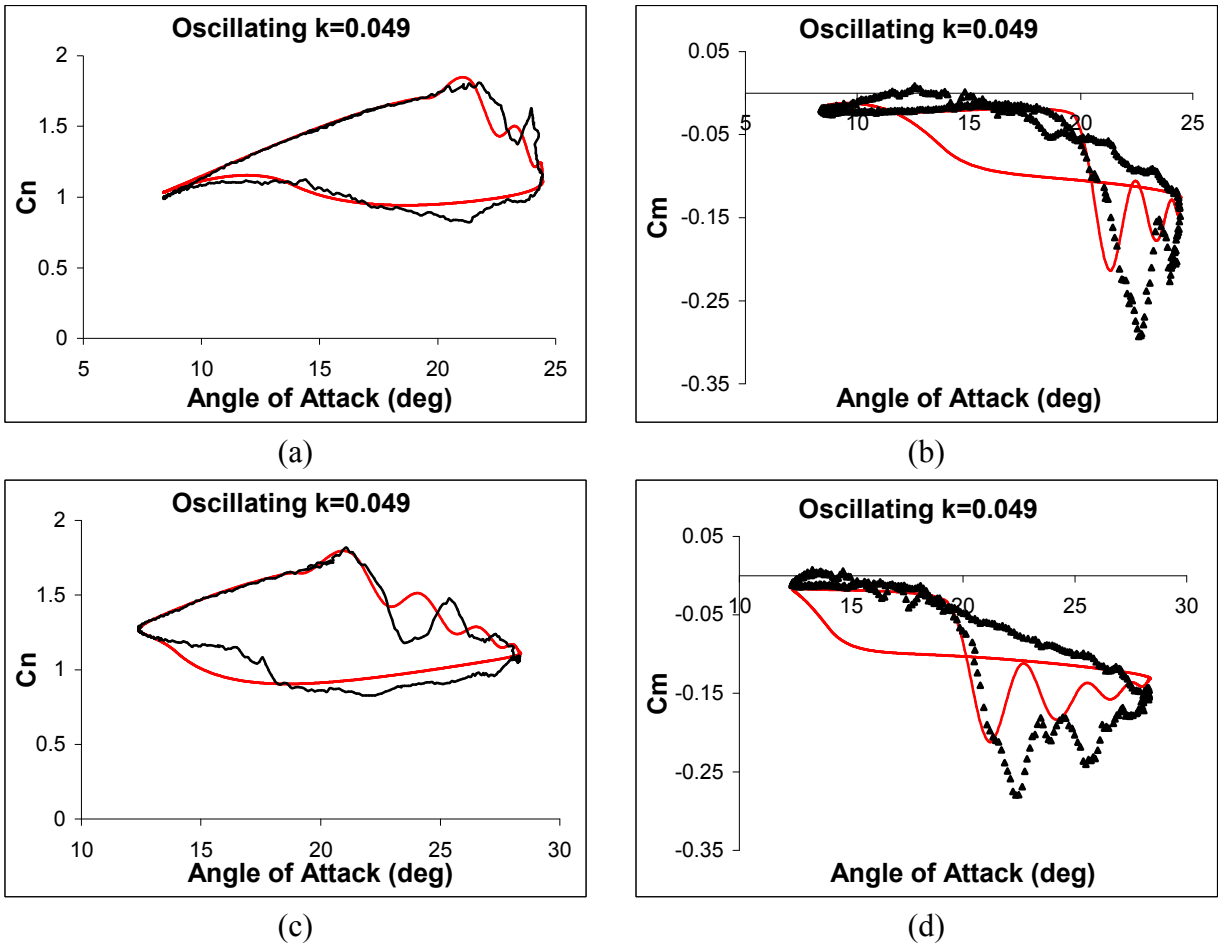

Figure 123 Beddoes' model reconstructions (red line) for the RAE9546 profile tested by University of Glasgow at 9.1rad/s for different mean angles and same amplitude

Increasing the reduced frequency highlights the aspects already mentioned and shows a new tendendecy of the Beddoes' model.

It has already been discussed (Chapter 4.1.2 and eq. A2.26) that, in low speed aerodynamics, the T_p lagging carried out with Beddoes' methodology is not enough to catch the onset of the dynamic-stall. Here, this lag was increased by adding an additional T_b lagging, as it was proposed by Niven [62]. However, when the reduced frequency is high enough, the additional T_b lag, obtained by the ramp-up data, may not be sufficient to capture the stall onset properly [70]. This happened for the two highest reduced frequency tests in Glasgow University data. It is clear from Figure 125 (a and c) and

Figure 126 (c and e) that the re-constructed stall onset occurs before the measured incidence.

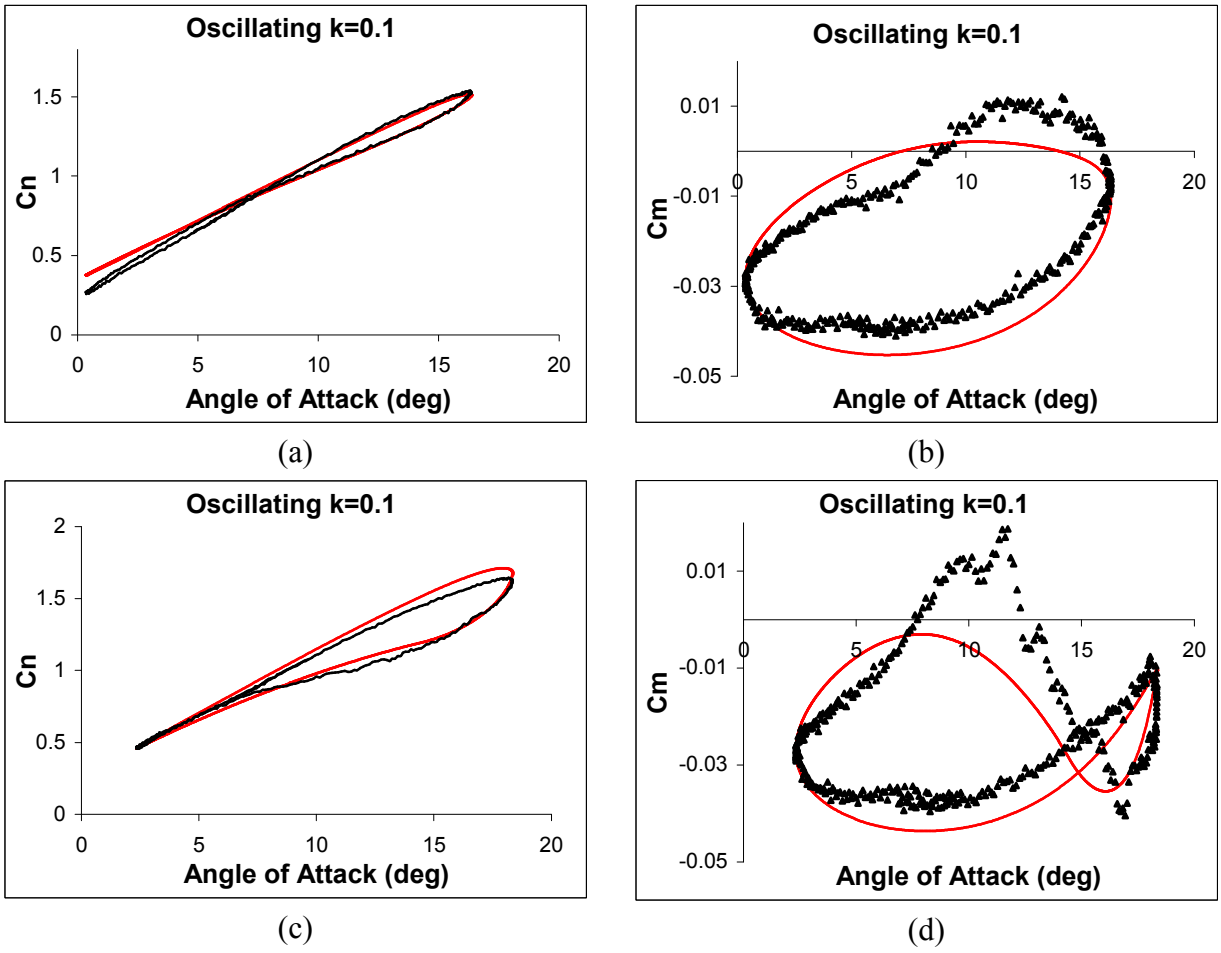

Figure 124 Beddoes' model reconstructions (red line) for the RAE9546 profile tested by University of Glasgow at 18.5rad/s for different mean angles and same amplitude

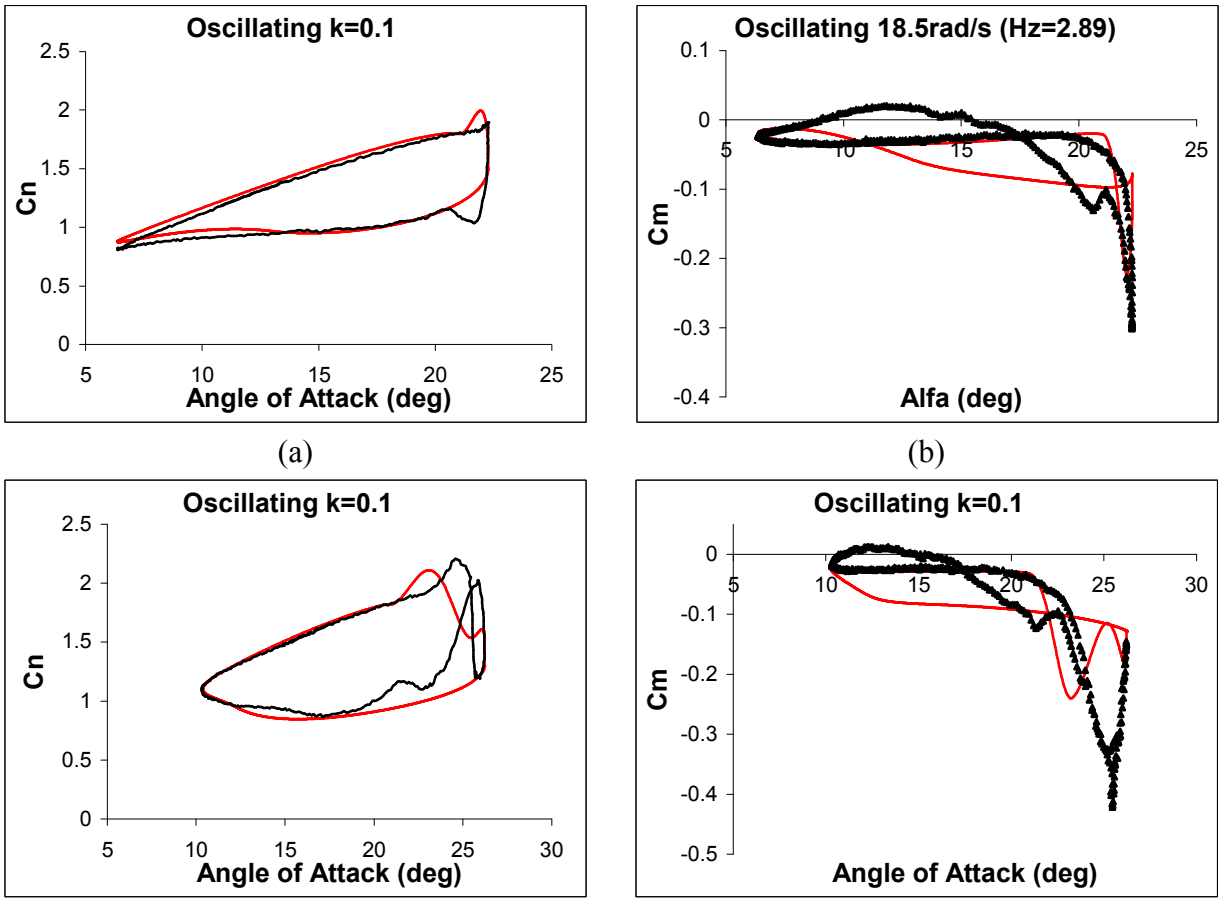

Figure 125 Beddoes' model reconstructions (red line) for the RAE9546 profile tested by University of Glasgow at 18.5rad/s for different mean angles and same amplitude

Moreover it was also observed that the "*f*" function (eq. A2.31) used by the model to match the data, is not always suitable for all the profiles. As happened for the RAE9645, the shape of the "*f*" function carried out from the static test may not be easily fitted by a continuous equation.

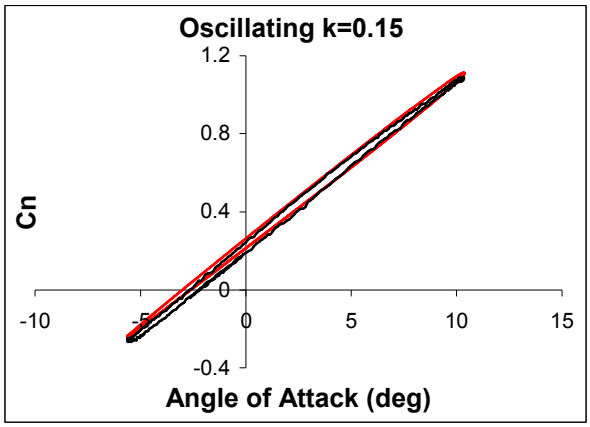

(a)

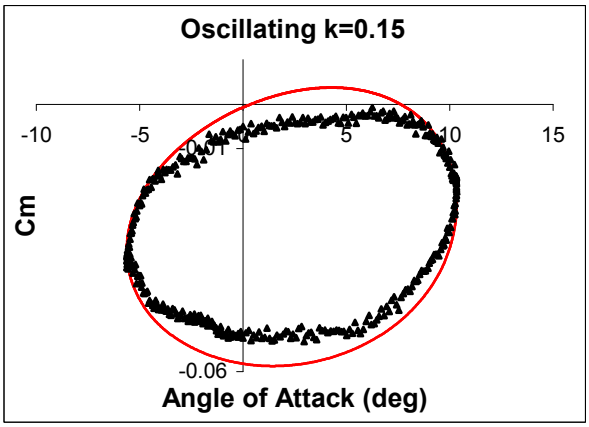

(b)

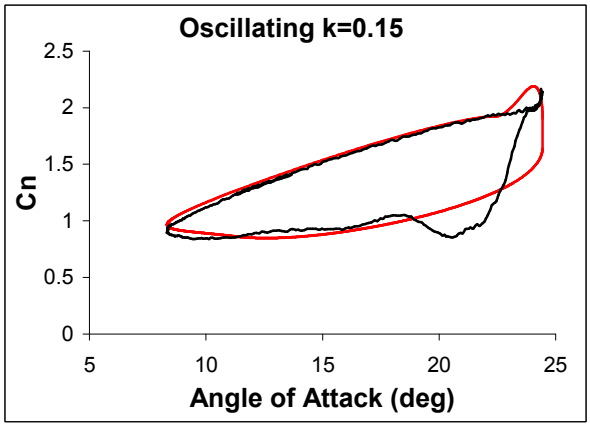

(c)

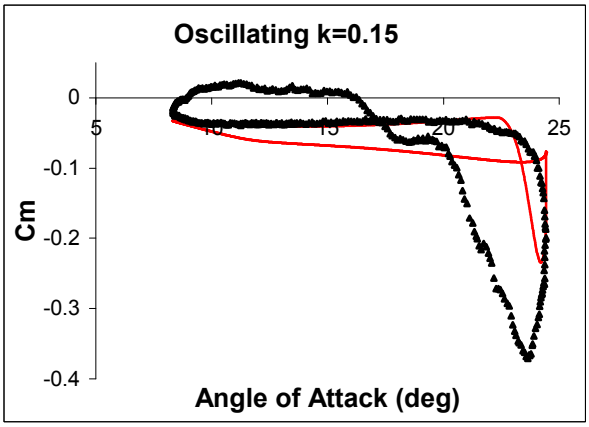

(d)

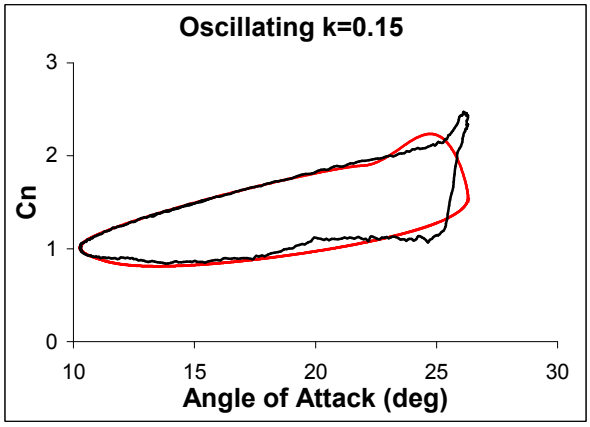

(e)

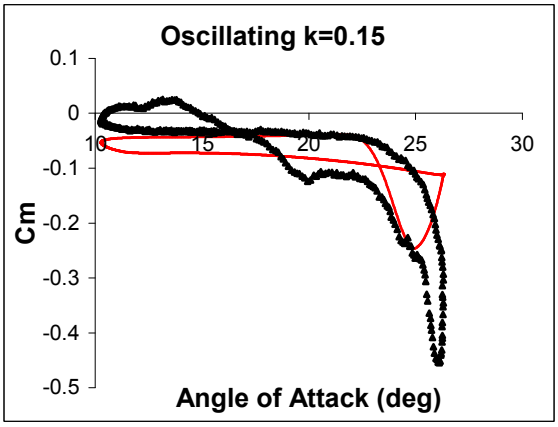

(f)

Figure 126 Beddoes' model reconstructions (red line) for the RAE9546 profile tested by University of Glasgow at 27.7rad/s for different mean angles and same amplitude

Figure 127 presents the "fitting" function, as described by the Kirchhoff equation, with the values obtained for each testing point of the static test. All the points for the attached flow above the unit were put equal to 1 in order to satisfy a Kirchhoff-theory requisite.

This does not effect the general observations and the method has a maximum of 1. It may be noticed that, in this case, the "*f*" line would be better matched by four linear curves rather than the two equations in Appendix 2 (eq.A2.31). The line is equivalent to one until the incidence reaches ~9 deg, at this angle of attack the second curve has a negative tangent up to 15 deg. At this point the next curve's tangent is less until an incidence of ~22 deg where the tangent becomes zero. Such behaviour is difficult to reproduce by other functions than straight lines (or look-up tables). Unfortunately these three incidences (e.g. 9, 15 and 22 deg for RAE9645) are very important for any aerofoil. In fact, for the pitching up part of the loop, they represent the beginning of the trailing edge separation, the Cm break and the minimum value of the Cm coefficient. During the subsequent pitch-down movement, they are important points to understand how and when the flow starts to re-attach and then to return to fully attached flow. They are significant steps for good reconstructions of the data and small differences at these angles of attack may lead to unfortunate discrepancy from the Beddoes' model. Moreover, the "*f*" function obtained from the pitch-down tests, empathizes this behaviour as being able to be fitted by two straight lines. An almost straight line parallel to the X axis (with few oscillations due to the instability conditions of the fluid) until the boundary layer starts to re-establish and a second branch tilted with the same tangent during that re-attachment process; shown in Figure 128.

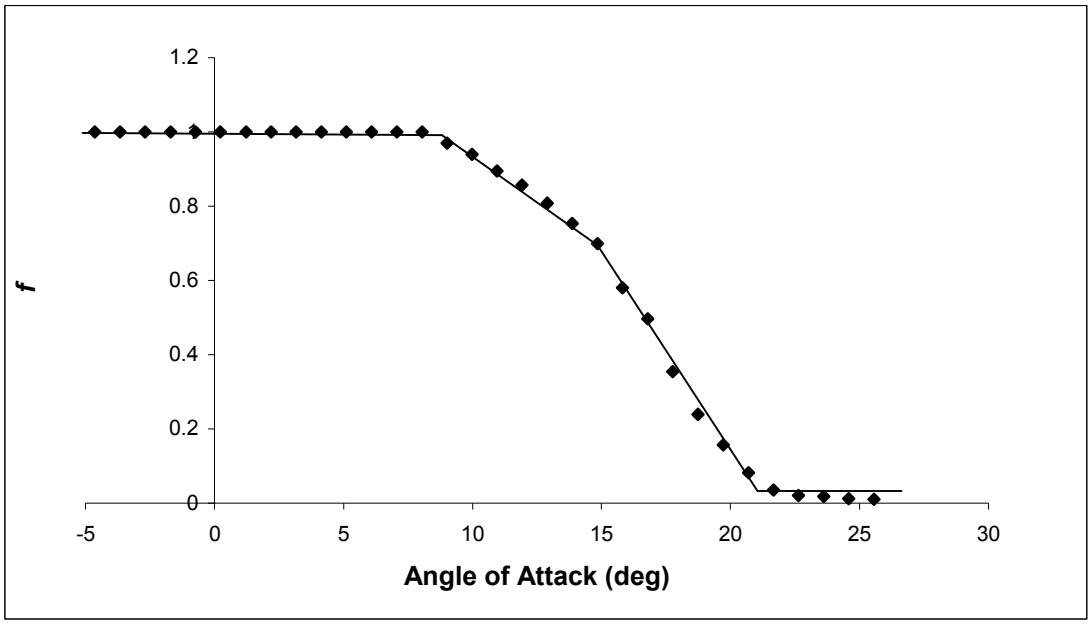

Figure 127 RAE9645 "*f*" function carried out from Cn experimental data for the static test (Glasgow)

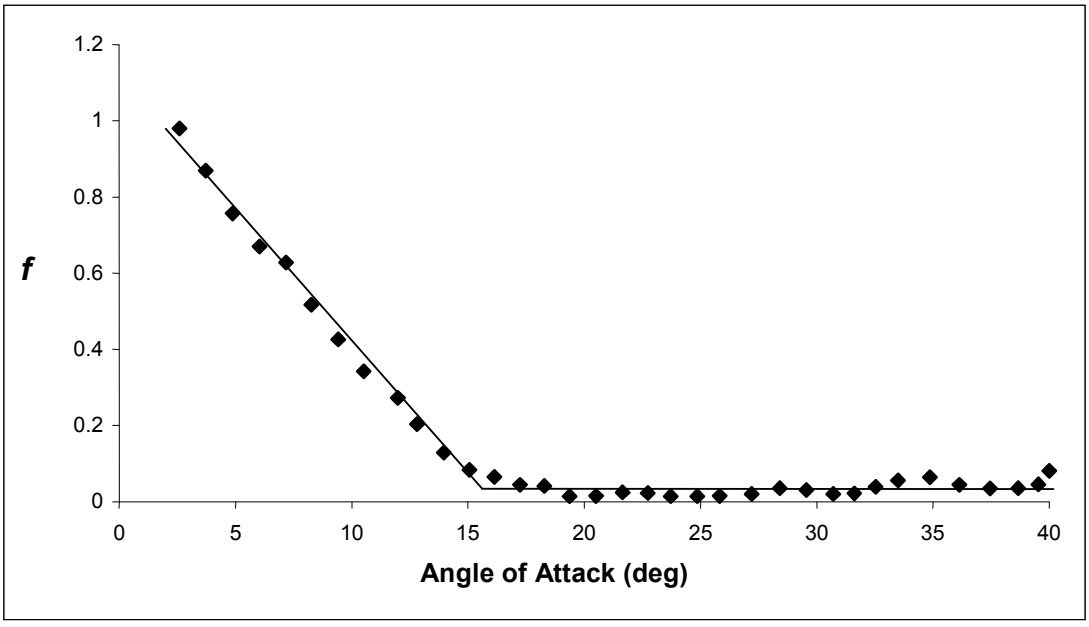

Figure 128 "*f*" function carried out from Cn data for ramp-down motion (University of Glasgow test n.317)

Similar behaviour may be noticed for the QinetiQ data. The simulations were run, with the coefficients presented in Table 18, and a few examples, for different frequencies, are given in Figure 129, Figure 130 and Figure 131.

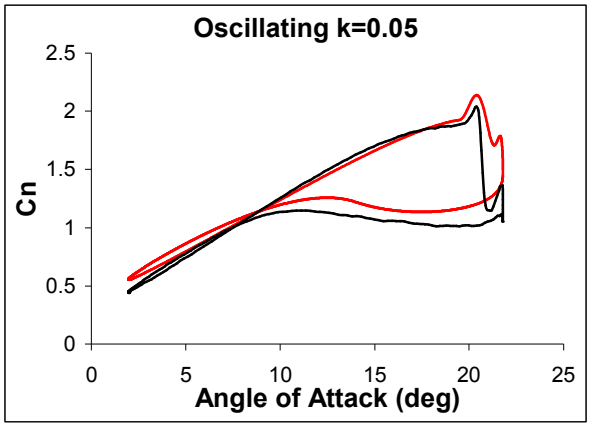

(a)

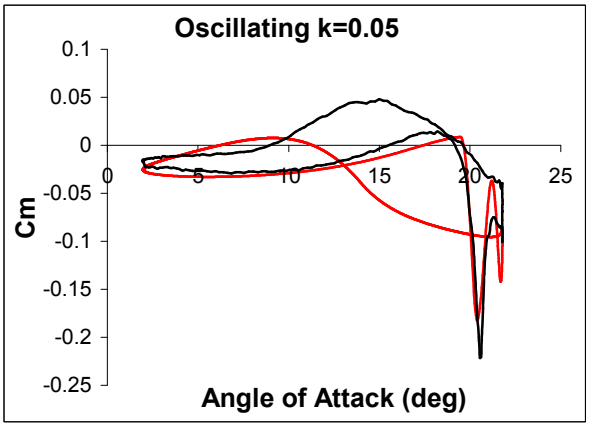

(b)

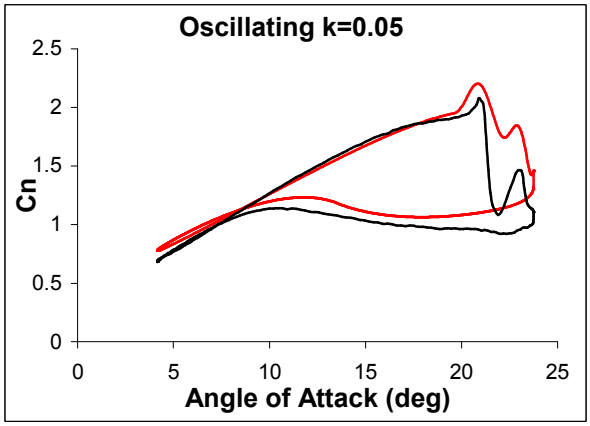

(c)

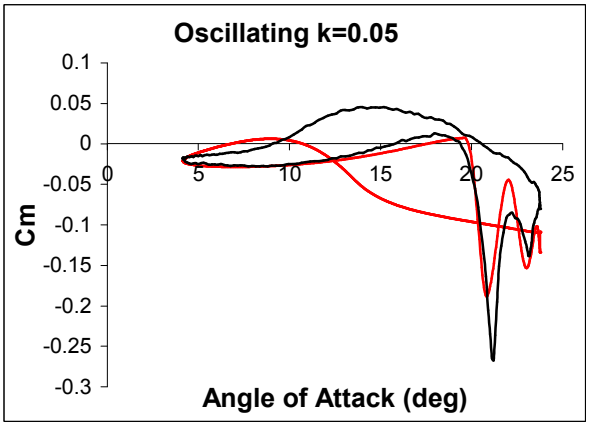

(d)

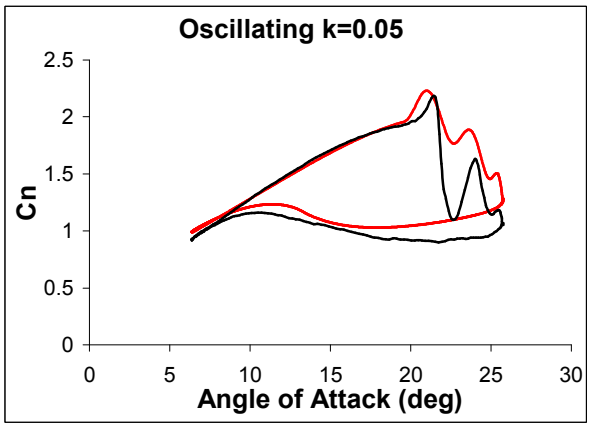

(e)

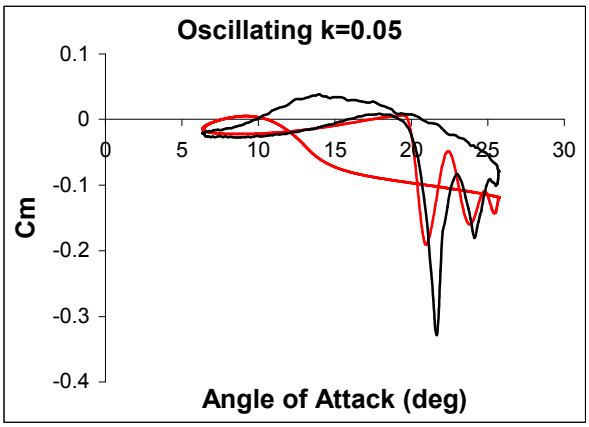

(f)

Figure 129 Beddoes' model reconstructions (red line) for the RAE9546 profile tested by QinetiQ for different frequencies, mean angles and same amplitude

As for the Glasgow data reconstructions, the QinetiQ reconstruction present smaller absolute values for the minimum Cm, a different path during the pitching down part of the loop and an earlier dynamic-stall onset for the higher frequency.

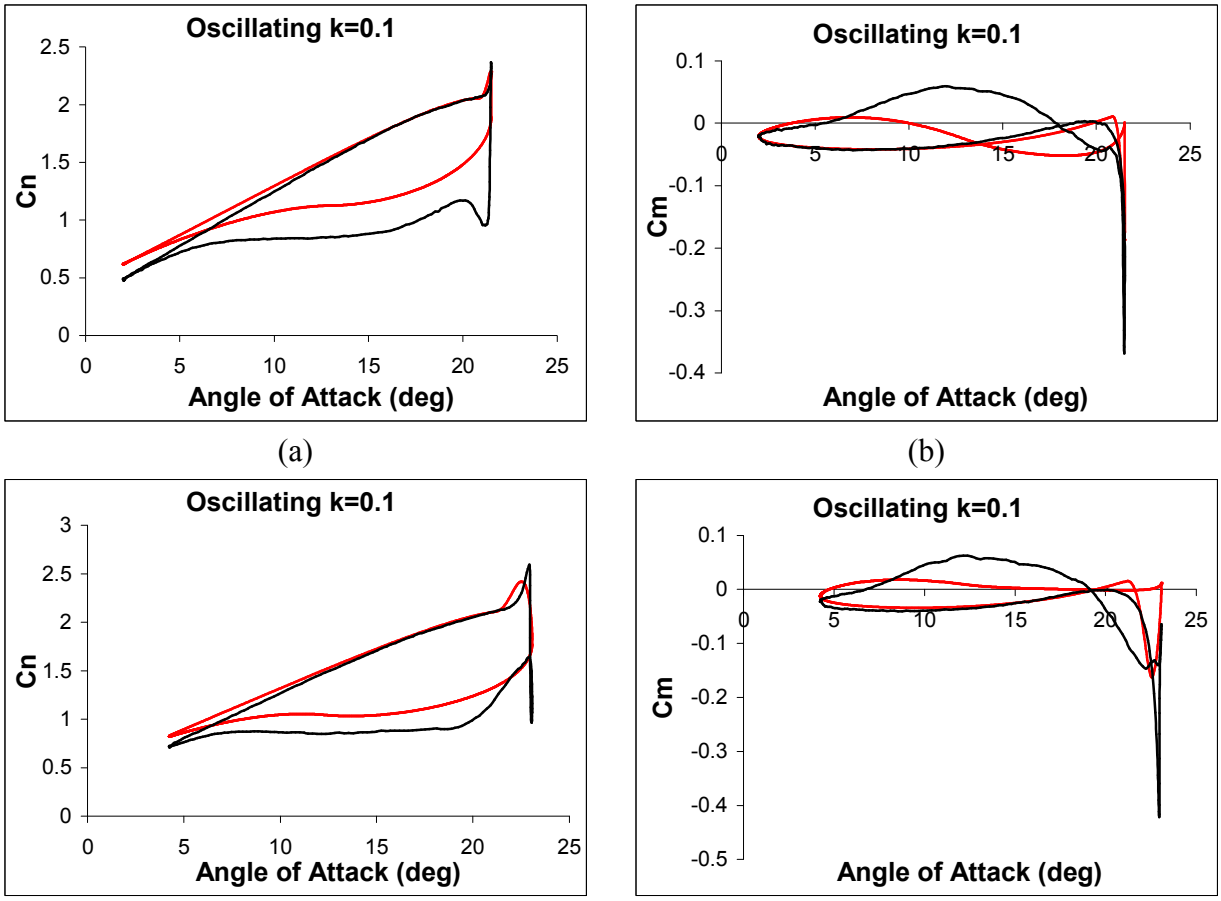

Figure 130 Beddoes' model reconstructions (red line) for the RAE9546 profile tested by QinetiQ for different frequencies, mean angles and same amplitude

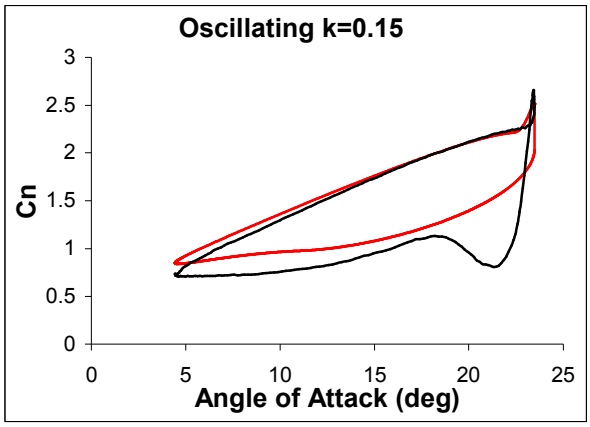

(a)

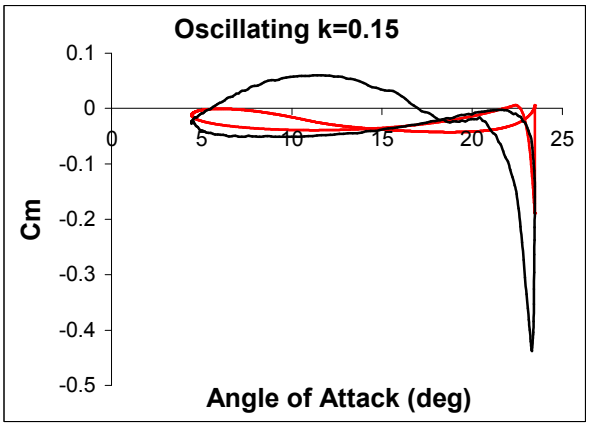

(b)

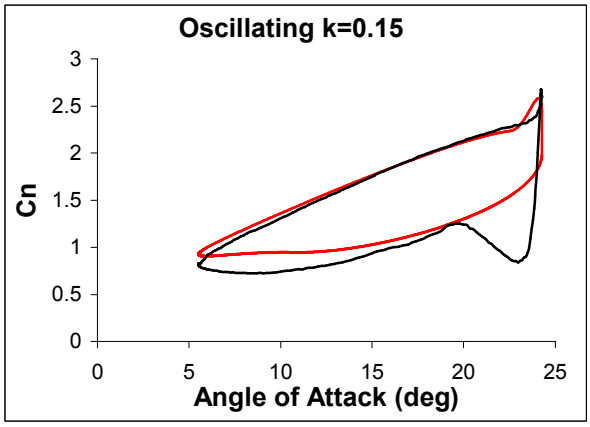

(c)

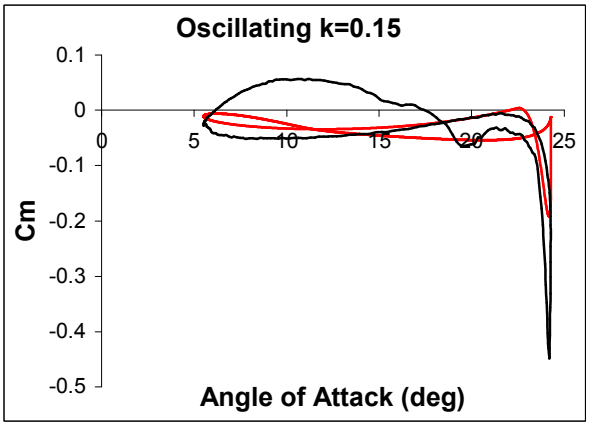

(d)

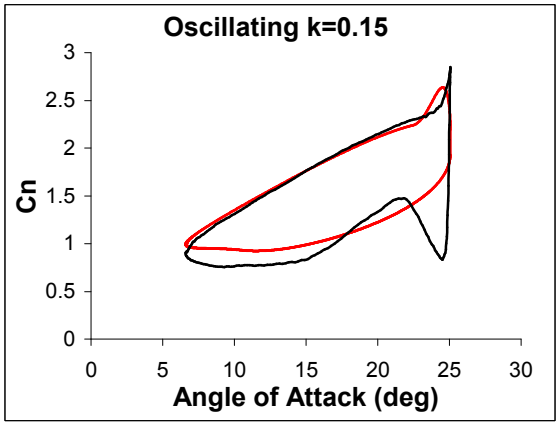

(e)

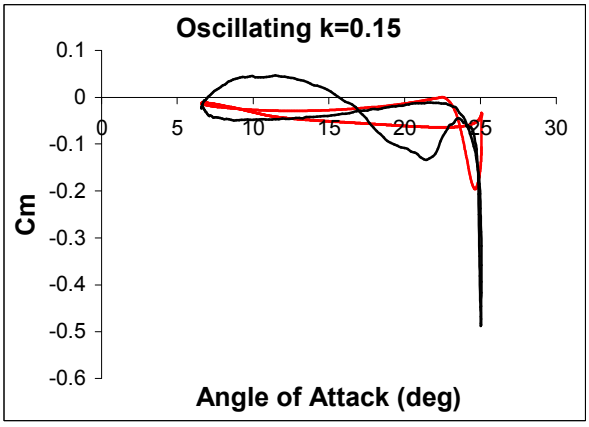

(f)

Figure 131 Beddoes' model reconstructions (red line) for the RAE9546 profile tested by QinetiQ for different frequencies, mean angles and same amplitude

5.4 Ramp-up

Ramp-up tests are very useful when evaluating or choosing many of the parameters that cannot be obtained from the static tests. This section presents some Beddoes' reconstructions with the coefficients listed in Table 17 and Table 18. In Figure 132 and Figure 133 it may be noticed, that the model gives a very close representation for the Cn coefficients. The choice of "unconventional" "s" (Table 17 and Table 18) parameters, usually smaller for other profiles, for the "*f*" function (eq. A2.31), that are included in these reconstructions, is well justified by the obvious agreement between the two data sets. What is also clear, is that the dynamic-stall onset is well caught, but the effects of the vortex shedding are underestimated; as was already noticed for the oscillating cases. When the profile stalls, the Cn does not drop far enough compared with the measured data. A similar difference may be observed in the Cm coefficients. As for the oscillating tests, the minimum value of Cm, obtained with the Beddoes' model, is always smaller, in absolute terms, than the measured data. The biggest discrepancy, however, is the onset of the deep stall for the Cm coefficient. The Beddoes' model always predicts it with too much delay applied compared to the measured data. Additionally the predicted Cm drops very suddenly when compared with the experimental data that always present a "smoother" Cm stall. This is due to the static test. In fact, it may be noticed in Figure 116, that the static behaviour presents a very sudden stall and an increase in Cm just before stall. This manner was also present in the oscillating cases when the dynamic-stall was either not present or light. In the Beddoes' model, the simulations follow that dictated by the coefficients obtained from the static test and so the simulations differ. It

can be noticed in Figure 132 that, for all the reconstructions, the Cm line presents a rapid stall and the "raising up" of the curve prior to this.

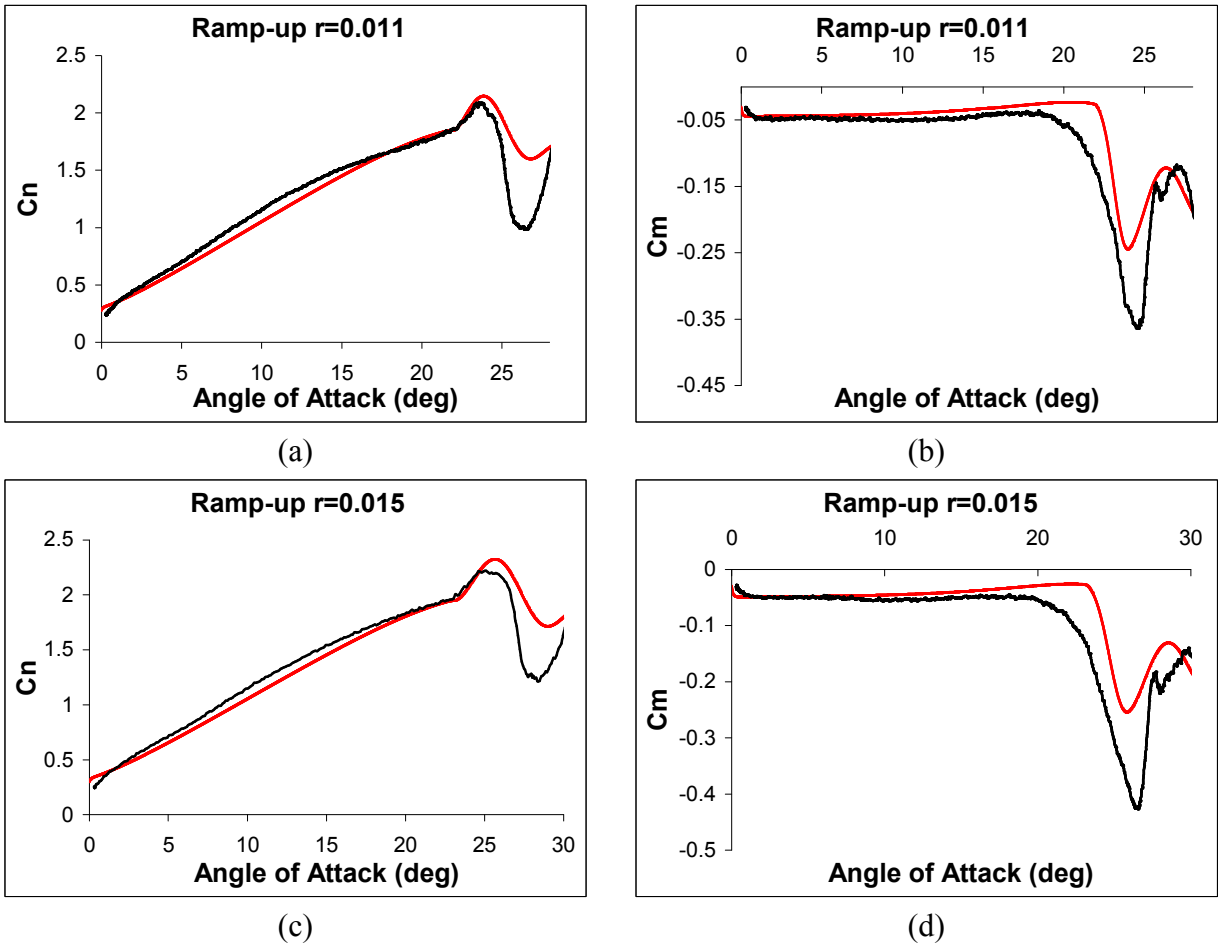

Figure 132 Beddoes' model reconstruction (red line) for Cn and Cm coefficients compared to the University of Glasgow's test data (black line)

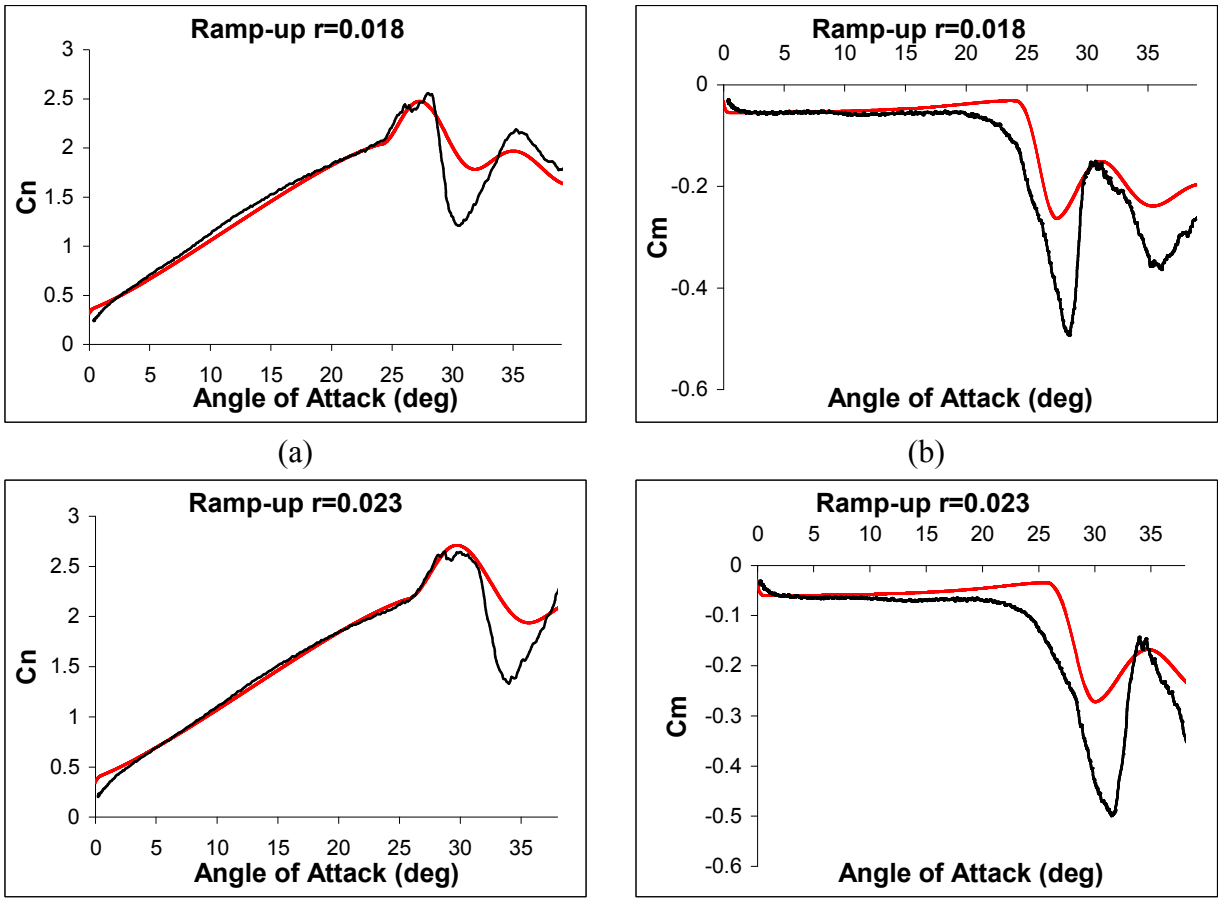

Figure 133 Beddoes' model reconstruction (red line) for Cn and Cm coefficients compared to the University of Glasgow's test data (black line)

For the QinetiQ data, similar observations may be made. Although in this case the agreement of the model with the Cm lines is better. In fact, it may be observed that the Cm coefficients have a closer behaviour to the one of the static test. In these tests the centre of pressure appears to move to the front of the profile and the line does not have a relatively constant value until the stall occurs. In Figure 134 and Figure 135 it may be seen that, for all the tests reported, the Cm curve always raises up towards positive values as the angle of attack increases.

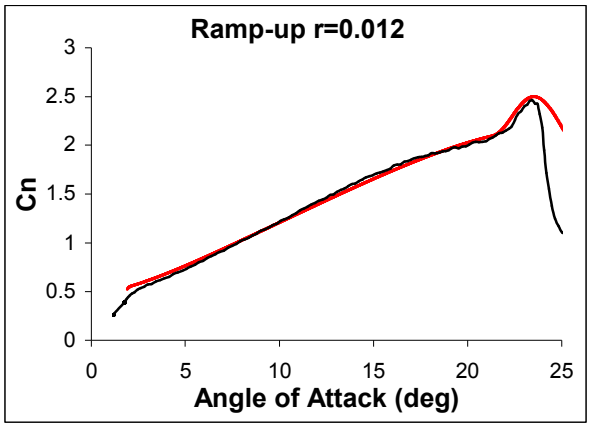

(a)

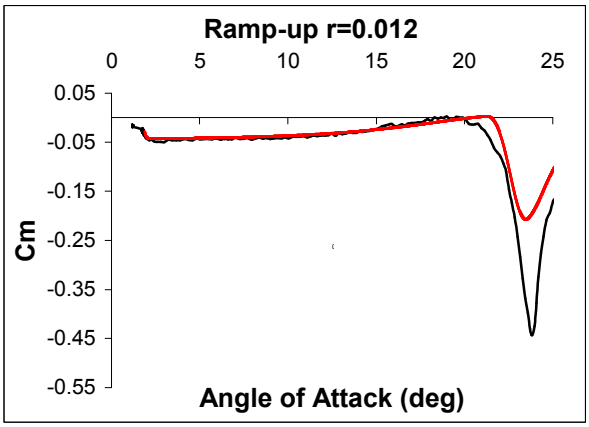

(b)

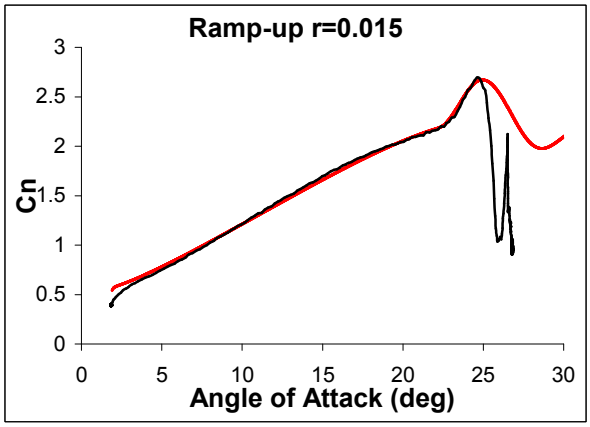

(c)

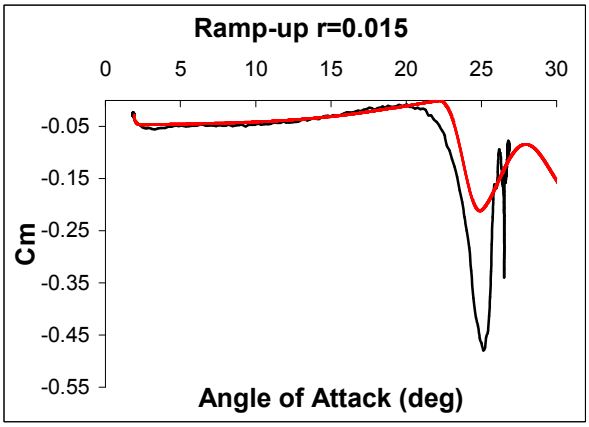

(d)

Figure 134 Beddoes' model reconstruction (red line) for Cn and Cm coefficients compared to the QinetiQ test data (black line)

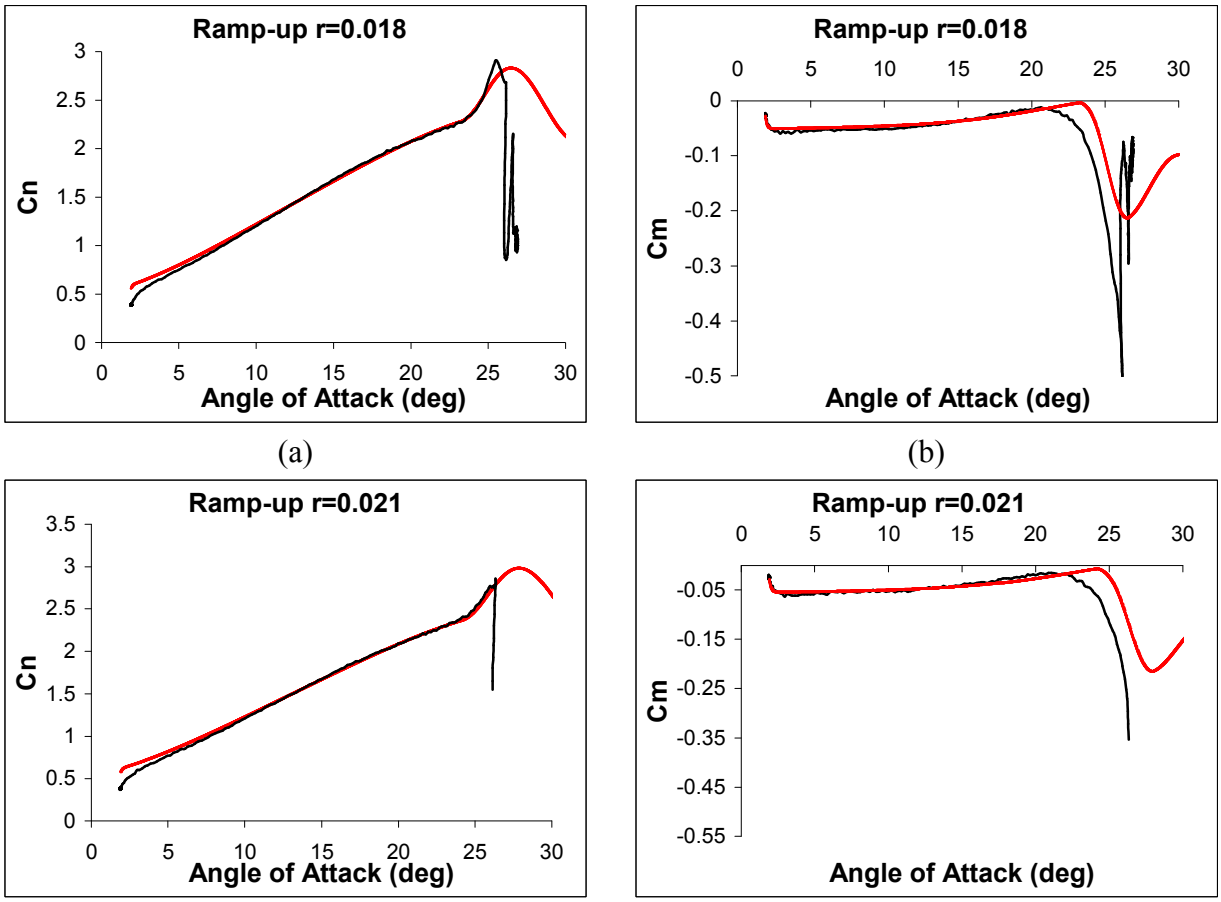

Figure 135 Beddoes' model reconstruction (red line) for Cn and Cm coefficients compared to the QinetiQ test data (black line)

5.4.1 Sensitiveness and improvement of the method

It has been illustrated how the Beddoes' model worked during the simulations of the ramp-ups and what were the points of weakness. This section investigates how the model, and its parameters, may be improved to yield better agreement with the measured data and to test the model's sensitivity to those parameters.

The Cn curves reconstructed by the method showed good agreement with the measured data and it was only after the stall that the agreement deteriorated. This suggests that the influence of the vortex generated is not modelled as well as could be.

The initial cycle of the vortex shedding involves its formation and growth over the chord. This is well represented by eq. A2.36 and the input parameter values used in the simulations were well coupled with the test results. The subsequent behaviour (eq.A2.37) involved the influence of vortex while it is convecting over the chord and leaving the trailing edge. It is when this second phase took place that the agreement between the model and the tests deteriorated. To force an improvement in the Cn reconstruction in this phase of the process, eq.A2.36 was modified to be:

$$V_x = \cos\left[\frac{\pi(\tau - T_v)}{T_{v1}}\right] \qquad \text{for } \tau > T_v \qquad 5.1$$

The cosine squared term has simple been replaced by the cosine. This was because the RAE9645 presents a very deep stall, after it achieves the maximum Cn, which could not be attained properly with eq. A2.37. Figure 136 and Figure 137 illustrates that this simple modification improves the ability of the method to achieve the measured minimum Cn post stall.

(No other modifications have been done to the Beddoes' model for these simulations).

With regard to the Cm reconstructions, the main discrepancies were found where the parameters obtained from the static test did not give the best representations. Accordingly another set of parameter/coefficients was developed in order to obtain improved agreement with the measured data. Table 19 lists these new parameters. The original parameters were changed to produce a smoother Cm-break and, also, to achieve

the minimum value of Cm. The modification of eq. A2.36 also influenced these changes to the parameters.

dCn/dα	Alf_0	Alf_1	S_1	S_2	K_0	K_1	K_2	Cm_0	C_{N1}	T_p	T_b	T_f	T_v	T_{vl}	m	n
0.095	-2.3	16.5	6	2	-0.015	-0.12	0.045	-0.03	1.62	3.5	1.8	5	3.2	3.2	2	4

Table 19 Beddoes' model parameters for University of Glasgow's data

In Figure 136 and Figure 137 are shown a few of the Beddoes' model simulations of the Glasgow's data set.

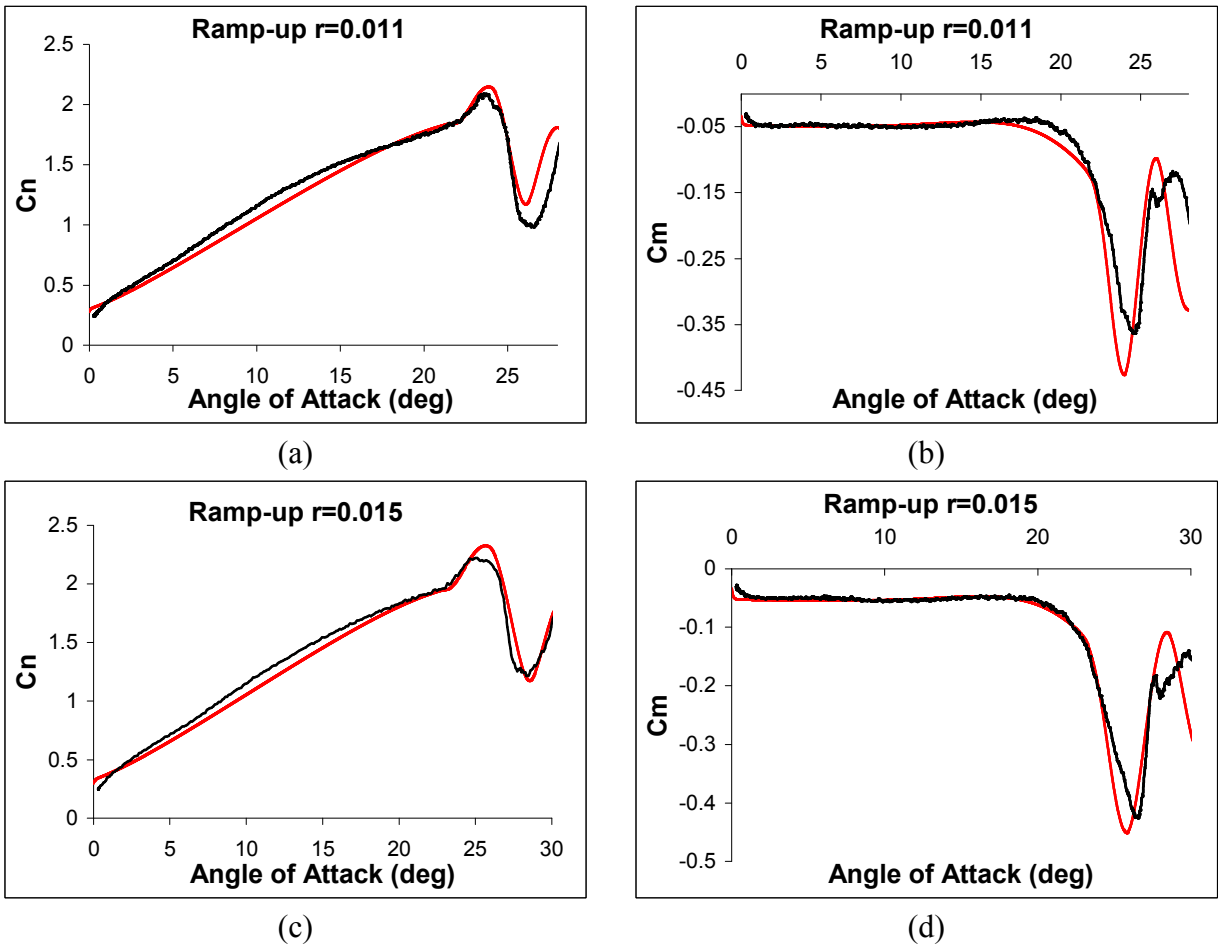

Figure 136 Beddoes' model reconstruction (red line) for Cn and Cm coefficients compared to the University of Glasgow's test data (black line)

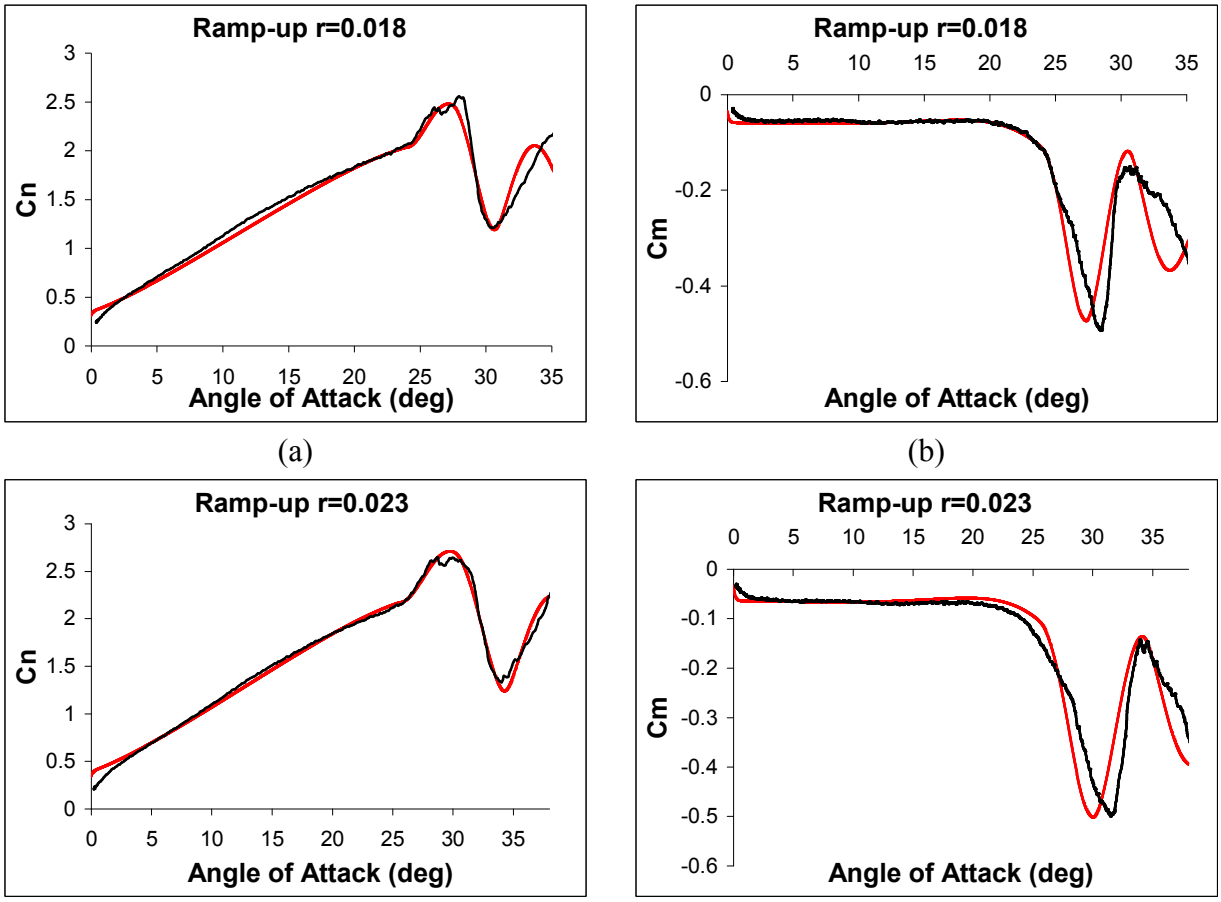

Figure 137 Beddoes' model reconstruction (red line) for Cn and Cm coefficients compared to the University of Glasgow's test data (black line)

In all the examples there is a good agreement between the reconstructions and measured data. Not all, however, is perfect and three aspects where further work may yield further improvement. It may be seen that for the modelled Cn coefficients, Figure 136 and Figure 137, the reconstructed dCn/dα, of the linear part of the curve, does not decrease in value, with the same ratio, than those of the measured data as the pitch rate increased. The tangent of the curve reduces, with the increasing pitch rate, faster in the test data. In Figure 136 (a), there is a visible gap between the two lines, and this reduces as pitch rate increases (Figure 137 (c)). The second aspect worthy of consideration is the evident

appreciable trailing edge separation (as shown in Figure 23). This is difficult to be represented by the Beddoes' model equation (A2.31), albeit the use of "non-conventional" "S" parameters. This suggests that the parameters of the *"f"* function require to be changed to gain a closer representation of the aerofoil's trailing edge separation. Finally an important aspect may be noticed in the Cm profiles (Figure 136 and Figure 137, b and d). The Beddoes' model appears unable to follow the deep dynamic-stall process. This may be appreciated by the earlier attainment of the minimum Cm, in terms of angles of attack, in all the reconstructions. However, was pointed out in Chapter 2, the increasing reduced pitch rate had the faculty, of "smoothing" and making less abrupt the dynamic-stall Cn profile.

In the Table 19, the only changed parameters, compared to Table 17, were the "K" coefficients and eq. 5.1 exponents for the Cm. The same modifications were then applied to the QinetiQ data. The Beddoes' model reconstructions for some pitch rates are presented in Figure 138 and Figure 139.

Figure 139 does not contain the highest pitch rates because the maximum angle of attack for these tests was insufficient to trigger any deep dynamic-stall onset and the aerofoil remained in the linear part of curve for both Cn and Cm coefficients.

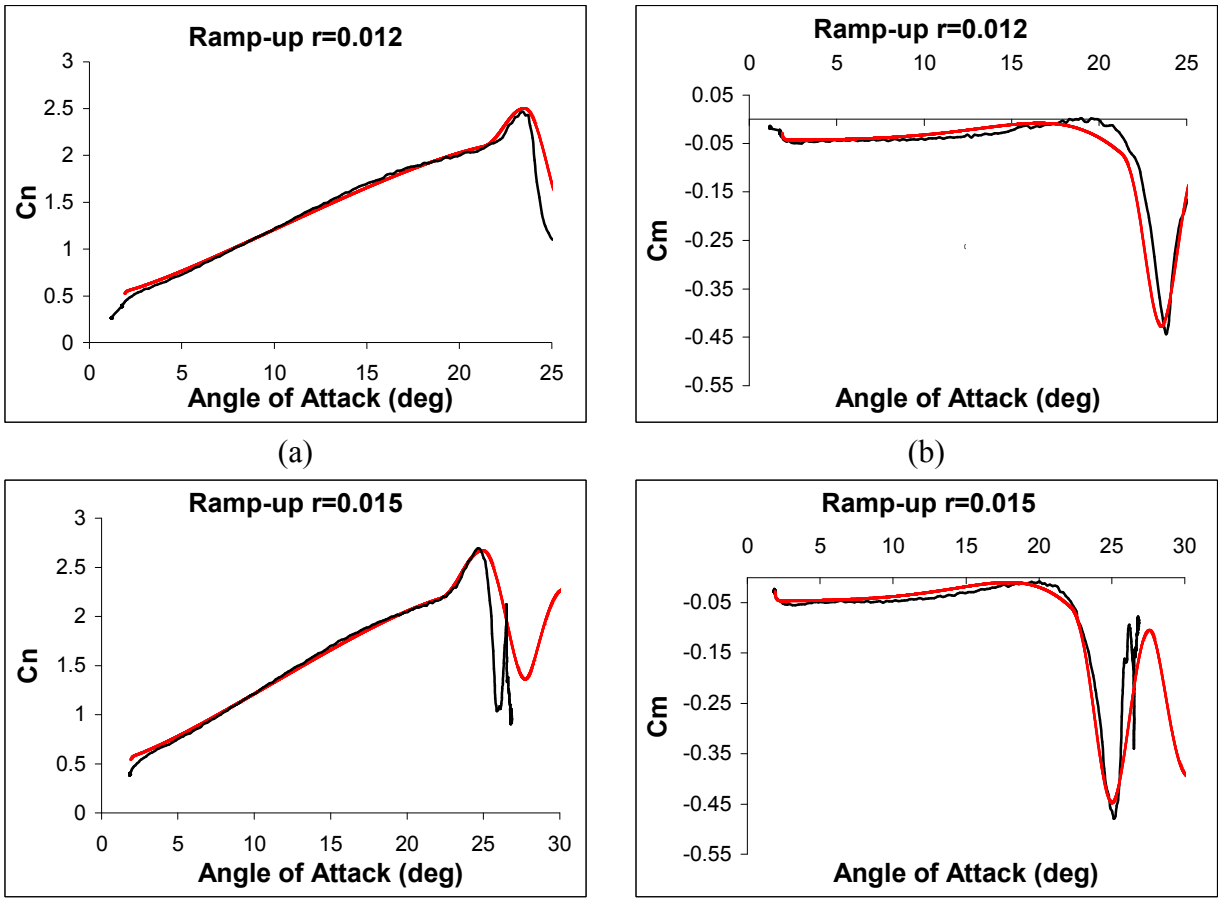

Figure 138 Beddoes' model reconstruction (red line) for Cn and Cm coefficients compared to the QinetiQ test data (black line)

It may be observed, in Figure 137, that, for the higher pitch rates, the onset of the deep dynamic-stall process was always above 25 degrees (see also Chapter 4.1.3). This is very close to the maximum incidence of the QinetiQ tests for the pitch rates of 240, 280 and 300 deg/s. The four tests represented in Figure 138 and Figure 139, however, are sufficient to permit a few modifications to the input parameters of the Beddoes' model so that the model can reproduce the data with good agreement.

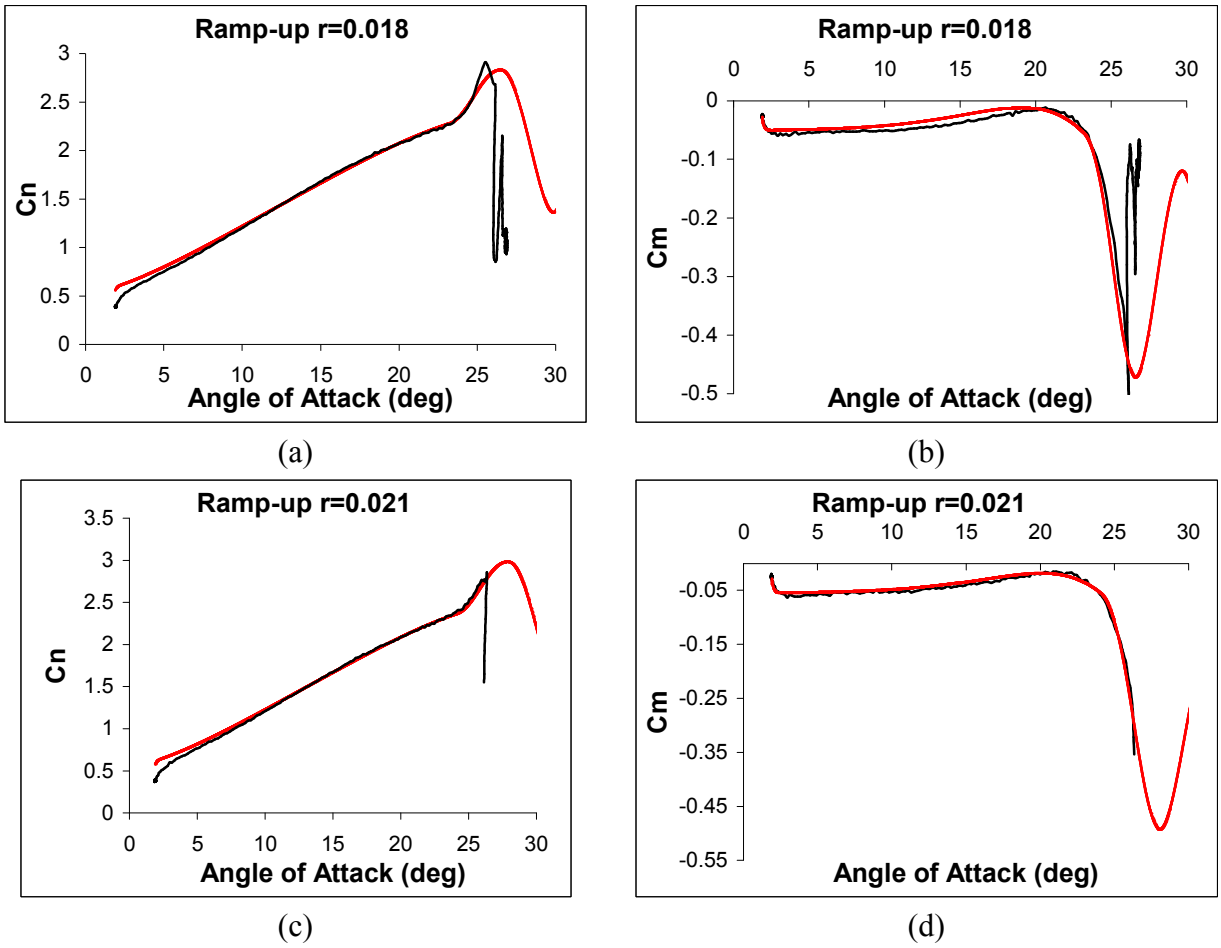

Figure 139 Beddoes' model reconstruction (red line) for Cn and Cm coefficients compared to the QinetiQ test data (black line)

Figure 138 and Figure 139 (a and c) show, once again, that the new dCn/dα and C_{N1} well predict the dynamic-stall onset, without necessity to change the time delays used with the Glasgow's data. Additionally the shape of the Cm lines and the Cm-breaks for both the reconstructions and measured data are in good agreement as shown in Figure 138 and Figure 139 (b and d). Unfortunately, because of the QinetiQ test limitations, it is not possible to compare the maximum and minimum values reached by the Cn and Cm coefficients throughout the whole range of pitch rates. Nonetheless, for the first two angular speeds, the maximum angle of attack of 27 degrees is sufficient for the flow to develop deep dynamic-stall with the associated stall vortex. In these two cases the

reconstructions appear to be in good accord with the measured data. As may be noticed that there appears to be a better agreement, of the Cm reconstruction, with the QinetiQ data when compared to Glasgow's.

5.5 Ramp-down

The Beddoes' model cannot reproduce to a satisfactory degree all the ramp-downs tested. The accuracy, of the re-attachment, diminishes as the pitch rate increases [11] because the original model does not contain a convective phase [34, 106]. As such, in the low speed aerodynamic ramp-down cases, here analyzed, the Beddoes' model yields poor reconstructions of the re-attachment process. Figure 140 presents the Cn coefficients, both measured and reconstructed, for a few pitch rates, from Glasgow data. The parameters used in the model are the same ones than Table 17 and Table 18 although the ramp-down motion does not use all of them, not requiring the ones related to the dynamic-stall onset and development as they are not all associated with the re-attachment process. Additionally, in an attempt to improve the model the Leishman's re-attachment modification [29, 95] was implemented.

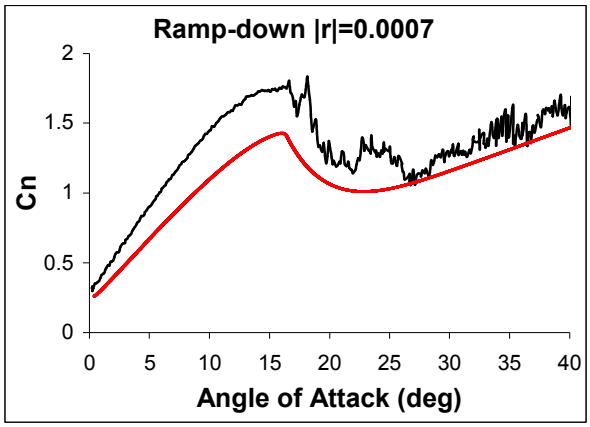

(a)

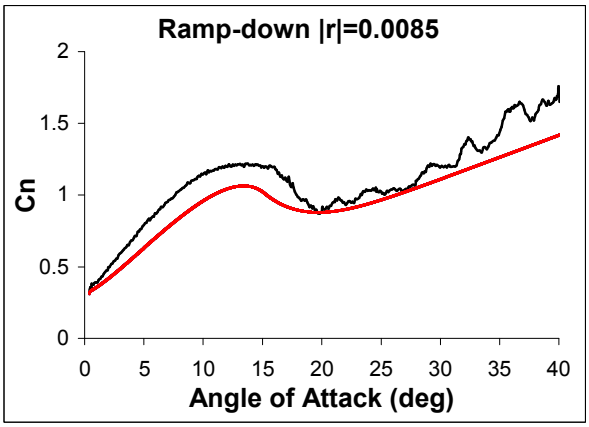

(b)

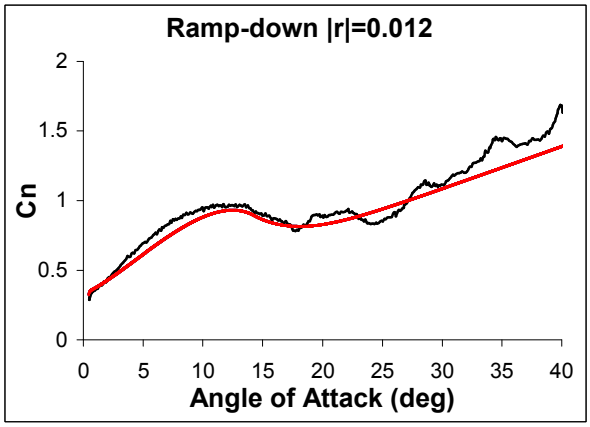

(c)

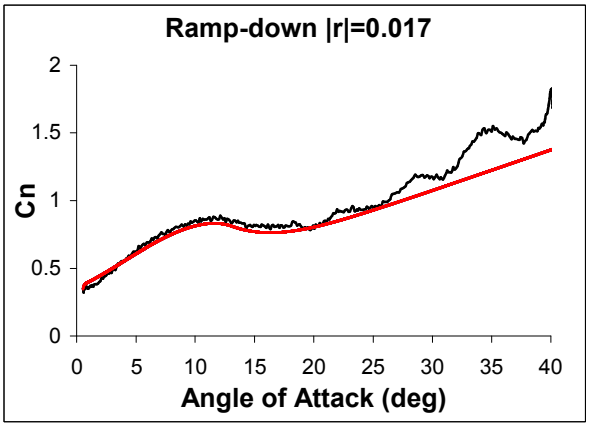

(d)

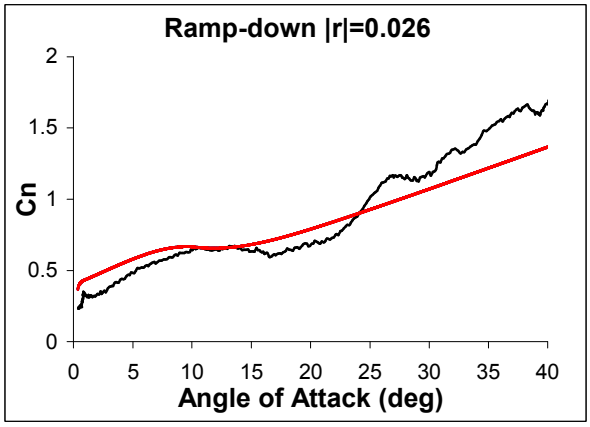

(e)

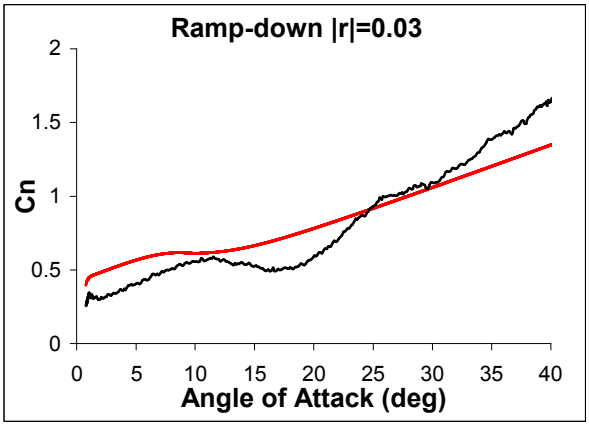

(e)

Figure 140 Beddoes' model reconstruction (red line) for Cn coefficients compared to the University of Glasgow's test data (black line)

It is very clear from Figure 140 that the Beddoes' model is deficient in reconstructing the re-attachment process at low speeds.

This is even clearer from the QinetiQ data, Figure 141, where the changes made have, almost, no effect on the final result [34].

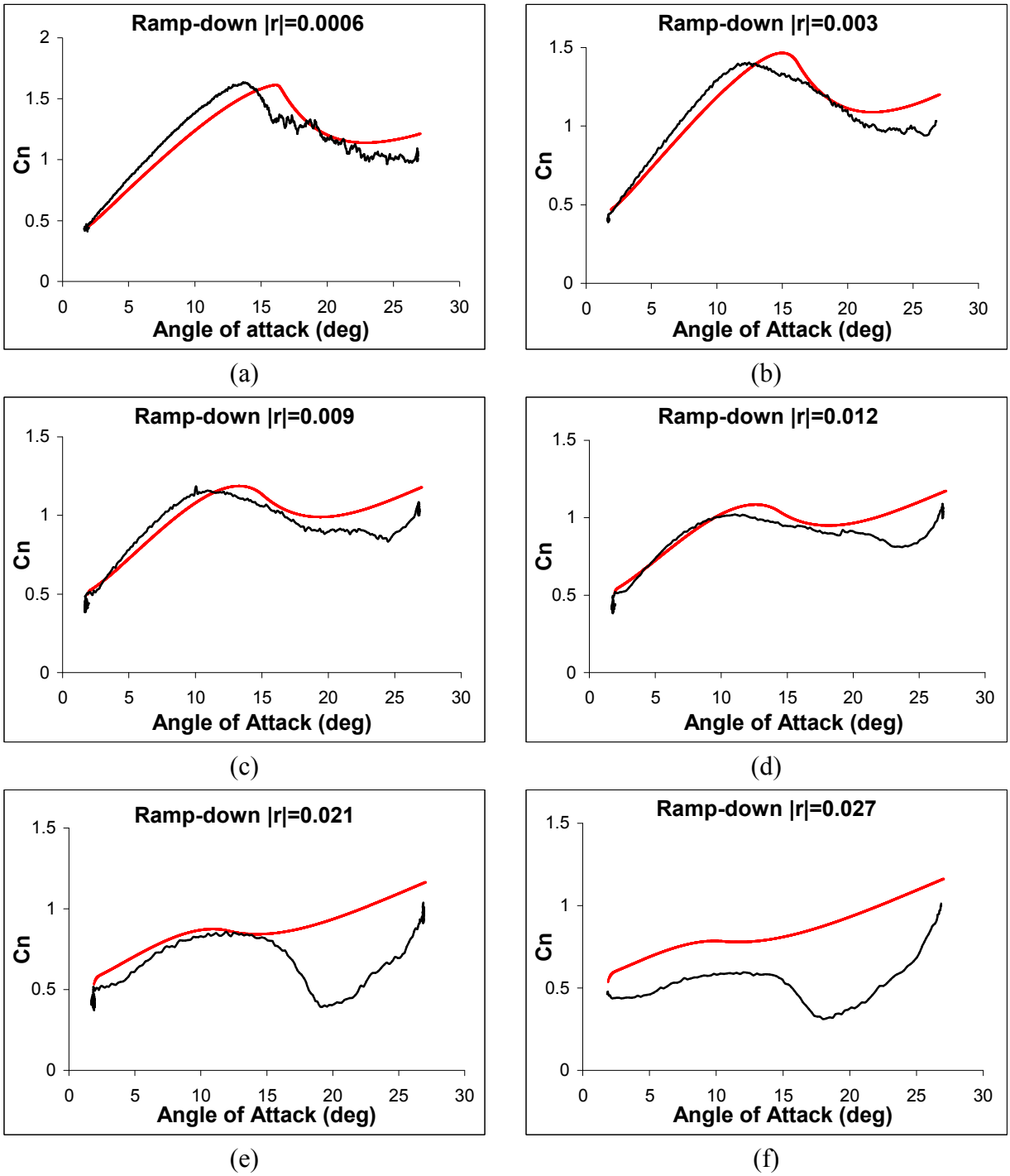

Figure 141 Beddoes' model reconstruction (red line) for Cn coefficients compared to the QinetiQ test data (black line)

The Cm coefficients, obtained using Cn (eq. A2.32), do not posses a good agreement with the data. This is only to be expected given the poor constructions of Cn. In these cases the Beddoes' model cannot be used as a reliable method to predict the pitching moment trend. In Figure 142 are shown few pitch rates for the University of Glasgow's data. It may be seen that the agreement becomes less as the pitch rate increases (highest angular speed ((c) and (d))). The same kind of trend was observed for the QinetiQ data (Figure 143).

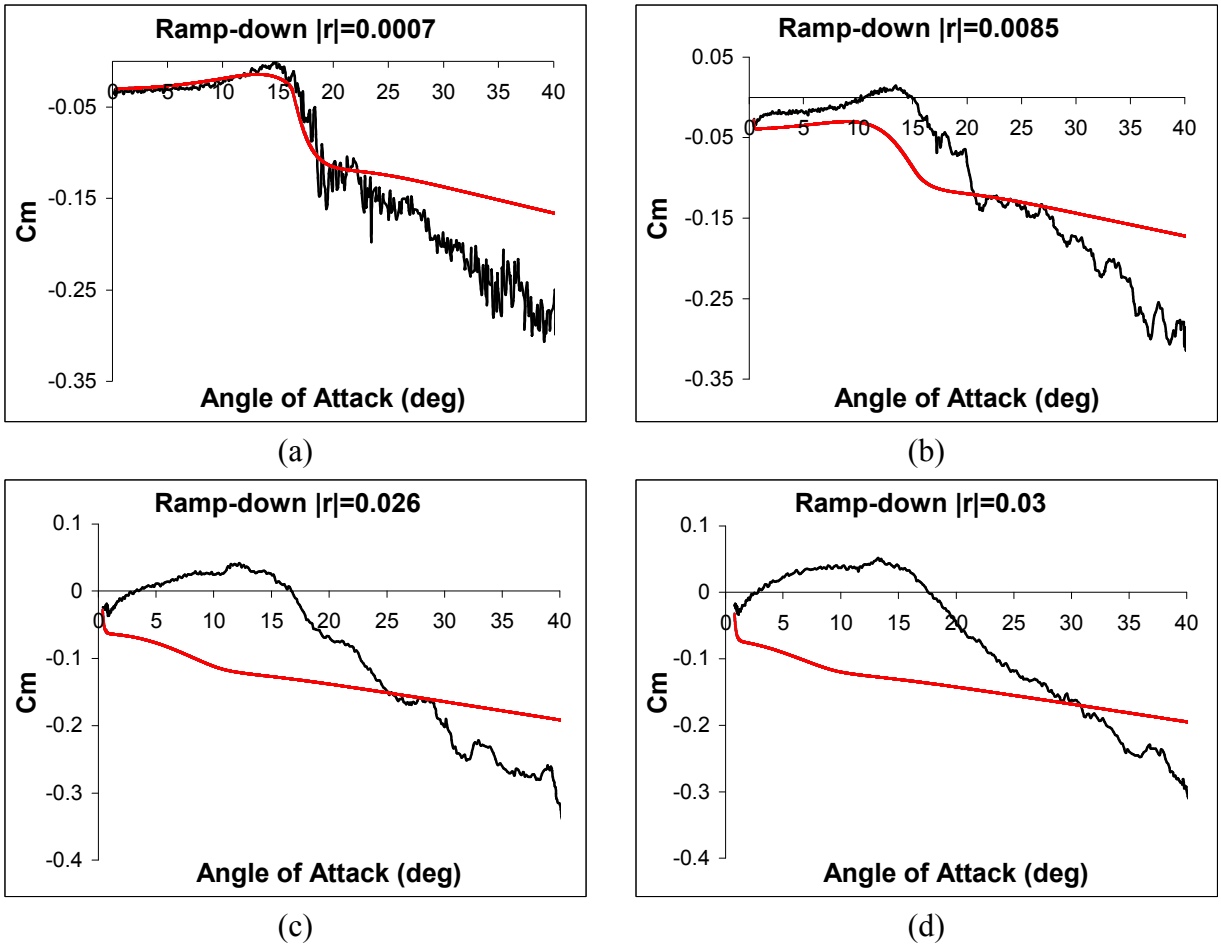

Figure 142 Beddoes' model reconstruction (red line) for Cm coefficients compared to the University of Glasgow's test data (black line)

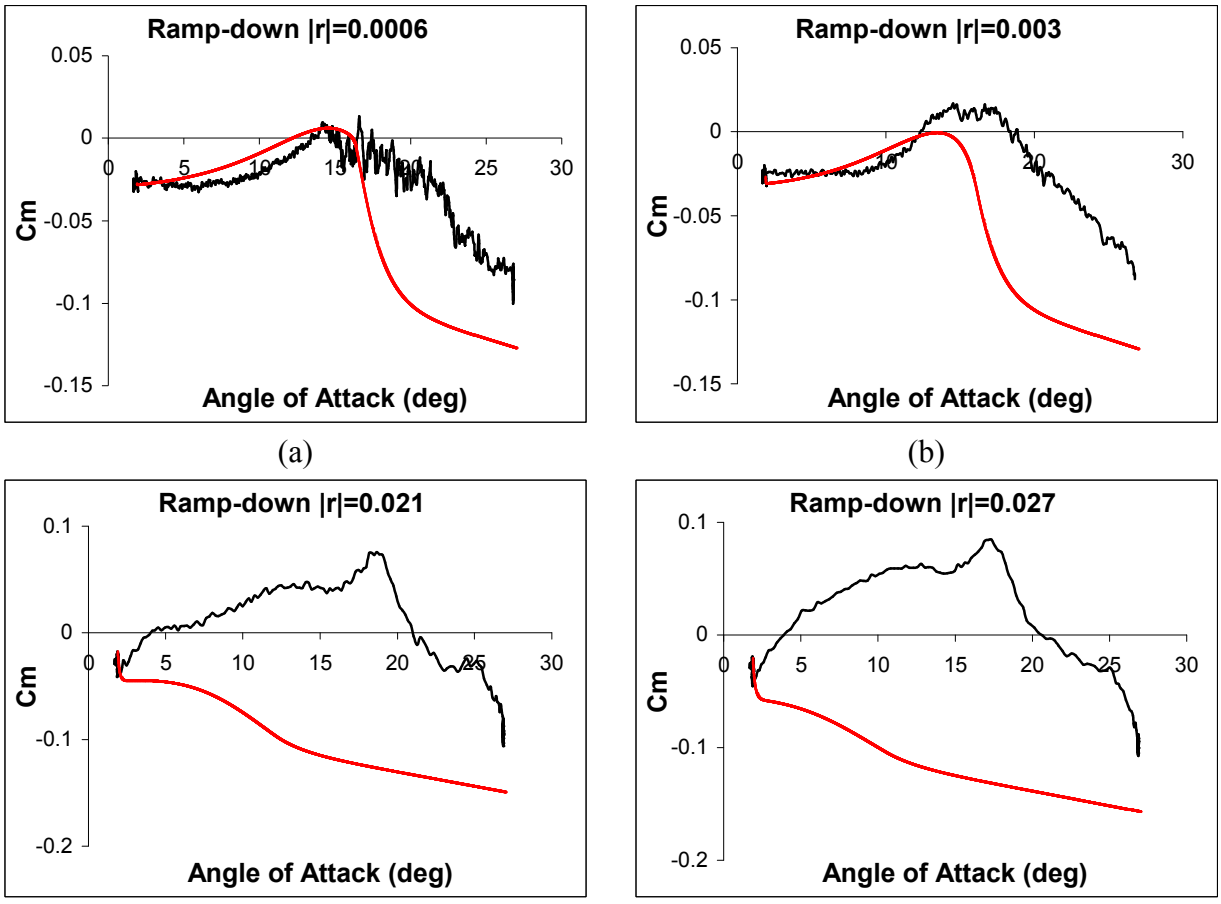

Figure 143 Beddoes' model reconstruction (red line) for Cm coefficients compared to the QinetiQ test data (black line)

It is suggested that there are mainly two reasons which may affect the poor reliability of the Beddoes' model during ramp-down reconstructions. In Section 5.3 it has already been noted that, for the oscillating tests, during the pitching down part of the loop, the method could not fit the data properly and that the reconstructions deteriorated with increased frequency. This was, in part, due to the RAE9645 profile's shape of the "*f*" function and its associated difficulty in obtaining a properly fitted curve via eq. A2.31 (Figure 128). This is obviously also the case for the ramp-down tests and even small changes in crucial phases illustrated in Section 5.3 (Figure 128) may lead to significant differences in the aerodynamics coefficients.

Moreover the ramp-downs highlighted an aspect of the re-attachment process which is not included in the Beddoes' model. This is the "convective phase" of the re-attachment process.

5.6 Modelling the Re-attachment Process

The author (along with R. Galbraith, F. Coton and W. Sheng) was involved in improving the methodology to determine a new non-dimensional time delay associated with re-attachment. The new method, along with reconstruction for some aerofoils, is presented by Sheng et al. in [34] and here only briefly recalled. As Niven et al. [11] had noted, the pitch rate did not affected significantly the incidence at which the maximum $|C_p|$-rise occurred. As shown in Figure 5, Figure 37 and Figure 58, the minimum normal force coefficient is linearly dependant on the reduced pitch rate.

Since the $|C_p|$-rise is, in effect, a horizontal line, only one linear fit is needed. The non-dimensional time constant is given by equation 5.2, where m_1 is the gradient of the linear fit applied to the Cn_{min} location, described in equation 5.3.

$$T_r = (\pi/180)m_1 \qquad 5.2$$

$$\alpha_{min} = \alpha_{min0} + m_1 r \qquad 5.3$$

In equation 5.2, α_{min} is the incidence of the minimum Cn values and α_{min0} is the incidence the linear fit cuts the y-axis. Applying a least squares fit to the data yields the values of α_{min0} and m_1, hence T_r. This methodology negates the requirement for assessing the location along the chord at which the $|C_p|$-rise occurs. The duration of the convective phase (T_r), the implied onset angle (α_{min0}) and the normal force gradient

(dCn/dα) can be easily obtained; these then provide the empirical contributions to Niven et al.'s improvement to the Beddoes' Model.

It should be also noted that, for the ramp-down experiments performed both by QinetiQ and the University of Glasgow, the airfoil was be held at the starting angle for few seconds. In these cases the airfoil acts like a bluff body and can exhibit bluff body phenomena [11]. Green and Galbraith [107] noted that and they performed a number of experiments to determine whether blockage was a major factor in the results of their tests and, as far as it could be determined, this was not of major importance to the results. On the other hand, there is the possibility that there is an unaccounted for complex three-dimensional flow structure within the wind tunnels. With regard to the Handley-Page wind tunnel, these aspects were evaluated (by R. Gordon, 1982) and they were not seen to be a contributing factor to the outputs.

5.7 Results and Discussion

As mentioned in the previous Section the improvement to the Beddoes' model arrives from an assessment of the convective part of the re-attachment process which was previously unknown. This plays a substantial role during the return from a fully stalled condition. The first step of this method is to find the two coefficients required to define the time lag T_r and to apply it to the modified Beddoes' model. The first coefficient here defined, is the average gradient of the ramp-down normal force curve (dCn/dα) for the fully detached flow. It may be noticed that, when the profile is completely stalled and it starts to pitch down, the slope of the Cn curve is always lower than the static case. This can be clearly seen comparing two different tests (i.e. Figure 34 and Figure 36). The

value of the tangent does not remain constant throughout the range of pitch rates tested, but varies with it. This is more noticeable for the QinetiQ data and can be appreciated clearly in Figure 57. The tangent of the totally stalled part of the line increases its value with the increasing reduced pitch rate. This is a general behaviour observed also in other profiles [11, 34]. In the present work, this aspect has been noticed, but not included during the computation of the new model. The phenomena behind this behaviour need further studies and the present work adopted an average of the ramp-down gradients. This procedure brings to two different tangent values depending on the test data used. In fact, in Chapter 3, where the three types of tests from each facility were compared, it was pointed out that, for ramp-up motions, two different gradients of the attached flow part were found. This indicates two different Cn slopes for the static tests depending on the profiles and facilities. Unfortunately it could not be proved, but only suggested, by the data because of the lack of the static test from QinetiQ.

5.7.1 Glasgow data

The first set of tests here analyzed was those from the Glasgow's data base. The Glasgow's data indicated a value for the linear part of dCn/dα of 0.096/0.097. For the current work the value adopted was 0.097. The second value needed is α_{min0}. According to Niven et al.'s procedure [11], simplified by the negation of the need for $|C_p|$-rise as previously explained, the angle of attack (α_{min0}) can be carried out from the following graph and table.

α_{Cnmin0}	r
16	0.03
16.5	0.027
17.6	0.017
18.5	0.013
19.5	0.0085
22	0.0039
22.5	0.002
23	0.00072
23.5	0.00021

Table 20 Angle of attacks at re-attachment start for each reduced pitch rate

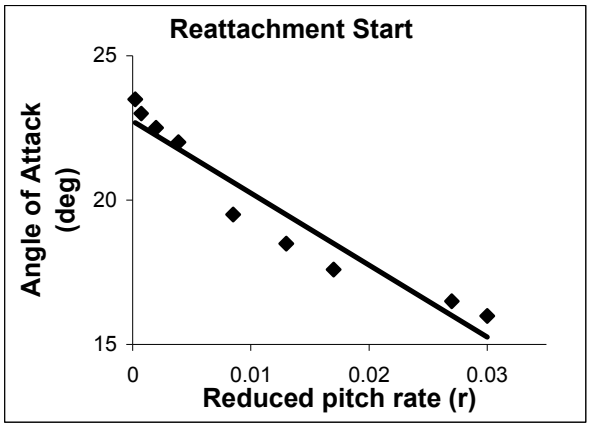

Figure 144 Re-attachment start for RAE9645 with Glasgow's data

Applying the linear fit, given by equation 5.3, the non-dimensional time delay T_r may be obtained using equation 5.2. A time delay (T_r) of ~4.3 was chosen. Once again this will not be the time delay used for the subsequent simulations. As before, the values for "T" laggings were averaged between the University of Glasgow and QinetiQ data. The T_r chosen, for all the calculations from now on, is equal to 4.5. With these two simple steps the method has all the parameters needed for the convective phase. The computation starts from a fully stalled incidence. It then follows, from a given Cn, a curve dictated by the value of (dCn/dα) obtained from the static test (or the pitch-up motion at low angular speeds when the static test is not available). When the decreasing incidence matches the incidence specified as "α_{min0}", the procedure does not change, but the T_r time begins its countdown. When this T lagging has expired it means that the convective phase is assumed to be complete and the re-establishment of the boundary layer dominates. An exponential return to the fully attached boundary layer is used to smooth the conjunction between the detached phase and the Beddoes' model. Figure 145 and Figure 146 illustrate the capacity of this method to reproduce the airfoil behaviours. The figures are presented in non-dimensional time and angle of attack domain. The three lines per each

graph are for the test data (black), the Beddoes' model (blue) and the T_r modification (red) respectively.

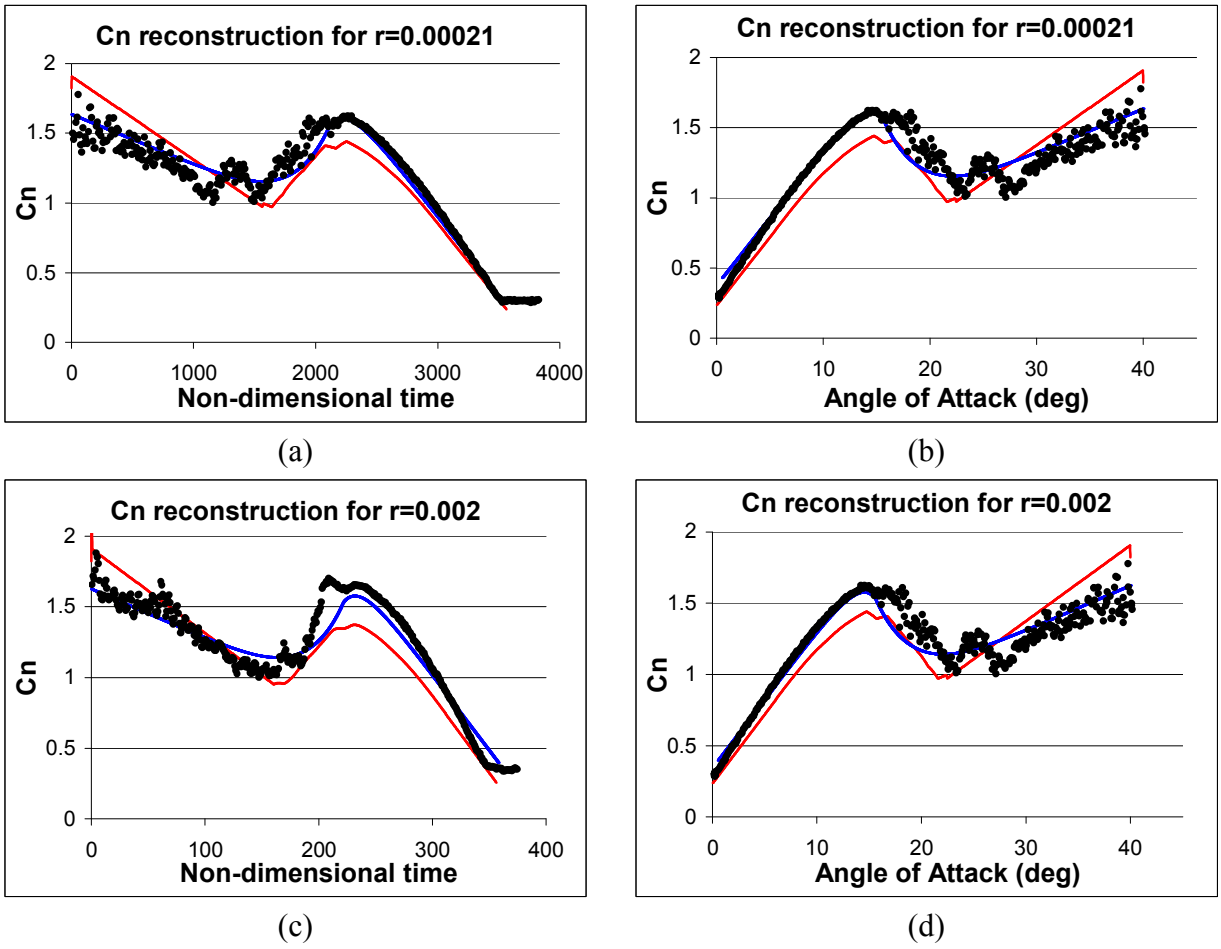

Figure 145 Cn reconstruction for ramp-down Glasgow's tests for RAE9645 for different reduced pitch rates. The test data are represented in black, the Beddoes' model in blue and the new T_r method in red

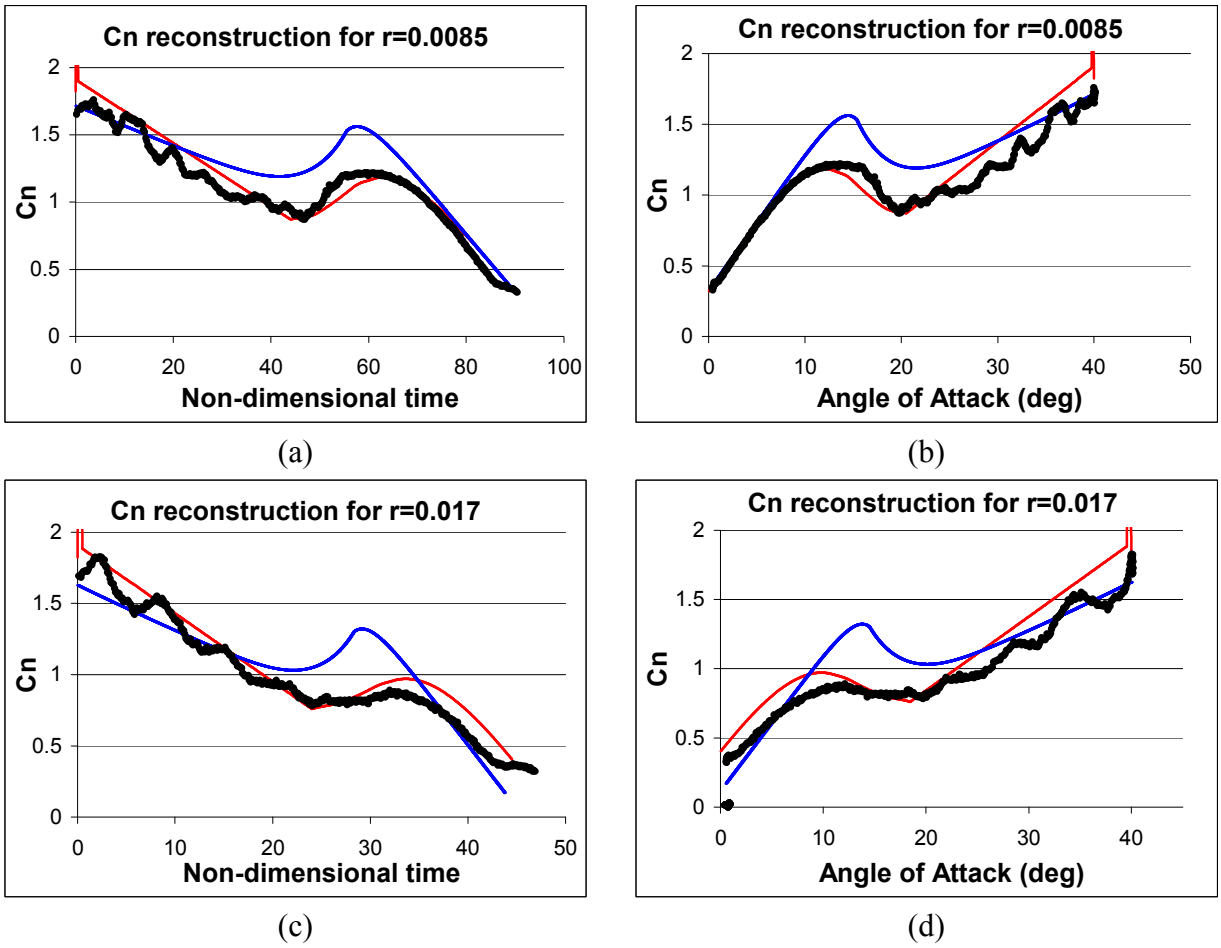

Figure 146 Cn reconstruction for ramp-down Glasgow's tests for RAE9645 for different reduced pitch rates. The test data are represented in black, the Beddoes' model in blue and the new T_r method in red

For the low pitch rate cases the new modelling is in good agreement with the measured data and the new re-attachment process is always better than the third generation model. This proves the necessity and importance of modelling the convective phase of the process. As the reduced pitch rate increases the new procedure may be seen to be much better than the original reproduction. It may be observed that the exponential return to the original model tends either to anticipate or over predict the measured data. However, the kernel of the new procedure is the representation of the convective phase. The same improvements may be seen for the QinetiQ data and its re-construction is now discussed.

5.7.2 QinetiQ data

It was shown in Chapter 3 that the ramp-down behaviour for the QinetiQ data was quite different from Glasgow's. As for the Glasgow data, the two necessary inputs are the Cn slope and T_r. also, because of the already noted differences in the two sets of data (Chapter 3) it is not possible to adopt the value of dCn/dα used for Glasgow's data. In the QinetiQ data, the tangent to the linear part of the Cn curve is ~0.107-0.108. Accordingly the value used for both Beddoes' and T_r simulations will be 0.108. The chosen value of the T_r delay is, the same as for the Glasgow data, 4.5. It may be recalled that this value is an average between the values found for the two different test facilities. In Figure 147 and Table 21 are represented the angles at the end of the convective phase against the reduced pitch rates for QinetiQ tests. The value of T_r ~ 4.6 was found from equations 5.2 and 5.3. This explains why the time delay for the entire test data has been given equal to 4.5.

α_{Cnmin0}	r
25	0.0003
25	0.0006
24.5	0.0015
24	0.003
23.8	0.006
23.5	0.012
21.3	0.0149
20.5	0.0178
19.8	0.0208
19	0.0238
18.1	0.0268
17.2	0.0297
16.2	0.0327

Table 21 Angle of attack at re-attachment start for each reduced pitch rate

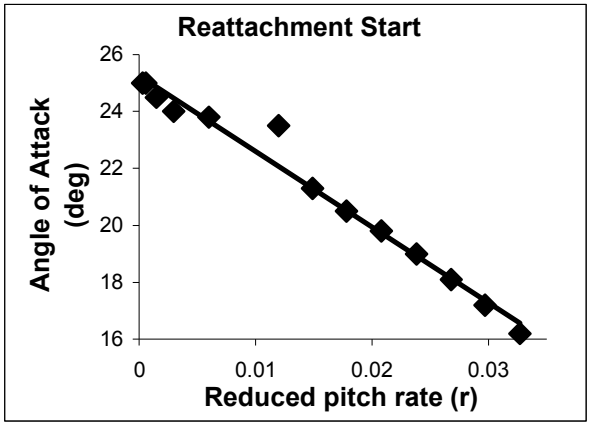

Figure 147 Re-attachment start for RAE9645 with QinetiQ data

The only other data that changed for the re-constructions was the value of the angle of attack which the T_r countdown begins. In fact, for the Glasgow's data the linear fit crossed the y-axis at a value of ~22.5. It is clear, from Figure 147, that this angle of attack does not compare with the QinetiQ data. The incidence indicated by the figure, and here chosen for this set of tests, is 25.2 deg. No other parameter was changed for the simulations. Figure 148 provides a sample of some of the cases tested by QinetiQ. The model (red line) was run using the new T_r value and from a starting angle of attack of 40 deg as for the Glasgow's data. Also included (blue line) is the original Beddoes' model using the starting value of 27 deg as for the test data. This does not, however, affect the final result as the method is independent of the starting angle. The most interesting reduced pitch rates are the higher ones for three reasons. First, the dependency on the test set-up is greatly reduced. Second, ramp-down data taken at University of Glasgow Argyll Wind Tunnel (QinetiQ data) start all from 27 deg and, for the slower ramp-downs, this is close to the conclusion of the convective phase of the re-attachment process (Figure 56 and Figure 57). For this reason the convective phase hardly exists. The third reason may be observed in the previous Figure 145 when, once again, considering the lower reduced pitch rates. For the tests (a) and (c) (Figure 145) the Beddoes' model does not perform as well as, the T_r method but is still quite close to the tests performed. Only when the pitch rate is increased, and the convective time starts to play an important role in the process, the major differences between the two methods can be observed.

In Figure 148 and Figure 149 there are four re-constructions with four different reduced pitch rates plotted against both the non dimensional time and the angle of attack.

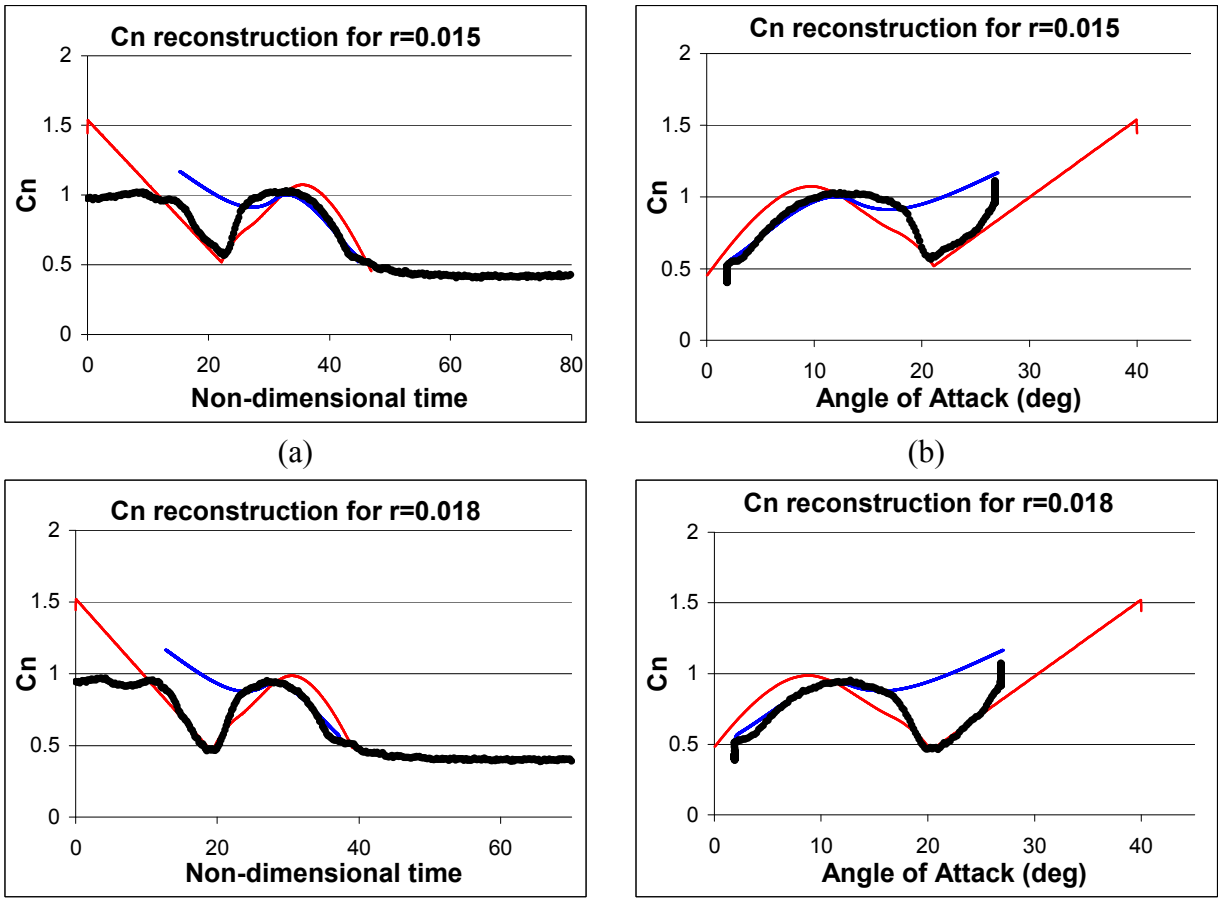

Figure 148 Cn reconstruction for ramp-down QinetiQ tests for RAE9645 for different reduced pitch rates. The test data are represented in black, the Beddoes' model in blue and the new *Tr* method in red

It is all too obvious that the original Beddoes' model [40] gives very poor re-constructions and this is particularly so for the high pitch rates. In contrast to this, however, the inclusion of the convective phase of the re-attachment process yields a significant improvement to the agreement between the measured data and the re-constructions. Clearly the physical description of the existence of the convective phase is correct and the necessary parameter assessments, by the improved method, are secure and easily obtained.

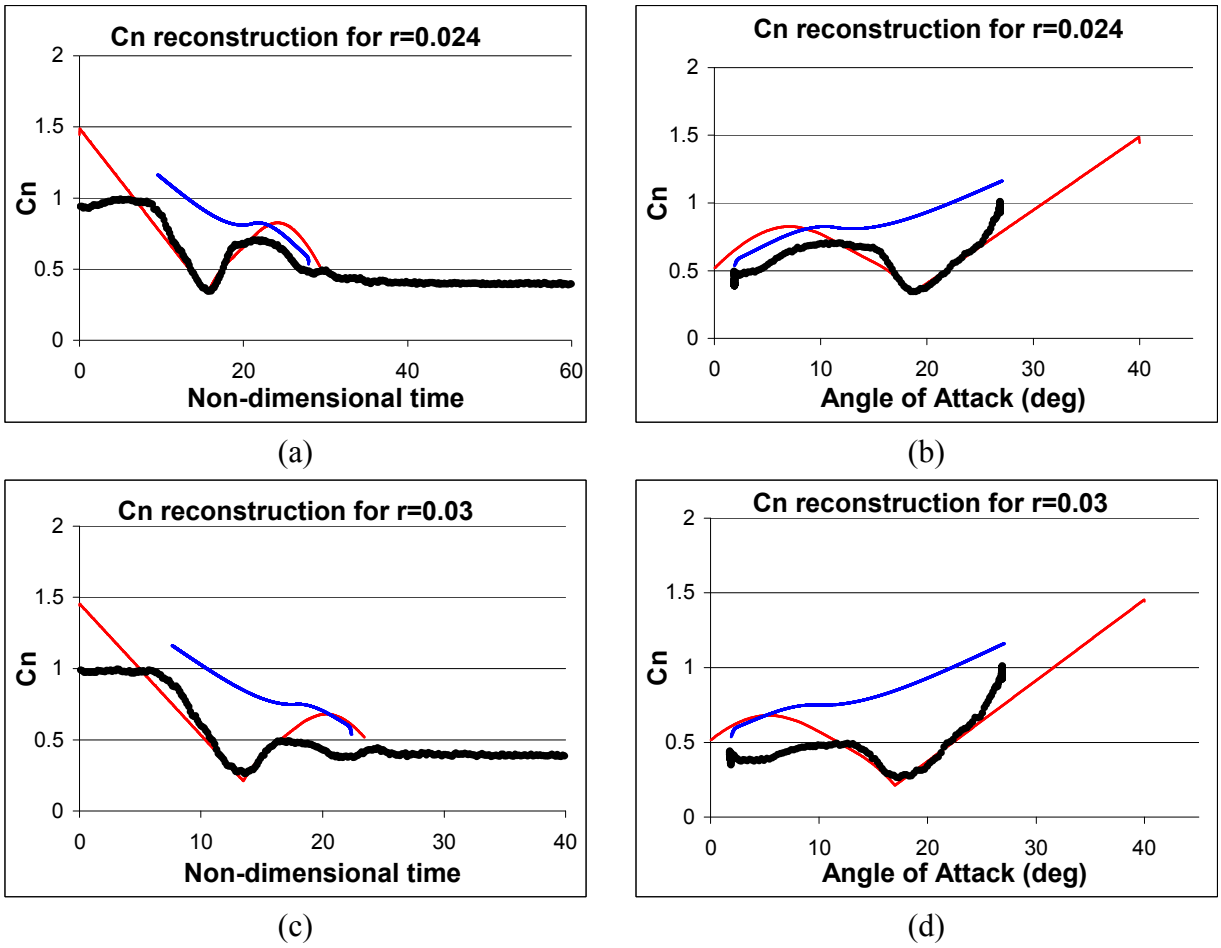

Figure 149 Cn reconstruction for ramp-down QinetiQ tests for RAE9645 for different reduced pitch rates. The test data are represented in black, the Beddoes' model in blue and the new *Tr* method in red

The alleviation of the obvious difficulty, with the original method, was attempted by Gutpa and Leishman and [108] via an increased lagging of the aerofoils separation location profile. It was not as successful as the dual process of convection and boundary layer formation.

It is also interesting to note that there were not only minor differences and the average value of T_r used, for the re-constructions, has proved to be very satisfactory.

The value of α_{min0} plays a key role because it allows one to distinguish between different profile behaviours and in different test settings, when the convective phase begins. Moreover the tests here presented show that for the same profile, tested in different wind

tunnels but with similar Reynolds and Mach numbers, the T_r delay remains similar. A simple average between them still yields acceptable results, as it happened for the T_α with ramp-up tests.

The T_r delay represents a very good enhancement since as was pointed out in Section 3.2, for ramp-downs, it was not possible to find a linear relationship, between the onset of the re-attachment process and its conclusion. Therefore it is difficult to find the common delay constants for the process that can satisfy both sets of data. Instead the T_r approach skips this problem by the dual process concept. Including the convective phase gives better results.

6 Conclusion and Future work

The aims of the present work, as stated in Chapter 1, were fulfilled. The analysis of the tests performed on the RAE9645 profile, in two different wind tunnels, highlighted the main characteristics of the aerofoil and allowed a full comparison between them for the different typologies of tests and facilities. Moreover, a conspicuous number of simulations with the Beddoes' 3rd generation model emphasized whether or not the method is suitable for low speed aerodynamics and allowed the exploration of new ways to improve the reliability of the reconstructions. In particular, new procedures, to which the author contributed, to catch the dynamic-stall onset for pitching up tests and the convective phase for the ramp-downs have been developed and tested. The new procedures have proved to yield a significant improvement to the original method for the RAE9645, especially for the re-attachment process. The following summary of the observations, made during the present research, attempts to give an overall view on all these aspects in details.

6.1 Profile Characteristics

Chapter 2 and Chapter 3 analyzed the unsteady aerofoil-data from the two different wind tunnels. For the both set of data is showed that:

Ramp-up:

1) At a certain incidence, depending on the pitch rate, the Cn curves exhibit the characteristics of trailing edge separation with the steady reduction in dCn/dα as α increases.

2) The tangent of the linear part of the Cn curves decreases its value along with the increasing reduced pitch rate. Although this behaviour was already noticed for other profiles, the RAE9645 drops the gradient value of the tangent below the static one only when the reduced pitch rate is fast enough to enable a deep dynamic stall to develop. For slower angular speed the dynamic tests stay above the static curve.

3) The deep dynamic stall, for the RAE9645, was observed to occur for reduced pitch rates r~>=0.005. This lowest value of r=0.005 is compatible with other data.

4) At the onset of deep dynamic stall, r>0.005, it was shown that a linear relationship exists between the maximum Ct (stall-onset indicator), achieved by the profile, and the corresponding reduced pitch rate. This relationship is important when implementing the new stall-onset criterion as per Sheng et al. [70].

Ramp-down:

1) For the "Ramp-down tests" the gross features of both data sets compatible in as much as the dual process of re-establishing fully attached flow was obvious. This entailed the initial process of convecting into the free stream all the stagnant air above the aerofoil (the convective phase) closely followed by, and sometimes overlapping this phase, the re-attachment of a fully attached boundary layer. The process was more evident at the higher pitch rates and less evident below a reduced pitch rate of |r|=0.012.

Although there are differences between the data sets, it was shown that, for both of them, there exists a linear relationship between the reduced pitch rate and the conclusion of the convective phase.

Oscillating:

The oscillating tests showed that the behaviour of the profile can be divided in:

1) *Maximum angle of attack below the static stall angle.*

For such oscillation the reduced frequency does not seriously affect the aerodynamic coefficients which, in general, follow the static behaviour both during the pitching up part of the loop and the pitching down one. Of course, for large reduced frequencies, a degree of hysteresis will be present.

2) *Maximum angle of attack above the static stall angle without deep dynamic stall.*

Accordingly to that stated by Leishman [73], the profile does not show any deep dynamic-stall if the reduced frequency is below 0.05. In these cases, however, the Cn coefficient follows a different path from the upstroke during the ramp down stroke resulting in a large hysteresis loop primarily due to a quasi-steady stall. The effect is more evident in the Cm curve. The result is the generation of a clockwise loop in the curve that reduces the torsional aerodynamic damping and may possibly lead to aeroelastic problems if the overall damping becomes negative.

3) *Maximum angle of attack above the static stall angle with deep dynamic stall.*

When the reduced frequency (k) and the maximum angle of attack are large enough, the profile undergoes a deep dynamic stall. A strong vortex develops over the upper surface of the aerofoil and convects across the chord. This is manifest by the typical rapid increase of Cn as the vortex builds up; followed by a plummeting of Cn as the vortex convects over and off the aerofoil. As the vortex convects it induces a rearward

movement of the centre of pressure resulting in an increased negative pitching moment. The Cn achieves the maximum when the vortex has just left the trailing edge and the induced secondary vortex, of opposite sign creates a significant suction at the trailing edge while the vortex is passing over the surface. A part from this not other main differences can be noticed for the coefficient respect the previous condition. The same can be said for the Cm curve which follows the aforementioned behaviours depending on the flow conditions.

Comparison between the two sets of data*:*

1) QinetiQ ramp-up tests have a higher Cn curve slope and present a delayed trailing edge separation, in terms of angle of attack. This is mainly addressed by the difference in aspect ratios, although there may be other factors (e.g. flow quality), which may influence the behaviour, that are unavailable at present.

Despite differences found in the profile behaviour, due to test procedure, data recording and different test environments, the two sets of ramp-up data exhibit a similar linear relationship between the dynamic-stall onset and the reduced pitch rate for r>=0.004. Albeit the tests are few, it is clear that a straight line closely fits the data and a linear approximation can be adopted. It can be seen, however, that, for the other tests with smaller r, another linear relationship exists but with a different gradient. The two lines meet at about 0.004 that can be assumed to be the first reduced pitch rate where the dynamic stall starts to appear for the RAE9645. In other words, it is the transition point at which the flow changes from quasi-static to fully dynamic stalling.

This leads to the same stall-onset criterion appropriate for inclusion in the Beddoes' model.

2) Comparing the ramp-down tests, a difference was found in the behaviour of the Cm lines during the re-attachment process when r is above ~0.015. This is due to two factors:

a. A much faster re-attachment process over the forepart of the profile in the QinetiQ data.
b. The transition from the stalled to the fully attached phase is smooth for the Glasgow data, but the QinetiQ data exhibit a reduction in suction prior to its rise to the fully attached state.

On the other hand the two data sets exhibit a linear relationship between the Cn_{min} and the reduced pitch rate. However, despite the similarity in dynamic-stall onset, the two lines have different gradient and lead to two different angles of attack for the beginning of the convective phase (Section 5.7). Hence, it is not possible to find only one appropriate value for inclusion in the modified Beddoes' model.

6.2 Beddoes' Model

Following the procedure illustrated by Beddoes, all the parameters needed by the model were obtained and simulations for each type of test (ramp-up, ramp-down and oscillating) were carried out. The parameters were chosen to suit the oscillating data which is more representative of the real blades environment.

The Beddoes' model has been enhanced, for low speed aerodynamics, by the inclusion of new stall-onset criterion and convective phase during the fully stalled state.

The new dynamic-stall onset criterion (Sheng et al. [70]) for low speed aerodynamics used can be summarized as follows and is applicable to the RAE9645 aerofoil:

1) Stall onset is well represented by the incidence at the maximum chord force coefficient.

2) For ramp-up data, beyond a certain reduced pitch rate (r>0.005) the dynamic-stall varies linearly with the reduced pitch rate

3) Extrapolating the stall data backwards to a reduced pitch rate of zero give an incidence value of α_{ds0}

4) From α_{ds0} an associated time delay T_α was obtained

5) A lagged incidence α', was obtained applying the time delay T_α

6) The dynamic-stall occurs when α'> α_{ds0}

7) The new formulation yielded improved predictions over the previous criterion [11, 62] and simplified the procedure to obtain the associated time delays.

Moreover a new method [11, 34, 107] of modelling the unsteady establishment of fully attached flow during pitch-down motions has been used for the RAE9645.

1) The method is based on the observation that the re-attachment process can be consists of two distinctive phases: a convective phase independent of the pitch rate and a frequency dependent phase associated with the re-establishment of the boundary layer.

2) By considering the minimum value of Cn over the reduced ramp rates, the acquisition of both the conclusion of the convective phase and its duration may be assessed.

3) The onset angle and the duration of the convective phase, together with the lift curve slope in the fully stalled region, provide the three empirical inputs.

4) The modelling procedure reduced the scatter associated with the methodology used by Niven et al. [11].

5) The resultant model displays a significant improvement, for the re-construction of ramp-down motions, over the third generation Beddoes' model for the RAE9645 profile; in low speed aerodynamics.

6.3 Future work

The new methods, for catching the onset of the dynamic stall and of the re-attachment process, used in the present work have shown a significant improvement, compared to the Beddoes' methodology, in low speed aerodynamics. Of course, even with these two new inputs to the Beddoes' model for the RAE9645, and all the attendant improvements to data re-construction, there remain several important aspects yet to be properly investigated. In essence, these are associated with motions where there exists an overlap in the observed phenomena. In both the ramp up and ramp down experiments no significant overlap took place for the stall and return from stall process. This was, of course, primarily why such tests were carried out. The overlaps that may occur, and need attention, are as follow.

1) When the stall-onset has been initiated and the process is incomplete before the initiation of the convective phase of the return from stall.
2) When the stall vortex has traveled the length of the chord and a new vortex is formed (bluff body type) prior to the initiation of the convective phase on the return from stall.

3) When the suction is such that the convective phase and the re-establishment of the boundary layer overlap significantly.

There are sufficient data at Glasgow to investigate all of the above, but the effort to do so is significant and should form the basis of future work.

The second major avenue for the future investigation relates to the differences between the behaviours of the RAE9645 in two different wind tunnels and the tunnels flow states. In particular, how the behaviour, prior the stall was influenced by the test environment and yet the stall onset angles were similar. A detailed study of both facilities and, perhaps, CFD associated with the linear phase, may suggest the specific reasons for these differences. It should be noted at this stage, however, that the QinetiQ model was originally designed for the Bedford 8'x8' transonic wind tunnel where it would have been tested up to Mach number of ~0.8. The Glasgow work was to be the comparison low speed tests at about Mach number 0.13. As such, and to accommodate the model in the Argyll tunnel, a compromise was required in which the RAE9645 model did not span the 9' width of the tunnel and an appropriate mounting inside the tunnel was constructed. Just how this obvious 3-D aspect of the set up affected the aerofoil aerodynamic coefficients is unknown, but probably would be an appropriate initial consideration whilst assessing the aerofoils differing behaviour.

Appendix 1

TABLE 1A: DETAILS OF STATIC TESTS

Run No.	Start angle (^{0})	Sweep (^{0})	Reynolds No ($\times 10^6$)
10000	-5	31 (1^0 interval)	1.5
10010	-5	27 (2^0 interval)	1.5
10020	10	16 (1^0 interval)	1.5
10030	26	4 (2^0 interval)	1.5

Table 1A.1: List of static tests

TABLE 2A: DETAILS OF SINUSOIDAL TESTS

Reynolds number	1.5×10^6									
Mean angle	2^0	4^0	6^0	8^0	10^0	12^0	14^0	16^0	18^0	20^0
Amplitude	8^0									
Oscillation frequency	0.72, 1.45, 2.89 and 4.34									

Table 2A.1: Summary of sinusoidal tests

Run No.	Mean angle	Amplitude	Oscillation frequency
11561	2	8	0.72
11571	4	8	0.72
11581	6	8	0.72
11591	8	8	0.72
11601	10	8	0.72
11611	12	8	0.72
11621	14	8	0.72
11631	16	8	0.72
11641	18	8	0.72
11651	20	8	0.72
11861	2	8	1.45
11871	4	8	1.45
11881	6	8	1.45
11891	8	8	1.45
11901	10	8	1.45
11911	12	8	1.45
11921	14	8	1.45
11931	16	8	1.45
11941	18	8	1.45
11951	20	8	1.45
12161	2	8	2.89

12171	4	8	2.89
12181	6	8	2.89
12191	8	8	2.89
12201	10	8	2.89
12211	12	8	2.89
12221	14	8	2.89
12231	16	8	2.89
12241	18	8	2.89
12251	20	8	2.89
12661	2	8	4.34
12671	4	8	4.34
12681	6	8	4.34
12691	8	8	4.34
12701	10	8	4.34
12711	12	8	4.34
12721	14	8	4.34
12731	16	8	4.34
12741	18	8	4.34
12751	20	8	4.34

Table 2A.2: List of sinusoidal tests. Not all the tests in the table are here presented.

TABLE 3A: DETAILS OF RAMP TESTS

Reynolds number	1.5×10^6		
Start angle	0^0	End angle	40^0
Start angle	40^0	End angle	0^0
Ramp rate (deg/s)	2, 7,20, 35, 79, 120, 160, 200, 240 and 280		

Table 3A.1: Summary of ramps tests

Run No.	Start Angle	End angle	Ramp rate
12802	0	40	2
12862	0	40	7
12922	0	40	20
12982	0	40	35
13042	0	40	79
13102	0	40	120
13162	0	40	160
13222	0	40	200
13282	0	40	240
13342	0	40	280
12813	40	0	2
12873	40	0	7
12933	40	0	20
12993	40	0	35

13053	40	0	79
13113	40	0	120
13173	40	0	160
13233	40	0	200
13293	40	0	240
13353	40	0	280

Table 3A.2: List of ramp tests

TABLE 4A: DETAILS OF SINUSOIDAL TESTS

Reynolds number	2 and 1.5×10^6						
Mean angle	8^0	10^0	12^0	14^0	16^0	18^0	20^0
Amplitude	4^0, 5^0, 6^0, 8^0, 10^0						
Oscillation frequency	0.28, 1.4, 2.8, 4.2, 5.6, and 7						

Table 4A.1: Summary of sinusoidal tests

File name	Mean angle	Amplitude	Oscillation frequency
84	14	5	0.28
85	16	5	0.28
86	18	5	0.28
87	20	5	0.28
88	8	5	1.401
89	10	5	1.401
90	12	5	1.401
91	14	5	1.401
92	16	5	1.401
93	18	5	1.401
94	20	5	1.401
95	8	5	2.801
96	10	5	2.801
97	12	5	2.801
98	14	5	2.801
99	16	5	2.801
100	16	5	2.801
101	18	5	2.801
102	20	5	2.801
103	8	5	4.202
104	10	5	4.202
105	12	5	4.202
106	14	5	4.202
107	16	5	4.202
108	18	5	4.202
109	20	5	4.202

110	8	5	5.602
111	10	5	5.602
112	12	5	5.602
113	14	5	5.602
114	16	5	5.602
115	18	5	5.602
116	20	5	5.602
117	8	5	7.003
118	10	5	7.003
119	12	5	7.003
120	14	5	7.003
121	14	5	7.003
123	18	5	7.003
124	20	5	7.003
126	8	8	0.28
127	12	8	0.28
128	14	8	0.28
129	16	8	0.28
130	18	8	0.28
131	10	8	1.401
132	12	8	1.401
133	14	8	1.401
134	16	8	1.401
135	18	8	1.401
136	10	8	2.801
137	10	8	2.801
138	12	8	2.801
139	14	8	2.801
140	16	8	2.801
141	18	8	2.801
142	10	8	4.202
143	12	8	4.202
144	14	8	4.202
145	16	8	4.202
146	18	8	4.202
147	10	8	5.602
148	12	8	5.602
149	14	8	5.602
150	16	8	5.602
151	18	8	5.602
152	8	8	7.003
153	10	8	7.003
154	12	8	7.003
155	14	8	7.003
156	16	8	7.003
157	18	8	7.003
158	10	4	0.28

159	10	6	0.28
160	10	8	0.28
161	10	4	1.401
162	10	6	1.401
163	10	8	1.401
164	10	4	2.801
165	10	6	2.801
166	10	8	2.801
167	10	4	4.202
168	10	6	4.202
169	10	8	4.202
170	10	4	5.602
171	10	6	5.602
172	10	8	5.602
173	10	4	7.003
174	10	6	7.003
175	10	8	7.003
176	12	10	0.28
177	13	10	0.28
178	14	10	0.28
179	15	10	0.28
180	16	10	0.28
181	12	10	1.401
182	13	10	1.401
183	14	10	1.401
184	15	10	1.401
185	16	10	1.401
186	12	10	2.801
187	13	10	2.801
188	14	10	2.801
189	15	10	2.801
190	16	10	2.801
191	12	10	4.202
192	13	10	4.202
193	14	10	4.202
194	15	10	4.202
195	16	10	4.202
196	8	5	0.1
203	8	5	0.05
210	8	5	0.374
211	10	5	0.374
212	12	5	0.374
213	14	5	0.374
214	16	5	0.374
215	18	5	0.374
216	20	5	0.374
217	8	5	1.868

218	10	5	1.868
219	12	5	1.868
220	14	5	1.868
221	16	5	1.868
222	18	5	1.868
223	20	5	1.868
224	8	5	3.735
225	10	5	3.735
226	12	5	3.735
227	14	5	3.735
228	16	5	3.735
229	18	5	3.735
230	20	5	3.735
231	8	5	5.603
232	10	5	5.603
233	12	5	5.603
234	14	5	5.603
235	16	5	5.603
236	18	5	5.603
237	20	5	5.603
238	8	5	7.47
239	10	5	7.47
240	12	5	7.47
242	8	5	1.868
243	10	5	1.868
244	12	5	1.868
245	14	5	1.868
246	16	5	1.868
247	18	5	1.868
248	20	5	1.868
249	8	5	3.735
250	8	5	3.735
251	10	5	3.735
252	12	5	3.735
253	14	5	3.735
254	16	5	3.735
255	18	5	3.735
256	20	5	3.735
257	8	5	5.603
258	10	5	5.603
259	12	5	5.603
260	14	5	5.603
261	14	5	5.603
262	16	5	5.603
263	18	5	5.603
264	20	5	5.603
265	8	5	7.47

266	10	5	7.47
267	12	5	7.47
268	14	5	7.47
269	16	5	7.47
270	18	5	7.47
271	20	5	7.47
272	8	5	9.338
273	10	5	9.338
274	12	5	9.338
275	14	5	9.338
276	16	5	9.338
277	18	5	9.338
278	20	5	9.338

Table 4A.2: List of sinusoidal tests

TABLE 5A: DETAILS OF RAMP TESTS

Reynolds number	1, 1.5 and 2 × 10^6		
Start angle	1.9^0	End angle	27^0
Start angle	27^0	End angle	1.9^0
Ramp rate (deg/s)	3, 6, 15, 30, 60, 90, 120, 150, 180, 210, 240, 270, 300, and 330		

Table 5A.1: Summary of ramps tests

File name	Start Angle (^{0})	End angle (^{0})	Ramp rate (deg/s)
443u	1.9	27	3
446u	1.9	27	6
4415u	1.9	27	15
4430u	1.9	27	30
4460u	1.9	27	60
4490u	1.9	27	90
44120u	1.9	27	120
44150u	1.9	27	150
44180u	1.9	27	180
44210u	1.9	27	210
44240u	1.9	27	240
44270u	1.9	27	270
44300u	1.9	27	300
44330u	1.9	27	330
443d	27	1.9	3
446d	27	1.9	6

4415d	27	1.9	15
4430d	27	1.9	30
4460d	27	1.9	60
4490d	27	1.9	90
44120d	27	1.9	120
44150d	27	1.9	150
44180d	27	1.9	180
44210d	27	1.9	210
44240d	27	1.9	240
44270d	27	1.9	270
44300d	27	1.9	300
2930u	1.9	27	30
29100u	1.9	27	100
29150u	1.9	27	150
29200u	1.9	27	200
29250u	1.9	27	250
29300u	1.9	27	300
5930u	1.9	27	30
59100u	1.9	27	100
59150u	1.9	27	150
59200u	1.9	27	200
59250u	1.9	27	250
59300u	1.9	27	300
2930d	27	1.9	30
29100d	27	1.9	100
29150d	27	1.9	150
29200d	27	1.9	200
29250d	27	1.7	250
29300d	27	1.9	300
5930d	27	1.9	30
59100d	27	1.9	100
59150d	27	1.9	150
59200d	27	1.9	200
59250d	27	1.9	250
59300d	27	1.9	300

Table 5A.2: List of ramp tests

Appendix 2

1 3rd Generation Dynamic-Stall Model

In Beddoes' 3rd generation dynamic-stall model, the forcing representations are no longer given in terms of angle of attack, pitch rate and plunging velocity separately, but by two circulatory and two impulsive forcing terms $\eta_N, \eta_M, \lambda_N, \lambda_M$.

1.1 Forcing Terms

In the first- and second-generation dynamic-stall models, the forcing terms were generally in the forms of angle of attack, of angular velocity, and of plunging motion. In 3rd generation model, however, the more general representations of forcing including chordwise effects were provided.

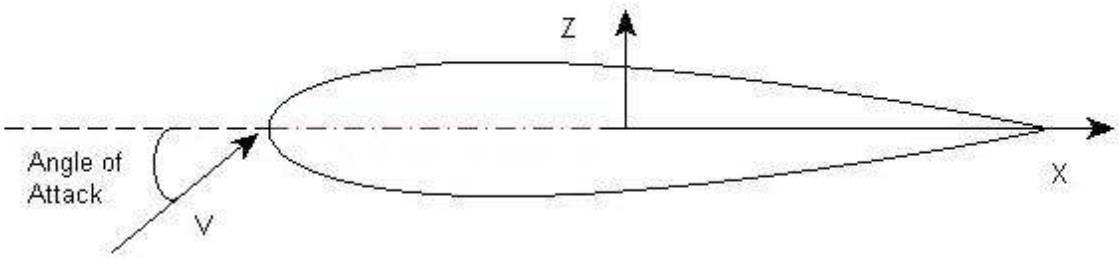

Figure 150 Coordinate system for thin airfoil

In classical linear aerodynamics, an actual aerofoil can be regarded as the linear superposition of a flat plate (see Figure 150 and the coordinate system), aerofoil thickness and a camberline. The airloads on the aerofoil can then be regarded as the superposition of the corresponding forces due to angle of attack, thickness and camber.

The details of this aerodynamic approach can be found in many books, Bertin et al. [109] and Katz et al. [110] are two good examples. In this work, similarly, the linear unsteady aerodynamics of aerofoil can be considered as the superposition of a thin aerofoil, thickness and camberline. This simplifies the practical problem to a thin aerofoil problem.

Following Theodorsen's theory, the unsteady force and moment are supposed to be composed of the sum of two parts: the initial non-circulatory loading and the circulatory loading. The former can be obtained from piston theory and decays very quickly with time. The latter builds up and reaches a steady value quickly.

Following the expressions of Beddoes' dynamic-stall model [40, 95, 111], the unsteady forcing is divided into several step changes, from which the indicial function [112] responses are obtained, and then the Duhamel integral is employed to get the total response in the time domain. From the indicial function responses employed by Beddoes, for a step change of forcing, the circulatory airloads can be regarded as those under the steady conditions modified by some special functions, such as Wagner or Kussner functions, which actually includes the effects of the shed vorticity into the wake. Therefore, the unsteady wake problem is much simplified by the indicial functions. For the non-circulatory components, we may get the results directly from piston theory [113].

1.1.1 Forcing for circulatory terms

As said before, the forcing terms in the Beddoes' 3rd Generation Model are not given in term of pitch rates (q) or angle of attack (α). They are expressed in terms of $w_a(\theta, s)$, that

represents the perturbation velocity normal to the chord where θ is the chordwise coordinate that can be defined in different ways depending on the different origins of coordinates, and s is the non dimensional time defined as $s = \frac{2Vt}{c}$. In this work, the two forcing terms for the circulatory effect are given, for the lift and the moment coefficient for the aerofoil which pitch axis is at ¼-chord, as follows:

$$\eta_L(s) = \frac{1}{\pi}\int_0^{\pi}(1+\cos\theta)\frac{w_a(\theta,s)}{V_\infty}d\theta \qquad \text{A2.1}$$

$$\eta_M(s) = \frac{2}{\pi}\int_0^{\pi}(\cos\theta+\cos 2\theta)\frac{w_a(\theta,s)}{V_\infty}d\theta \qquad \text{A2.2}$$

1.1.2 Forcing for non-circulatory terms

If it is supposed that a step change in normal velocity Δw_a occurs, then piston theory gives the difference in pressure across the airfoil as

$$\Delta p(x,s)\big|_{s=0} = 2\rho a \Delta w_a(x) \qquad \text{A2.3}$$

and the pressure coefficient by

$$\Delta C_p(x,s)\Big|_{s=0} = \frac{2\rho a \Delta w_a(x)}{\frac{1}{2}\rho V_\infty^2} = \frac{4}{M}\frac{\Delta w_a(x)}{V_\infty} \qquad \text{A2.4}$$

After integrating the ΔC_p along the chord for the non-circulatory lift and pitching moment for a single change in Δw_a, and dividing x by half of the profile chord (x^*), the forcing for the non circulatory terms are found to be:

$$\Delta\lambda_L = \frac{1}{2}\int_{-1}^{1}\frac{\Delta w_a(x^*)}{V_\infty}dx^* \qquad \text{A2.5}$$

$$\Delta\lambda_M = \frac{1}{2}\int_{-1}^{1}\frac{\Delta w_a(x^*)}{V_\infty}(x^* - a)dx^* \qquad \text{A2.6}$$

For the unsteady case, the force due to a step change in forcing is modified by an indicial function. In 3rd generation dynamic-stall model, a refined Kussner function $\psi(s)$ was employed:

$$\Delta C_L(s) = 2\pi\Delta\eta_L(s)\psi(s) \qquad \text{A2.7}$$

For an actual aerofoil, the more general form is often used,

$$\Delta C_L(s) = C_{L\alpha}\Delta\eta_L(s)\psi(s) \qquad \text{A2.8}$$

Where s is the non-dimensional time in terms of half chord, $C_{L\alpha}$ is the lift curve slope, obtained from static test.

Similarly, for the unsteady case, the indicial response for circulatory pitching moment is

$$\Delta C_M(s) = \frac{\pi}{4}\Delta\eta_M(s)\left(1 - e^{-\frac{s}{T_M}}\right) \qquad \text{A2.9}$$

Again, for an unsteady aerofoil flow, a step change of the forcing in non-circulatory, or impulsive, lift and pitching moment, the indicial responses are as follows:

$$\begin{cases} \Delta C_L^I(s) = \dfrac{4}{M}\Delta\lambda_L(s)e^{-\frac{s}{T_I}} \\ \Delta C_M^I(s) = -\dfrac{4}{M}\Delta\lambda_M(s)e^{-\frac{s}{T_I}} \end{cases} \qquad \text{A2.10}$$

1.2 Attached flow

Like in the early versions of Beddoes' dynamic-stall models, in 3rd generation dynamic-stall model, the attached flow air loads are calculated using indicial response functions,

and the total responses of the aerofoil under dynamic conditions are obtained via Duhamel's integral.

For a step change in forcing, the indicial responses are given with a Mach number scaled time $s' = \beta^2 s$ and $\beta = \sqrt{1-M^2}$,

Circulatory normal force:

$$\Delta C_N^C(s') = C_{N\alpha}\Delta\eta_N(1 - A_1 e^{-b_1 s'} - A_2 e^{-b_2 s'} - A_3 e^{-b_3 s'}) \quad \text{A2.11}$$

Circulatory moment:

$$\Delta C_M^C(s') = \Delta\eta_M \frac{\pi}{4\sqrt{1-M^2}}(1 - e^{-s'/T_M}) \quad \text{A2.12}$$

Impulsive normal force:

$$\Delta C_N^I(s') = \Delta\lambda_N \frac{4}{M} e^{-s'/T_I} \quad \text{A2.13}$$

Impulsive moment:

$$\Delta C_M^I(s') = -\Delta\lambda_M \frac{4}{M} e^{-s'/T_I} \quad \text{A2.14}$$

With the revised constants

A_1=0.165, A_2=0.335, A_3=0.5

$b_1 = 0.05$, $b_2 = 0.222$, $b_3 = 0.8/M$

$$T_M = M/2,\ T_I = \frac{M(1+3M)}{2} \quad \text{A2.15}$$

For the equations, Beddoes developed the efficient numerical algorithms for the discrete time superposition in time domain, as

$$C_N^C(s') = C_{N\alpha}\left[\eta_N(s') - X_1(s') - Y_1(s') - Z_1(s')\right] \quad \text{A2.16}$$

$$C_M^C(s') = \frac{\pi}{4\sqrt{1-M^2}}\left[\eta_M(s') - X_2(s')\right] \quad \text{A2.17}$$

$$C_N^I(s') = \frac{4}{M} X_3(s') \quad \text{A2.18}$$

$$C_M^I(s') = -\frac{4}{M} X_4(s') \quad \text{A2.19}$$

With the deficiency functions in the discrete time samples

$$X_1(s') = X_1(s' - \Delta s')\exp(-b_1\Delta s') + A_1\Delta\eta_N(s')\exp(-b_1\Delta s'/2) \quad \text{A2.20}$$

$$Y_1(s') = Y_1(s' - \Delta s')\exp(-b_2\Delta s') + A_2\Delta\eta_N(s')\exp(-b_2\Delta s'/2) \quad \text{A2.21}$$

$$Z_1(s') = Z_1(s' - \Delta s')\exp(-b_3\Delta s') + A_3\Delta\eta_N(s')\exp(-b_3\Delta s'/2) \quad \text{A2.22}$$

$$X_2(s') = X_2(s' - \Delta s')\exp(-\Delta s'/T_M) + \Delta\eta_M(s')\exp(-\Delta s'/2T_M) \quad \text{A2.23}$$

$$X_3(s') = X_3(s' - \Delta s')\exp(-\Delta s'/T_I) + \Delta\lambda_L(s')\exp(-\Delta s'/2T_I) \quad \text{A2.24}$$

$$X_4(s') = X_4(s' - \Delta s')\exp(-\Delta s'/T_I) + \Delta\lambda_M(s')\exp(-\Delta s'/2T_I) \quad \text{A2.25}$$

As mentioned in previous Chapters, a positive pitch rate decreases the leading edge pressure due to the induced camber effect. For practical purposes, and analogous to the static case, in order to use Evans-Mort correlation to denote the onset of dynamic-stall, Beddoes introduced a time constant T_p to lag the normal force, to account for the dynamic effects. The lagging is performed by

$$\Delta C_N'(s') = \Delta C_N(s')\left(1 - e^{-s'/T_p}\right) \quad \text{A2.26}$$

Figure 151 shows the lagged C_N' for a ramp-up test compared to the static normal force.

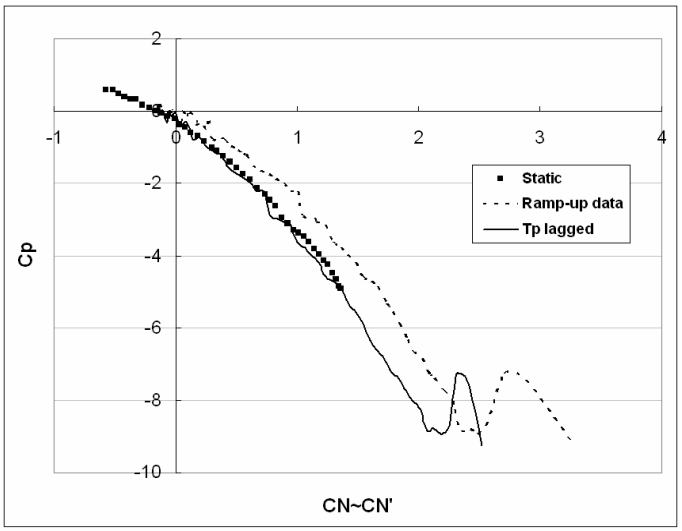

Figure 151 Normal force lagging for a ramp-up test [70]

However, Niven et al. [62] found that T_p lagging was not enough for the delay of boundary layer separation for low speed aerofoils, and introduced another time delay constant T_b, the further lagging is performed by

$$\Delta C_N''(s') = \Delta C_N'(s')\left(1 - e^{-s'/T_b}\right) \qquad \text{A2.27}$$

When the Mach number is bigger than 0.3 a shock reversal condition is adopted [12] while, for less than 0.3, a leading edge criterion, developed from the work of Evans and Mort [114] was applied. The lagged normal force C_N' is then compared with the critical normal force value C_{N1} for that defined Mach number (Figure 152). If it is greater than that value, the dynamic-stall onset is triggered. Figure 153 shows that with T_p lagging only, onset of dynamic vortex is predicted too early (Δ), while the further T_b modification gives the more accurate assessment of the onset of dynamic-stall. This is an example of a NACA0012 ramp-up test at reduced pitch rate 0.0245, and the Evans-Mort critical normal force C_{N1} is obtained from Figure 152.

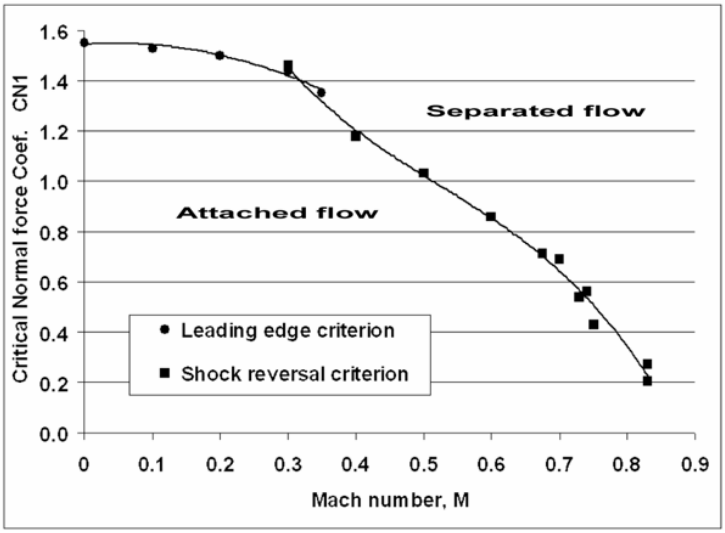

Figure 152 Beddoes' critical normal force C_{N1} for NACA0012 aerofoil

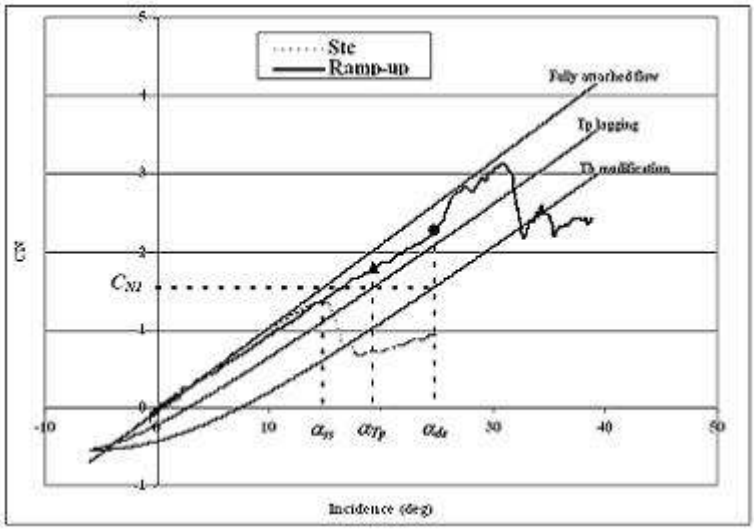

Figure 153 T_p lagging and T_b modification to denote onset of dynamic vortex

From the lagged normal force C'_N or C''_N, the corresponding effective angle of attack is calculated by

$$\alpha_{eff} = \frac{C'_N}{C_{N\alpha}} \qquad \text{For } T_p \text{ lagging only} \qquad \text{A2.28}$$

Or

$$\alpha_{eff} = \frac{C''_N}{C_{N\alpha}} \qquad \text{With } T_b \text{ modification} \qquad \text{A2.29}$$

1.3 Separated flow

In Beddoes dynamic-stall model, Kirchhoff theory [40] is employed to account for the airloads during separated flow, where the normal force is calculated by

$$C_N = C_{N\alpha} \times (\alpha - \alpha_0) \times \left(\frac{1+\sqrt{f}}{2} \right)^2 \qquad \text{A2.30}$$

Where α_0 is the angle of attack of zero normal force.

Beddoes (1993) used two functions to fit the separation point f

$$\begin{cases} f = 1 - 0.4 \exp\left(\dfrac{\alpha - \alpha_1}{S_1} \right) & \alpha \le \alpha_1 \\ f = 0.02 + 0.58 \exp\left(\dfrac{\alpha_1 - \alpha}{S_2} \right) & \alpha > \alpha_1 \end{cases} \qquad \text{A2.31}$$

Where

α_1 angle of attack at separation point f=0.6

S_1, S_2 parameters for fitting experimental data f

Pitching moment is reconstructed by following equation:

$$\frac{C_M}{C_N} = K_0 + K_1(1 - f^n) + K_2(f - f_b) e^{-(f-f_b)^2/m} \qquad \text{A2.32}$$

K_0, K_1 and K_2 are the parameters for fitting C_M, which can be obtained by least square method from the static test data. Three more parameters n, f_b and m are normally decided empirically for better fitting of C_M. Figure 154 illustrates the comparisons of the reconstructed normal force, pitching moment and separation point and experimental data. It can be seen that the reconstructions are good.

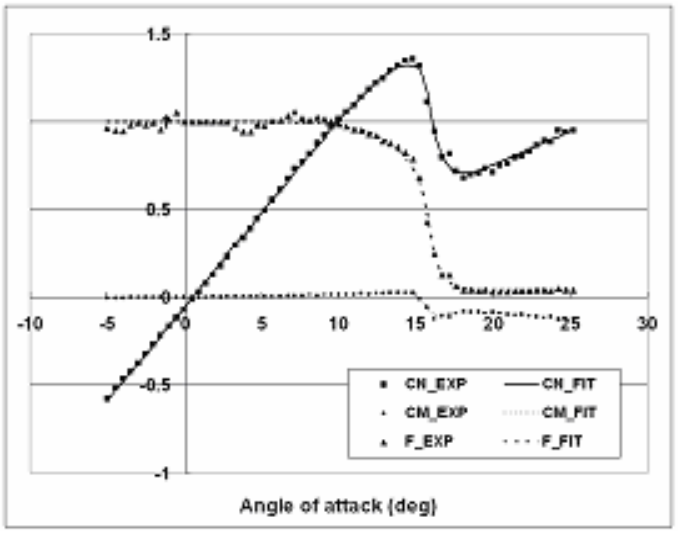

Figure 154 Normal force and separation point reconstructions [70]

Under dynamic conditions, the boundary layer separation is delayed. For the effective angles of attack α_{eff} given by formulations (A2.28 or A2.29), from equation A2.33, the delayed separation point f' can be calculated, as

$$\begin{cases} f' = 1 - 0.4\exp\left(\dfrac{\alpha_{eff} - \alpha_1}{S_1}\right) & \alpha_{eff} \le \alpha_1 \\ f' = 0.02 + 0.58\exp\left(\dfrac{\alpha_1 - \alpha_{eff}}{S_2}\right) & \alpha_{eff} > \alpha_1 \end{cases} \qquad \text{A2.33}$$

Boundary layer separation delay

In Beddoes 3rd generation model the boundary layer separation, due to dynamic effects, is lagged by a further time delay. In practice the delay is performed by lagging with a time constant T_f, as

$$\Delta f''(s') = \Delta f'(s')\left(1 - e^{-s'/T_f}\right) \qquad \text{A2.34}$$

where

$$\Delta f'(s') = f'(s'_{i+1}) - f'(s_i) \qquad \text{A2.35}$$

1.4 Dynamic vortex induced airloads

Vortex growth

With the vortex strength increasing, an added overshoot in normal force is produced. In Beddoes 3rd generation dynamic stall, the strength of the growing vortex is given by a function of the difference between the current location of the separation point and the steady state value ([40] and [115]) via a modulation parameter V_x. Hence the effects of vortex shedding are modified by the modifications of separation point.

Vortex growth

$$V_x = \sin^{3/2}\left(\frac{\pi\tau}{2T_v}\right) \qquad \text{for } 0 < \tau < T_v \qquad \text{A2.36}$$

Vortex convection

$$V_x = \cos^2\left[\frac{\pi(\tau - T_v)}{T_{v1}}\right] \qquad \text{for } \tau > T_v \qquad \text{A2.37}$$

Where T_v and T_{v1} represents the non-dimensional period of the initial vortex formation and convection respectively.

The modification value of separation point is given by

$$df(s') = \Delta f(s') \times V_x \qquad \text{A2.38}$$

where

$$\Delta f(s') = f''(s') - f'(s)$$

Since the effects of vortex shedding on normal force and pitching moment have 180^0 phase difference, therefore

$$\begin{cases} f_L = f''(s') + df \\ f_M = f''(s') - df \end{cases} \tag{A2.39}$$

Finally, the pressure drag is given by

$$C_d = C_N \sin\alpha - \eta_d C_t \cos\alpha K_n^{3/2}\left(1 - \frac{0.8C_p}{K_0 + K_1}\right) \tag{A2.40}$$

References

[1] DaVinci L., c. 1487-1490, "Ms. 2173 B", folio 83r, Bibliotheque L' Institut de France, Paris

[2] Davenport F. J., Front J. V., 1966, "Airfoil Sections for Rotor Blades- a Reconsideration", 22nd *Annual national Forum of the American Helicopter Society*

[3] Dadone L., 1978, "Rotor Airfoil Optimization: An Understanding of the Physical Limits", 34th *Annual National Forum of the American Helicopter Society*

[4] Harris F. D., Pruyn R. R., 1968, "Blade Stall – Half Fact, Half Fiction", 23rd *Annual National Forum of the American Helicopter Society*, n. 101

[5] Krama M., 1932, "Increase in the Maximum Lift of an Aerofoil Due to a Sudden Increase in Its Effective Angle of Attack Resulting from a Gust", NACA Technical Memorandum 678

[6] Liiva J., Davenport F. J., Gray L., Walton I. C., 1969, "Two-Dimensional Tests of Airfoil Oscillating near Stall, Vol. 1: Summary and Evaluation of Results", U.S. Army Aviation Material Lab., Tech. Report 68-13A

[7] Johnson W., Ham N. D., 1972, "On the Mechanism of Dynamic-stall", *J. American Helicopter Society*, Vol. 17, No. 4, pp. 36-45

[8] Mc Croskey W. J., Fisher R. K., 1972, "Detailed Aerodynamic Measurements on a Model Rotor in the Blade Stall Regime", *J. American Helicopter Society*, Vol. 17, No. 1, pp. 20-30

[9] Carr L.W., 1988 "Progress in Analysis and Prediction of Dynamic-stall", *Journal of Aircraft* 25: 6-17

[10] Carr L.W., McAlister K.W., McCroskey W.J., January 1977, "Analysis of the Development of Dynamic-stall Based on Oscillating Airfoil Experiments", NASA TN D-8382

[11] Niven A.J, Galbraith R.A.McD, Herring D.G.F, 1989, "Analysis of Reattachment during Ramp Down Tests", *Vertica* 13: 187-196

[12] Niven A.J, Galbraith R.A.McD, 1990, "Experiments on the Establishment of Fully Attached Aerofoil Flow from the Fully Stalled Condition During Ramp-Down Motions", 17th ICAS, Stockholm, Sweden

[13] Green R. B., Galbraith R.A.McD., 1995, "Dynamic Recovery to Fully Attached Flow from Deep Stall", AIAA Journal, Vol. 33, No. 8, pp. 1433-1440

[14] Green R. B., Galbraith R.A.McD., 1994, "Phenomena Observed During Ramp-down Tests from the Fully Stalled State", Aeronautical Journal, Vol. 98, pp. 349-356

[15] Ham M. D., 1968, "Aerodynamic Loading on a Two-Dimensional Airfoil During Dyanmic Stall", *AIAA Journal*, Vol. 6, No. 10

[16] Mc Croskey W. J, McAlister K. W., Carr L. W., Pucci S. L., Lambert O., Indergand R. F., 1980, "Dynamic-stall on Advanced Airfoil Sections", American Helicopter Society Prepint 80-01

[17] Nash J. F., Scruggs R. M., 1977, " Unsteady Boundry Layers with Reversal and Separation", AGARD CP-227

[18] Vezza M., 1986, "Numerical Methods for Design and Analysis of Aerofoils", Ph.D. Thesis, University of Glasgow

[19] Leishman J.G, Beddoes T.S, June 1986, "A Generalised Model For Airfoil Unsteady Aerodynamic Behaviour And Dynamic-stall Using The Indicial Method", 42nd *Annual Forum of the American Helicopter Society*

[20] Gangwani S.T., 1983, "Synthesized Airfoil Data method for Prediction of Dynamic-stall and Unsteady Airloads", *Vertica 8*:93-118

[21] Beddoes T. B., 1980, "Prediction of Unsteady Separated Flows", AGARD Report 679, Paper 15

[22] Galbraith R.A.McD., 1985, "Comments on the Prediction of Dynamic-stall", Glasgow University Aero Report No. 8501

[23] McCroskey W.J, February 1978, "Prediction of Unsteady Separated Flows on Oscillating Airfolis", AGARD-94

[24] Robinson M. C., Luttges M. W., 1983, "Unsteady Flow Separation and Attachment Induced by Pitching Aerofoils", AIAA 21st Aerospace Sciences Meeting

[25] Aihara Y., Koyama H., Murachige A., 1985, "Transient Aerodynamic Characteristics of a Two-Dimensional Airfoil during Stepwise Incidence Variation", Journal of Aircraft, 12.

[26] Jumper E. J., Shreck S. J., 1986, "Lift Curve Characteristics for an Airfoil Pitch at Constant Rate", 24th Aerospace Science Meeting

[27] Lorber P.F., Carta F.O., 1987, "Unsteady Stall Penetration Experiment at High Reynolds Number", UTRC Report R87-956939-3

[28] Seto L. Y., Galbraith R.A.McD, 1985, "The Effect Of Pitch-Rate On The Dynamic-stall of a Naca23012 Aerofoil", 11th European Rotorcrat Forum, London

[29] Leishman J.G, Beddoes T.S, 1989, "A Semi-Empirical Model for Dynamic-stall", *Journal of the American Helicopter Society,* Vol. 34: 3-17

[30] Kline S. J., Bardina J., Strawn R., 1981, "Correlation and Computation of Detachment and Reattachment of Turbulent Boundary Layers on Two-Dimensional faired Surfaces", AIAA Paper 81-1220

[31] Ericsson L. E., 1995, "Dynamic Airfoil Flow Separation and Reattachment", *Journal of Aircraft*, Vol. 32, pp. 1191-1197

[32] Ahmed S., Chandrasekhara M. S., 1994, "Reattachment Studies of an Oscillating Airfoil Dynamic-stall Flowfield", *AIAA Journal*, Vol.33, pp. 1006-1012

[33] Schreck S. J., Faller W. E., Luttges M. W., 1996, "Dynamic Reattachment on a Downward Pitching Finite Wing", *Journal of Aircraft*, Vol. 33, pp. 279-288

[34] Sheng W., Galbraith R.A.McD, Coton F. N., 2007, "On the Return from Aerofoil Stall during Ramp-down Pitching Motions", 45th AIAA Aerospace Sciences Meeting and Exhibit, Reno, Nevada (AIAA-2007-0626)

[35] Beddoes T.S, 1980, "Prediction Methods for Unsteady Separated Flows", AGARD Report 679, Paper 15

[36] McCroskey W. J., 1981, "The Phenomenon of Dynamic-stall", NASA TM-81264

[37] Johnson W., 1986, "Recent Development in Rotary-Wing Aerodynamic Theory", *AIAA Journal*, Vol. 24, No. 8

[38] Ericsson L. E., Reding J. P., 1988, "Fluid Mechanics of Dynamic-stall Part 1: Unsteady Flow Concepts", J.Fluids and Structures, Vol. 2, pp. 1-33

[39] Ekaterinaris J.A, Platzer M. F, 1997, "Computational Prediction of Airfoil Dynamic-stall", *Progress in Aerospace Science* 33: 759-846

[40] Beddoes T.S, 1993,"A Third Generation Model for Unsteady Aerodynamics and Dynamic-stall", Westland Helicopter Limited, RP-908

[41] Geissler W., Dietz G., Mai H., 2005, "Dynamic-stall on a Supercritical Airfoil", *Aerospace Science and Technology*, Vol.9, pp. 390-399

[42] Tan C. M., Carr L. W., 1996, "The AFDD International Dynamic-stall Workshop on Correction of Dynamic-stall Models with 3-D Dynamic-stall Data2, NASA Technical Memorandum 110375, also USAATCOM technical report 96-A009

[43] Petot D., Arnaud G., Stevens J., Dieterich O., van der Wall B. G., Young C., Szechenyi E., 1999, "Stall Effects and Blade Torsion-An Evaluation of Predictive Tools", *Journal of the American Helicopter society*, Vol. 44, pp. 320-331

[44] Johnson W., 1998, "Rotorcraft Aerodynamics Models for a Comprehensive Analysis", Presented at 54th AHS Annual Forum, Washington DC

[45] Mc Croskey W. J, Pucci S. L., 1981"Viscous-Inviscid interaction on Oscillating Airfoils", AIAA pper 81-0051

[46] Galbraith R.A.McD, 1985, "Comments on the Prediction of Dynamic-stall", Glasgow University, Aeronautics Report No. 8501

[47] Agarwal R., 1999, "Computational Fluid Dynamics of Whole-Body Aircraft", Annual Review of Fluid Mechanics , Vol. 31, pp. 125-169

[48] Sears W., 1976 "Unsteady Motion of Airfoils with Boundary-Layer Separation", A.I.A.A. Journal 14, pp. 216-220.

[49] Clement R. R., Maull D. J,. 1975, "The Representation of Sheets of Vorticity by Discrete Vortices". *Prog. AeroSpace Sci.* 16, pp129-146.

[50] Oshima K., Oshima Y, 1982, "Flow simulation by discrete vortex method", Lecture in Physics, Vol. 170, Springer Berlin/Heidelberg editor

[51] Jones L. E., Sandberg R. D., Sandham N. D., 2006, "Direct Numerical Simulation of the Flow around an Airfoil with Unsteady Wake", Wesseling P., Onate E., and Periaux J., editors, *European Conference on Computational Fluid Dynamics, ECCOMAS CFD 2006*

[52] Beddoes T.S, 1984, 'Practical Computational of Unsteady Lift', *Vertica* 8: 55-71

[53] Leishman J.G, 1988, "Validation of Approximate Indicial Aerodynamic Functions for Two-Dimensional Subsonic Flow", Journal of Aircraft, Vol.25, No. 10, pp. 914-922

[54] Galbraith R.A.McD, Leishman J. G., 1983, “A Micro-Computer Based on Test Facility for the Investigation of Dynamic-stall”, International Conference on the Use of Micros in Fluid Engineering, Paper E3

[55] Lober P. F., Carter F. O., 1987, “Unsteady Stall Penetration Experiments at High Reynolds Number”, United Technologies Research Centre Report R87-956939-3, also AFOSR TR-87-1202

[56] Niven A. J., 1991, “An Experimental Investigation into the Influence of Trailing Edge Separation on an Aerofoil’s Dynamic-stall Performance”, Universtity of Glasgoow, Ph.D. Thesis

[57] Gracey M. W., 1991, “The Design and Low Mach Number Wind Tunnel Performance of a Modified NACA 23012 Aerofoil, with an Ivestigation of Dynamic-stall onset”, University of Glasgow, Ph. D. Thesis

[58] North Atlantic Treaty Organization – RTO TECHNICAL REPORT 26, October 2000, “Verification and Validation Data for Computational Unsteady Aerodynamics”, 22-E Dynamic-stall Data for 2-D and 3-D Test Cases,

[59] Gobbi G., Singh C., Galbraith R.A.McD., Coton F., Peake D., Kokkalis A., Gilmour R., 2006, “Collected Data For Tests On A Rae 9645 Aerofoil”, G.U. AERO REPORT: 0602

[60] Gobbi G., Singh C., Galbraith R.A.McD., Coton F., Peake D., Kokkalis A., Gilmour R., 2006, “Collected Data For Tests On A Rae 9645 Aerofoil”, G.U. AERO REPORT: 0603

[61] Wilby P. G., 1980, “The Aerodynamic Characteristics of Some New RAE Blade Sections and Their Potential Influence on Rotor Performance”, Vertical, Vol. 4, 121-133

[62] Niven A.J., Galbraith R.A.McD, February 1997, “Modelling Dynamic-stall Vortex Inception at Low Mach Numbers”, *The Aeronautical Journal*

[63] Leishman J.G, 1988, “Two-Dimensional Model for Airfoil Unsteady Drag Below Stall”, Journal of Aircraft, Vol. 25, No.7, pp. 665-666

[64] Leishman J.G, 1993, “Indicial Lift Approximation for Two-Dimensional Subsonic Flow as Obtained from Oscillatory Measurement”, Journal of Aircraft, Vol. 30, No. 3, pp. 340-351

[65] Kenneth W., McAlister, Lawrence W., Carr, William J. McCroskey, 1978, “Dynamic-stall experiments on the NACA 0012Airfoil”, NASA Technical Paper 1100

[66] Angel R.K., Musgrove P.J., Galbraith R.A.McD, 1988, “Collected Data for Tests on a NACA 0030 Aerofoil”, G.U. AERO REPORT: 8825, 8826, 8827

[67] Angel R.K., Musgrove P.J., Galbraith R.A.McD, 1988, "Collected Data for Tests on a NACA 0015 Aerofoil", G.U. AERO REPORT: 8801, 8802, 8803

[68] Sheng W., Galbraith R.A.McD, Coton F. N., Jan.2007, "A Modified Dynamic-stall Model for Low Speed Mach Numbers", 45th AIAA Aerospace Sciences Meeting and Exhibit, Reno, Nevada (AIAA-2007-1075)

[69] Beddoes T.S, 1978, "Onset Of Leading Edge Separation Effects Under Dynamic Conditions And Low Mach Number", presented at the 34th Annual National Forum of the American Helicopter Society, Washington D.C.

[70] Sheng W., Galbraith R.A.McD., Coton F. N.,2006, "A New Stall-Onset Criterion for Low Speed Dynamic-Stall", *Journal of Solar Energy Engineering*, Vol. 128, pp. 61-471

[71] Sebag O., 2005, "Analysis of Reattachment During Ramp-down Tests for Low-Speed Dynamic-stall on Helicopters", Final Year Report, University of Glasgow, Department of Aerospace Engineering

[72] McCroskey W. J., Mc Alister K. W., Pucci S. L., Lambert O., Indergrand R. F., 1981, "Dynamic-stall on Advanced Airfoil Sections", *Journal of the American Helicopter Society*, Vol 26, pp. 40-50

[73] Leishman J.G., 2000, "Principles Of Helicopter Aerodynamics", Cambridge University Press, U.S.A.

[74] McCroskey W. J., 1976, "Dynamic-stall Experiments on Oscillating Airfoils", *AIAA Journal* 14: 57-63

[75] McCroskey W.J, 1982, "Unsteady Airfoils", *Annual Review of Fluid Mechanics* 14: 285-311

[76] Gobbi G., Galbraith R.A.McD., Coton F., Gilmour R., 2006, "Collected Data For Tests On A Rae 9645 Aerofoil", G.U. AERO REPORT: 0604

[77] Gobbi G., Galbraith R.A.McD., Coton F., Gilmour R., 2006, "Collected Data For Tests On A Rae 9645 Aerofoil", G.U. AERO REPORT: 0605

[78] Angell R.K., Musgrove P.J., Galbraith R.A.McD., Green R.B. 1990, "Summary of the Collected Data for Tests on the NACA 0015, NACA 0018, NACA 0021, NACA 0025 and NACA 0030 Aerofoils", G.U. REPORT 9005

[79] Wilby P.G., 2001, "The Development of Airfoil Testing in the UK", Journal of American Helicopter Society46: 210-220

[80] Sheng W., Galbraith R. A. McD., Coton F. N., "*On the S809 Aerofoil's Unsteady Aerodynamic Characteristics*", To be published

[81] Jones K.D, Platzer M.F, 1998, "On the prediction of Dynamic-stall Onset on Airfoils in Low Speed Flow", *Proceedings of the 8th International Symposium on Unsteady Aerodynamics and Aeroelasticity of Turbomachines*, Dordrecht, Netherlands

[82] Guilmineau E., Queutey P., 1999, "Numerical Study of Dynamic-stall on Several Airfoil Sections", AIAA *Journal*, Vol. 37, pp. 128-130

[83] Spentzos A., Barakos G. N., Badcock K. J., Richards B. E., Wernert P., Schreck S., Raffel M., "Investigation of Three-Dimensional Dynamic-stall Using Computational Fluid Dynamics", AIAA Journal, Vol. 43, pp. 1023-1033

[84] Gross D.W., Harris F.D., 1969, "Prediction of In-Flight Stalled Airloads from Oscillating Airfoil Data", 25th Annual Forum of AHS, Washington DC

[85] Johnson W., 1969, "The Effect of Dynamic-stall on the Response and Airloading of Helicopter Rotor Blades", *Journal of American Helicopter Society 14*:68-77

[86] Carta F.O. et al., 1970, "Analytical Study of Helicopter Rotor Stall flutter", 26th Annual Forum of AHS, Washington DC

[87] Tran C.T., Petot D., 1981, "Semi-Empirical Model for the Dynamic-stall Airloads in View of the Application to the Calculation of Responses of a Helicopter Blade in Forward Flight", *Vertica 5*:35-53

[88] McCrosky W.J., March 1977, "Some Current Research in Unsteady Fluid Dynamics", Trans. of the ASME, Journal of Fluids Engineering

[89] Beddoes T.S, 1984, 'Practical Computational of Unsteady Lift', *Vertica* 8: 55-71

[90] Beddoes T. S., "Application of Indicial Aerodynamic Functions"

[91] Beddoes T. S., 1976,"A Synthesis of Unsteady Aerodynamic Effects Including Stall Hysteresis", *Vertical 1*: 113-123,

[92] Beddoes T.S, 1983, "Representation of Airfoil Behaviour", *Vertica* 7: 183-197,

[93] Beddoes T.S, 1984, 'Practical Computational of Unsteady Lift', *Vertica* 8: 55-71,

[94] Leishman J.G, 1987, "Practical Modelling of Unsteady Airfoil Behaviour in Nominally Attached Two-Dimensional Compressible Flow", UM-AERO-87-6, Department of Aerospace Engineering, University of Maryland

[95] Leishman J.G, 1987, "A Semi-Empirical Model for Dynamic-stall', UM-AERO-87-24, Department of Aerospace Engineering, University of Maryland

[96] Lomax H. et al., 1952, "Two and Three Dimensional, Unsteady Lift Problems in High-Speed", NACA Report 1077

[97] Leishman J.G., 2002, "Challenges in Modelling the Unsteady Aerodynamics of Wind Turbines", AIAA -0037

[98] Ormiston R. A., 1974, "Comparison of Several Methods for Predicting Loads on a Hypothetical Helicopter Rotor", *Journal of the American Helicopter Society*, Vol. 19, No. 4, pp. 2-13

[99] Reddy T. S. R., Kaza K. R. V., 1987, "A Comparative Study of some Dynamic-stall Models", NASA TM 88917

[100] Beddoes T. S., 1976, "A Synthesis of Unsteady Aerodynamic Effects Including Stall Hysteresis", *Vertical 1*: 113-123

[101] Scruggs R.M, Nash J. F., Singleton R. E., 1974, "Analysis of Dynamic-stall Using Unsteady Boundary-Layer Theory", NASA CR-2462

[102] Wilby P.G., 1984, "An Experimental Investigation of the Influence of a Range of Aerofoil Design Features on Dynamic-stall", presented at 10th European Rotorcraft Forum

[103] Lorber P.F., Carta F.O., 1987, "Airfoil Dynamic-stall as Constant Pitch Rate and High Reynolds Number", presented at AIAA 19th Fluid Dynamics, Plasma Dynamics and Lasers Conference, AIAA 87-1329

[104] Daley D.C., Jumper E.J, 1984, "Experimental Investigation of Dynamic-stall for a Pitching Airfoil", Journal of Aircraft 21

[105] Beddoes T.S., 1978, "Onset of Leading Edge Separation Effects Under Dynamic Conditions and Low Mach Number", 34th Annual National Forum of the American Helicopter Society

[106] Green R.B., Galbraith R.A.McD., Niven A. J., 1992, "Measurements of the Dynamic-stall Vortex Convection Speed", *Aeronautical Journal*, Vol. 96, pp. 319-327

[107] Green R. B., Galbraith R.A.McD., 1995 "Dynamic Recovery to Fully Attached Flow from Deep Stall", AIAA Journal, Vol. 33, No. 8. pp. 1433-1440

[108] Gutpa S., Leishman J. G., 2006, "Dynamic Stall Modelling of the S809 Airfoil and Comparison with Experiments", Wind Energy; 9, pp. 512-547

[109] Bertin J.J, Smith M.L, 1998, "Aerodynamics for Engineers" (3rd Ed.), Prentice Hall

[110] Katz J., Plotkin A., 2001, "Low Speed Aerodynamics", Cambridge University Press

[111] Beddoes T.S, “Two and Three Dimensional Indicial Methods for Rotor Dynamic Airloads”, presented at AHS/National Specialist’s Meeting on Rotorcraft Dynamics, Nov. 1989, Texas,US

[112] Lomax H., “Indicial Aerodynamics”, Part II, Chapter 6, AGARD Manual on Aeroelasticity

[113] Bisplinghoff R. L., Ashley H., Halfman R. L., 1955, “Aeroelasticity”, Addison-Wesley, Reading, MA

[114] Evans W.T., Mort K. W., 1959, “Analysis of Computed Flow Parameters for a Set of Suddenly Stalls in Low Speed Two-Dimensional Flow”, NACA TND-85

[115] GKN Westland Helicopter Ltd, Glasgow University, July 1999, *Korean Lecture Series*